REMOVAL OF HALOACETONITRILES BY ADSORPTION ON MODIFIED INORGANIC POROUS MATERIALS

Miss Panida Prarat

A Dissertation Submitted in Partial Fulfillment of the Requirements
for the Degree of Doctor of Philosophy Program in Environmental Management
(Interdisciplinary Program)
Graduate School
Chulalongkorn University
Academic Year 2011

การกำจัดสารฮาโลแอซิโตไนไตรล์โดยการดูดซับบนวัสดุมีรูพรุนที่ดัดแปร

นางสาวพนิดา ปรารัตน์

วิทยานิพนธ์นี้เป็นส่วนหนึ่งของการศึกษาตามหลักสูตรปริญญาวิทยาศาสตรดุษฎีบัณฑิต
สาขาวิชาการจัดการสิ่งแวดล้อม (สหสาขาวิชา)
บัณฑิตวิทยาลัย จุฬาลงกรณ์มหาวิทยาลัย
ปีการศึกษา 2554

Thesis Title	REMOVAL OF HALOACETONITRILES BY ADSORPTION ON MODIFIED INORGANIC POROUS MATERIALS
By	Miss Panida Prarat
Field of Study	Environmental Management
Thesis Advisor	Assistant Professor Patiparn Punyapalakul, Ph.D.
Thesis Co-advisor	Associate Professor Sutha Khaodhiar, Ph.D.

Accepted by the Graduate School, Chulalongkorn University in Partial Fulfillment of the Requirements for the Doctoral Degree

…….. Dean of the Graduate School
(Associate Professor Pornpote Piumsomboon,Ph.D.)

THESIS COMMITTEE

…….. Chairman
(Assistant Professor Chantra Tongcumpou, Ph.D.)

……..…… Thesis Advisor
(Assistant Professor Patiparn Punyapalakul, Ph.D.)

…….. Thesis Co-advisor
(Associate Professor Sutha Khaodhiar, Ph.D.)

…….. Examiner
(Associate Professor Jin Anotai, Ph.D.)

…….. Examiner
(Assistant Professor Chawalit Ngamcharussrivichai, Ph.D.)

…….. External Examiner
(Emma Asnachinda, Ph.D.)

พนิดา ปรารัตน์ : การกำจัดสารฮาโลแอซิโตไนไตรล์โดยการดูดซับบนวัสดุมีรูพรุนอนินทรีย์ที่ดัดแปร (REMOVAL OF HALOACETONITRILES BY ADSORPTION ON MODIFIED INORGANIC POROUS MATERIALS) อ.ที่ปรึกษาวิทยานิพนธ์หลัก: ผศ.ดร.ปฏิภาณ ปัญญาพลกุล, อ.ที่ปรึกษาวิทยานิพนธ์ร่วม: รศ.ดร.สุธา ขาวเธียร, 200 หน้า.

งานวิจัยนี้มีวัตถุประสงค์เพื่อศึกษาการกำจัดสารฮาโลแอซิโตไนไตรล์ (HANs) ในน้ำด้วยกระบวนการดูดซับบนวัสดุมีรูพรุนอนินทรีย์ที่ถูกดัดแปรพื้นผิว ตัวดูดซับสังเคราะห์ชนิดเมโซพอรัสซิลิเกต (HMS) ถูกต่อติดหมู่ฟังก์ชั่นอินทรีย์ 3 ชนิด (ได้แก่ หมู่อะมิโน หมู่เมอร์แคปโต และหมู่อัคคิล) เพื่อศึกษาผลของการต่อติดหมู่ฟังก์ชั่นอินทรีย์ต่อประสิทธิภาพและกลไกการดูดซับสาร HANs เปรียบเทียบกับถ่านกัมมันต์ชนิดผง (PAC) นอกจากนี้ HMS ถูกดัดแปรโดยแทนที่ด้วยโลหะไททาเนียมในโครงสร้างเมโซพอรัสซิลิเกตเพื่อศึกษาความสัมพันธ์ระหว่างโครงสร้างรูพรุนกับประสิทธิภาพการดูดซับเปรียบเทียบกับเมโซพอรัสซิลิเกตชนิด SBA-15 และซีโอไลต์ NaY จากผลการศึกษาพบว่าโครงสร้างรูพรุนที่แตกต่างกันและชนิดของหมู่ฟังก์ชั่นอินทรีย์ที่ต่อติดบนพื้นผิวมีอิทธิพลต่ออัตราเร็ว และประสิทธิภาพการดูดซับ ซึ่งหมู่เมอร์แคปโตบน HMS (M-HMS) มีประสิทธิภาพการดูดซับสูงสุดเมื่อเปรียบเทียบกับหมู่ฟังก์ชั่นอินทรีย์ชนิดอื่น และมีประสิทธิภาพการดูดซับสาร HANs ได้เทียบเท่า PAC โครงสร้างของสาร HANs ที่แตกต่างกันส่งผลต่อประสิทธิภาพการดูดซับและสมบัติการดูดซับแบบคัดเลือกของ M-HMS ในขณะที่ไม่พบสมบัติการดูดซับแบบคัดเลือกของ PAC นอกจากนี้ผลกระทบของของอิเล็กโตรไลท์ที่มีอยู่ในน้ำประปาต่อการดูดซับสาร HANs และการมีอยู่ร่วมกันของสารไตรฮาโลมีเทน (THMs) และสารฮาโลแอซิติก แอซิด (HAAs) ไม่ส่งผลกระทบต่อสมบัติการดูดซับแบบคัดเลือกของ HANs บนตัวกลางทั้งสองชนิด กลไกการดูดซับสาร HANs คาดว่ามีความซับซ้อนซึ่งเกิดจากแรงทางประจุไฟฟ้าระหว่างไอออนและคู่ขั้วรวมถึงการดูดซับทางเคมี และผลจากการศึกษาการฟื้นฟูสภาพตัวดูดซับพบว่าเกิดการดูดซับแบบไม่ผันกลับบนพื้นผิวของตัวดูดซับ

นอกจากนี้เมโซพอรัสซิลิเกตชนิด SBA-CHX ถูกดัดแปรพื้นผิวโดยการดูดซับสารลดแรงตึงผิวแบบสองหัวที่สามารถเกิดปฏิกิริยาโพลีเมอร์ไรซ์ได้ (PG-SBA-CHX) เพื่อศึกษาอิทธิพลของกระบวนการแอดโซลูบิไลเซชั่นต่อประสิทธิภาพการดูดซับสาร HANs จากการศึกษาพบว่า PG-SBA-CHX มีประสิทธิภาพในการดูดซับสารได้ดีเมื่อเปรียบเทียบกับตัวดูดซับที่ไม่มีการดัดแปรพื้นผิวโดยเฉพาะอย่างยิ่ง HANs ชนิดไม่ชอบน้ำ อย่างไรก็ตามการดูดซับสารที่มีความชอบน้ำยังคงมีประสิทธิภาพต่ำกว่า ชี้บ่งว่ากระบวนการแอดโซลูบิไลเซชั่นมีบทบาทสำคัญต่อการดูดซับสาร HANs ซึ่งสัมพันธ์กับความชอบน้ำ / ไม่ชอบน้ำของตัวถูกดูดซับ

สาขาวิชา การจัดการสิ่งแวดล้อม ลายมือชื่อนิสิต .....

ปีการศึกษา 2554 ลายมือชื่อ อ.ที่ปรึกษาวิทยานิพนธ์หลัก.....

ลายมือชื่อ อ.ที่ปรึกษาวิทยานิพนธ์ร่วม .....

5087878520 : MAJOR ENVIRONMENTAL MANAGEMENT
KEYWORDS : HALOACETONITRILE / HEXAGONAL MESOPOROUS SILICATE / ADSORPTION/ADSOLUBILIZATION / SURFACE FUNCTIONAL GROUP / POLYMERIZABLE SURFACTANT / ZEOLITE

PANIDA PRARAT : REMOVAL OF HALOACETONITRILES BY ADSORPTION ON MODIFIED INORGANIC POROUS MATERIALS. ADVISOR : ASST. PROF. PATIPARN PUNYAPALAKUL, Ph.D., CO-ADVISOR : ASSOC. PROF. SUTHA KHAODHIAR, Ph.D., 200 pp.

The main objective of this study was to investigate the removal of haloacetonitriles (HANs) in aqueous solution by adsorption on various surface-modified inorganic porous materials. Hexagonal mesoporous silicate (HMS) was synthesized and modified surface with various organic functional groups (amino-, mercapto- and octyl groups) to investigate the effect of surface functional group on adsorption efficiency and mechanism compared with powder activated carbon (PAC). In addition, HMS then modified by substitution of titanium in silicate structure to investigate the relationship between the porous structure and the resultant adsorption capacities, compared to the similar mesopore SBA-15. Zeolite NaY was used so as to investigate the effect of crystalline structure. The results indicated that the adsorption rate and capacity of HANs both significantly influenced by the different porous and crystalline structures as well as by the surface functional group of adsorbent. M-HMS provided higher adsorption capacity of HANs than the other organic-functionalized adsorbents and had a comparable the adsorption capacity to PAC. The different molecular structure of HANs obviously affected the adsorption capacity and selectivity over M-HMS whereas selective adsorption over PAC was not observed. Moreover, the effect of electrolyte in tap water and in the presence of co-existing DBPs (trihalomethanes and haloacetic acids) did not affect the selective adsorption of both adsorbents significantly. The adsorption mechanism is believed to occur via a more complex interplay between an ion-dipole electrostatic interaction and chemisorption. Adsorbent regeneration study by extraction method revealed an irreversible adsorption on adsorbent surface which confirmed the chemisorption mechanism.

Furthermore, mesoporous silicate SBA-CHX was modified surface by polymerizable gemini surfactant (PG-SBA-CHX) adsorption to investigate the influence of adsolubilization on HAN adsorption efficiency. PG-SBA-CHX could efficiently adsorb the HANs especially hydrophobic HANs compared with unmodified adsorbent, however, hydrophilic HANs were the lower adsorption capacity. This indicated that the partition process (adsolubilization) plays crucial role on the adsorption related to hydrophilic / hydrophobicity of adsorbate.

Field of Study : Environmental Management Student's Signature .....

Academic Year : 2011 Advisor's Signature .....

Co-advisor's Signature .....

ACKNOWLEDGEMENTS

I would like to express my sincere gratitude to my advisor, Assist. Prof. Dr. Patiparn Punyapalakul. I appreciate very much for his patience and guidance that I have been able to complete this process. I would like to thank for his encouragement and valuable comments, and I am grateful for all of the opportunities that he has provided me. Through his actions he has shown me how research should be done, and it has been a privilege to study under his guidance. I express my gratitude to my co-advisor, Assoc. Prof. Dr. Sutha Khaodhiar for his time, continuous support and helpful suggestions. I am also grateful to Assist. Prof. Dr. Chawalit Ngamcharussrivichai who has assisted me throughout my study, and I would also like to thank for his time, continuous support and many beneficial discussions. I would like to take this opportunity to thank Assist. Prof. Dr. Chantra Tongcumpou, chairman of the committee, Assoc. Prof. Dr. Jin Anotai, and Dr. Emma Asnachinda, the member of my committee, for their useful and valuable comments.

I express my gratitude to the Thai Industrial Standards Institute, Ministry of Industry, which has provided the opportunity to me for studying Ph.D. program. I would like to thank the Center of Excellence for Environmental and Hazardous Waste Management (EHWM), Chulalongkorn University, for providing my tuition and thesis grants. In addition, the financial support from the 90th Anniversary of Chulalongkorn University Fund (Ratchadaphiseksomphot Endowment Fund), 2010 TTSF Science & Technology Research Grant from Thailand Toray Science Foundation and 2010 Overseas Research Grants from the Asahi Glass Foundation and the technical support from the Department of Environmental Engineering, Faculty of Engineering, Chulalongkorn University are also acknowledged.

Lastly, I would like to thank Miss Ramnaree for her assistance in the laboratory and for her patience with my questions regarding frequency response. I would like to express my sincere gratitude to my beloved family. Thank are, P'Kung, Pin, Palm, Ple and Ohm, five of my friend, greatly helped me during the program of my Ph.D., and my friends in research group for their love, encouragement and their support in any respect.

CONTENTS

Page

Page

Page

Page

Page

.

Page

Page

LIST OF TABLES

LIST OF FIGURES

Figure **Page**

Figure **Page**

Figure **Page**

ABBREVIATIONS

AC	=	Activated carbon
A-HMS	=	Amino-functionalized hexagonal mesoporous silicate
APTES	=	3-aminopropyltriethoxysilane
BAC	=	Biological activated carbon
BET	=	Brunner-Eller-Teller
BJH	=	Barret-Joyner-Halenda
CMC	=	Critical micelle concentration
CHX		Cyclohexane
DBAN	=	Dibromoacetonitrile
DCAA	=	Dichloroacetic acid
DCAN	=	Dichloroacetonitrile
DDA	=	Dodecylamine
FT-IR	=	Fourier transform infrared
GAC	=	Granular activated carbon
GC/ECD	=	Gas chromatograph equipped with electron capture detector
HAAs	=	Haloacetic acids
HANs	=	Haloacetonitriles
HMS	=	Hexagonal mesoporous silicate
ICP-AES	=	Inductively couple plasma atomic emission
IS	=	Ionic strength
IUPAC		International Union of Pure and Applied Chemistry
MBAN	=	Monobromoacetonitrile
MCAN	=	Monochloroacetonitrile
M-HMS	=	Mercapto-functionalized hexagonal mesoporous silicate
MPTMS	=	3-mercaptopropyltrimethoxysilane
MtBE	=	Methyl-*tert* -butyl ether
NaY	=	Na-form faujasite zeolite
NF	=	Nanofiltration
OD-HMS	=	Octyl-functionalized hexagonal mesoporous silicate
PAC	=	Powder Activated Carbon

PG	=	Polymerlizable gemini surfactant
PG-SBA-CHX	=	Polymerizable Gemini surfactant adsorbed on Santa Barbara Acid expanded pore size by cyclohexane
SBA-15	=	Santa Barbara Acid mesoporous silicate no.15
SBA-CHX	=	Santa Barbara Acid mesoporous silicate expanded pore size by cyclohexane
SEM	=	Scanning electron microscope
TCAN	=	Trichloroacetonitrile
TCM	=	Trichloromethane
TEOS	=	Tetraethylorthosilicate or tetraethoxysilane
THMs	=	Trihalomethanes
Ti-HMS	=	Titanium-substituted hexagonal mesoporous silicate
TIPOT	=	Tetraisopropylorthotitanate
TPN	=	Total persulfate nitrogen
XRD	=	X-ray diffraction

NOMENCLATURE

ΔG	=	Gibbs free energy (kJ mol^{-1})
ΔH	=	Enthalpy (kJ mol^{-1})
$\triangle q$ (%)	=	Normalized standard deviation (percentage)
ΔS	=	Entropy (kJ mol^{-1} K^{-1})
$1/n$	=	Freundlich constant related to sorption intensity of the adsorbent
C_0	=	Initial concentration (μg L^{-1} or mg L^{-1})
C_e	=	Concentration at equilibrium (μg L^{-1} or mg L^{-1})
h	=	Initial adsorption rate (mg g^{-1} h^{-1})
k_1	=	Pseudo-first-order rate constant (h^{-1})
k_2	=	Pseudo-second-order rate constant (g mg^{-1} h^{-1})
k_{iP}	=	Intraparticle rate constant (mg g^{-1} $h^{-0.5}$)
K_F	=	Freundlich constant (mg g^{-1})
K_L	=	Langmuir constant (L mg^{-1})
K_p	=	Linear partition coefficient
k_s	=	External diffusion (mg g^{-1} h^{-1})
K_S	=	Sips isotherm constant (L mg^{-1})
M	=	Mass (gram)
q_e	=	Adsorption capacity at equilibrium (mg g^{-1})
q_m	=	Maximum adsorption capacity (mg g^{-1})
q_t	=	Adsorption capacity at time (mg g^{-1})
R	=	Universal gas constant (8.314 J mol^{-1} K^{-1})
R^2	=	The correlation coefficient
S_{BET}	=	Specific surface area (m^2 g^{-1})
t	=	Time (hour)
$t_{1/2}$	=	Half-life (hour)
T	=	Temperature (Kelvin)
V	=	Volume (Liter)
V_p	=	Pore volume (mm^3 g^{-1})

CHAPTER I

INTRODUCTION

1.1 STATE OF PROBLEM

Haloacetonitriles (HANs) are nitrogenous disinfection by-products (DBPs) that have been recently reported to have a much higher toxicity than the two other major groups of DBPs, the trihalomethans (THMs) and haloacetic acids (HAAs) (Plewa et al., 2008). Therefore, the World Health Organization has suggested guideline maximal permitted values of HANs presenting in drinking water supplies. Moreover, they have been included in the US Environmental Protection Agency Information Collection Rules and they may be considered in future US Environmental Protection Agency regulations. Several diverse techniques have been employed to remove the DBPs from the (aqueous) environment, such as by adsorption (Tung et al., 2006; Babi et al., 2007; Kim and Kang, 2008; Ratasuk et al., 2008), ozonation (Ratasuk et al., 2008), and membrane filtration (Uyak et al., 2008). Among them, the adsorption process has been favored for water treatment due to its advantages of low relatively cost and simplicity. Although activated carbon is predominantly used as the adsorbent because of its availability and high efficiency for the removal of a number of DBPs, especially the hydrophobic molecules, however, the surface characteristics are not suitable for the adsorption of hydrophilic compounds (Tung et al., 2006; Babi et al., 2007). In addition, the use of activated carbon is sometimes problematic due to its low adsorption-selective nature and difficulty in its regeneration. Consequently, a lot of effort has been focused upon the development various materials for the removal of DBPs from an aqueous phase.

Among the porous materials, mesoporous silicates offer a number of potential advantages as adsorbents due to their high surface area, large pore volume and narrow pore size distribution. Moreover, their surface modification, via the reaction of silanol groups with various organosilanes, is very helpful in improving the adsorptive capacity and selectivity as a result of specific interactions between the surface functional groups and adsorbate molecules. In literature, only a limited amount of information on the adsorption of DBPs over microporous and mesoporous

materials has been reported previously. Various organic functionalized hexagonal mesoporous silicate (HMS) derivatives have been shown to be effective adsorbents for dichloroacetic acid (DCAA) adsorption at which the amino-functionalized HMS showing excellent adsorption properties of DCAA at high concentration (ppm level) (Punyapalakul and Takizawa, 2004). Recently, Punyapalakul and coworkers found that the crystalline structure and surface area of adsorbents also affected the adsorption of DCAA at low concentration (Punyapalakul et al., 2009). Furthermore, micropore size, relative pore volume, and surface characteristic have all been reported to be important factors in determining the adsorption of *N*-nitrosodimethylamine (NDMA) (Dai et al., 2009). According to the literature, it indicated that the characteristics of the adsorbent such as surface functional groups and the porous structure play crucial roles on the adsorption.

Surfactant-modified adsorbents have drawn much attention in separation process and the removal efficiency of various organic/inorganic compounds have been reported in literature, such as phenol and derivatives (Rawajfih and Nsour, 2006; Alkaram et al., 2009; Damjanovic et al., 2010), dyes (Jin et al., 2008; Li et al., 2008; Oei et al., 2009), heavy metals (Choi et al., 2009; Chutia et al., 2009; Nadeem et al., 2009; Su et al., 2011), and etc. The adsorbents can be modified by surfactant to form bilayer micelle structures, called “admicelle”, on their surface having the potential to solubilize organic molecules (Adak et al., 2005). Even though the surfactant-modified adsorbent has been found to be a promising adsorbent for environmental approach, however, its use is sometimes problematic due to the loss of surfactant from the solid surface. In order to reduce the surfactant loss, polymerizable surfactants are of interest because the crosslink of adsorbed surfactant after polymerization is expected to increase a stability of the surfactant coverage on adsorbent surface. Additionally, previous report has found that admicelle polymerization could reduce surfactant desorption from solid surface without reducing the adsolubilization potential (Attaphong et al., 2010).

To the best of our knowledge, the adsorption of HANs by mesoporous silicate HMS in aqueous solution has not been studied. Towards a better understanding of the adsorption mechanism, however, a comparative study is still needed to evaluate the impact of the molecular structure of DBPs on the adsorption

behavior of the synthesized adsorbents. Thus, the purpose of this study emphasized the investigation of the effects of surface functional groups, porous or crystalline structures, and surface modification by surfactant on the HAN adsorption efficiency and mechanism. The modification of HMS with three organic functional groups (amino-, mercapto- and octyl groups) was employed to investigate the effect of surface functional groups on HAN adsorption capacity comparing with powdered activated carbon (PAC). Because the effect of porous and crystalline structures on adsorption is poorly understood or defined and needs further investigation, therefore, similar mesoporous structure HMS and SBA-15, and one metal substitution by incorporating titanium into silicate structure (Ti-HMS) compared with micropore NaY were employed to investigate the relationship between the porous structure of adsorbents and the adsorption efficiency and mechanism for HANs. In addition, mesoporous silicate was modified surface with polymerizable surfactant and was investigated the influence of adsolubilization process on HAN adsorption compared with the unmodified-surface adsorbent.

The adsorption experiments were carried out using batch adsorption experiments. The adsorption kinetics, adsorption isotherms and the effects of pH of solution and temperature were studied to investigate the adsorption mechanism. The adsorption selectivity of adsorbent for the adsorption of mixed HAN_s, in the presence of co-existing electrolytes in tap water, and competitive DBPs in mixed solute solution were investigated. In addition, the possibility of regeneration of used adsorbents by extraction method was also evaluated.

1.2 OBJECTIVES

The main objective of this study is to investigate the removal of haloacetonitriles (HANs) in aqueous solution by adsorption on various surface-modified inorganic porous materials. The sub-objectives are as follow:

1. To investigate the effects of surface functional group, porous and crystalline structures, and surface modification by surfactant on adsorption capacities and mechanism of HANs.

2. To investigate the effects of pH of solution and temperature on adsorption capacities and mechanism of HANs.

3. To investigate the effect of molecular structure of five-different HANs (halogen type and degree of substitution) on adsorption selectivity of adsorbent.

4. To investigate the adsorption selectivity of adsorbent on the adsorption of HANs in the presence of co-existing electrolytes in tap water, and competitive disinfection by-products (DBPs) under mixed solute solution.

5. To determine the regeneration efficiency of used adsorbents by extraction method.

1.3 HYPOTHESES

The hypotheses of this study are as follow:

1. Different surface function group and porous structure of adsorbents can affect the adsorption capacities and mechanism of HAN adsorption; such as positive surface charge of amino-functionalized HMS efficiently adsorbs HAN by interacting with negative dipole position of HAN molecule, HAN can diffuse more easily in a larger pore size of mesoporous material than microporous zeolite, and hydrophilic HANs are more favorable adsorption on hydrophilic adsorbent than hydrophobic HANs.

2. HANs can be adsorbed on the parental HMS and the functionalized HMS derivatives by hydrogen bonding and/or ion-dipole electrostatic interaction between organic functional group of adsorbents and adsorbates, and Lewis acid site of titanium substituted HMS plays more crucial role on adsorption than acidic silanol group leading to higher adsorption capacity and selectivity.

3. Adsorption capacities of HANs in aqueous phase increase by increasing the pH of solution which is higher than pH_{PZC} because a higher negative surface charge of adsorbent can enhance ion-dipole electrostatic interaction.

4. The adsorption mechanism of surfactant-modified adsorbent involves a more complex interplay between the partition process (adsolubilization) and the surface adsorption, and high hydrophobic HANs are favorable to partition into a high hydrophobic part of surfactant aggregate at the surface of adsorbent.

5. Molecular structure of HAN in term of amount halogen type and degree of substitution affects the adsorption selectivity of adsorbent, and the larger molecular weight of HAN molecule obtains more adsorption capacity and selectivity.

6. The presence of electrolytes in tap water does not affect the adsorption capacity of HANs in mixed solute solution due to low concentration of electrolytes, and the presence of co-existing DBPs affect the selective adsorption of adsorbent on HAN adsorption.

7. The used adsorbents can be regenerated by solvent extraction method and their physico-chemical characteristics of regenerated adsorbents may change due to collapse of mesopore structure.

1.4 SCOPE OF STUDY

The scope of this study is as follow and the experimental framework is shown in Figure 1.1.

1. Five different species of HANs, i.e. monochloroacetonitrile (MCAN), dichloroacetonitrile (DCAN), trichloroacetonitrile (TCAN), monobromoacetonitrile (MBAN) and dibromoacetonitrile (DBAN), were used as model of HANs to investigate the adsorption capacity and mechanism.

2. Synthesized adsorbents in this study were hexagonal mesoporous silicate (HMS) based materials which were modified surface by grafting with the three types of surface functional groups (i.e. *n*-octyldimethyl, 3-aminopropyltriethoxy, and 3-mercaptopropyltrimethoxy) and by incorporating titanium metal into mesopore framework of HMS. In addition, a large pore size of silicate material (SBA-15) was synthesized and modified surface with the polymerizable cationic gemini surfactant by adsorption to form admicelle structure.

3. The physicochemical properties of adsorbents, such as surface area, mean pore size, pore structure, surface functional group, elemental analysis (total nitrogen and sulfur content), surface charge density, hydrophilic/hydrophobic surface characteristic, were characterized using a number of physical and chemical techniques and then compared those physicochemical properties of each synthesized adsorbents.

4. The adsorption experiments of HANs on the synthesized adsorbents were investigated under the batch condition. For adsorption kinetics, the equilibrium time for HAN adsorption was performed by varying the contact time from 0 to 48 h. The pseudo-first-order, the pseudo-second-order and the intraparticle diffusion models were used to analyzed the adsorption rate and mechanisms.

5. Adsorption isotherms were performed by varying concentration of HAN solution. The experimentally derived equilibrium data were fitted with various adsorption isotherm models, i.e. Linear, Langmuir, Freundlich and Sips isotherm models, and the isotherm parameters were calculated to determine the likely adsorption mechanisms. Moreover, the adsorption experiments were performed under various temperatures (15, 25, and 40 ^{o}C), and the solution of pH values (5, 7 and 9) for studying the influence of various factors on adsorption capacity.

6. Selective adsorption of adsorbents on adsorption of five-HANs in mixed solute solution were investigated and compared with the results in single solute solution. In addition, the effect of electrolytes in tap water and in the presence of co-existing DBPs such as THMs and HAAs, trichloromethane and dichloroacetic acid were used as the model of THMs and HAAs, respectively, on adsorption of HANs were investigated the adsorption selectivity of adsorbents.

7. The used adsorbents were evaluated the efficiency of regeneration by using solvent and water extraction methods. Various kinds of solvent (methanol, ethanol, acetone, and MtBE) and various pH values of DI water were applied to extract HANs form adsorbent surface.

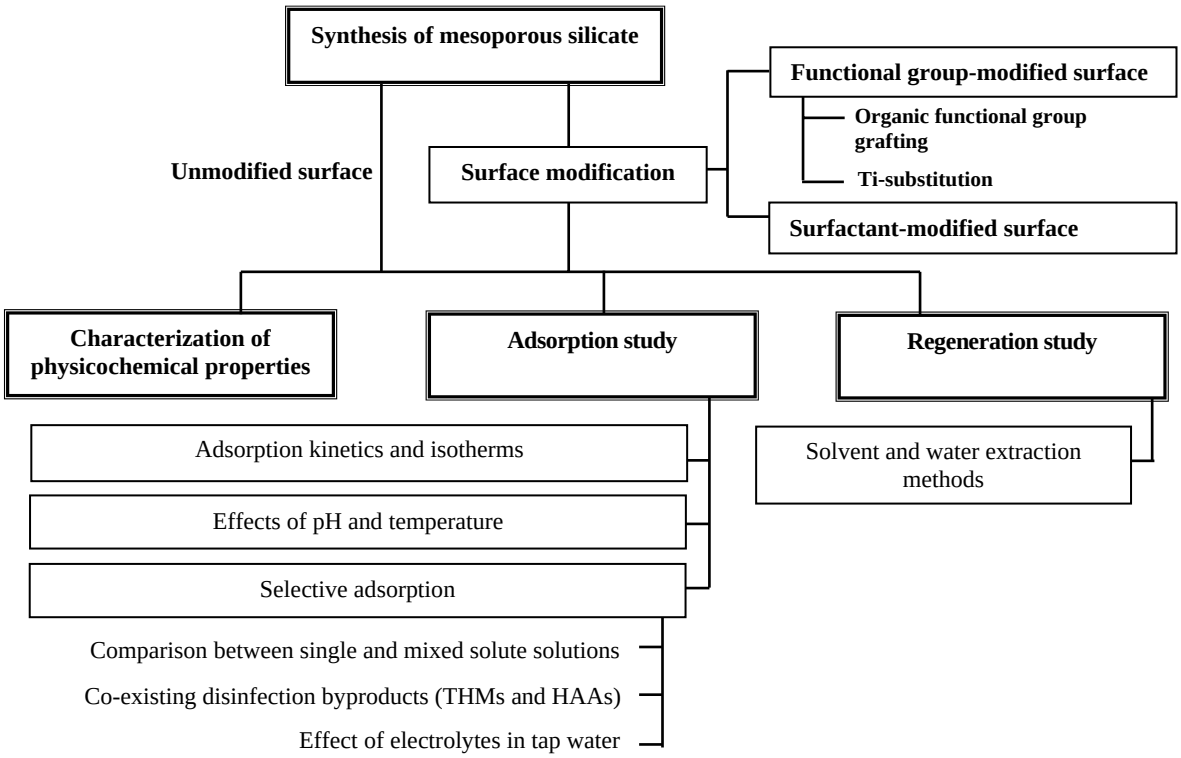

Figure 1.1 Experimental framework of this study

CHAPTER II

THEORETICAL BACKGROUND AND LITERATURE REVIEWS

2.1 DISINFECTION BY-PRODUCTS

Disinfection by-products (DBPs) are several organic and inorganic compounds that are formed by reactions between aqueous free chlorine and natural organic matter (NOM) presenting in water (Grunwald et al., 2002). The major halogenated DBPs that are commonly identified of chlorination by-products, in order of abundance, are the trihalomethanes (THMs), haloacetic acids (HAAs), haloacetonitriles (HANs), cyanohalides, and halopicrins (Krasner et al., 2006). The relative amount of DBPs as propotional of the total assimilable organic carbon (AOC) in drinking water (representative chlorination plant) is shown in Figure 2.1.

Organic matter + free chlorine ⟶ **THMs + HAAs + HANs + cyanogens halides + other DBPs**

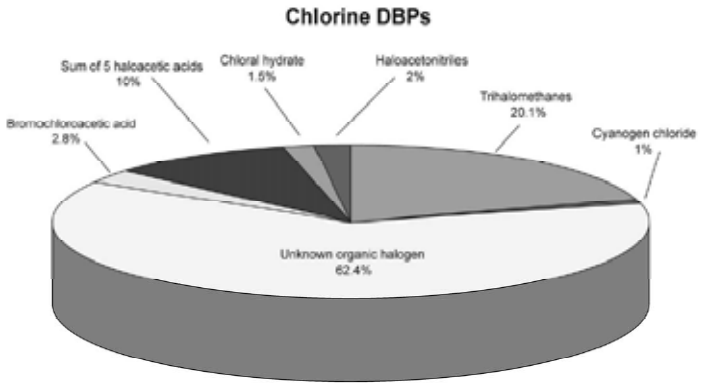

Figure 2.1 Relatives amount of DBPs in chlorinated drinking water (Richardson, 2003).

Many of these DBPs are usually present at low concentrations, but are considered to be either probable or possible carcinogens, genotoxic, and mutagenic. Exposure to low levels of DBPs over long periods of time through the use of

chlorinated water for drinking, washing, and cooking is believed to be deleterious to human health. The health effect of DBPs is summarized in Table 2.1.

Table 2.1 Disinfection byproduct and its health effects (Gopal et al., 2007).

Class of DBPs	Compounds	Health effects
Trihalomethanes (THMs)	Chloroform	Cancer, liver, kidney and reproductive effects
	Dibromochloromethane	Nervous system, liver, kidney and reproductive effects
	Bromodichloromethane	Cancer, liver, kidney and reproductive effects
	Bromoform	Cancer, liver, kidney and reproductive effects
Haloacetonitriles (HANs)	Trichloroacetonitrile	Cancer, mutagenic and clastogenic effects
Halogenated aldehydes and ketones	Formaldehyde	Mutagenic
Halophenol	2-Chlorophenol	Cancer and tumor promoter
Haloacetic acids (HAAs)	Dichloroacetic acid	Cancer and reproductive and developmental effects
	Trichloroacetic acid	Liver, kidney, spleen and developmental effects

2.2 HALOACETONITRILES (HANs)

2.2.1 Haloacetonitrile Formation in Drinking Water System

Haloacetonitriles (HANs) are nitrogenous species of disinfection by-products (DBPs) which can be formed by reaction between chlorine or chloramine or bromine disinfectants and natural organic matter (NOM) presenting in drinking water supplies. HANs are semi-volatile DBPs which are newer generation of DBPs that are emerging as concerns as brominated and iodinated compound (such as iodo-trihalomethane). They are less frequently studied as compared to the more abundant THMs and HAAs. The most abundant HANs after water chlorination are dichloroacetonitrile (DCAN) and its brominated analogs, dibromoacetonitrile (DBAN) and bromochloroacetonitrile (BCAN). In general, increasing temperature and/or decreasing pH have been associated with increasing concentrations of HANs (Siddiqui and Amy, 1993).

The level of HANs concentration reported by some researchers showed a tendency a wide variation. The di-haloacetonitriles in South Florida drinking water at concentrations up to 42 ug L^{-1}, while DCAN in a drinking water located in Canada were measured to be 10 ug L^{-1} in maximum concentration (Oliver, 1983; Trehy et al., 1986). The average concentration of di-haloacetonitriles in finished drinking/tap water has been found to be approximately 10% of the THMs (Oliver, 1983; Richardson, 2003).

2.2.2 Physico-chemical Properties

The physico-chemical properties of HANs are summarized in Table 2.2**.**

Table 2.2 The physico-chemical properties of haloacetonitrile (HANs)

HANs	**Molecular structure**	**MW (g mol^{-1})**	**BP (^oC)**	**Kow**	**Water solubility (mg mL^{-1})**
Monochloroacetonitrile (MCAN): CH_2ClCN	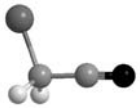	75.50	126	0.23	100
Dichloroacetonitrile (DCAN): $CHCl_2CN$	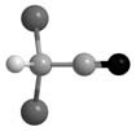	109.94	112	0.14	10-50
Trichloroacetonitrile (TCAN): CCl_3CN	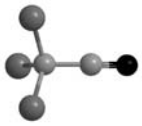	144.39	181	-	<1
Monobromoacetonitrile (MBAN): CH_2BrCN		119.95	150	-	50-100
Dibromoacetonitrile (DBAN): $CHBr_2CN$		198.85	170	0.42	50
Bromocholoroacetonitrile (BCAN): CHBrClCN		154.39	10	0.28	-

2.2.3 Environmental Fate

HANs are produced during water chlorination or chloramination from naturally occurring substances, including algae, fulvic acid and proteinaceous material (Oliver, 1983). In general, increasing temperature and/or decreasing pH have been associated with increasing concentrations of HANs (Glezer et al., 1999). Many factors between the source and the tap can influence the DBPs to which consumers are exposed. HANs form rapidly and are able to decay in the distribution system as a result of hydrolysis (Oliver, 1983). Different trends were observed in the HANs concentrations of different source waters. For instance, HAN levels formed rapidly for the first 8 h and continued to increase slowly or leveled off after 96 h. MBAN levels remained relatively stable over the 96 h, as did BCAN and DCAN levels. For the other sources, levels of HANs, consisting mostly of DCAN, increased rapidly up to 4-8 h and began to decline by the end of the 96-h period. For these sources, BCAN appeared to be slightly more stable than DCAN.

Bromide levels appear to influence, the speciation of HANs compounds generation. DCAN is the most predominant HAN species detected in drinking-water from sources with bromide levels of 20 μg L^{-1}. In chlorinated or chloraminated water from sources with higher bromide levels (50–80 μg L^{-1}), BCAN was the second most prevalent compound.

2.2.4 Toxicity

HANs have been reported to be genotoxic and potentially carcinogenic for human health (Bull et al., 1985; Daniel et al., 1986). Plewa and co-workers (Plewa et al., 2008) reported that HANs toxicity were much higher than the THMs and HAAs, even though, HAAs and THMs were more significant in regards to the mass concentration than the HANs. The comparison of cytotoxicity and genotoxicity indices between DBPs group are shown in Figure 2.2.

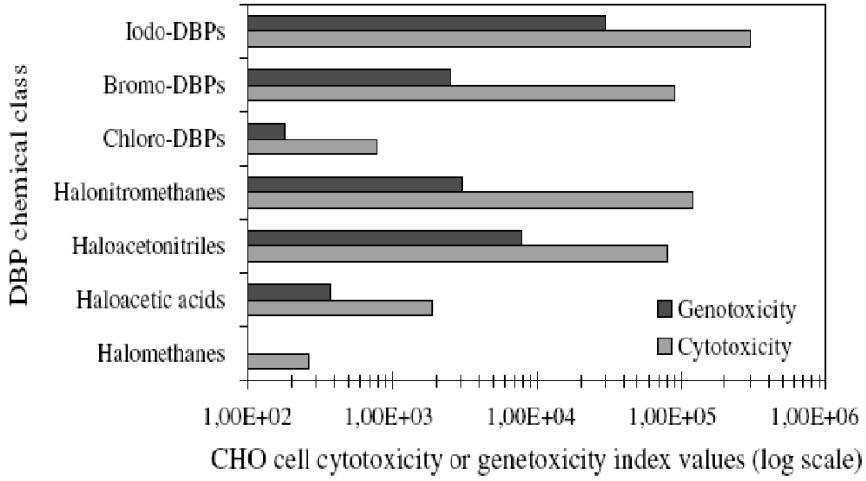

Figure 2.2 Cytotoxicity and genotoxicity indices for different classes of DBPs and for chloro-, bromo- and iodo-DBPs (adapted from Plewa et al., 2008)

2.2.5 Regulation of HANs

Nowadays, there is no regulatory of contaminant level of HANs in drinking water as THMs and HAAs, however, the World Health Organization (WHO) has suggested guideline values of DCAN, DBAN and TCAN due to their potential health effects (Table 2.3). Moreover, HANs have been included in the US Environmental Protection Agency Information Collection Rules (ICR) and they may be considered in future US EPA regulation.

Table 2.3 WHO guideline of concentration of HANs in drinking/tap water after chlorination

HANs	Year 2006 [a] ($ug\ L^{-1}$)	Year 2008 [b] ($ug\ L^{-1}$)
Dichloroacetonitrile (DCAN)	90	20
Dibromoacetonitrile (DBAN)	100	70
Trichloroacetonitrile (TCAN)	1	1

[a] Reference: (Richardson, 2003)
[b] Reference: (WHO., 2008)

2.3 DBPs REMOVAL METHODS

There are three approaches for the control of DBPs in drinking/tap water: (i) removal of precursors prior to disinfection, and (ii) use of alternative disinfectants which create fewer DBPs, and (iii) removal of DBPs after their formation. The first and second approaches can be used to control the formation of contaminant while the third approach removes the DBPs after generation by treatment methods.

2.3.1 Removal of DBPs Precursor prior to disinfection

2.3.1.1 Adsorption by Granular Activated Carbon (GAC) and Coagulation Process

One of the most effective and economical methods to control DBPs in the conventional water treatment plants is to remove precursors before they react with disinfectants. US Environmental Protection Agency (EPA) has proposed techniques including an enhanced coagulation or granular activated carbon (GAC) treatment in order to achieve the DBPs standards indicated in the regulation. Therefore, early researches have been investigated DBPs precursor removal by activated carbon adsorption. Snoeyink et al. studied the adsorption of NOM by activated carbon. The results showed that NOMs are more adsorbable than DBPs; therefore, adsorption by activated carbon is generally applied before chlorination. Uyak et al. (2007) studied DBPs precursor removal by using coagulation and PAC adsorption. They found that the enhanced coagulation by ferric chloride was preferentially large organic molecules with negatively charged NOM removal, and PAC adsorption removed mostly low molecular weight and uncharged NOM substances. This observation is also consistent with previous research. Najm et al. (Najm et al., 1991) noted that the low molecular weight of NOM was adsorbed onto the PAC, whilst the high molecular weight portion of the NOM took much longer adsorbed time onto the PAC. Some previous researches noted that neither enhanced coagulation nor activated carbon effectively removes bromide; as a result in a shift to the formation of more brominated DBPs (Jacangelo et al., 1995; Richardson, 2003).

2.3.1.2 Ozonation

DBPs precursor removal by chemical oxidation has been investigated using various oxidants. Among the oxidants, ozone has been widely used in research studies. Amy et al. (1991) studied DBPs precursor removal processes by comparing activated carbon adsorption and ozone oxidation. The study indicated that ozone degraded the humic substances into low molecular weight compound that were less reactive towards chlorine; however, ozonation appeared to transform bromide ion to hypobromous acid, leading to an increase in the percentage of brominated DBPs while activated adsorption had little effect on bromide.

2.3.1.3 Membrane Filtration

Membrane processes including microfiltration (MF), ultrafiltration (UF) and nanofiltration (NF) in drinking water treatment have been considered to be an effective means of removing turbidity, organics, microorganisms, and DBP precursors and to comply with the more stringent regulations (Visvanathan et al., 1998; Thorsen, 1999). Previous research has shown that DBP precursor reductions can be succeeded in different efficiencies by membrane filtration processes. However, there are different findings in the literature in terms of the impact of NOM characteristics and various NOM fractions on membrane fouling. Cho et al. (1998) reported that non-charged NOM fractions were important foulant materials in both types of source waters containing relatively hydrophilic and hydrophobic NOM. Furthermore, Amy and Cho (1999) stated that NOM containing a significant amount of hydrophobic fractions might play a role in fouling. The efficiency of membrane process is mainly due to the variations in the characteristics of DBP precursors and different types of membranes used in various studies.

2.3.2 Use of Alternative Disinfectants

2.3.2.1 Chloramination

In order to comply with DBPs regulation, another alternative method by changing the type of disinfectant from chlorine to chloramines has drawn

much attention to use in water supply system due to reduced DBP formation. Its ability provides residuals in water distribution systems as chlorination. Monochloramine is known to only form trace amounts of THMs and HAAs, but also lead to an increase in other DBPs such as HANs and iodo-THMs (*i*-THMs) (Bichsel and von Gunten, 2000). Lee et al. (2007) investigated the formation of upon adding free chlorine and monochloramine. The results showed that chloramine formed 10 times lower concentration of THMs (especially chloroform) but 5 times higher of dichloroacetonitrile (DCAN) as compared with free chlorine addition.

2.3.3 DBPs Removal after Formation

2.3.3.1 Adsorption by Activated Carbon

For DBPs removal after formation, the intensive research work has been done by using activated carbon as the adsorbent. Tung et al. (2006) studied the physical adsorption characteristics of HAAs onto GAC. They found that GAC had a much lower adsorption capacity for HAAs especially trichloroacetic acid (TCAA) than for THMs, and this may be attributable to biodegradation. This result of HAAs biodegradation was in accordance with the reports in the relevant literature. Xie and Zhou (2002) and Ratasuk et al. (2008) reported that biological activated carbon (BAC) is more efficient for HAAs removal.

2.3.3.2 Membrane Filtration

As the limitations of conventional water treatment processes to meet increasingly stringent drinking water regulations become more apparent, membrane processes are gaining support within the water treatment industry as a better means of addressing existing and anticipated regulatory requirements in the world wide. Several researches have focused on nanofiltration (NF) that appears to be promising for controlling DBP in drinking water (Visvanathan et al., 1998; Ates et al., 2009). In addition, solute properties of dipole moment and hydrophobic also affect the separation efficiency by adsorbing or interacting with membrane surfaces (Visvanathan et al., 1998; Kimura et al., 2003).

The advantages and drawbacks of each DBPs removal method are summarized in Table 2.4

Table 2.4 Summary of the advantages and drawbacks of each DBPs removal method

Methods	Advantages	Drawbacks
• Removal of DBPs precursors (adsorption, coagulation)	Reduce DBPs formation Low cost	Low efficiency (low NOM adsorption capacity due to the short contact time)
• Change of disinfection process (ozone, membrane filtration)	Good efficiency	High cost and generate other DBPs such as carboxylic acids.
• Removal of DBPs after formation (AC adsorption)	Low cost	Inefficient removal for hydrophilic DBPs
• Use of alternative disinfectants (chloroamines)	Stable in distribution system Reduce THMs and HAAs (10 times lower concentration) (Lee et al., 2007)	Increase HANs formation (5 times higher concentration) (Lee et al., 2007)

Reference: Kim and Kang, (2008)

2.4 POROUS MATERIALS

Porous materials are used technically as adsorbents, catalysts and catalyst supports owing to their high surface areas. According to the IUPAC definition (Lu and Zhao, 2004), porous materials are divided into three classes: microporous (<2 nm), mesoporous (2–50 nm) and macroporous (>50 nm). Well-known members of the microporous class are the zeolites, which provide excellent catalytic properties by their crystalline aluminosilicate network. However, their applications are limited due to small pore openings; therefore, porous materials with larger pores preferably in the mesoporous range would be interested (Ciesla and Schuth, 1999).

2.5 MESOPOROUS SILICATES

Mesoporous silicates are subset of porous material which were first described in 1992 as a result of the self-assembly of a structure directing agent and the silica source. The most important characteristics of the mesoporous silicas are the large surface area, high mesopore volume, and narrow pore size distribution in the range of mesopores (Zhao et al., 2005; Rockmann and Kalies, 2007; Anbia and Lashgari, 2009; Asouhidou et al., 2009a; Qin et al., 2009); therefore, they have attracted much attention from the industry as catalysts or catalyst supports in the pharmaceutical and fine chemical industries, in adsorption and separation process and in other areas of heterogeneous catalysis applications processing macromolecules.

2.5.1 Synthesis Method of Mesoporous Silicates

There are three kinds of relevant materials of mesoporous silicate obtained by using different synthetic procedures. Based on the template used for synthesis and the interaction of inorganic species and organic surfactant molecule, the mesoporous silicate can be grouped as follow:

2.5.1.1 Ionic Surfactant and Ionic Inorganic Precursor

The first route is the so-called M41S family of silica and aluminosilicates introduced by the Mobil group. The preparation of M41S materials is based on charge matching between ionic surfactants and ionic inorganic reagents. The original preparation of the materials involves direct co-condensation of a cationic surfactant (S^+) and anionic species (I^-) to produce assembled ion pairs (S^+I^-). In addition, depending on the synthesis conditions and principally the surfactant/SiO_2 ratio, different phases could be obtained, like the hexagonal phase MCM-41, the cubic one MCM-48 as well as the lamellar compound MCM-50.

The schematic representation of the mesoporous silicate MCM-41 is shown in Figure 2.3. Formation mechanism is that surfactant micelle aggregate into a hexagonal array of rods, followed by interaction of silicate or aluminates anions present in the reaction mixture with the surfactant cationic head groups. Thereafter condensation of the silicate species occurs, leading to the formation of an inorganic

polymeric species. After combusting of the surfactant template by calcinations, hexagonally arranged inorganic hollow cylinders are obtained.

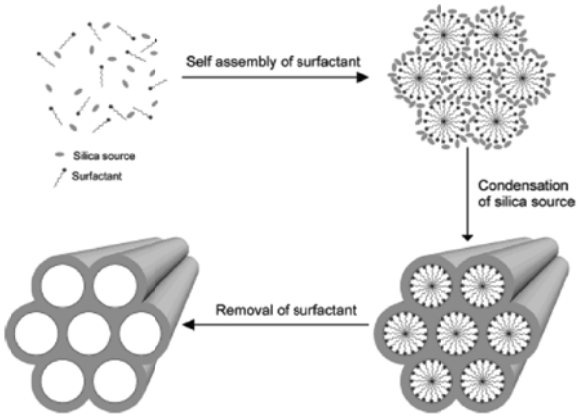

Figure 2.3 Schematic representative of the synthesis of MCM-41

In 1994, Stucky and coworker extended this mechanism including the charge reversal situation i.e., an anionic template (S^-) was used to direct the self-assembly of cationic inorganic species (I^+) through S^-I^+ ion pairs. The next mechanisms involved counterion (X^- or M^+) mediated assemblies of surfactants and inorganic species of similar charge, These counterion-mediated mechanisms produces assembled solution species of the type $S^+ X^- I^+$ (where $X^- = Cl^-$ or Br^-) or $S^- M^+ I^-$ (where $M^+ = Na^+$ or K^+), respectively. The ionic surfactant or template is recovered by ion exchange in cation donor solutions.

2.5.1.2 Neutral Surfactant and Inorganic Precursor

The second route of mesoporous silicate was introduced by Tanev and coworker by using two neutral routes based on hydrogen bonding and self assembly between neutral primary amine micelles (S^0) and neutral or inorganic precursors (I^o) (Tanev and Pinnavaia, 1996). This mechanism produces neutral S^oI^o templating route. Mesoporous siliocate's produced by this technique are hexagonal mesoporous silica (HMS and MSU). These materials are less ordered than mesoporous silicate's produced with ionic surfactants. One of the most important advantages of HMS compared with MCM-41 is that the organic phase can be totally removed from as-synthesized samples by solvent extraction.

2.5.1.3 Using Ampliphilic Di- and Tri-block Copolymer

A new synthesis route involving amphiphilic di- and tri-block copolymers as the organic structure directing agents was introduced by Stucky and co-workers (Zhao et al., 1998). Poly(ethylene oxide) monoethers were used to form materials showing worm-like disordered or hexagonally ordered mesopores with pore sizes of ca. 5nm. One of the most useful groups of surfactants are the triblock co-polymers consisting of poly(ethylene oxide)x‑poly- (propylene oxide)y‑poly(ethylene oxide)x, (PEO)x(PPO)y- (PEO)x, (trade name: Pluronics) which show the ability to form liquid‑crystal structures. A 2D hexagonal mesoporous material formed via this pathway (denoted as SBA-15, Santa Barbara Acid No.15) exhibits a thick wall of 3‑7nm thickness and large pore sizes adjustable between 6 and about 15nm. The thick wall of this material significantly improves the thermal and hydrothermal stability compared to mesoporous MCM-41 and related silicates.

Interactions between the inorganic species and the head group of the surfactant with consideration of the possible synthetic pathway in acidic, basic, or neutral media are depicted in Figure 2.4 (Hoffmann et al., 2006). Depending on the synthesis conditions and the silica source or the type of surfactant used, many other mesoporous silicate materials (HMS, MSU, KIT, SBA) can be synthesized with properties different as reflected in Table 2.5 (Linssen et al., 2003; Taguchi and SchÜth, 2005).

Table 2.5 Possible pathways for the synthesis of mesoporous silicates

Template condition	**Interaction**		**Synthesis condition**	**Mesoporous materials**
Ionic surfactant	*Strong* (*electrostatic*) *interactions*			
	- Direct interaction	S^+I^-	Basic	MCM-41, MCM-48, MCM-50
		S^-I^+	Neutral-basic	
	- Anion mediated interaction	S+X-I+ or	Acidic	SBA-1, SBA-2, SBA-3
		S+X+I-	Basic	
Nonionic surfactant	*Weak interactions*			
	- Hydrogen boning interaction	S^0I^0	Acidic	HMS
Co-polymer	- Hydrogen boning interaction	N^0I^0	Acidic	SBA-15

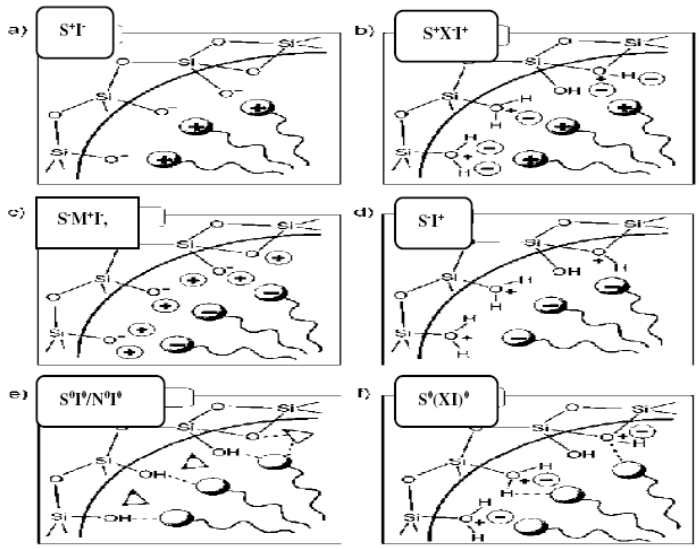

Figure 2.4 Interactions between the inorganic species and the head group of the surfactant with consideration of the possible synthesis pathway in acidic, basic, or neutral media. Electrostatic: S^+I^-, $S^+X^-I^+$, $S^-M^+I^-$, S^-I^+; through hydrogen bonds: S^0I^0/N^0I^0, $S^0(XI)^0$ (Hoffmann et al., 2006).

2.6 HEXAGONAL MESOPOROUS SILICATE

2.6.1 Synthesis of Hexagonal Mesoporous Silicate

Hexagonal mesoporous silicate (HMS) is a kind of mesoporous silicates produced by the neutral synthesis pathway (S^0I^0) which was firstly proposed by Tanev and Pinnavaia (1996). HMS was synthesized in the presence of neutral inorganic precursors and uncharged surfactants (i.e. primary amines). The schematic of synthesis pathway is shown in Figure 2.5. The pore systems of the latter silicas have been shown to have rather worm-like structures than long-range ordered hexagonal arrays which are characteristic for MCM-41. If these nonionic surfactants are used instead of ionic ones, hydrogen bonding is the driving force for the formation of mesophases. Therefore, the surfactant can be recovered by extraction, which is advantageous both from an economical and an ecological point of view. More than 90% of the template molecules can be recovered by a simple extraction with ethanol.

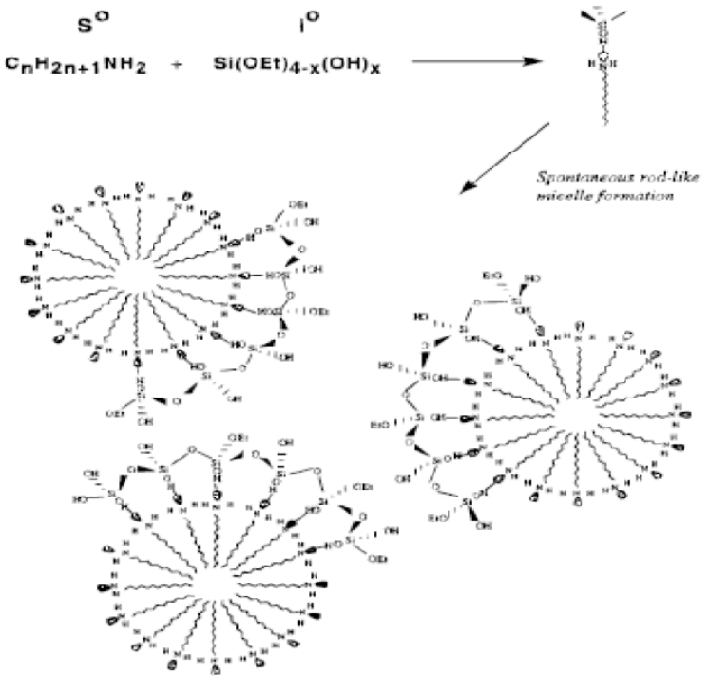

Figure 2.5 Schematic representation of the S^0I^0 template mechanism of formation of HMS mesoporous molecular sieves (Tanev and Pinnavaia, 1996)

2.6.2 Surface and Structure modifications

The application of mesoporous silicate itself is restricted because of the limitations in the active sites. Hence, in order to utilize the unique properties of the mesoporous material for specific applications, such as catalysis and adsorption, reactive functional groups by the incorporation of organic functional group or metal substitution remains the key issues. The advantages of the functionalization of these solids can provide the tuning of the surface properties (such as hydrophilicity/ hydrophobicity), thermal and structural stability. In addition, the organic functional group or metal element can be modified for various specific applications.

2.6.2.1 Organic Grafting Modification

To enhance specific characteristic of mesoporous silicates, their surface can be modified with organosilanes generally through 2 approaches which are post synthesis and direct co-condensation methods.

(a) Post Synthesis Method

The preparation method refers to attachment part of functional group to terminal hydroxyl groups or silanol groups (Si-OH) (Figure 2.6). In this process, the silanol groups of the silica walls react with the organosilane molecules precursors of the organic chain to form a layer of covalently coupled surface functional groups (Chong et al., 2004). Typically, this method is accomplished by one of the following procedures:

$$\equiv \text{Si-OH} + \text{Cl-SiR}_3 \xrightarrow{25\ ^{o}\text{C}} \equiv \text{Si-OSiR}_3 + \text{HCl} \qquad (2.1)$$

$$\equiv \text{Si-OH} + \text{R´O-SiR}_3 \xrightarrow{100\ ^{o}\text{C}} \equiv \text{Si-OSiR}_3 + \text{HOR´} \qquad (2.2)$$

$$2\equiv \text{Si-OH} + \text{HN(SiR}_3)_2 \xrightarrow{25\ ^{o}\text{C}} 2\equiv \text{Si-OSiR}_3 + \text{NH}_3 \qquad (2.3)$$

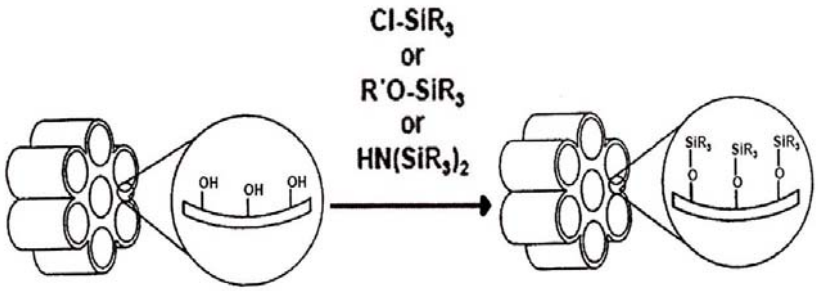

Figure 2.6 Functionalization of inner walls of mesoporous silicates by post synthesis method (Tanev and Pinnavaia, 1996)

The most apparent advantage is good preservation of the mesostructure after post-modification, but decrease of pore volume diameter. This method is suitable for organic and inorganic, which do not include every kind of functional group due to limitation of access to silanol group, and also the heterogeneity of surface functional group.

(a) Co-condensation Method

The direct co-condensation method allows preparation of organic-functionalized materials in a limited time. Typically, this method involves the one-step co-condensation between silica sources with one or more organosilanes through a sol-gel process in presence of a surfactant. The advantages of this method are the stability of the inorganic framework even at higher organic loadings,

homogenous distribution of the organic groups in the pore channels as well as the single step preparation procedures. However, the structural ordering was highly dependent on the relative amount of organic precursor used and the organosilane precursor must be chosen carefully to avoid phase separations and Si–C bond cleavages during the synthesis and the afterward surfactant removal process. The schematic of the direct co-condensation method is shown in Figure 2.7.

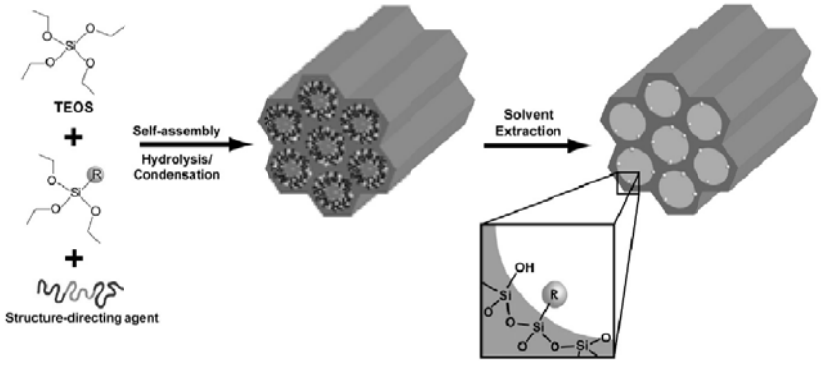

Figure 2.7 Co-condensation approach to the functionalization of mesoporous silicates by direct co-condensation and incorporation of the functional moiety (R) species during synthesis (Athens et al., 2009)

The comparison between post synthesis and co-condensation methods is summarized in Table 2.6.

Table 2.6 Summary of advantage and drawback of two organic functionalized modification methods

Post synthesis method	**Co-condensation method**
Advantage: • Good preservation of the mesostructure after post-modification	**Advantage:** • Higher and more uniform surface coverage of functionality • Capable control in surface properties.
Drawback: • Reduce pore size and pore volumn • limited loading level of the functional groups can be grafted because of the limited density of the reactive surface silanols • Time consuming • Ineffective due to partial cross-linking of the functional groups with the silica-surface silanol groups • Obtain low density and non uniformity of functionality	**Drawback:** • Loss in original structure ordering such as aminopropyltriethoxysilane (APTES) functionalization**.**

2.6.2.2 Structure Modification by Metal Substitution

Mesoporous silicates are beneficial in the field of catalysis, due to the relatively large pores and the very high surface area, which allows a high concentration of active sites per mass of material. Therefore, mesoporous silicate can be modified with various heteroatoms by incorporation them into the pore channels of mesoporous supports. The degree of metal incorporation as well as coordination of metal sites in the mesopore structure is dependent on the nature of metal precursor used. When trivalent cations like Al^{3+}, B^{3+}, Ga^{3+}, and Fe^{3+} substitute in the walls of the mesoporous silicates, the framework possesses negative charges that can be compensated by protons and solids can be used in acidic reactions. When other cations like Ti^{4+}, V^{4+}, Sn^{4+}, and Zr^{4+} are introduced, the electroneutrality is maintained and the corresponding mesoporous materials are used rather in specific reactions like in redox catalysis.

(a) Titanium-containing Mesoporous Silicate

Titanium-containing mesoporous silicates (such as Ti-MCM-41, Ti-HMS and Ti-SBA-15) are well-known oxidation catalysts for the selective oxidation of bulky organic substrates in the presence of aqueous oxidants. These mesoporous titanosilicate materials have pore diameters of 30–60 A ° and exhibit exhibit oxidative properties for a series of bulky reactants under mild reaction conditions. Among them, Ti-HMS, prepared by a neutral templating pathway (Tanev et al., 1994), offers certain advantages over the electrostatically template MCM-41 material due to different in textural properties, and has been reported to be more active in the catalytic activities such as hydrodesulfurization of dibenzothiophene (DBT) (Zepeda et al., 2005) and epoxidation of cyclohexane and 2,6-di-*tert*-butyl phenol (2,6-DTBP) (Jang et al., 2005).

Moreover, titanium-containing mesoporous silicate has been proved to be an adsorbent to remove the contaminants in aqueous solution for adsorption process. For instance, Messina and Schulz (2006) modified silica mesoporous materials by TiO_2 for adsorption of reactive dyes. The presence of TiO_2 enhanced the adsorption capacities of reactive dyes due to possible degradation of the

dye molecule in contact with the TiO_2 particles in the adsorbent interior. Punyapalakul and Takizawa (2004) studied adsorption mechanism of alkylphenon polyethoxylate compound on HMS and modified HMSs (Ti-HMS, OD-HMS and MP-HMS) compared with PAC. The results showed that hydrophilic adsorbents (HMS and Ti-HMS) had higher adsorption capacities of APnEOs than hydrophobic adsorbents (PAC, OD-HMS and MP-HMS) because hydrophilic surface caused by silanol groups enhanced aggregation adsorption on the external surface.

(b) Aluminum-containing Mesoporous Silicate

The incorporation of trivalent cations, like aluminum, in mesoporous silicate material is performed in order to create the adsorption sites for adsorption field. It has been reported that the density of Brönsted acid sites of Al-MCM-41 is superior to that of pristine MCM-41(Nowinska et al., 2003). The inserted Al in the pore wall of mesoporous silicate through direct co-condensation method forming Brönsted acid sites to promote adsorption of volatile nitrosamines because the proton of Brönsted acid sites interact with the nitroso group of nitrosamines to promote the adsorption (Shi et al., 2005). The promotional effect has been studied as the Al-content increased, the direct synthesized sample had the declined porous structure and at the same time the accessibility of the new-formed Brönsted acid sites decreased (Gu et al., 2009).

2.7 CHARACTERIZATION OF HEXAGONAL MESOPOROUS SILICATE

2.7.1 Porous Structure Confirmation by X-Ray Powder Diffraction (XRD)

X-ray diffraction (XRD) has become the method of choice for structure analysis of crystalline materials. The method is based on the scattering of X-rays by the electrons of atoms. XRD gives the distance of regions with highest electron density, which is the distance from one crystal plane to the next. This distance is called the *d*-spacing. The geometry of the corresponding diffraction events can be described by Bragg's law (Equation 2.4), which combines a measure of the distance (*d*) between lattice planes, the wavelength (λ) of the X-ray radiation and the diffraction angle (θ):

$$2d \sin \theta = \lambda \qquad (2.4)$$

The scattering occurs at each of the atom layers of the crystal, resulting in characteristic sets of sharp lines. Since each crystalline structure is unique, the angles of constructive interference form a unique pattern. By comparing the positions and intensities of the diffraction peaks against a library of known crystalline materials, samples of unknown composition can be identified. The example of X-ray diffractograms of mesoporous thin films is shown in Figure 2.8.

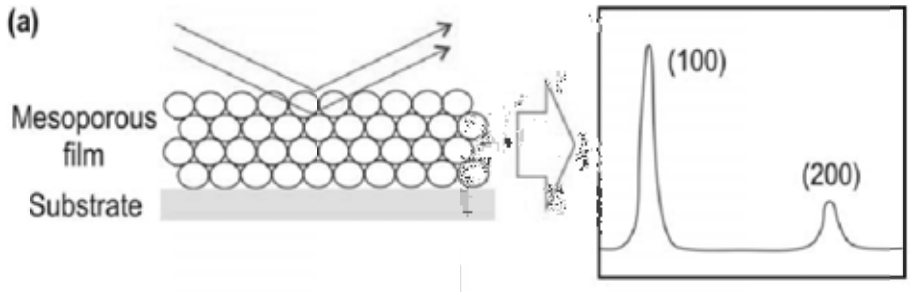

Figure 2.8 The incident X-rays are scattered on the planes of pores and collected under the same angle (θ–θ geometry), resulting in characteristic diffractograms

2.7.2 Determination of Surface Area and Pore Diameter of Mesoporous Silicate by Nitrogen Adsorption isotherms

The correct characterization of the textural properties of nanoporous materials is very helpful to verify the success of the synthesis process. N2 adsorption desorption isotherm is primary method to determined pore diameter, pore volume and surface area. The relationship of the amount of gas adsorbed onto a particle at a given gas-phase pressure results in an isotherm which, when analyzed, will provide the physical characteristics of the porous materials. Six different types of isotherms have been recognized by the International Union of Pure and Applied Chemistry (IUPAC) (Figure 2.9).

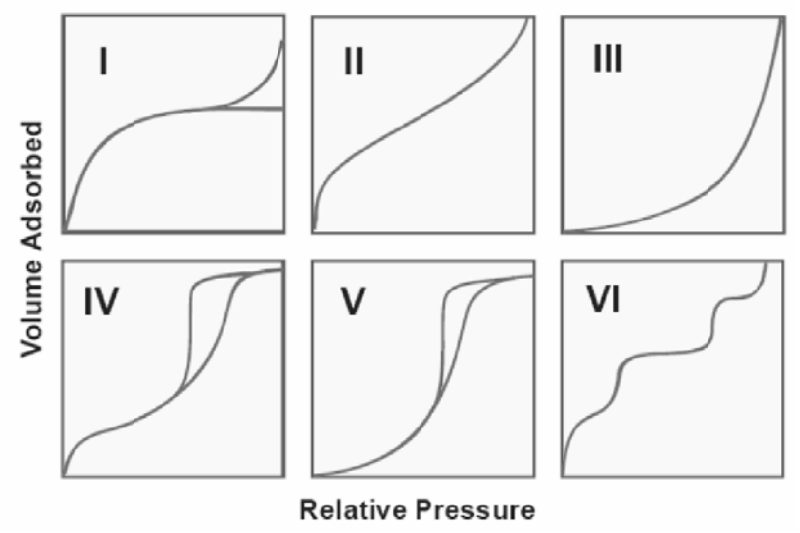

Figure 2.9 Type of isotherm shapes classified by IUPAC

The adsorption isotherms for mesoporous materials are type IV according to IUPAC classification, with capillary condensation at medium relative pressure being indicative of mesoporosity. In some cases the desorption branch is different to the adsorption path, the isotherm then exhibiting a hysteresis loop. The shape of the hysteresis loop provides information about the shape and the size of the mesopores.

The surface area is usually calculated by application of the BET equation to the N_2 adsorption isotherm. The model calculates the volume of the monolayer of adsorbed molecules on the surface and the surface area is directly obtained by application of the following equation:

$$\frac{p}{v(p_0-p)} = \frac{1}{cv_m} + \frac{c-1}{cv_m}\frac{p}{p_0} \qquad (2.5)$$

where v is volume of N_2 adsorbed by the sample under pressure p; P_0 is saturated vapor pressure at the same temperature; v_m is volume of N_2 adsorbed when the surface is covered with a unimolecular layer; and c is constant for a given adsorbate

The specific surface areas of samples were calculated from the adsorption data by Equation 2.6:

$$S = \frac{N_0 V_m A}{22414\, m} \qquad (2.6)$$

where S is specific surface area; N_0 is Avogadro number; m is amount of solid adsorbent; and A is cross-section of the gas molecules (16.2 $A°^2$ for N_2).

The pore diameter and pore size distribution in the mesopore range can be obtained using the BJH (Barret–Joyner–Halenda) method. The method is based on the Kelvin equation, predicting the formation of liquid N_2, at the capillary condensation step, in the larger pores of the material. The equation expresses the relation between the condensation of N_2 in the mesopores of a certain size. The Kelvin equation can be expressed as Equation 2.7:

$$\ln \frac{p_0}{p} = \frac{2\gamma V_L}{rRT} \qquad (2.7)$$

where p_0 is the saturated vapor pressure, p equilibrium pressure, V_L is the molar volume of the liquid and γ is the surface tension.

2.7.3 Fourier Transform Infrared (FT-IR) Spectroscopy

Fourier transform infrared spectroscopy (FT-IR) is an economic and multidisciplinary analytical tool, which yields information concerning the structural details of a siliceous inorganic material. In addition, it can be used to confirm surface characteristics and isomorphous substitution by other elements in the material. Analysis by FT-IR is based on the fact that molecules have specific frequencies of internal vibrations. These frequencies occur in the infrared region of the electromagnetic spectrum. When a sample is placed in a beam of infrared radiation, the sample will absorb radiation at frequencies corresponding to molecular vibrational frequencies, and this is being measured in the infrared spectrometer.

The mid-infrared region of the spectrum (4000 to 400 cm^{-1}) is the most interesting part of the spectrum when dealing with siliceous materials as it contains the fundamental framework vibrations of the $Si(Al)O_4$ groupings. Table 2.7 shows the frequencies of various functional groups that contained in silicate surface investigation.

Table 2.7 Infrared adsorption frequencies of various surface functional groups

Functional groups	Wavenumber (cm^{-1})	References
O-H stretching, free hydroxyl	3,750	(Punyapalakul et al., 2009)
H-O-H	3,430	(Asouhidou et al., 2009a)
N-H stretching	3,300-3,400	(Li et al., 2008; Asouhidou et al., 2009a)
C-H stretching	2,850-2,920	(Asouhidou et al., 2009a)
S-H stretching	2,560	(Liang et al., 2009)
O-H bending	1,620-1,650	(Li et al., 2008; Liang et al., 2009)
N-H bending	1523	(Asouhidou et al., 2009a)
C-H bending	1,450	(Liang et al., 2009)
Si-O stretching	1,080	(Liang et al., 2009; Punyapalakul et al., 2009)
Si-O-Ti	964	(Punyapalakul and Takizawa, 2006)
Si-O stretching	800	(Liang et al., 2009)
O-Si-O	470	(Liang et al., 2009; Punyapalakul et al., 2009)

2.7.4 Scanning Electron Microscopy (SEM)

Scanning electron microscopy characterization is used primarily for the study of surface topography and morphology of solid materials on a scale down to about 10 nm. Topographical features, void content, particle agglomeration as well as compositional and structural differences within the material can be revealed. The technique works on the principle that an electron beam is passing through an evacuated column and focused by electromagnetic lenses onto the material. The beam is scanned over the specimen surface in synchronism with the beam of a cathode ray tube (CRT) display screen. Inelastically scattered secondary electrons are emitted from the sample surface and collected by a scintillator, the signal from which is used to modulate the brightness of the cathode ray tube. In this way the secondary electron emission from the sample is used to form an image on the CRT display screen.

Materials can only be studied properly when they are electrically conducting, as the electrons otherwise give rise to charging phenomena resulting in blurred images. Non-conducting materials (amongst which silica-based materials) need to be sputtered with a thin layer of conducting material before being inserted into the SEM, and connected to a conducting sample holder. In general, Au is used for sputtering in a plasma sputter-coater.

2.7.5 Elemental Analysis by Inductively Coupled Plasma-Atomic Emission Spectroscopy (ICP-AES)

Inductively coupled plasma-atomic emission spectroscopy (ICP-AES), is an analytical technique used to determine concentrations of a wide range of elements in solution. ICP-AES is a fast multi-element technique with a dynamic linear range and moderate-low detection limits (0.2–100 ppb). ICP-AES makes use of the fact that the atoms of elements can take up energy from inductively coupled plasma, are thereby excited, and fall back into their ground state again emitting electromagnetic radiation at wavelengths characteristic of a particular element. The identification of this radiation permits the qualitative analysis of a sample. Digestion methods such as microwave, high-pressure, fusion, and acid digestion can be employed for the liquid sample preparation of solid sample material. High number of measurable elements– elements that are difficult to analyze in atomic absorption spectrometry such as Zr, Ta, rare earth, P and B can be easily analyzed.

2.7.6 Surface Charge Density

The principle of electroneutrality must hold true for every point on all titration curves, i.e., the sum of all negative charges is equal to the sum of all positive charges (Al-Ghouti et al., 2003).

$$\Sigma \text{ negative charges} = \Sigma \text{ positive charges} \qquad (2.8)$$

For example, their titration of an oxide surface with HCl or NaOH in the presence of NaCl electrolyte solution would result in:

$$[OH^-] + [Cl^-] + [\text{negative surface}] = [H^+] + [Na^+] + [\text{positive surface}] \quad (2.9)$$

or

$$\sigma_0 = [\text{positive surface}] - [\text{negative surface}]$$

$$= [C_A - C_B] - [H^+ - OH^-] \quad (2.10)$$

where σ_0 = surface charge

[negative surface] = the concentration of negative charges

[positive surface] = the concentration of positive charges

$[H^+] = 10^{-pH}$

$[OH^-] = 10^{pH-pKw}$

$[Cl^-] = [NaCl]_{added} + [HCl]_{added}$

$[Na^+] = [Nacl]_{added} + [NaOH]_{added}$ and

$[C_A - C_B] = [Cl^-] - [Na^+]$

$= [HCl]_{added} - [NaOH]_{added}$

When the surface charge is neutral, the negative and positive charges are equal, and the surface become to have zero charge. At the pH of point of zero charge (pH_{PZC}), equation (2.10) simplified to:

$$[C_A - C_B] = [H^+ - OH^-] \quad (2.11)$$

Hydroxyl groups present on the surface of silicate materials can gain or lose a proton, resulting in a surface charge that varies with changing pH. At low pH, surface sites are protonated and the surface becomes positively charged:

$$pH < pH_{PZC} : \quad Si\text{-}OH + H^+ \longrightarrow Si\text{-}OH^{2+} \quad (2.12)$$

While at high pH, the surface hydroxides lose their protons, and the surface becomes anionic.

$$pH > pH_{PZC} : \quad Si\text{-}OH + OH^- \longrightarrow Si\text{-}O^- + H_2O \quad (2.11)$$

pH_{PZC} values of silicate materials were reported by several researchers depending of types of silicate materials.

2.8 SURFACTANT-MODIFIED ADSORBENT

2.8.1 Surfactant Phenomena

Surfactants have an amphipathic molecular structure which consists of hydrophilic head group and hydrophobic tail group. The hydrophilic head group is attracted to polar environments, such as water, while the hydrophobic tail comprised a long chain hydrocarbon is attracted to nonpolar environments, (e.g. oil). Consequently, the surfactants can dissolve either in water or oil and have the capability to solubilize water or oil to create homogeneous system. Surfactants are classified into 4 types based on the charge of their hydrophilic head group which are anionic, cationic, nonionic and zwitterionic (Rosen, 2004).

At low surfactants concentration, surfactants monomers will act independently in the solution phase and accumulate at the surface of the system. As surfactants concentration increase to a certain level, these monomers will form into aggregates called *micelles*. The concentration where the first micelle is formed is called the critical micelle concentration (CMC). When a solid phase is added to the surfactant solution, surfactant will adsorb at the solid-liquid interface. At low surfactant concentrations, the surfactant begins to adsorb and form micelle-like structure called *hemimicelles or admicelles*, depending on whether the aggregates are monolayer or bilayer. Once the CMC is reached, additional surfactant does not increase the amount of adsorbed surfactant, but rather increase the concentration of micelles in aqueous solution (West and Harwell, 1992).

2.8.2 Surfactant Adsorption on Solid Surface

Surfactant adsorption is a complex process that transfers the surfactant molecules from bulk solution phase to the surface/ interface. This process can occur by various mechanisms which are ion exchange, ion pairing, acid-base interaction, hydrophobic bonding, adsorption by polarization of π electrons and adsorption by dispersion force (Paria and Khilar, 2004). In addition, this process is characterized by an adsorption isotherm, as S-shaped isotherm, which is usually divided into 4 regions as shown in Figure 2.10.

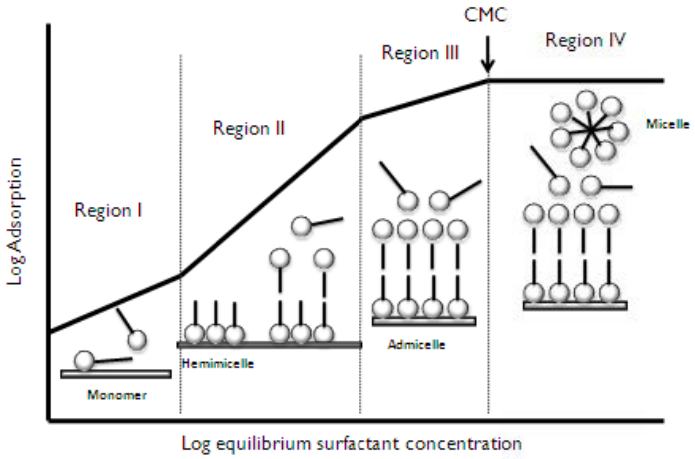

Figure 2.10 Schematic diagram of adsorption isotherm of a surfactant onto a solid surface (Charoensaeng et al., 2008)

Region I or Henry's Law region occurs at very low surfactant concentration. In this region, the surfactant adsorbs in a linear manner mainly by ion exchange. Adsorbed surfactants in this region are proportional to surfactant concentration and adsorb without forming any surfactant aggregates.

Region II is characterized by a sharp change in the isotherm slope between region I and region II. This marked increase in adsorption resulting from interaction of hydrophobic chains of oncoming surfactant ions with those of previously adsorbed surfactant. This aggregation of the hydrophobic groups which occurs at concentrations well below the critical micelle concentration (CMC) of the surfactant is known as hemimicelle or admicelle, depending on whether the aggregates are monolayer or bilayer.

Region III is indicated by the decreasing of isotherm slope since adsorption now must overcome electrostatic repulsion between the oncoming ions and the similarly charged solid and the beginning of admicelle formation on lower energy surface patches.

Region IV is the plateau adsorption region. In this region, the critical micelle concentration (CMC) is reached and the first micelle is formed. The

adsorption in this region is constant with increasing surfactant concentration because of the maximum bilayer coverage of ionic surfactant adsorbed onto oppositely charged surfaces or the completed adsorption on hydrophobic surfaces.

2.8.3 Adsolubilization of Organic Solute

The admicelle provides three main regions for adsolubilization (Dickson and O'Haver, 2002), i.e. surfactant headgroup, palisade and core regions, and where a solute partition is dependent upon the physicochemical compatibility between each region and the adsolubilized solute as shown in Figure 2.11. The headgroup, palisade and core regions typically accommodate the partition of solutes possessing high, medium and low polarity, respectively. At very high solute concentration, some hydrophobic solutes may demonstrate phase separation in admicelles as also seen in micelles.

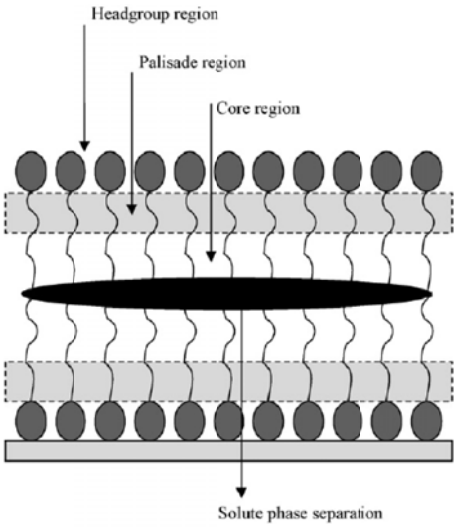

Figure 2.11 Schematic model of an extensive admicelle bilayer with solute phase separation. Polar solutes are expected to primarily partition within the palisade and headgroup regions, while less polar solutes would primarily partition in the core. The solute phase separation may exist for some highly hydrophobic solutes at high solute concentration (Saphanuchart et al., 2007)

2.8.4 Polymerizable Gemini Surfactant

Polymerizable gemini surfactants (PG) have been investigated as a novel surfactant for a number of application. This surfactant contains two cationic monomeric parts linked with an ethylene spacer at the level of the quaternary ammonium groups, and polymerizable methacryloxy groups covalently attached to the terminal of the hydrocarbon tail chains (Abe et al., 2009). The tighter packing of the hydrophilic group of gemini surfactants results in a more cohesive and stable interfacial film (Asnachinda et al., 2009). The molecular structure of PG surfactant is shown in Figure 2.12.

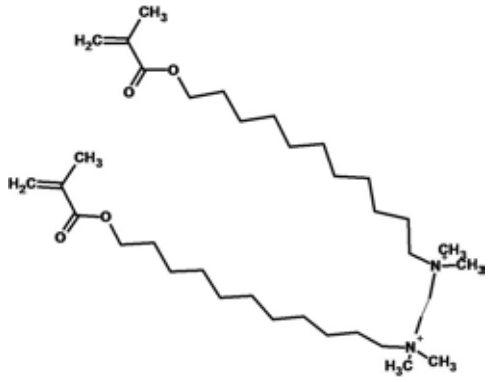

Figure 2.12 Molecular structure of polymerizable cationic gemini surfactant (PG)

2.8.5 Polymerization of Surfactant

Polymerizable surfactants are molecules having hydrophilic and hydrophobic regions together with a polymerizable group such as a double bond in their structure. Polymerizable surfactants have a characteristic property of forming micelles in water in the same manner as conventional surfactants. Some polymerizable surfactants can spontaneously polymerize at 35-80 ^{o}C without initiator when the surfactants form micelles. In contrast, some vinyl monomers, such as styrene, polymerize spontaneously on heating above 100 ^{o}C. The mechanism of polymerization has two steps. In the first step, aggregates of surfactant molecules are formed on the solid substrates as admicelles (or hemimicelles). These surfactant aggregates can achieve bilayer coverage of the entire surface. In the second step, polymerization on the solid surface is initiated by chemical, thermal, or

photochemical processes such as UV irradiation (Esumi et al., 1991). Schematic of the polymerization process is illustrated in Figure 2.13. The admicelle polymerization has been used as a novel technique in a number of surface modification such as poly(methyl methacrylate) on polyester fiber (Siriviriyanun et al., 2007); poly(methyl methacrylate) on silica (Luna-Xavier et al., 2002); and polystyrene on cotton (Pongprayoon et al., 2002).

Recently, polymerizable surfactants have received increasing interest in water and soil remediation. Previous reports noted that admicelle polymerizable surfactant can enhance the stability of surfactant on solid surface; therefore, reduce surfactant desorption from the solid surface (Asnachinda et al., 2009; Attaphong et al., 2010) without reducing the adsolubilization potential.

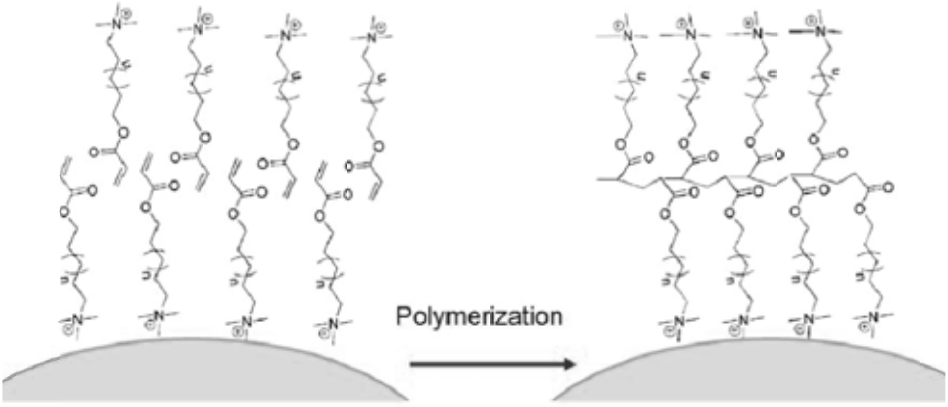

Figure 2.13 Demonstrating the bilayer of polymerizable surfactant on the solid surface and subsequent polymerization on the surface (Alkilany and Murphy, 2009)

2.9 ZEOLITES

Zeolites are microporous crystalline solids with well-defined structures. Generally, they contain silicon, aluminum and oxygen in their framework. The basic unit of a zeolite structure is the TO_4 tetrahedron, where T is normally a silicon or aluminum atom/ion (or phosphorous in an aluminophosphate). The general formula of the aluminosilicate zeolites is $M_{x/n}\,[(AlO_2)_x\,(SiO_2)_y].mH_2O$. The zeolite framework is composed of $[(AlO_2)_x\,(SiO_2)_y]$ and M is a non-framework, exchangeable cation. The

great variety of zeolites is made possible by the different arrangements of linked TO_4 tetrahedral within secondary building units (SBUs), which are linked themselves together in numerous three-dimensional networks. The two simplest SBUs are rings of four and six tetrahedral and others comprise larger single and double ring up to 16 T atoms. The unit cell always contains an integral number of SBUs.

Zeolite Y is the faujasite-type zeolite (Figure 2.14). It crystallizes with cubic symmetry. The general composition of the unit cell of faujasite is (Na, Ca, $Mg)_{29}[Al_{58}Si_{134}O_{384}].240H_2O$. The faujasite structure is formed by quite wide supercages accessed through 12-membered silicate ring with 0.74 nm diameter. Because of their unique porous properties, zeolites are used in a variety of applications. Major uses are in petrochemical cracking, ion exchange (water softening and purification), separation and adsorption. For adsorption process, Al^{3+} replaces Si^{4+} in crystalline aluminosilicate structure brings the formation bridging hydroxyl group, so-called BrÖnsted acid site. The proton of BrÖnsted acid site inside the channel can introduce an electrostatic interaction towards negatively charged adsorbates. Furthermore, zeolites have narrow diameter of pore (smaller than 0.8 nm) which provides a geometric confinement for small molecule adsorbate (Gu et al., 2009).

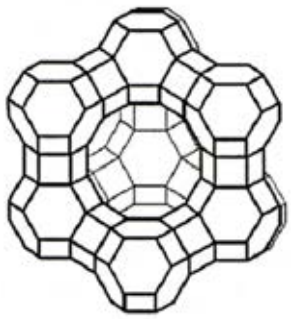

Figure 2.14 Structure of faujasite-type zeolite

2.10 ADSORPTION THEORY

2.10.1 Adsorption mechanism

Adsorption is the inter-phase accumulation of one or more components in an interfacial layer (i.e. between two bulk phases) (Rouquerol et al., 1999). This

process can occur at an interface of any two phases by the imbalance of concentration between two phases as the driving force. Generally, for a solid–liquid adsorption process, three steps are involved in the adsorption process as following:

(i) Film diffusion, which involves the movement of adsorbate molecules from the bulk of the solution towards the external surface of the adsorbent.

(ii) Particle diffusion, where the adsorbate molecules move in the interior of the adsorbent particles.

(iii) Adsorption of the adsorbate molecules onto active sites interior of adsorbent particle.

2.10.2 Diffusion Controlled Process

It is important to predict the rate-controlling step in an adsorption process to understand the mechanism of the sorption. According to the three mass transfer steps for solid-liquid adsorption process; (i) film or external diffusion, (ii) pore diffusion and (iii) adsorption onto active sites (Liu et al., 2010). The third step being very rapid for adsorption of organic compounds on porous adsorbent, does not represent the rate-controlling step, so result this step can be negligible. The slowest step determines the rate-controlling parameter in the adsorption process. However, the rate-controlling parameter might be distributed between particle and film diffusion mechanisms. *If external transport > internal transport*, rate is governed by particle diffusion. *If external transport < internal transport*, rate is governed by film diffusion. So it is important to distinguish between film diffusion and particle diffusion.

An intraparticle diffusion model developed by Weber and Morris (Weber and Morris, 1963) is used to investigate whether the adsorption process was limited by mass transfer within the film layer or by diffusion inside the adsorbent particles. The model can be defined as shown in Equation 2.12:

$$q_t = k_{iP} t^{0.5} + C \qquad (2.12)$$

where k_{iP} is the intraparticle diffusion rate constant (mg $g^{-1}h^{-0.5}$) and C (mg g^{-1}) is a constant that gives the idea about the thickness of the boundary layer.

2.10.3 Adsorption Interaction

Adsorption is a surface phenomenon that is defined as the increase in concentration of adsorbate at the surface or interface between two phases such as liquid-liquid, gas-liquid, gas-solid, or solid-liquid interfaces. For solid-liquid interface, the imbalance between the two environments amounts is a driving force for adsorption process. Two kinds of surface phenomenon of adsorption are involved i.e. physical adsorption and chemisorptions.

The physical adsorption involves only relative weak intermolecule forces which can be identified as follows:

(a) *Electrostratic interaction*: is a type of adsorptive interaction that involves the attractive forces of charged adsorbate onto oppositely charged sites of adsorbent.

(b) Hydrogen bonding: is a strong dipole-dipole interaction between hydrogen atoms with strongly electronegative atom such as oxygen, nitrogen or fluorine. (O, F, or N)

(c) *Hydrophobic bonding*: is an attraction between a hydrophobic group of adsorbed molecule and the hydrophobic surface adsorbent presented in the solution.

(d) *Van der Waals force*: are the attractive or repulsive forces between molecules (or between parts of the same molecules) with one another molecule. The adsorption by van der Waals force between adsorbate and adsorbent increases with the increasing molecular weight of the adsorbate.

The chemisorption involves essentially the formation of a chemical bond between the adsorbate molecules and the surface of adsorbent. The chemisorption involves the sharing or transfer of electrons. Furthermore,

chemisorptions is site specific while the adsorbed molecules by physical adsorption are free to cover the entire surface.

Many factors influence the mechanism of adsorption on porous materials. First, there are the adsorbate properties of group functionality, branching or geometry, polarity, hydrophobicity, dipole moment, molecular weight and size and aqueous solubility. Second, there are solution conditions such as pH, temperature, adsorbate concentration, ionic strength and competitive solutes. Third, there is the nature of the adsorbent with its surface area, pore size and distribution of functional groups.

2.10.4 Adsorption Kinetic

The main purpose of the kinetic study is to identify the adsorption rate which gives important information for designing and modeling the process. Adsorption kinetic mechanisms can be based on diffusion mass transfer processes or chemical reaction kinetics. There are many mathematical models are reported in literature, all attempting to describe quantitatively in the kinetic study during the adsorption process. Among these models, the pseudo-first order model and pseudo-second order model equations are the commonly used to represent the adsorption behavior.

2.10.4.1 Pseudo-first-order Model

Pseudo-first order model is one of the most widely used procedures for the adsorption of a solute from aqueous solution. The rate constant of pseudo-first-order adsorption is determined from the Lagergren equation, can be expressed as Equation (2.13):

$$\frac{dq_t}{dt} = k_1(q_e - q_t) \qquad (2.13)$$

where q_e and qt (mg/g) are the amount of adsorbed contaminant at equilibrium and at time (h), respectively, and k_1 is the first-order rate constant for adsorption (h^{-1}).

Integrating Equation 2.13 with the boundary conditions of t = 0 to $t = t$, and q_t = 0 to $q_t = q_t$ to yield the linear form equation as shown in Equation (2.14):

$$\log(q_e - q_{t)} = \log q_e - \frac{k_1 t}{2.303} \qquad (2.14)$$

A straight line of log (q_e - q_t) versus t suggests the applicability of the kinetic model. Values of q_e and k_1 are determined from the intercept and slope of plot, respectively.

And the non-linear form equation of this model is given as Equation (2.15), and k_1 value is obtained from the plot of q_t versus t.

$$q_t = q_e(1 - exp^{(-k_1 t)}) \qquad (2.15)$$

2.10.4.1 Pseudo-second-order Model

Pseudo-second-order equation is based on a chemisorption. The pseudo-second-order equation can be expressed as Equation (2.16):

$$\frac{dq_t}{dt} = k_2(q_e - q_t)^2 \qquad (2.16)$$

Here k_2 (g mg^{-1} h^{-1}) is the rate constant of pseudo-second-order adsorption. Separating the variables in Equation (2.16) gives:

$$\frac{dq_t}{(q_e - q_t)^2} = k_2 dt \qquad (2.17)$$

Integrating and applying boundary conditions of t = 0 to $t = t$, and q_t = 0 to $q_t = q_t$ to yield the non-linear form equation of the pseudo-second-order model as shown in Equation (2.18):

$$q_t = \frac{q_e^2 k_2 t}{1 + q_e k_2 t} \qquad (2.18)$$

Equation (2.18) can be rearranged to obtain as Equation (2.19), and the linear form of this model can be expressed as Equation (2.20). Values of k_2 and q_e are calculated from the intercept and slope of the plot of t/qt versus t.

$$q_t = \frac{1}{\frac{1}{k_2 q_e^2} + \frac{t}{q_t}} \quad (2.19)$$

$$\frac{t}{q_t} = \frac{1}{k_2 q_e^2} + \frac{t}{q_e} \quad (2.20)$$

2.10.5 Error Function

In order to confirm the best model for the adsorption process, the applicability of the kinetic model is further validated by the error function. A normalized standard deviation $\triangle q$ (%) is employed to find out the most suitable kinetic model in fitting to the data. This error function has been used previously by the number of researchers in the adsorption study (Gűnay et al., 2007; Qin et al., 2009; Shaarani and Hameed, 2011), is given as shown in Equation (2.21):

$$\Delta q(\%) = 100\, x \sqrt{\frac{\sum\left[\frac{q_{exp} - q_{cal}}{q_{exp}}\right]^2}{N-1}} \quad (2.21)$$

where N is the number of data points, and q_{exp} and q_{cal} (mg g^{-1}) are the experimental and the calculated adsorption capacities, respectively. The best-fit models should have the least $\triangle q$ (%) values.

2.10.6 Adsorption Isotherm

Theoretically, the relationship between the amount of a substance adsorbed per unit mass of adsorbent at constant temperature and its concentration in the equilibrium solution of the solid-liquid interface determines the adsorption isotherm (Foo and Hameed, 2010). For adsorption isotherms, the equilibrium adsorption capacity (q_e) and the final equilibrium concentration of the residual solute remaining in the solution (C_e) are plotted to study their relationship. The adsorption capacity (q_e) can be calculated as Equation (2.22):

$$q_e = \frac{V(C_0 - C_e)}{M} \quad (2.22)$$

where q_e is the adsorption capacity (mg g^{-1}), C_0 and C_e are the initial and equilibrium concentration (mg L^{-1}), respectively. V is the volume of the solution (L) and M is the mass of adsorbent (g).

The adsorption isotherm relationship can also be mathematically expressed by many models. The Langmuir and Freundlich models are the simplest and most commonly used isotherms. Moreover, a compromise between Langmuir and Freundlich systems is an interesting trend in the isotherm modeling.

2.10.5.1 Langmuir Model

The Langmuir sorption isotherm (Langmuir, 1916) has been successfully applied to many contaminant adsorption processes and has been the most widely used to describe the adsorption of a solute in aqueous solution. A basic assumption of the Langmuir theory is that adsorption takes place at specific homogeneous sites on the surface of the adsorbent. It is then assumed that once a adsorbate molecule occupies a site, no further adsorption can take place at that site. The Langmuir model can be written as Equation (2.23):

$$q_e = \frac{q_m K_L C_e}{1 + K_L C_e} \qquad (2.23)$$

Equation (2.23) can be rewritten in the linear form equation as follows:

$$\frac{C_e}{q_e} = \frac{C_e}{q_m} + \frac{1}{q_m K_L} \qquad (2.24)$$

where q_m (mg g^{-1}) is the maximum amount of the adsorbate per unit mass of the adsorbent to form a complete monolayer on the surface, and K_L is Langmuir constant related to the affinity of the binding sites.

2.10.5.2 Freundlich Model

Freundlich model is an empirical equation to describe the adsorption process based on the assumption that the adsorbent had a heterogeneous surface composed of different classes of adsorption sites, with adsorption on each class of sites following the Langmuir isotherm. The Freundlich

model demonstrates that the ratio of the amount of solute adsorbed onto a given mass of an adsorbent to the concentration of the solute in the solution was not constant at different solution concentrations. This isotherm does not predict any saturation of the sorbent by the sorbate; thus infinite surface coverage is predicted mathematically, indicating multilayer adsorption of the surface. It can be written as equation (2.25):

$$q_e = K_F {C_e}^{1/n} \qquad (2.25)$$

where K_F (L g^{-1}) is a constant related to the extent of adsorption, and *n* is a constant releated to the intensity of adsorption or the degree of dependence of adsorption on concentration. This equation can be represented in linear form as shown in Equation (2.26):

$$\ln(q_e) = \ln(K_F) + \frac{1}{n}\ln(C_e) \qquad (2.26)$$

The value of K_F and *n* depend on temperature, the nature of the adsorbent, and the adsorbate property to be adsorbed.

2.10.5.3 Sips Model

Sips model is widely used as a compromise between Langmuir and Freundlich systems, which incorporate three parameters into an empirical equation. At low adsorbate concentrations, it reduces to Freundlich isotherm; while at high concentrations, it predicts a monolayer adsorption capacity characteristic of the Langmuir isotherm. The equation parameters are governed mainly by the operating conditions such as the alteration of pH, temperature and concentration. Hence, Sips model can be applied either in homogeneous or heterogeneous systems (Gimbert et al., 2008). This isotherm is expressed as equation (2.27):

$$q_e = \frac{q_m K_S C_e^{1/n}}{1 + K_S C_e^{1/n}} \qquad (2.27)$$

where K_S is the Sips adsorption constant.

2.10.5.4 Linear Model

Linear model (Samuel and Osman, 1987) is the simplest isotherm in which the amount adsorbed varies directly with the equilibrium concentration of adsobate. It is often called Henry's Law after the analogous isotherm for the solution of gases in liquid. The Linear isotherm can be written as shown in Equation (2.28):

$$q_e = K_p C_e \qquad (2.28)$$

where K_p is linear constant that obtained from the slope of plotted q_e *versus* C_e.

This isotherm is obtained under condition of low concentration of adsorbate. In such system, the adsorbed layer is extremely dilute and the amount of adsorbed molecule is only a fraction of the monolayer capacity. Usually, the linear relationship is observed at the low concentration levels of a total adsorption isotherm. Hence, the application of Henry's Law equation should be restrict to that region of the isotherm obtained from experiment.

2.10.7 Influence of Various Parameters on Adsorption Mechanism

2.10.7.1 Effect of pH

The pH of solution not only influences the properties of the sorbent surface, but also affects the adsorbate speciation in solution. Therefore, it is an important parameter affecting adsorption behaviors in many cases of the ionic adsorption, in which the influence of pH has directly relation with the surface charge of adsorbents. Such pH value that gives zero surface charge is called the point of zero charge (pH_{PZC}). At this pH cationic surface groups and anionic surface groups, posses equal amount of electric charge.

Moreover, the surface of adsorbents can gain or lose protons, which vary the surface charge with changing pH. At low pH, most of the surface sites are protonated and the surface becomes positively charged, while at high pH, the surface sites lose protons, and the surface become anionic. Thus, the electrostatic

attraction between adsorbents and adsorbates usually plays a crucial role on adsorption process.

2.10.7.2 Effect of Ionic Strength

The influence of ionic strength is significantly affected ion adsorption by the electrostatic attraction. Since a lower IS value usually weakens the electrostatic interaction and consequently decreases the adsorption capacity (Bjelopavlic et al., 1999). However, some literature reported that the adsorption of adsorbate did not change significantly at low IS value. For instance, Yu et al. (2008) reported that the adsorption of perfluorooctane sulfonate (PFOS) on chitosan-based polymer adsorbent did not change with increasing of NaCl concentrations from 0 to 50 mM (Yu et al., 2008). Su et al. (2011) reported that the adsorption capacity of As(III) on surfactant-modified bentonite was not significantly affected when the IS increased from 0 to 500 mM (Su et al., 2011).

2.10.7.3 Effect of Temperature

Temperature is an important parameter for the adsorption process. Several studies in literature found that the temperature influence the adsorption capacity. For instance, the adsorption of dye on the mesoporous carbon increased with increasing temperature (Asouhidou et al., 2009b). Because the increase in temperature increased the rate of diffusion of the adsorbate molecules across the external boundary layer and in the internal pores of adsorbent particle, owing to decrease on viscosity of the solution (Wang and Zhu, 2007). However, the adsorption of some substituted phenol derivatives on activated carbon fiber (Liu et al., 2010), and cationic dyes on mesoporous SBA-15 (Huang et al., 2011) exhibited the reverse results.

The adsorption parameters obtained from isotherm study can be used for described the adsorption mechanism by using a thermodynamic basis. The thermodynamic of the surface was originally formulated by Gibbs in 1878, and subsequent studies were directed mostly to gas-liquid, gas-solid, and solid-liquid interfaces. The concept of thermodynamic assumes that in an isolated system where energy cannot be gained or lost, the entropy change is the driving force (Kumar and

Kumaran, 2005). The thermodynamic parameters that must be considered to determine the adsorption process are changes in entropy (ΔS) and heat of adsorption (enthalpy, ΔH) and free energy (ΔG) due to transfer of unit mole of adsorbate from solution onto the solid-liquid interface (Tan et al., 2009). The ΔG, ΔS, and ΔH can be calculated according to the following equation:

$$\Delta G = -RT\ lnK \qquad (2.29)$$

$$\ln K = -\frac{\Delta H}{RT} + \frac{\Delta S}{R} \qquad (2.30)$$

where ΔG is the free energy change (kJ mol^{-1}) and K corresponds to K_L in the Langmuir equation. ΔH is the change in enthalpy (kJ mol^{-1}); ΔS is the entropy change (kJ mol^{-1} K^{-1}), R is universal gas constant (8.314 J mol^{-1} K^{-1}), and T is the absolute temperature (^oK). The value of ΔH and ΔS can be calculated, respectively form the slope and the intercept of the van't Hoff plot of ln$K$ versus 1/T.

2.11 LITERATURE REVIEWS

2.11.1 Adsorption of DBPs by Porous Materials

Various processes, such as adsorption (Tung et al., 2006; Babi et al., 2007; Kim and Kang, 2008; Ratasuk et al., 2008), ozonation (Ratasuk et al., 2008) and membrane filtration (Uyak et al., 2008), have been employed to remove the disinfection by-products (DBPs) from the aqueous phase. According to the advantage and drawback of each process as mentioned earlier, adsorption technology has been favored for DBP removal due to its advantages of low cost and simplicity. Intensive research has been done on the adsorptive removal of DBPs using porous materials (Babi et al., 2007; Kim and Kang, 2008). Therefore, early researches have been investigated DBPs removal by activated carbon adsorption. Tung et al. (2006) studied the physical adsorption characteristics of HAAs onto GAC. They found that GAC had a much lower adsorption capacity for HAAs especially trichloroacetic acid (TCAA) than for THMs, and this may be attributable to biodegradation. This result of HAAs biodegradation was in accordance with the reports in the relevant literature. Xie and

Zhou (2002) and Ratasuk et al. (2008) reported that biological activated carbon (BAC) is more efficient for HAAs removal.

Form the literature reviews as mention above, adsorption process by activated carbon is found to be the most suitable and significant for DBPs removal because of its availability and high efficiency for the removal of a number of DBPs, especially the hydrophobic molecules, however, the surface characteristics are not suitable for the adsorption of hydrophilic compounds (Tung et al., 2006; Babi et al., 2007). In addition, the use of activated carbon is sometimes problematic due to its low adsorption-selective nature and difficulty in its regeneration. Therefore, the development of alternative adsorbents with specific surface characteristics and high adsorption selectivity is of importance to improve the removal efficiency, particularly when treating water pollutants with a small molecular size, high molecular polarity and high solubility but found at low concentrations in water.

Among the porous materials, mesoporous silicates offer a number of potential advantages as adsorbents due to their high surface area, large pore volume and narrow pore size distribution. Moreover, their surface modification, via the reaction of silanol groups with various organosilanes, is very helpful in improving the adsorptive capacity and selectivity as a result of specific interactions between the surface functional groups and adsorbate molecules. A limited amount of work on the adsorption of DBPs over synthetic micoporous and mesoporous materials has been reported previously. Hexagonal mesoporous silicates (HMSs) with a pure silica framework and different functionalized surfaces were shown to be effective adsorbents for the removal of dichloroacetic acid (DCAA), with the amino-functionalized HMS showing excellent adsorption properties of DCAA at the ppm concentration (Punyapalakul and Takizawa, 2004). In addition, they also found that a combination of mercapto- and amino- functional groups caused a higher surface complexity, produced more active surface sites, gave a higher DCAA adsorption capacity than amino-functionalized HMS. These results indicated that the effect of surface functional group obviously play crucial role in adsorption.

As to adsorption on porous materials, the adsorption phenomena may be significantly different as a consequence of their porous structure (Zhang et al.,

2006). Recently, Punyapalakul and coworkers found that the crystalline structure and surface area of adsorbents also affected the adsorption of DCAA at low concentration (Punyapalakul et al., 2009). Furthermore, some studies reported that micropore size, relative pore volume, and surface characteristic were important factors for the adsorption of *N*-nitrosodimethylamine (NDMA) which is nitrogenous –DBPs (Dai et al., 2009). Until now, the study of the effect of porous structure on adsorption is limited and needs further investigation.

To the best of our knowledge, the adsorption of HANs by mesoporous silicate in aqueous solution has not been studied. Evidence from literature, it is possible that HANs are able to be adsorbed by mesoporous materials. The adsorption of nitrile compounds on adsorbent is mainly associated with the surface characteristics of the adsorbent and the nature of adsorption sites. For instance, the removal of acetonitrile from gaseous stream by adsorption on various inorganic solids was found, using Fourier transformed infra-red spectroscopy (FT-IR) based analysis, to be mediated by hydrogen bonding between acetonitrile and the silanol groups of the silica aerogel, and titanium oxide (TiO_2) exhibited both physisorption and chemisorptions of bases on surface silanol groups and acid sites, respectively (Busca et al., 2008). Similarly, modification of TiO_2-modified activated carbons resulted in enhanced nitrogenous-DBPs, namely N-nitrosodimethylamine (NDMA), due to the increased number of surface adsorption sites (Dai et al., 2009). Furthermore, the acetonitrile was adsorbed on microporous material such as Na-faujasite (NaY) by the interaction of a nitrile group with a cation and/or a hydroxyl site (silanol group) through a nitrogen atom (Kozyra et al., 2006).

2.11.2 Removal of Contaminants from Aqueous Solution by Surfactant Modified Adsorbent

The adsorbents can be modified by surfactant to form bilayer micelle structures, called “admicelle”, on their surface having the potential to solubilize organic molecules (Adak et al., 2005). In several research studies, various adsorbents, such as metal oxides (Asnachinda et al., 2009; Attaphong et al., 2010), titanium dioxide (Esumi, 2001), zeolites (Jin et al., 2008; Chutia et al., 2009; Zhan et al.,

2011), bentonites (Rawajfih and Nsour, 2006; Alkaram et al., 2009; Su et al., 2011), montmorillonites (Wang and Wang, 2008) and etc., have been used to modify surface by anionic/cationic surfactant adsorption. Surfactant adsorption and adsolubilization behavior are important in various application such as chemical separation (Nayyar et al., 1994), surface modification (Esumi et al., 1991), drug delivery and soil remediation.

In recent two decades, surfactant-modified adsorbents have drawn much attention in separation process and have proved in the removal efficiency for various organic/inorganic compounds. For instance, Adak et al. (2005) modified surface of natural alumina by adsorption with sodium dodecyl sulfate (SDS); denoted as SMA, and studied the removal of cationic dye (crystal violet: CV) in aqueous solution. The results showed that SMA was found to be good efficient adsorbent, and 99% efficiency could be achieved at a high concentration level. The pH value affected to the removal efficiency but not affected by temperature. At pH greater than pH_{zpc}, SDS molecules were desorbed from alumina surface and caused less removal. Valsaraj et al. (1998) also modified activated ϒ-alumina surface by adsorption of SDS and was used to remove a phenanthrene in aqueous solution. They found that the adsorption of phenanthrene was directly related to the concentration of surfactant adsorbed, and the partitioning of phenanthrene normalized to the adsorbed surfactant concentration was independent of pH. Moreover, the surfactant modified adsorbents were investigated the effect of surfactant modifcation on the removal of various contaminants from aqueous solution such as phenol and derivatives (Rawajfih and Nsour, 2006; Alkaram et al., 2009; Damjanovic et al., 2010), dyes (Jin et al., 2008; Wang and Wang, 2008; Oei et al., 2009), heavy metals (Choi et al., 2009; Chutia et al., 2009; Nadeem et al., 2009; Su et al., 2011), and etc. However, the adsorption of surfactant molecules on these adsorbents is limited due to small pore size and low specific surface area resulted in the amount of surfactant coverage on surface was low and limited to sites of external surface only.

A major problem in using surfactant-modified adsorbents is the loss of surfactant molecules during application due to desorption when changes in system pH. Therefore, to reduce the amount of surfactant desorbed from the surface,

polymerization of the admicelle has been proposed to create a fixed surfactant film (Esumi et al., 1991; Esumi et al., 1993). Asnachinda et al. (2009) investigated the surfactant desorption by comparing the efficiency of polymerized and non-polymerized surfactants using gemini cationic surfactant, monomeric cationic surfactant and conventional cationic surfactants. The results demonstrate that the increased stability of the polymerized surfactant-modified surface can reduce the desorption of surfactant from the silica surface. Further, Attaphong et al. (2010) studied the styrene and ethycyclohexane adsolubilization of polymerizable anionic surfactants on aluminum oxide. They also found that admicelles polymerization reduces surfactant desorption from alumina surface without reducing the adsolubilization potential.

The comparison of organic contaminants removal efficiency between surfactant-modified zeolite and mesoporous silicate has been investigated by Ghiaci et al. (2004). They studied the removal of chromate from aqueous solution using hexadecyltrimethylammonium (HDTMA) bromide and *n*-cetylpyridinium bromide (CPB) modified natural clinoptilolite and zeolites, compared with uncalcined mesoporous MCM-41. The results showed that the maximum chromate adsorption by uncalcined MCM-41 was much greater than that of the natural clinoptilolite and surfactant-modified zeolites which might be related to high surfactant aggregates on the inner surfaces of this mesoporous material.

From the literature reviews, removal of haloacetonitriles (HANs) which are new generation of DBPs by adsorption onto mesoporous material has not yet been studied. The finding of surfactant-modified mesoporous material which was found to be good efficient adsorbent has interested in. Therefore, the mesoporous silicate adsorbents were synthesized and modified surface with organic functional group and polymerizable surfactant to investigate the possibility of these adsorbents for haloacetonitrile removal in aqueous solution.

CHAPTER III

RESEARCH METHODOLOGY

3.1 MATERIALS

3.1.1 Chemical Reagents

-	Acetone	HPLC	LAB SCAN
-	Ammonium fluoride	>98%	CARLO ERBA
-	Cyclohexane	>98%	CARLO ERBA
-	Dichloroacetic acid	>99%	ACROSS ORGANICS
-	Dipotassium hydrogenphosphate	>97%	Ajax Finechem
-	Dodecylamine	98%	ACROSS ORGANICS
-	Ethyl alcohol absolute	RPE-ACS	CARLO ERBA
-	Hydrochloric acid	37%	CARLO ERBA
-	Methanol	HPLC	Fisher Scientific
-	Methyl-tert butyl ether	HPLC	LAB SCAN
-	Poly(ethylene oxide)-poly(propylene oxide)-poly(ethylene oxide) triblock copolymer: Pluronic 123		BASF Corporation
-	Potassium dihydrogenphosphate	>97%	VOLCHEM
-	Potassium persulfate	>97%	Ajax Finechem
-	Potassium nitrate	>97%	Ajax Finechem
-	Sodium hydroxide	99%	MERCK
-	Sodium bromide	>99%	Sigma-Aldrich
-	Sodium chloride	>99.5%	BDH Chemicals
-	Sodium sulfate	>98.5%	Scharlau
-	Sulfuric acid	96%	CARLO ERBA
-	Sodium bicarbonate	>98%	CARLO ERBA

- Tetraethoxysilane 98% Fluka
- Trichloromethane 99.8% LAB SCAN
- 3-aminopropyltriethoxysilane >98% Fluka
- 3-mercaptopropyltrimethoxysilane >98% Fluka
- *N*-dimethyloctylchlorosilane >98% Fluka
- 2,3-dibromopropionic acid >98% Fluka
- 2,2'-azobis(2-methylpropionamidine) dihydrochloride 95% WAKO Japan

3.1.2 Haloacetonitriles (HANs)

Monochloroacetonitrile (MCAN), dichloroacetonitrile (DCAN), trichloacetonitrile (TCAN), monobromoacetonitrile (MBAN), and dibromoacetonitrile (DBAN) were products of Wako Pure Chemical Industries (Japan). The physicochemical properties and molecular structure of five-HANs were shown in Table 3.1.

Table 3.1 The physicochemical properties and molecular structure of five-HANs

HANs	Molecular structure	MW ($g\ mol^{-1}$)	Water solubility ($mg\ mL^{-1}$)
Monochloroacetonitrile (MCAN): CH_2ClCN	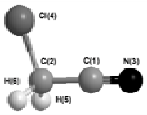	75.50	100
Dichloroacetonitrile (DCAN): $CHCl_2CN$	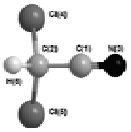	109.94	10-50
Trichloroacetonitrile (TCAN): CCl_3CN	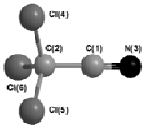	144.39	<1
Monobromoacetonitrile (MBAN): CH_2BrCN	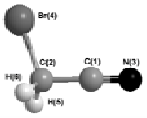	119.95	50-100
Dibromoacetonitrile (DBAN): $CHBr_2CN$	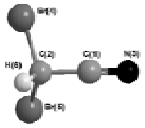	198.85	50

3.1.3 Polymerizable Cationic Gemini Surfactant

Polymerizable cationic gemini surfactant (PG) was kindly supplied by Faculty of Science and Technology, and the Institute of Colloid and Interface Science, Tokyo University of Science. The physicochemical properties and molecular structure of PG were shown in Table 3.2.

Table 3.2 Properties of polymerizable cationic gemini surfactant

Surfactant	Type	MW	Active (%)	Molecular structure
Polymerizable cationic gemini surfactant	Cationic	690.8	97	$CH_2=C(CH_3)COO(CH_2)_{11}N^+(CH_3)_2$ | CH_2 $2Br^-$ | CH_2 | $CH_2=C(CH_3)COO(CH_2)_{11}N^+(CH_3)_2$

Reference: Abe et al. (2006) and Asnachinda et al. (2009)

3.2 PREPATION OF ADSORBENTS

3.2.1 Hexagonal Mesoporous Silicate (HMS) Synthesis

Synthesis of HMS followed the procedure described by Lee et al. (2001). Typically, 1 mol of tetraethoxysilane (TEOS) was dissolved in a clear solution of dodecylamine (DDA) (0.25 mol), water (50 mol) and ethanol (12.5 mol), giving a DDA: TEOS: H_2O: ethanol molar composition of 1:4:200:50. The resulting mixture was vigorously stirred at room temperature for 18 h. The white solid product was filtered and dried in air for 24 h. Subsequently, the solid was calcined in a muffle furnace at 650 ^oC for 4 h with a heating rate of 1 $^oC\ min^{-1}$ to remove the surfactant template.

3.2.2 Titanium-Substituted HMS Synthesis

Titanium substituted HMS (Ti-HMS) was synthesized according to the previous procedure (Tanev et al., 1994; Punyapalakul and Takizawa, 2006). A 0.01 mol of tetraisopropylorthotitanate (TIPOT) and 1 mol of TEOS was added at the same time into a mixture of DDA (0.27 mol), water (29.6 mol) and ethanol (9.09 mol) under vigorous stirring, and aged at room temperature for 20 h to obtain a white gel.

Then, the solid product was filtered, dried in air at room temperature, and calcined in a muffle furnace at 650 ^{o}C for 4 h with a heating rate of 1 ^{o}C min^{-1}.

3.2.3 Organic-Functionalized HMS Synthesis

Amine- and mercapto-functionalized HMS derivatives obtained by co-condensation method were prepared following the procedure of HMS as described above, except that a certain amount of an organosilane was added. 1.0 mol of TEOS was dissolved in the mixture of DDA (0.25 mol), water (50.0 mol) and ethanol (12.5 mol) under vigorous stirring. After 30 min, 0.25 mol of either 3-aminopropyltriethoxysilane (APTES) or 3-mercaptopropyltrimethoxysilane (MPTMS) was added. The synthesis mixtures were continually stirred at room temperature for 20 h, and then filtrated and dried in air for 24 h. Finally, residual organosilane and surfactant template were extracted by refluxing in ethanol for 24 h, followed by drying at 90 ^{o}C under vacuum for at least 2 h. The resulting adsorbents were named as A-HMS and M-HMS, respectively.

Octyl-functionalized HMS derivative, denoted as OD-HMS, was prepared by post-synthesis method according to previously reported (Inumaru et al., 2006). The synthesis procedure was slightly modified as follows: 0.5 g of calcined HMS was dehydrated at 105 ^{o}C in oven for 24 h, and then stirred in 30 mL of dried toluene containing 0.5 g of *n*-dimethyoctylchlorosilane under refluxing conditions for 24 h. The product was filtered, followed by washing with toluene, and then subsequently dried at 90 ^{o}C under vacuum for at least 2 h.

3.2.4 Santa Babara Acid 15 (SBA-15) Synthesis

SBA-15 was prepared using Pluronic P123 as the template according to previously reported (Imperor-Clerc et al., 2000). Pluronic P123 (4 g) was dissolved in a mixture of water (6.46 mol) and HCl (0.24 mol) at 40 ^{o}C. Once the mixture became homogeneous, TEOS (0.0409 mol) was then added dropwise and the white slurry was stirred at 40 ^{o}C for 24 h and then transferred to a Teflon-lined bottle and heated at 100 ^{o}C for 24 h. The slurry product was filtered and dried in air for 24 h. The organic template that occuled in the mesopore was removed by calcination in a muffle furnace at 550 ^{o}C for 5 h with a heating rate of 1 ^{o}C min^{-1}.

3.2.5 Polymerizable Surfactant-Modified Mesoporous Silicate Synthesis

3.2.5.1 Pore Expansion of SBA-15 Synthesis

A large-pore SBA-15 was synthesized using cyclohexane as a swelling agent according to previously reported (Cao et al., 2009). A 2.4 g of Pluronic 123 was dissolved in 84 mL HCl solution (1.30 M) and 0.027 g of NH_4F. The solution was then stirred at 40 ^oC (500 rpm) to yield a clear solution. Subsequently, the solution was transferred to a water bath set at 15 ^oC. After at least 1 h, 8.5 g of cyclohexane was added under stirring. After 2 h, 5.5 mL TEOS then introduced into the solution, and the slurry solution was stirred at 15 ^oC for 24 h. Then, the product was transferred to a Teflon-lined bottle and heated at 100 ^oC for 48 h. The slurry product was filtered and dried in air for 24 h. The organic template was removed by calcination in a muffle furnace at 550 ^oC for 5 h with a heating rate of 1 $^oC\ min^{-1}$. The large pore SBA-15 was obtained; denoted as SBA-CHX.

3.2.5.2 Admicelle Polymerizable Surfactant on SBA-CHX and Polymerization Procedure

Preparation of polymerizable surfactant-modified adsorbent under optimized condition was described in previous report (Asnachinda et al., 2009). Due to different adsorbent media, the amount of surfactant coverage on SBA-CHX was determined by isotherm study. In this study, the concentration of polymerizable cationic gemini surfactant (PG) was varied from 0.05 to 40 mM. The initial pH of solution was fixed at pH 7 and ionic strength (IS) at 1 mM by NaBr solution. The samples were shaken at 25°C, 200 rpm for 48 h. The concentration of PG at initial and equilibrium were then determined by UV/visible spectrophotometer at maximum wavelength (λmax = 230 nm). Based on isotherm study, it was found that the maximum adsorption capacity of PG on SBA-CHX was 1.35 mmol g^{-1} derived from the initial PG concentration at 14 mM. Thus, this initial PG concentration was applied for PG-modified mesoporous silicate preparation.

A 0.3 g of large pore SBA-CHX was equilibrated with 50 mL of PG surfactant at initial concentration of 14 mM in NaBr solution (ionic strength 1 mM). The pH of the solution was periodically measured and adjusted to pH of

7±0.5. After being equilibrated, the concentration of PG at initial and equilibrium were determined by UV/visible spectrophotometer at maximum wavelength (λmax = 230 nm) to confirm the adsorption capacity of surfactant on surface.

Polymerization procedure was performed according to previously reported (Alkilany and Murphy, 2009). The polymerization procedure was slightly modified as follows: 10 mL of slurry product was then placed in a 25 mL of two-neck round-bottomed flask, and the solution was purged with nitrogen for 2 h under stirring at 100 rpm to remove dissolved oxygen (a polymerization inhibitor). Then, the solution was heated in a water bath to 60 ^{o}C, and 100 μL of (25 mg mL^{-1}) of the cationic initiator (2,2'-azobis(2-methylpropionamidine) dihydrochloride) was added via syringe. The slurry was stirred at 150 rpm for 5 h under a positive pressure of nitrogen. Finally, the product was corrected by filtration, washed thoroughly with Deionized water (DI) and dried in an oven at 60 ^{o}C for 24 h. The polymerizable surfactant-modified SBA-CHX was obtained; denoted as PG-SBA-CHX.

3.2.6 Preparation of NaY zeolite

Commercial Na-form Y zeolite (Si/Al ratio at 1.8), denoted as NaY, was purchased from Tosoh Corporation. Prior to use in an adsorption experiment, it was thermally pretreated under static conditions at 400 ^{o}C for 3 h with a heating rate of 1 ^{o}C min^{-1} (Punyapalakul et al., 2009).

3.3 MATERIAL CHARACTERIZATION PROCEDURE

3.3.1 Porous Structure

Structural analysis of adsorbents was performed on a Rigaku DMAX 2200 powder X-ray diffractometer equipped with Cu Kα radiation. The XRD patterns were collected in the range of 2θ = 0.5-6^{o}, except for NaY was collected in range 2θ = 0.5-50^{o}.

3.3.2 Surface Area and Pore Size

Specific surface area, mean pore diameter and pore volume were determined by nitrogen adsorption-desorption isotherm using an Autosorb-1 Quantachrome automatic volumetric sorption analyzer at 77 ^{o}K. Before operation, 0.05 g of sample was degassed at 300 ^{o}C for 3 h to remove any contaminant that may be present at the surface. The specific surface area (S_{BET}) was calculated according to Brunner-Eller-Teller (BET) equation using N_2 adsorption isotherm data. Mean pore diameter and pore volume (V_P) were calculated according to Barrett-Joyner-Halenda (BJH) equation.

3.3.3 Surface Functional Groups

A Perkin Elmer Spectrum One Fourier-transform infrared (FT-IR) spectrometer was used to identify the organic functional groups on HMS derivatives, the presence of surfactant coverage and polymerization performance. The adsorbent powder mixed with KBr was compressed to form a self-support wafer, and the FT-IR spectra were recorded in the transmittance mode between 4000 and 400 cm^{-1}. Before measurement, the samples were heated at 105 °C in oven for 24 h, and then kept in desiccators until analysis.

3.3.4 Elemental Analysis

3.3.4.1 Nitrogen Content Determination

An autoclave digestion in the presence of potassium persulfate in an alkaline media was conducted for determining the nitrogen content of amino-functionalized HMS derivative (A-HMS) as described in previous report (Smart et al., 1983). The oxidizing reagent was prepared by dissolved 3 g $K_2S_2O_8$ and 4 g sodium hydroxide (NaOH) in 100 mL of DI water. The reagent was analytical grade and contained low levels of nitrogen. The oxidizing reagent was prepared daily.

The experiment procedure for analysis of nitrogen content was slightly modified as follows: 0.05 g of A-HMS adsorbent was mixed with 50 mL DI water in a 100-mL of Duran bottle. A 10 mL of oxidizing solution was added to the sample which was then autoclaved for at 120 °C for 30 min. This mixture was cooled to room temperature, and then filtered the mixture solution to remove the solid

adsorbent. A 25 mL extract solution was transferred to 50 mL of volumetric flask for nitrate analysis. Prior to analysis, bicarbonate was removed by acidifying extract with 5 mL of HCl solution (1 mL of concentrated HCl and 15 mL of DI water) to reduce the pH of extract solution approximately to pH 2-3, and then the solution volume was adjusted to 50 mL by DI water. Blank was performed with the same condition without adsorbent addition.

Nitrate standard stock solution (0.1 mg-N mL^{-1}) was prepared by dissolved 0.0722 g of dried-potassium nitrate (KNO_3) in 100 mL DI water. The stock solution was diluted to 0.01 mg-N mL^{-1} before calibration curve preparation. The calibration curve was prepared in 50 mL of volumetric flask by varying the volume of diluted-NO_3 standard from 1 to 15 mL, 5 mL of HCl solution was added, and the solution volume was adjusted to 50 mL by DI water. The samples, blank and standards were measured by UV-visible spectrophotometer at maximum wavelength (220 nm).

Amount of nitrogen was plotted *vs*. UV absorbance. The total persulfate nitrogen (TPN) in the sample (mg g^{-1}) was then calculated with the following equation:

$$TPN\ (mg\ g^{-1}) = \frac{a*(V_s/V_a)}{b} \qquad (3.1)$$

where a is amount of nitrogen obtained from calibration curve (mg); b is amount of adsorbent (g); V_s is volume of extract solution (60 mL) and V_a is volume of analyzed extract solution (25 mL).

3.3.4.2 Sulfur Content Determination

The amount of sulfur of mercapto-functionalized HMS derivative (M-HMS) was measured by using a LECO SC132 sulfur analyzer. Coal reference material (S = 1.14 ± 0.5%) was used as a sulfur standard. A 0.3 g of sample is burned in furnace at 2,462 ^{o}F (1,350 ^{o}C) under static condition. The sulfur content is calculated as % (wt/wt) by comparing with sulfur in coal reference material.

3.3.5 Scanning Electron Microscope (SEM)

Micrograph and particle size of the adsorbent samples were taken using a JEOL JSM-5410LV scanning electron microscope (SEM). Before observation of SEM, all samples were fixed on aluminum stubs and coated with gold.

3.3.6 Surface Charge Measurement

3.3.6.1 Acid-base Titration Method

Surface charge density of the adsorbents were determined by acid-base titration method according to previously reported (Punyapalakul and Takizawa, 2004). NaOH and HCL stock solutions were prepared at 25 mM in ultrapure (UP) water (18.2 mΩ). The amount ratio of adsorbent to mixture solution was 1.0 g L^{-1}. For analysis, the different volume of NaOH or HCl stock solutions was mixed with 0.025 g of adsorbent in order to vary the pH of solution. The ionic strength (IS) was fixed at 10 mM by adding 2.5 mL of NaCl solution (0.1 M). The samples were diluted with UP water to obtain a 25 mL of final volume. Then, the samples were shaken at 200 rpm (25 ^{o}C). After completion of 12 h, the pH of solution for each condition was measured and calculated the surface charge density as Coulombs m^{-2} was calculated as following equation:

$$Surface\ charge(C\ m^{-2}) = \frac{\{[HCl]-[NaOH]-[H^+]+[OH^-]\}}{M\ x\ S_{BET}} x\ 96{,}500 \qquad (3.2)$$

where [HCl], [NaOH] are concentration (M) of added HCl and NaOH, respectively. $[H^+]$ is the concentration of hydrogen ion (M) as calculated from pH = -log $[H^+]$; $[OH^-]$ is the concentration of hydroxide ion (M) as calculated from pOH = -log $[OH^-]$ and pOH=14-pH; 96,500 is Faraday constant (Coulomb mol^{-1}); *M* is mass of adsorbent (g L^{-1}) and S_{BET} is specific area of adsorbents (m^2 g^{-1}).

3.3.6.2 Zeta Potential Measurement

Surface charge of adsorbents was measured by an electrophoresis apparatus (Zeta-Meter System 3.0, Zeta-Meter Inc.). Before measurement, 0.005 g of the adsorbent was suspended in 35 mL of aqueous solution which was fixed by 10 mM phosphate buffers at the pH range 3-10. After completion of 24 h, 15-20 mL of

suspension was transferred into a measuring cell, and the zeta potential (millivolt: mV) for each condition was measured.

3.3.7 Hydrophilic/hydrophobic Surface Characteristic

Hydrophobic/hydrophilic surface characteristic of the adsorbents were evaluated by measuring the water contact angle (θ) using a Dataphysics DCAT-11 tensiometer in a powder contact angle mode. The water contact angle degree was more than 50^{o} which was characterized as the hydrophobic adsorbent.

3.4 ADSORPTION EXPERIMENTS

An evaluation of aqueous-phase adsorption of HANs was conducted under batch experiment. Stock solutions of HANs were prepared in DI water at which the pH of solution and 10 mM of ionic strength (IS) were adjusted by using phosphate buffer. In a typical procedure, 0.025 g of adsorbent and 35 mL of HAN solution were mixed in a 100-mL Erlenmeyer flask covered with a glass stopper. The slurry was then stirred in a rotary shaker at 200 rpm (25 ^{o}C). The solid was removed by a glass microfiber filter (GF/C) and the supernatant was analyzed by a gas chromatograph equipped with an electron capture detector (GC/ECD) according to the EPA method 551.1 (1990). Each experiment was performed under duplication of identical conditions. Blank experiment without the adsorbent addition was carried out for comparison and a loss due to vaporization was considered.

The HAN adsorption amount was calculated according to Equation 3.3:

$$q_e = \frac{(C_0 - C_e)}{M} V \qquad (3.3)$$

where q_e is the equilibrium adsorption capacity (μg g^{-1}), C_0 and C_e are initial and equilibrium concentration of HANs in the solution (μg L^{-1}), V is the volume of solution (L), and M is the mass of adsorbent (g).

3.4.1 Adsorption Kinetic Study

The evaluation of kinetic study was performed by varying equilibrate time from 0 to 48 h. DCAN was selected as a model HANs for batch adsorption kinetic. The initial DCAN concentration for the parental HMS, organic-functionalized HMS derivatives, Ti-HMS, SBA-15, SBA-CHX, PG-SBA-CHX and NaY zeolite was 100 μg L^{-1}, for M-HMS and PAC was 50 mg L^{-1} at pH 7, while the ionic strength remain fixed at 10 mM adjusted by a phosphate buffer. The samples were shaken in a rotary shaker at 25 ^{o}C (200 rpm), and then the solid adsorbent was separated at time intervals. The concentration of DCAN in supernatant was analyzed by GC/ECD according to the EPA method 551.1.

3.4.2 Adsorption Isotherm Study

3.4.2.1 Effect of Initial Concentration

The adsorption isotherm was performed following the similar procedure with different initial concentration of HANs at pH 7 and IS of 10 mM. The initial of each HAN (i.e. MCAN, DCAN, TCAN, MBAN and DBAN) for the parental HMS, organic-functionalized HMS derivatives, Ti-HMS, SBA-15, SBA-CHX, PG-SBA-CHX and NaY zeolite was varied from 25 to 300 μg L^{-1} in single solute solution while for M-HMS and PAC was 0.05 to 80 mg L^{-1}. The contact time was obtained from the kinetic studies. After equilibrium, the mixture was separated through a glass microfiber filter (GF/C) to remove the solids, and then the initial and equilibrium concentrations in supernatant were analyzed by GC/ECD according to EPA method 551.1.

3.4.2.2 Effect of pH of Solution

Effect of the solution pH on the adsorption capacity of DCAN was evaluated at pH 5, 7 and 9. The IS was fixed at 10 mM by using phosphate buffer. The initial DCAN concentration for all adsorbents was varied from 25 to 300 μg L^{-1}, excepted for M-HMS and PAC were performed at high concentration (ppm level) in range 0.1 to 50 mg L^{-1}. The samples were shaken in a rotary shaker at 25 ^{o}C (200 rpm). After equilibrium, the solid adsorbent was separated, and then the initial and equilibrium concentrations in supernatant were analyzed by GC/ECD according to the EPA method 551.1.

3.4.2.3 Effect of Temperature

Effects of temperature on adsorption of DCAN on M-HMS and PAC were conducted at pH 7 with IS of 10 mM. The initial concentration of DCAN was varied from 1 to 50 mg L^{-1}. The samples were shaken in a rotary shaker at various temperatures (15, 25 and 40 ^{o}C) at 200 rpm. After equilibrium, the solid adsorbent was separated, and then the initial and equilibrium concentrations in supernatant were analyzed by GC/ECD according to the EPA method 551.1

3.4.3 Selective Adsorption Study

3.4.3.1 Selective Adsorption of Five-HANs in Mixed Solute Solution

The effect of the HAN molecular structure on the selective adsorption was evaluated using mixed solute of the five-HANs (MCAN, DCAN, TCAN, MBAN and DBAN) at the same concentration at pH 7 with IS of 10 mM. The samples were shaken in a rotary shaker at 25 ^{o}C at 200 rpm. After equilibrium, the solid adsorbent was separated, and then the initial and equilibrium concentrations in supernatant were analyzed by GC/ECD according to the EPA method 551.1. The adsorption capacities results were compared with that of single solute study.

3.4.3.2 Effect of Co-existing Electrolytes in Tap Water on Selective Adsorption

The effect of electrolytes in tap water on the selective adsorption of M-HMS and PAC was performed by mixing the five-HANs (MCAN, DCAN, TCAN, MBAN and DBAN) at the same concentration in tap water. The samples were shaken in a rotary shaker at 25 ^{o}C at 200 rpm. After equilibrium, the solid adsorbent was separated, and then the initial and equilibrium concentrations in supernatant were analyzed by GC/ECD according to the EPA method 551.1. The concentration of electrolytes in tap water, such as Na^{+}, Mg^{2+}, Ca^{2+}, Fe^{2+}, F^{-}, Cl^{-}, Br^{-}, NO_3^{-}, SO_4^{2-} and etc., was determined by an ion chromatograph (Dionex LC25) equipped with electrochemical detector. The background concentration of HANs in tap water was also measured.

3.4.3.3 Selective Adsorption in the Presence of Co-existing DBPs in Mixed Solute Solution

The selective adsorption of adsorbents in the presence of co-existing DBPs on M-HMS and PAC was performed by mixing the three abundant DBPs species, i.e. trichloromethane (TCM), dichloroacetic acid (DCAA) and DCAN, at the same concentration at pH 7 with IS of 10 mM. The initial concentration of the three DBPs was varied from 0.025 to 0.8 mg L^{-1}. The samples were shaken in a rotary shaker at 25 ^{o}C at 200 rpm. After equilibrium, the solid adsorbent was separated. The concentration of TCM and DCAN at initial and equilibrium in supernatant were analyzed by GC/ECD according to the EPA method 551.1, and DCAA concentration was determined following the EPA method 552.2.

3.4.4 Regeneration study

The adsorbent regeneration study was carried out using extraction method. Adsorbed DCAN on the parental HMS, M-HMS and PAC were extracted by varying various kinds of solvent (such as methanol, ethanol and acetone, and MtBE), and various pH values of DI water (pH 5, 7, and 9 with IS of 10 mM) at 25 ^{o}C for 24 h. Extract solution-adsorbent ratio was fixed at 500 v/w (mL g^{-1}) for M-HMS and PAC while at 250 v/w (mL g^{-1}) for HMS due to low adsorption capacity. The concentration of desorbed DCAN was analyzed by using GC/ECD. Regeneration efficiency was calculated as Equation 3.4 (Ahmaruzzaman and Laxmi Gayatri, 2010):

$$\% \text{ Regeneration efficiency} = \frac{C_d \times V_d}{M \times q_e \times 1000} \times 100 \qquad (3.4)$$

where C_d is the desorbed DCAN concentration (mg L^{-1}), V_d is the volume of the extracted solution (mL), M is the mass of adsorbent (g), q_e is the amount of the DCAN pre-adsorbed on the adsorbent (mg g^{-1}).

3.5 ANALYTICAL METHOD

3.5.1 Determination of Haloacetonitriles (HANs) and Trichloromethane (TCM)

Haloacetonitriles (HANs) and trichloromethane (TCM) were analyzed according to a modified EPA Method 551.1 (Cancho et al., 1999). Typically, a sample solution (30 mL) was placed in a 40 mL glass vial with a polypropylene screw cap and PTFE faced septum. Into each sample, 5 g of anhydrous sodium sulfate (Na_2SO_4) was added in order to increase the ionic strength of the aqueous matrix together with 2 mL of methyl *tert*-butyl ether (MtBE). The vial was then sealed with Teflon-faced septa and shaken for 2 min. After standing the resulting solution for 3 min, 500 μL of the MtBE layer was transferred into a 2-mL GC vial. The organic layer (1 μL) was injected into an Agilent GC6890 gas chromatograph equipped with an electron capture detector (GC/ECD).

The gas chromatograph condition and parameters were performed as follows: the velocity of helium-carrier gas was established at 25 cm sec^{-1} and nitrogen was used as a make-up gas. The column used for GC/ECD analysis was fused silica capillary column (HP-1, 30 m x 0.32 mm i.d. x 0.25 μm film thickness). The injection temperature was set at 200 ^oC with splitless mode, and ECD detector temperature was maintained at 300 ^oC. The temperature of column oven was programmed as follows:

[1] initial temperature of 30 ^oC for 5.5 min,

[2] ramping to 35 ^oC at 10 ^oC min^{-1} and holding for 4 min,

[3] ramping to 40 ^oC at 10 ^oC $min^{-1}$and holding for 3 min, and

[4] ramping to 150 ^oC at 15 ^oC min^{-1}.

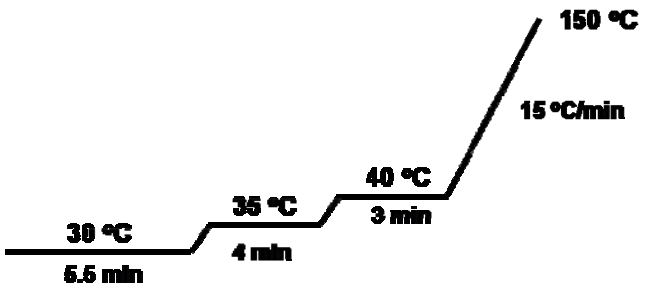

Figure 3.1 Temperature program of GC condition for HANs and TCM determination

3.5.2 Determination of Dichloroacetic Acid (DCAA)

Dichloroacetic acid (DCAA) was analyzed using an acidic methanol esterification according to a modified EPA Method 552.2 as describe by elsewhere (Nikolaou et al., 2005). The analytical method was slightly modified as follows:

3.5.2.1 Derivatization Step

A 15 ml of sample solution was placed in a 40 mL glass vial with a polypropylene screw cap and PTFE faced septum. The 25 μL of surrogate standard, 30 mg L^{-1} of 2,3-dibromopropionic acid which was dissolved in MtBE was added. Then, 0.5 mL of concentrated sulfuric acid (H_2SO_4) (so that pH <0.5), and 4 g of Na_2SO_4 were added and shaken until dissolved. The sample was then quickly added with 1.5 g of copper sulfate pentahydrate ($CuSO_4.5H_2O$) and 2.5 mL of MTBE was added. The vial was then sealed with Teflon-faced septa and shaken for 2 min and allowed to stand for 5 min.

3.5.2.2 Methylation Step

A 1.625 mL of the MtBE layer was transferred into a 14 mL of vial that containing 2 mL of a solution of H_2SO_4 in methanol (10%), and the vial was placed in a water bath at 50°C for 2 h. Then, it was cooled to 4°C for 3 min and then 5 mL of saturated sodium bicarbonate ($NaHCO_3$) was added. The vial was shaken again for 2 min and was frequently vented to release carbon dioxide (CO_2) and allowed to stand for 5 min. The upper layer (1 mL) was transferred into a 2-mL GC vial. The organic layer (1 μL) was injected into an Agilent GC6890 gas chromatograph equipped with an electron capture detector (GC/ECD). Extracts were always analyzed within 24 h.

The gas chromatograph condition and parameters were conducted as follows: the velocity of helium-carrier gas was established at 25 cm sec^{-1} and nitrogen was used as a make-up gas. The column used for GC/ECD analysis was fused silica capillary column (VF-X Varian, 30 m x 0.32 mm i.d. x 0.10 μm film thickness). The injection temperature was set at 200 ^oC with splitless mode, and ECD detector temperature was maintained at 290 ^oC. The temperature of column oven was programmed as follows:

[1] initial temperature of 35 ^{o}C for 7 min,

[2] ramping to 55 ^{o}C at 5 ^{o}C min^{-1}, and

[3] ramping to 110 ^{o}C at 7.5 ^{o}C min^{-1}.

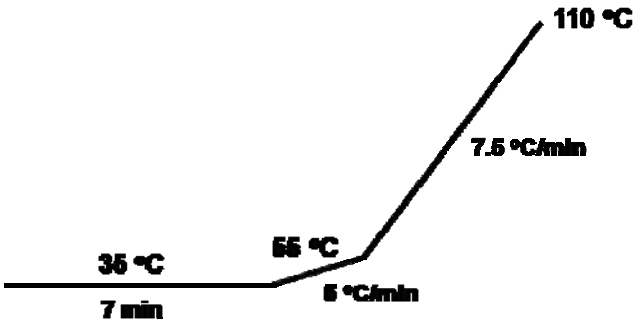

Figure 3.2 Temperature program of GC condition for DCAA determination

3.5.3 Determination of Electrolyte in Tap Water

The concentration of electrolytes in tap water, such as Na^{+}, Mg^{2+}, Ca^{2+}, Fe^{2+}, F^{-}, Cl^{-}, Br^{-}, NO_3^{-}, and SO_4^{2-}, was determined by an ion chromatograph (Dionex LC25) equipped with electrochemical detector. Anion/cation standard solution was prepared in UP water (18.2 mΩ). The standard solution of each ion was prepared daily before the analysis.

3.5.4 Determination of Polymerizable Gemini Surfactant (PG)

The concentration of PG in a supernatant at initial and equilibrium was determined by UV/visible spectrophotometer (GENESYS 10S) at maximum wavelength (λmax = 230 nm) using 5-cm quartz cells.

CHAPTER IV

MATERIALS CHARACTERIZATION

4.1 INTRODUCTION

In this study, hexagonal mesoporous silicate (HMS) was synthesized and modified surface by two methods (direct co-condensation and post grafting method) of organic-ligand grafting onto pristine HMS, with three different types of organosilanes, i.e. amino-, mercapto- and octyl- functional groups to investigate the effects of different physicochemical characteristics on the adsorption capacities for haloacetonitriles (HANs) compared to the similar mesopore SBA-15. Titanium-substitution modification in mosoporous silicate structure (Ti-HMS) was also applied in this study. NaY zeolite was used so as to investigate the effect of a crystalline structure. Furthermore, the effect of surface modification by polymerizable surfactant on adsorption was also investigated. Therefore, the physicochemical characteristics of all synthesized adsorbents were investigated comparing with powder activated carbon (PAC). The obtained characterized data were combined with adsorption experiment results for study the relationships between physicochemical characteristics (such as porous structure, surface area, surface charges, surface characteristics, and etc.) and adsorption phenomena of HANs. Summary of synthesized adsorbents used in this study of which surface functional groups of all adsorbents are shown in Table 4.1.

Table 4.1 List of the inorganic porous materials used in this study

Adsorbents	Surface functional groups
1. Mesoporous materials	
1.1 Parental mesoporous material	
• HMS	Silanol (SiOH)
• SBA-15	Silanol (SiOH)
• Large pore SBA-CHX	Silanol (SiOH)
1.2 Transition element substituted HMS	
• Ti-HMS	Lewis acid site, Silanol (SiOH)
1.3 Organic-functionalized HMS derivatives	
• A-HMS	Amino ($-NH_2$), Silanol (SiOH)
• OD-HMS	Octyl ($-C_8H_{17}$), Silanol (SiOH)
• M-HMS	Mercapto (-SH), Silanol (SiOH)
2. Microporous materials	
• NaY zeolite	Na^+, Lewis acid site, Silanol (SiOH)
• PAC	Carboxyl, phenyl and others
3. Surfactant-modified adsorbent	
• PG-SBA-CHX	Cationic surfactant

4.2 HEXAGONAL STRUCTURE CONFIRMATION BY POWDER XRD TECHNIQUE

XRD patterns of the parental HMS and the four functionalized HMS derivatives are shown in Figure 4.1a. HMS exhibited more correspondingly the hexagonal porous structure with a clear (100) plane at $2\theta = 2.2^{o}$. A shift of (100) plane to higher angles was observed for Ti-containing HMS ($2\theta = 2.32°$). This can be attributed to a partial collapse of HMS framework during adsorbent synthesis. A-HMS and M-HMS exhibited a broad low intensity peak, indicating a decrease in the level of structure orders. This is likely to be due to the interaction of the organofunctional groups preventing the self-assembly of the surfactant and silica precursor during the co-condensation process (Maria et al., 2004). In contrast, the XRD pattern of the OD-HMS remained virtually intact, in comparison to that of the parental HMS, suggesting that the functionalization via the post-synthesis method only slightly affected the framework of the ordered porous structure. Similar XRD pattern of OD-HMS was also reported by Inumura et al. (2006).

In the case of SBA-15 (Figure 4.1b), three diffraction peaks appeared at $2\theta = 0.92^{o}$, 1.58^{o} and 1.84^{o} corresponding to (100), (110) and (200) plane, respectively, were clearly revealed, reflecting the well-defined hexagonal array of mesopore structure. The standard peaks of the NaY were 6^{o}, 10^{o}, 12^{o}, 15^{o}, 18^{o}, 20^{o}, 24^{o}, 27^{o} and 31^{o} (Figure 4.1c). The patterns attained from synthesized SBA-15 and commercial NaY were similar to those found in the literature (Wei et al., 2005; Aguado et al., 2009; Sue-aok et al., 2010; Tao et al., 2010).

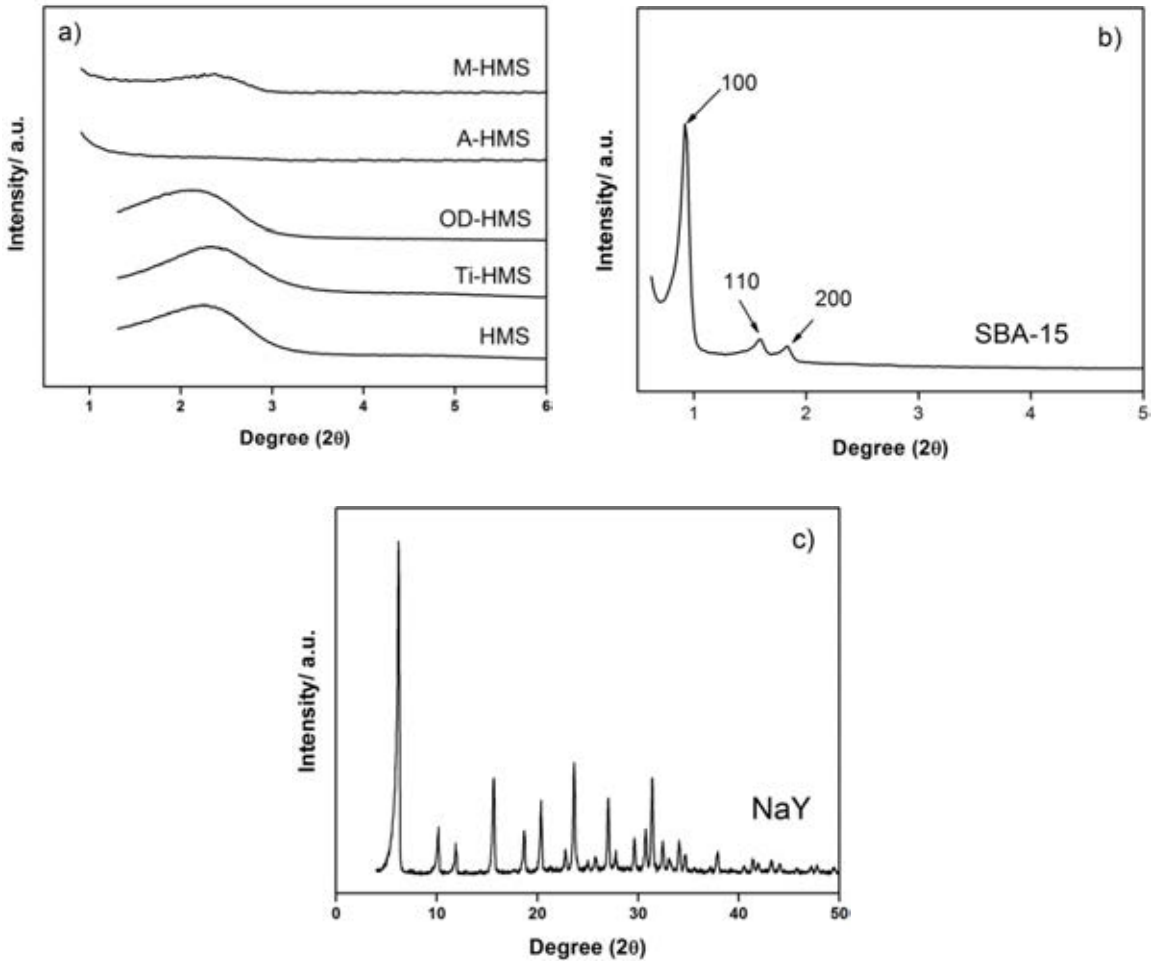

Figure 4.1 Representatives of X-ray powder diffraction patterns of (a) HMS and functionalized HMS derivatives; (b) SBA-15 and (c) NaY

4.3 SURFACE AREA AND PORE STRUCTURE CHARATERISTICS CALCULATED FROM N_2 ADSORPTION-DESORPTION ISOTHERMS

As seen in Figure 4.2a, N_2 adsorption-desorption isotherms of HMS, functionalized HMS derivatives, SBA-15 and SBA-CHX showed type IV isotherm classified by IUPAC, which was typical of materials containing mesopores. NaY and PAC showed type I isotherm which indicates the presence of micropores (Figure 4.2b). Comparison between SBA-15 and SBA-CHX, the capillary condensation at midpoint of relative pressure of SBA-CHX was shift up to 0.90 (Figure 4.2c). The highest relative pressure of capillary condensation observed for SBA-CHX provides strong evidence that SBA-CHX has higher pore diameter than SBA-15 and other silica-based adsorbents.

Based on the N_2 adsorption-desorption isotherms, the BET surface area pore size (as diameter) and pore volume were estimated and are summarized in Table 4.2. PAC possessed higher BET surface area than all five of the HMS-based adsorbents. Compared to the parental HMS, a decrease in the BET specific surface area was noted for OD-HMS and especially A-HMS, which was a direct consequence of the functionalized process as mentioned in the XRD results (but these are different in terms of OD-HMS and M-HMS). More precisely, the poorly ordered structure of A-HMS, yielding the lowest BET surface area, should be derived from a strong hydrogen bonding of the amine precursor during the micelle aggregation as well as the silicate condensation. However, M-HMS exhibited a significantly larger surface area than A-HMS, and was even larger than that of HMS, despite being similarly functionalized via the co-condensation method.

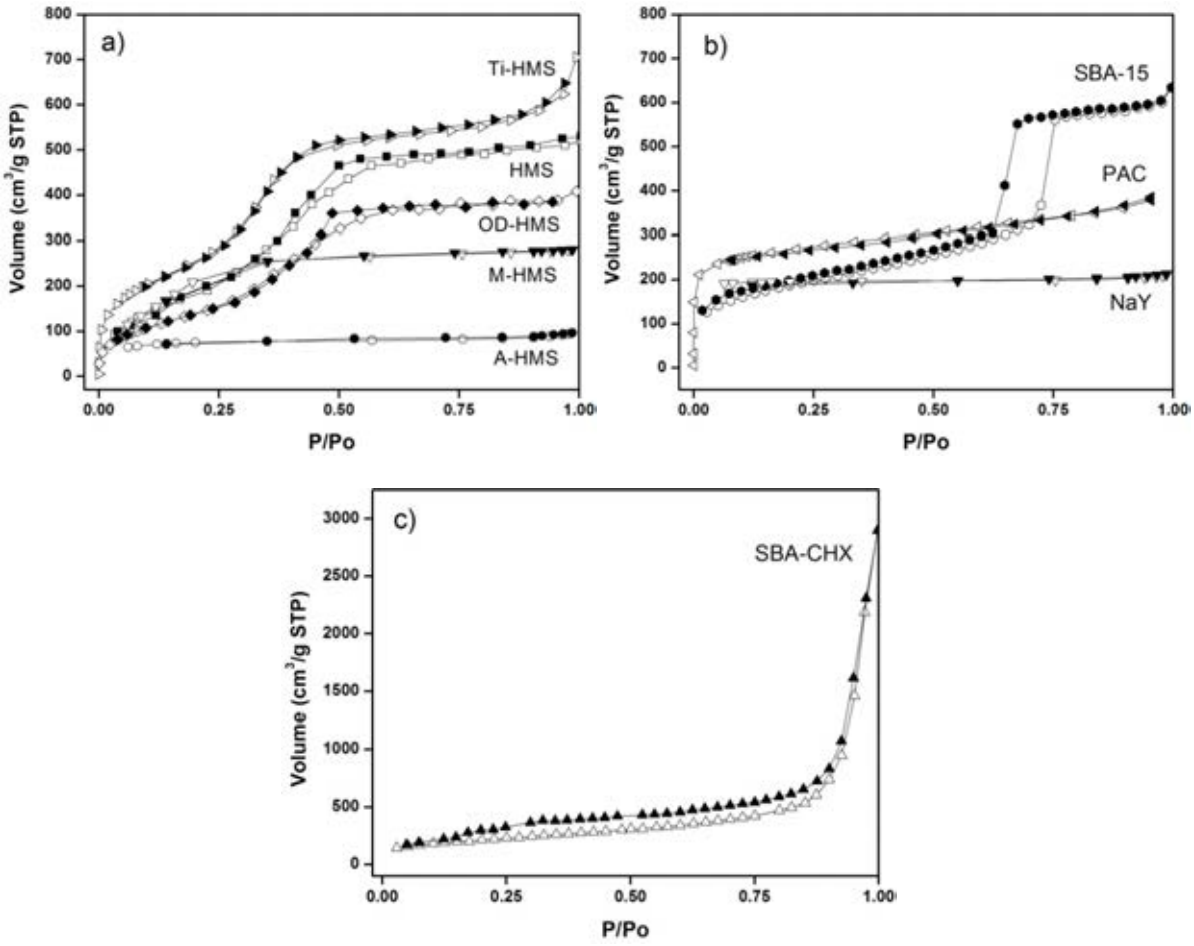

Figure 4.2 N_2 Adsorption-desorption isotherms of (a) HMS and functionalized HMS derivatives; (b) SBA-15, NaY and PAC; and (c) SBA-CHX. Open and closed symbols represent N_2 adsorption and N_2 desorption, respectively

Table 4.2 Mean pore diameter, pore volume and BET surface area of HMS, functionalized HMS derivatives, SBA-15, SBA-CHX, NaY and PAC.

Adsorbents	Functional groups	Mean pore diameter (nm)	V_P ($mm^3\ g^{-1}$)	S_{BET} ($m^2\ g^{-1}$)
HMS	Silanol	2.60[a]	773[a]	712[a]
Ti-HMS	Lewis acid site and silanol	3.18[b]	1276[b]	767[b]
A-HMS	Amine and silanol	3.95[a]	147[a]	262[a]
M-HMS	Thiol and silanol	2.48[a]	433[a]	912[a]
OD-HMS	Octyl and silanol	2.36[b]	500[b]	477[b]
SBA-15	Silanol	6.00	981	654
SBA-CHX	Silanol	23.41	448	766
NaY	Na^+ Lewis acid site and silanol	0.74[a]	326[a]	653[a]
PAC	Carboxyl, phenyl and oxygen-containing groups	1.90[a]	276[a]	980[a]

[a] Reference: Punyapalakul et al., (2009)

[b] Reference: Punyapalakul and Takizawa (2006)

4.4 SURFACE FUNCTIONAL GROUP CHARACTERIZATION OF ORGANIC-FUNCTIONALIZED HMS DERIVATIVES BY FT-IR SPECTROSCOPY

The functional groups presenting on the surface of the adsorbents were identified by using FT-IR spectroscopy (Figure 4.3). The O-H stretching of free surface silanol groups was observed at 3746 cm^{-1} and the Si-O stretching was detected around 1111 cm^{-1}. The FT-IR spectrum of Ti-HMS was similar to that of the original HMS, except for the weak band at 992 cm^{-1} that could be assigned to the Ti-O vibration (Punyapalakul and Takizawa, 2006). For the functionalized HMS delivatives, the presence of organofunctional groups could be verified by the bands located in the range of 2850–2965 cm^{-1}, corresponding to the C-H stretching, and by the band at 2560 cm^{-1} derived from the S-H stretching for M-HMS. For A-HMS, the located of stretching of the N-H group at 3300-3400 cm^{-1} could not be identified because the broad characteristic of the IR bands was revealed due to the physisorbed water molecules. The functionalization degree was reflected by a significant decrease in the free O-H vibration at 3746 cm^{-1} concomitantly with an increase in the bands related to the organic groups of the HMS surface.

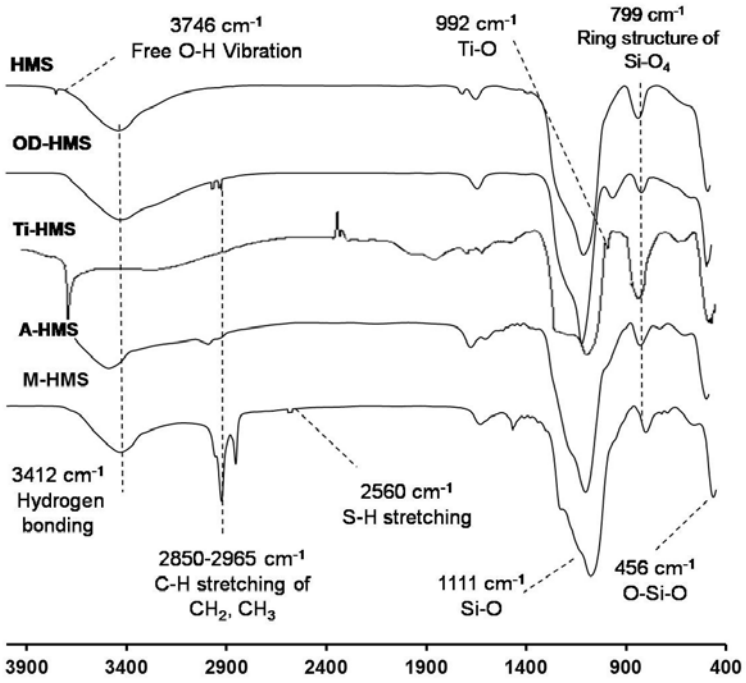

Figure 4.3 Representative FT-IR spectra of HMS and the four functionalized HMS derivatives

4.5 POLYMERIZABLE GEMINI SURFACTANT ADSORPTION AND POLYMERIZATION DEGREE CHARACTERIZATION

4.5.1 Adsorption of PG on SBA-CHX

The adsorption isotherm of cationic polymerizable cationic gemini surfactant (PG) on the parental SBA-CHX at pH 7, the ionic strength was fixed at 1 mM by NaBr solution, is shown in Figure 4.4. It was observed that the adsorption isotherm could be defined into 4 regions. Region I was occurred at low concentration of the surfactant whilst region II and III indicated monolayer and bilayer PG structures on the SBA-CHX surface, respectively. The transition from region III to IV also indicated a critical micelle concentration (CMC). From this isotherm study, the maximum adsorption capacity (q_{max}) was found to be 1.35 mmol g^{-1} derived from the initial PG concentration at 14 mM which was ca. 2 times higher than that was reported in previous literature (Asnachinda et al., 2009). This result indicated that a larger pore size offered the accessible channels for PG surfactant to internal pore of SBA-CHX which did not be limited only the external surface coverage, leading to

higher adsorption capacity. In order to maximize the adsolubilization of organic solute, the maximum bilayer coverage is desired; hence this condition was applied for the preparation of PG-modified SBA-CHX.

Considering the effective area per head molecule (94.04 A^{o2} $molecule^{-1}$), based on the maximum adsorption capacity (q_{max} = 1.35 mmol g^{-1}), this was 3 times higher than surface area of PG headgroup (32.26 A^{o2} $molecule^{-1}$ as calculated by ACD/ChemSketch software). It might be caused that the coiling effect of long alkyl chain of hydrophobic tail, and the repulsive force between adsorbed PG headgroup onto solid surface causing an increase in the area per head molecule. Moreover, this is possible that surfactant-modified SBA-CHX may have the remaining silanol groups on its surface which are available to interact with HAN molecules.

Based on N_2 adsorption-desorption isotherm (Figure 4.2c), the determined mean pore diameter of SBA-CHX was 23.41 nm (Table 4.2). According to the molecular dimension of PG as calculated by ACD/ChemSketch software, is 0.69, 1.07 and 2.08 nm in width of headgroup side, width of tail side and length, respectively, it was clear that PG was able to access to the inner mesoporosity of the parental SBA-CHX suggesting that pore blocking effect can be neglected.

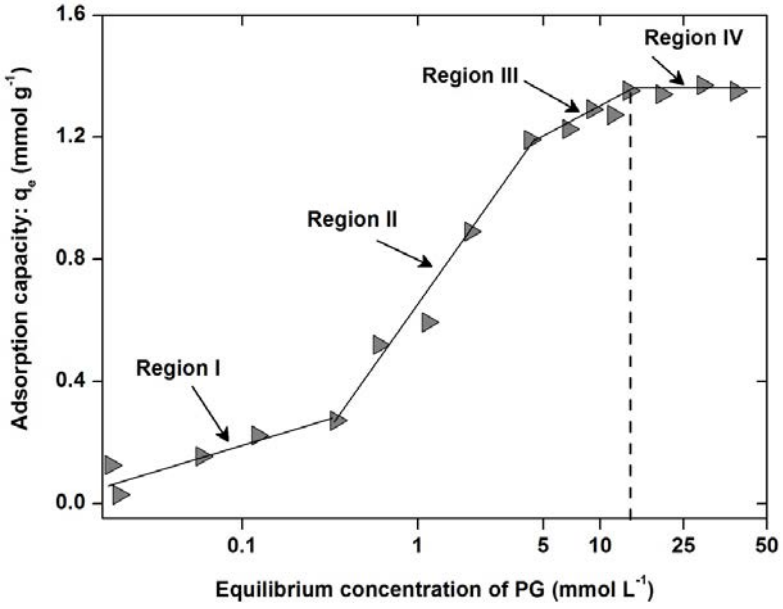

Figure 4.4 Adsorption isotherm of PG on the parental SBA-CHX at pH 7 in NaBr solution with ionic strength 1 mM

4.5.2 The presence of PG surfactant on adsorbent surface and polymerization degree characterization by FT-IR

FT-IR analysis was used in order to identify the presence of PG surfactant on the parental SBA-CHX surface as shown in Fig. 4.5. The O-H stretching of free-OH was observed at 3746 cm^{-1} for the parental of SBA-CHX. The sharp bands at 1087 cm^{-1} and 804 cm^{-1} are due to Si-O-Si and Si-O stretching vibrations, respectively. With regard to the spectra of SBA-CHX after surfactant adsorption, the presence of new specific bands could be verified by the bands located in the range of 2850–2950 cm^{-1} and around 1460 cm^{-1}, corresponding to the C-H stretching and C-H bending, respectively; and by the band at around 1720 cm^{-1} derived from the C=O stretching of methacryloxy group (CH_2=C(CH_3)C=O).

The degree of polymerization can be confirmed by FT-IR evidences as shown in Figure 4.6 which was analyzed by IGOR Pro 6.0 software. The band at 1631cm^{-1} represented the physisorbed water molecules. Before polymerization, an appearance of weak band at 1579 cm^{-1} could be assigned to C=C stretching corresponds to the methacryloxy group at which this band located at 1550-1600 cm^{-1}. In contrast, this stretching band disappeared totally on polymerized PG-SBA-CHX, indicating the conversion of this group by the polymerization process.

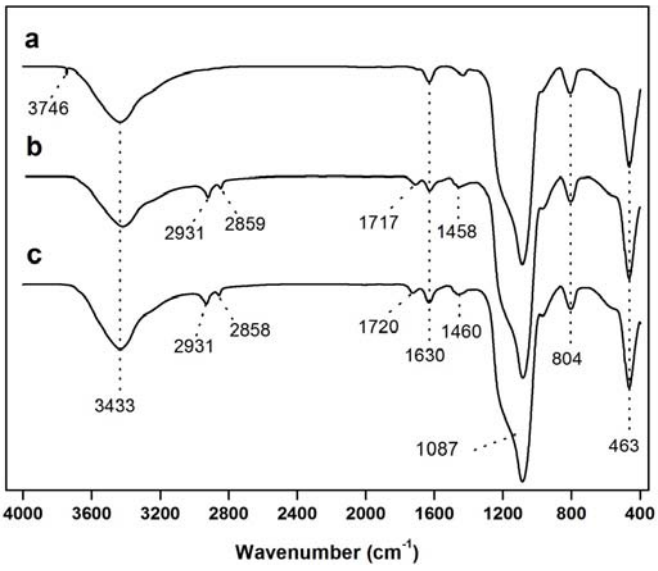

Figure 4.5 FT-IR spectra of adsorbents: (a) Parental SBA-CHX; (b) PG-SBA-CHX before polymerization; and (c) PG-SBA-CHX after polymerization

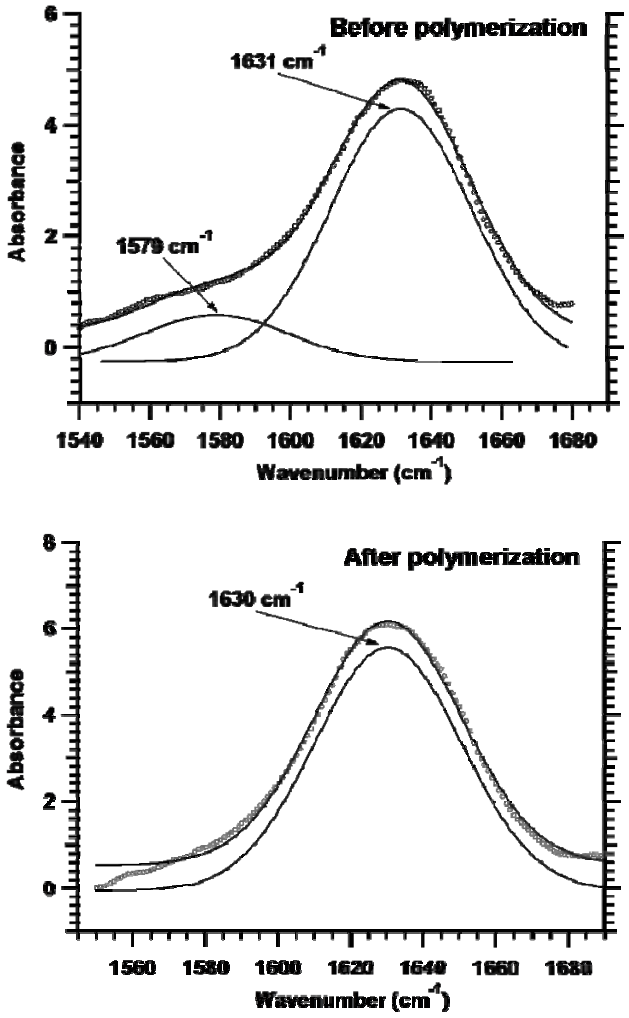

Figure 4.6 FT-IR spectra in region of C=C stretching of PG-SBA-CHX before and after polymerization

4.6 MORPHOLOGY AND PARTICLE SIZE OF ADSORBENT CHARACTERIZATION BY SEM

The morphologies of the parental HMS, functionalized HMS derivatives, SBA-15 and SBA-CHX were observed using a scanning electron microscope (SEM) and the images are shown in Figure 4.7. The image of HMS exhibit aggregated spherical particle of ca. 0.1 to 1μm in size which is consistent with the report of Asouhidou et al. (2009). A similar morphology can be seen for A-HMS and M-HMS except that the particles of two functionalized HMSs were slightly larger compared to

those of parental HMS. Moreover, SEM image of SBA-15 was continuous rod shaped particles with average size around 1 μm while pore expansion SBA-15, i.e. SBA-CHX, exhibited the some spherical morphology and some others irregular shapes with ca. 0.5 to 1.5 μm in size. It can be concluded that the morphology was changed largely after the pore expansion. Similar result has been reported in previous literature (Nguyen et al., 2008).

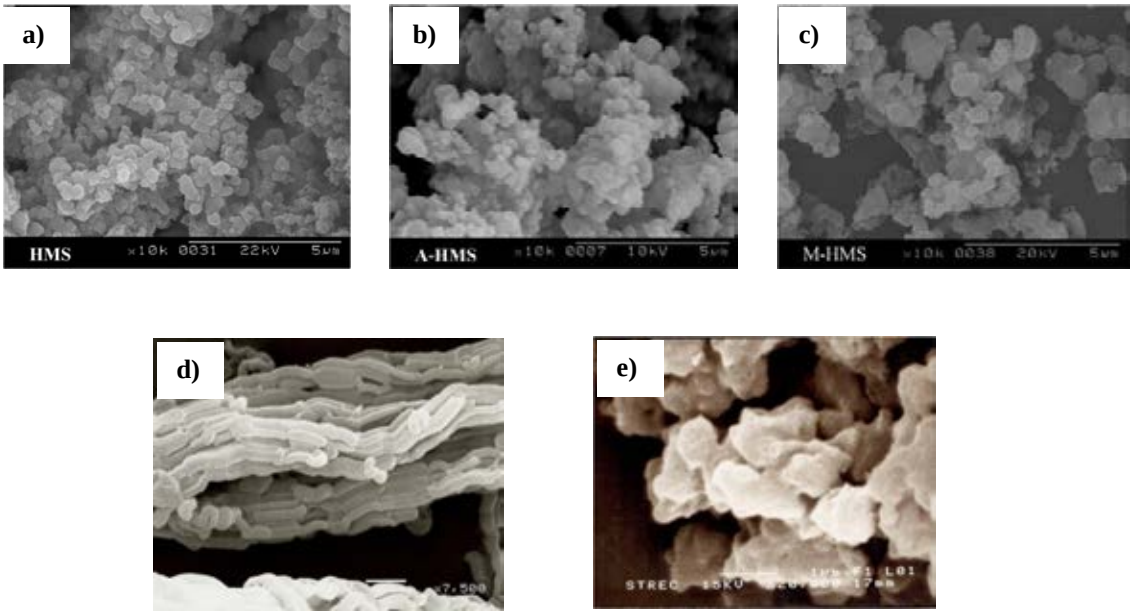

Figure 4.7 Representative SEM images of (a) HMS; (b) A-HMS; (c) M-HMS; (d) SBA-15; and (e) Large pore SBA-CHX

4.7 NITROGEN AND SULFUR CONTENTS OF A-HMS AND M-HMS

The functionalization of organosilanes on HMS was further quantitively indentify nitrogen and sulfur composition by elemental analysis. Autoclave digestion by potassium persulfate in alkaline condition was conducted for nitrogen quantitative analysis of A-HMS. The sulfur analyzer technique was applied for sulfur quantification. The quantification of organosilanes revealed that the amine group content of A-HMS was equal to 9.037 $\mu mol_N\ m^{-2}$ (3.315 wt%) and the sulfur content of M-HMS was 2.554 $\mu mol_S\ m^{-2}$ (7.47 wt.%), confirming the presence of amine- and mercapto- functional groups on the surface of A-HMS and M-HMS, respectively, which is consistent with the FT-IR spectra (Figure 4.3).

4.8 SURFACE CHARGE DENSITY OF ADSORBENTS

An acid/base titration technique was used to determine the surface charge per square meter of adsorbents. The ionic strength (IS) was fixed at 10 mM by NaCl solution. After equilibrium, the pH of solutions was measured and calculated the surface charge density as Equation 3.2 (see Chapter 3).

The surface charge density, as Coulombs m^{-2}, of the parental HMS, the four functionalized HMS derivatives, SBA-15, NaY and PAC *vs*. the pH are plotted in Figure 4.8a and are summarized in Table 4.3. As seen, the surface charge density decreases as increasing the pH from acidic region to basic region. Theoretically, the silanol and organic functional groups are ionizable under different pH, resulting in a surface charge variation at different pH values. At low pH, the surface sites of HMSs were protonated leading to positively charged surfaces; whereas the surface hydroxides lose their protons at high pH values, and so resulted in negatively charged surfaces (Yu et al., 2008; Punyapalakul et al., 2009). The pH_{PZC} of the parental HMS and Ti-HMS were in the range of 4.5 to 5.0 whilst that of OD-HMS was found to shift slightly towards lower charged value (~4.0). On the other hand, A-HMS and M-HMS exhibited higher pH_{PZC} (9.5 and 6.2, respectively) due to the protonation of the amine- and mercapto-groups, respectively, which undergo protonation at low / moderate pH values. Moreover, the pH_{PZC} of SBA-15, NaY and PAC were 4.8, 7.8, and 9.5, respectively.

Surface charges of the parental SBA-CHX and surfactant-modified SBA-CHX; denoted as PG-SBA-CHX, were measured by zeta potential analyzer. Figure 4.8b shows the zeta potential *vs.* pH values. It can be seen that the pH_{PZC} of parental SBA-CHX and PG-SBA-CHX were 3.5 and 9.6, respectively. The higher pH_{PZC} of PG-SBA-CHX after surface modification reflected the bilayer formation of positively charged PG surfactant resulted in a charge reversal on the external surface of the parental SBA-CHX from negatively to positively charged surfaces.

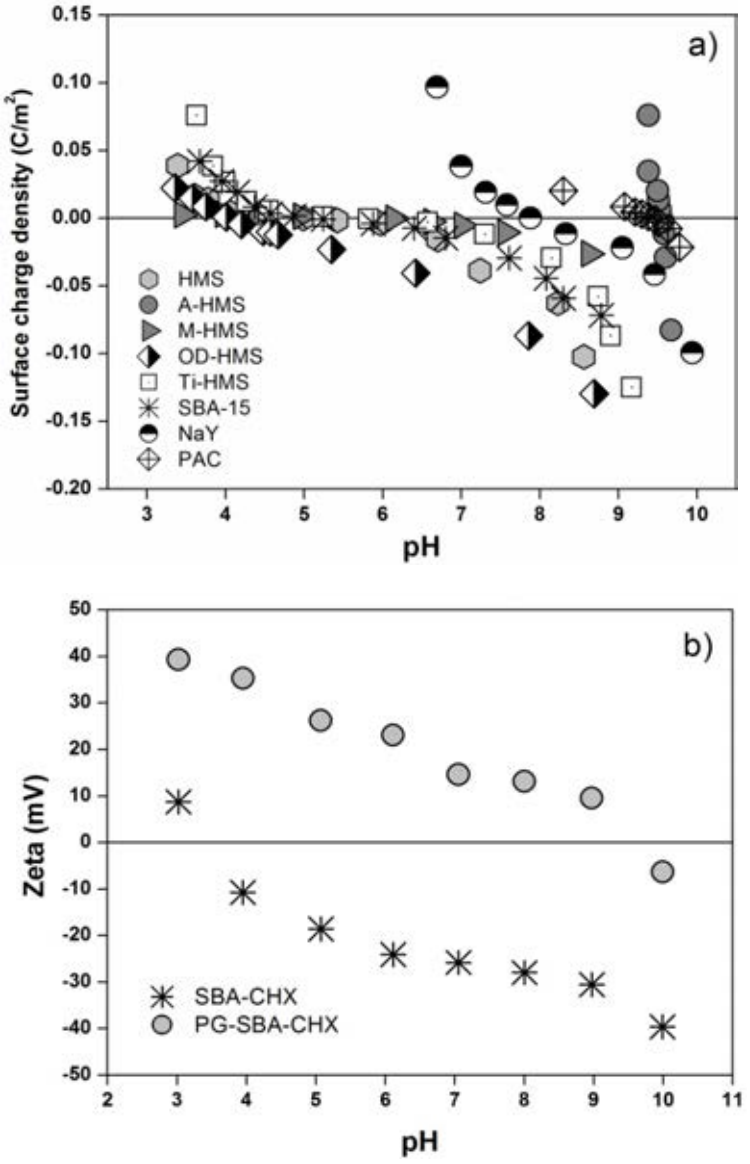

Figure 4.8 Surface charges of the adsorbents as a function of pH solution (a) HMS, functionalized HMS derivatives, SBA-15, NaY and PAC (Acid-Base titration method); and (b) SBA-CHX and PG-SBA-CHX (Zeta potential measurement)

4.9 HYDROPHOBICITY OF ADSORBENTS

Hydrophilic/hydrophobic surface characteristics were reflected by the water affinity of the adsorbents. In this study, the adsorbents were analyzed for contact angle (θ) by using a tensiometer (powder contact angle mode) and are summarized in Table 4.3. In general, the smaller the contact angle is, the greater the adsorbent surface exhibits hydrophilic character. As results, the hydrophobic surface characteristics were ranked in order of OD-HMS > M-HMS > PG-SBA-CHX > PAC

> HMS > SBA-15 > A-HMS > SBA-CHX > Ti-HMS > NaY. Among the hydrophobic surface adsorbents, OD-HMS exhibited the highest hydrophobic character which agrees with an aliphatic long chain structure of octyl group. The water contact angle attained from the M-HMS adsorbent was similar to that of the OD-HMS, but significantly larger than that for PAC (Table 4.3). Thus, PAC is more hydrophilic than either M-HMS or OD-HMS. Furthermore, the water contact angle PG-SBA-CHX adsorbent ($\theta = 80.45^{o}$) was significantly larger than unmodified SBA-CHX ($\theta = 32.56^{o}$). The hydrophobic character of PG-SBA-CHX was due to the long alkyl chain of hydrophobic tail of PG surfactant.

For hydrophilic surface adsorbents, it can be observed that the functionalized HMS derivatives (A-HMS, and Ti-HMS) were more hydrophilic than the parental HMS. It might be caused that amine group and Lewis acid sites are stronger acidity than weak acidic silanol group of pure silica-based HMS and SBA-15, therefore; they are more easily interacted with water molecules than silanol group resulted in higher hydrophilic surface characteristics. Interestingly, the water contact angle of SBA-15 and SBA-CHX were quite different. This result implies that pore expansion did not only modify the porous structure but also the surface characteristic was also changed.

Table 4.3 The pH_{PZC} and water contact angle of HMS, functionalized HMS derivatives, SBA-15, SBA-CHX, PG-SBA-CHX, NaY and PAC

Adsorbents	Functional groups	pH_{PZC}	Water contact angle (degree)
HMS	Silanol	4.5-5.0[a]	45.06
Ti-HMS	Lewis acid site and silanol	4.7[b]	30.90
A-HMS	Amine and silanol	9.5[a]	40.18
M-HMS	Thiol and silanol	6.2[a]	89.65
OD-HMS	Octyl and silanol	4.0[b]	89.83
SBA-15	Silanol	4.8	44.19
SBA-CHX	Silanol	3.5	32.56
PG-SBA-CHX	Cationic surfactant and silanol	9.6	80.45
NaY	Na^{+}, Lewis acid site and silanol	7.8[a]	20.43
PAC	Carboxyl, phenyl and oxygen-containing groups	9.5[a]	58.34

[a] Reference: Punyapalakul et al., (2009)

[b] Reference: Punyapalakul and Takizawa (2006)

4.10 CONCLUSIONS

Functionalization of hexagonal mesoporous silicate (HMS) was carried out by direct co-condensation method of TEOS and 3-aminopropyltriethoxysilane, and 3-mercaptopropyltrimethoxysilane, by post-grafting method for *n*-octyldimethysilane, and by incorporating titanium into silicate structure. Similar mesoporous structure SBA-15 was synthesized and modified by pore expansion using cyclohexane as swelling agent. Obtained large pore mesoporous SBA-CHX was modified surface by polymerizable cationic gemini surfactant. These synthesized materials were extensively characterized using a number of physical and chemical techniques. From results, X-ray powder diffraction (XRD) patterns and nitrogen adsorption isotherm results showed different levels of disorder of the mesopore structures upon incorporation of the functional groups, which are dependent upon the type of organosilanes present in the synthesis mixtures. Elemental analysis data and FT-IR spectra demonstrated the presence of the functional groups and PG surfactant coverage on the adsorbent surface, including polymerization degree. Surface characteristic of adsorbents, i.e. surface charge and hydrophilic/hydrophobic characteristic, were changed after surface modification with organosilanes and surfactant. The physicochemical characteristics of adsorbents are summarized in Table 4.4.

Table 4.4 Physicochemical characteristics of the synthesized adsorbents

Adsorbents	Surface functional groups	Mean pore diameter (nm)	S_{BET} (m^2/g)	V_P (mm^3/g)	pH_{PZC}	Density of functional group (µmol /m^2)	Contact angle (degree)	Surface characteristic
HMS	Silanol	2.60	712	773	4.5-5	-	45.06	Hydrophilic
A-HMS	Amine, Silanol	3.95	262	147	9.5	9.04	40.18	Hydrophilic
M-HMS	Mercapto, Silanol	2.48	912	433	6.2	2.55	89.65	Hydrophobic
OD-HMS	Octyl, Silanol	2.36	476	499	4.0	-	89.83	Hydrophobic
Ti-HMS	Lewis acid site, Silanol	3.18	766	1276	4.7	-	30.90	Hydrophilic
SBA-15	Silanol	6.00	981	654	4.8	-	44.19	Hydrophilic
SBA-CHX	Silanol	23.41	448	766	3.5	-	32.56	Hydrophilic
PG-SBA-CHX	Cationic surfactant, silanol	-	-	-	9.6	-	80.45	Hydrophobic
NaY	Na^+, Lewis acid site, Silanol	0.74	653	326	7.8	-	20.43	Hydrophilic
PAC	Carboxyl, and others	1.90	980	276	9.5	-	58.34	Hydrophobic

CHAPTER V

ADSORPTION KINETICS AND INTRAPARTICLE DIFFUSION MECHANISM

5.1 INTRODUCTION

The kinetic of adsorption describes the rate of adsorbate uptake on the adsorbent and rate limiting step, which controls the equilibrium time. Kinetic parameters are helpful for the prediction of adsorption rate which gives important information for design and modeling the process. In addition, adsorption mechanism bases on diffusion mass transfer processes, which depends on the property of the adsorbate and adsorbent, including the experimental conditions (temperature and pH value).

Towards a better understand of the adsorption mechanism, thus the purpose in this study focused on the analysis of the kinetics of adsorption process. Three different adsorption kinetic models, i.e. pseudo-first-order, pseudo-second-order, and intraparticle diffusion models, were employed to determine the adsorption order and rate constant of the adsorption process between DCAN molecule and synthesized adsorbents in aqueous solution. The parental HMS and organic-functionalized HMS derivatives (A-HMS, OD-HMS, and M-HMS) were performed to investigate the effect of surface functional group on DCAN adsorption kinetic, along with PAC. Moreover, similar mesoporous structure of pure silica HMS and SBA-15, and one metal substitution by incorporating titanium into silicate structure (Ti-HMS) compared with micropore NaY were employed to investigate the role of porous and crystalline structures on the adsorption. The experimentally derived data were fitted with adsorption kinetic models and kinetic parameters were calculated to determine the likely adsorption mechanism.

5.2 DICHLOROACETONITRILE (DCAN) ADSORPTION KINETICS

5.2.1 Effect of Surface Functional Group

Kinetic curves for DCAN adsorption on the porous adsorbents are shown in Figure 5.1. Note that the data for DCAN adsorption on PAC and M-HMS are plotted with a different Y-axis scale to the others due to the much higher (ca. 2300- to 4600-fold) adsorption capacities. A large amount of DCAN was adsorbed over PAC and M-HMS, but with PAC the equilibrium was reached within a short contact time (1 h) whereas with M-HMS it did not reach equilibrium but tended towards it at 36 - 48 h and was half maximal at ~5 h. In accordance, the acrylonitrile adsorption on PAC was reported to take about 1 h to attain equilibrium at an initial concentration of 100 mg L^{-1} (Kumar et al., 2008). For HMS and OD-HMS, the amount of adsorbed DCAN reached the equilibrium stage at approximately 18 h. Interestingly, the kinetic curves of M-HMS and A-HMS both showed a multi-step biphasic adsorption process. M-HMS reached to equilibrium plateau at 36 h whereas A-HMS was without reaching the equilibrium in the 48 h period (equilibrium time ca. 60 h). This is probably related to their low degree of pore order and wide pore size distribution, as reflected by the XRD results (see Figure 4.1 in Chapter 4).

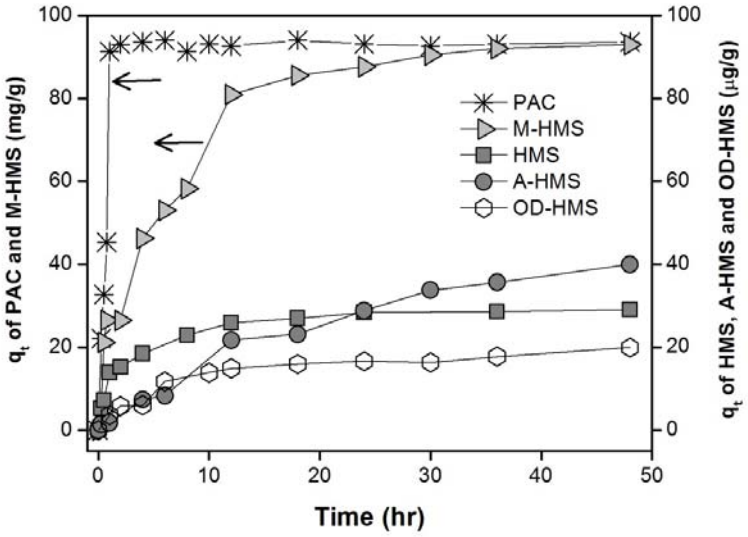

Figure 5.1 DCAN adsorption kinetics of PAC and M-HMS at 50 mg L^{-1}, and HMS, A-HMS and OD-HMS at 100 μg L^{-1}

Kinetic modeling not only allows an estimation of the adsorption rate but also explains characteristics of the possible adsorption mechanism. In this respect, pseudo-first-order and pseudo-second-order models were employed to investigate the

likely adsorption mechanism by fitting the experimental data obtained from the batch experiment.

The pseudo-first-order equation can be represented as given in Equation (5.1):

$$q_t = q_e(1 - exp^{(-k_1 t)}) \qquad (5.1)$$

where q_t and q_e are the amount of DCAN adsorbed at any given time (t) and at equilibrium (μg g^{-1}), respectively, and k_1 is the first order rate constant (h^{-1}).

The pseudo-second-order equation is given by Equation (5.2):

$$q_t = \frac{q_e^2 k_2 t}{1 + q_e k_2 t} \qquad (5.2)$$

where k_2 is the rate constant for pseudo-second order adsorption (g μg^{-1} h^{-1}).

In order to measure the adsorption rate, the initial adsorption rate, h (μg g^{-1} h^{-1}) at t = 0, and the half-life time, $t_{1/2}$ (h), can be determined according to Equations (5.3) and (5.4), respectively:

$$h = k_2 q_e^2 \qquad (5.3)$$

$$t_{1/2} = \frac{1}{k_2 q_e} \qquad (5.4)$$

A normalized standard deviation $\triangle q$ (%) was employed in this study to find out the most suitable kinetic model in fitting to the data. This error function has been used previously by the number of researchers in the adsorption study (Gűnay et al., 2007; Qin et al., 2009; Shaarani and Hameed, 2011), is given as shown in Equation (5.5):

$$\Delta q(\%) = 100\, x \sqrt{\frac{\sum\left[\frac{q_{exp} - q_{cal}}{q_{exp}}\right]^2}{N-1}} \qquad (5.5)$$

where N is the number of data points, and q_{exp} and q_{cal} (μg g^{-1}) are the experimental and the calculated adsorption capacities, respectively. The best-fit models should have the least $\triangle q$ (%) values.

The kinetic parameters, the correlation coefficients (R^2) and $\triangle q$ (%) from the nonlinear equation for the pseudo-first-order and pseudo-second-order models, were calculated using the ORIGIN version 8.0 software and the results are shown in Table 5.1. Both models provided high and significant R^2 values, but these were not significantly different between the two models although numerically those from the pseudo-second order rate model had slightly higher R^2 values than those from the pseudo-first rate model. However, the $\triangle q$ (%) of the pseudo-second-order model was significantly smaller, regardless of the adsorbents, compared with those of the pseudo-first-order model.

The adsorption mechanism on adsorbent surface should be proportional to the driving force and area of adsorbent. In this study, the driving force is the adsorbate concentration in the solution, and the area is the amount of active sites on the adsorbent surface. Due to at a low concentration of DCAN in this study, the effect of water on adsorption mechanism essentially can be excluded. Therefore, the pseudo-second-order model is more suitable to describe the adsorption kinetics of DCAN on these porous adsorbents at a low solute concentration. Consistent with this notion is that Wu et al. reported that the pseudo-second order model was suitable to explain the adsorption of low molecular weight compounds on small adsorbent particles (Wu et al., 2009). Regardless, the initial adsorption rate (h) followed the order of PAC > M-HMS > HMS > OD-HMS > A-HMS.

Considering the pseudo-second-order kinetic parameters by comparison between the parental HMS, A-HMS and OD-HMS, it was observed that amino-functionalized HMS (A-HMS) had quite lower values of the initial adsorption rate (h) and the half-life time ($t_{1/2}$) than those for the two adsorbents. This might be caused by an increasing of liquid film thickness surrounding the adsorbent particle due to its high hydrophilicity. Indeed, the surface functional group not only plays a key factor on adsorption rate but also the characteristic of porous structure of adsorbent, i.e. pore size and pore volume, would be concerned. The effect of porous and crystalline structure on adsorption kinetic was more discussed in detail as described in Section 5.5.2.

Table 5.1 Kinetic parameters of DCAN adsorption on HMS, three functionalized HMS derivatives, and PAC adsorbents

Adsorbents	$q_{e,exp}$	Pseudo-first-order				Pseudo-second-order					
	($\mu g\ g^{-1}$)	$q_{e,cal}$ ($\mu g\ g^{-1}$)	k_1 (h^{-1})	R^2	$\triangle q$ (%)	$q_{e,cal}$ ($\mu g\ g^{-1}$)	k_2 ($g\ \mu g^{-1}h^{-1}$)	R^2	$\triangle q$ (%)	h ($\mu g\ g^{-1}h^{-1}$)	$t_{½}$ (h)
PAC[a]	94,060	94,025	1.283	0.984	1.782	98,604	19.27	0.999	0.035	170,490	0.55
M-HMS[a]	95,030	91,311	0.178	0.960	2.900	102,430	2.46	0.972	0.162	22,210	4.37
HMS[b]	29.10	26.87	0.452	0.942	4.398	29.29	0.0213	0.962	2.008	18.06	1.61
A-HMS[b]	73.45[C]	75.79	0.021	0.988	0.815	75.83	0.0003	0.989	0.451	0.67	45.38
OD-HMS[b]	18.94	17.53	0.156	0.970	1.677	20.68	0.0086	0.973	0.202	3.09	6.13

[a] Initial DCAN concentration was 50 mg L^{-1}
[b] Initial DCAN concentration was 100 μg L^{-1}
[c] $q_{e,\,exp}$ of A-HMS was obtained by prolonging the contact time to 72 h, and equilibrium time was 60 h.

5.2.2 Effect of Porous and Crystalline Structures

The kinetic curves of the DCAN adsorption on the porous materials, as plot of the relative adsorption capacity (q_t) versus time, are shown in Figure 5.2. The DCAN uptake by all four adsorbents (HMS, Ti-HMS, SBA-15 and NaY) was rapid at the beginning (within the first 4 h) and reached the equilibrium stage after ca. 18 h. However, the amount of adsorbed DCAN (q_t) varied between the four adsorbents being highest for HMS followed by NaY > Ti-HMS > SBA-15. To describe the adsorption phenomena, the experimental data obtained from the batch experiment were fitted with the pseudo-first order and pseudo-second order equations. The correlation coefficients (R^2) and $\triangle q$ (%), from the nonlinear regression were calculated and the results are shown in Table 5.2.

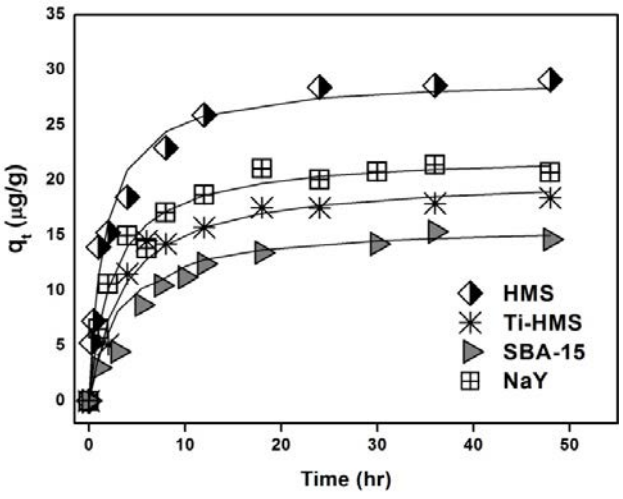

Figure 5.2 DCAN adsorption kinetics of HMS, Ti-HMS, SBA-15 and NaY at 100 μg L^{-1} (pH 7 and IS 10 mM)

The fitting results show that the pseudo-second order model gave a better fit to the data, as defined by the higher R^2 and significantly smaller $\triangle q$ (%), than the pseudo-first order model. As discussed above, the effect of water can be classified as a control due to at a low concentration of DCAN in this study. Therefore, the pseudo-second order model is more suitable to describe the adsorption kinetics of DCAN on these porous adsorbents at a low solute concentration.

Comparison between mesopore HMS and micropore NaY, the pseudo-second order rate constant (k_2) value obtained was highest for HMS, followed by that for NaY, and so a higher amount of HMS sample is needed to adsorb a given amount of DCAN. In other word, it can be concluded that overall NaY has a better adsorption performance (i.e. adsorption capacity and adsorption rate) for DCAN. Nevertheless, the initial adsorption rate (h) and the half-life time ($t_{1/2}$) of HMS was 2.13–fold higher and 1.56-fold lower, respectively, than that for NaY. Thus, NaY requires almost twice the time to achieve two-thirds the maximal level of DCAN uptake at the equilibrium stage, compared with that seen with HMS. Traditionally, the adsorption rate of porous material is related to the porous structure of the adsorbents (Ruiz et al., 2010), and so the different adsorption behavior of HMS and NaY might be caused directly by the intrinsic characteristic of their porous structures. HMS has a much larger (3.51-fold) pore size and higher (2.37-fold) total pore volume (see Table 4.2 in Chapter 4) than NaY, which certainly favors a quicker initial adsorption rate. The molecular dimension of DCAN, as calculated by the ACD/ChemSketch software, is 0.29 and 0.36 nm in width and length, respectively, and so the pore size clearly did not affect the accessibility of DCAN to the inner pores of the micropore NaY adsorbent.

For comparison of the h values between HMS and Ti-HMS, Ti-HMS had a ~3.5-fold lower initial adsorption rate than that for HMS even though Ti-HMS has a 1.22-fold larger pore size and 1.65-fold larger total pore volume than HMS. This different in adsorption rate then might be because the surface of Ti-HMS is more hydrophilic than that of HMS, based on water contact angle results (Table 1). Water contact angle (θ) of HMS and Ti-HMS are 45.06 and 30.90, respectively, and so Ti-HMS particle can be surrounded by water molecules, causing a lower adsorption rate onto the Ti-HMS. Surprisingly, the initial adsorption rate (h) of the mesopore

SBA-15, with a pore size 6.0 nm, showed the lowest value, for which faster adsorption rate would have been expected. This is probably related to its pore feature which contains a combined micropore and mesopore structure within the hexagonally ordered mesopore structure.

Table 5.2 Kinetic parameters of DCAN adsorption on HMS, Ti-HMS, SBA-15 and NaY adsorbents

Adsorbents	$q_{e,exp}$	Pseudo-first-order				Pseudo-second-order					
	(μg g^{-1})	$q_{e,cal}$ (μg g^{-1})	k_1 (h^{-1})	R^2	$\triangle q$ (%)	$q_{e,cal}$ (μg g^{-1})	k_2 (g μg$^{-1}h^{-1}$)	R^2	$\triangle q$ (%)	h (μg $g^{-1}h^{-1}$)	$t_{½}$ (h)
HMS	29.10	26.87	0.452	0.942	4.398	29.29	0.021	0.962	2.008	18.06	1.61
Ti-HMS	18.41	17.86	0.225	0.968	0.852	20.33	0.015	0.979	0.063	4.75	3.88
SBA-15	15.35	15.06	0.113	0.978	2.361	18.29	0.007	0.984	1.304	1.53	7.81
NaY	21.39	20.29	0.289	0.958	1.595	22.36	0.018	0.982	0.068	8.50	2.52

5.3 INTRAPARTICLE DIFFUSION MECHANISM

The adsorption process over any porous adsorbent involves three consecutive mass transfer steps; (i) film or external diffusion, (ii) pore diffusion and (iii) adsorption at the site on the adsorbent surface. Any of these three steps can be the rate-limiting step. However, the final step is assumed to be rapid and so is usually omitted in the kinetic analysis.

The intraparticle diffusion model developed by Weber and Morris (1963) was also applied to investigate whether the adsorption process was limited by mass transfer within the film layer or by diffusion inside the adsorbent particles. The model can be defined as shown in Equation (5.6):

$$q_t = k_{iP} t^{0.5} + C \qquad (5.6)$$

where k_{iP} is the intraparticle diffusion rate constant (μg $g^{-1}hr^{-0.5}$) and C (μg g^{-1}) is a constant that gives an idea of the thickness of the boundary layer.

5.3.1 Effect of Surface Functional Group

The data-fitting curves (q_t versus $t^{0.5}$ relations) are shown in Figure 5.3. Note that since the HMS and OD-HMS adsorbents showed very similar adsorption kinetics, only the fitting curve for HMS is presented for simplicity. The q_t versus $t^{0.5}$ relations were found to display multi-linearity, indicating that multiple adsorption

steps are involved in the adsorption process. Similar behaviors have been reported for the retention of various molecules on mesoporous silicates (Wang and Wang, 2008; Qin et al., 2009; Tao et al., 2010). It can be seen that the adsorption over HMS (and OD-HMS, not shown) and M-HMS displayed three different regimes. The first regime represented the external mass transfer in the boundary layer while the second one was accounted for the diffusion of DCAN molecules through the pores of the adsorbent simultaneously with a gradual adsorption on the surface. Finally, the horizontal line at longer time points illustrated attaining the adsorption equilibrium. In the case of PAC, the boundary diffusion is not observed; the first linear regime can be reasonably correlated to the intraparticle diffusion. The adsorption of DCAN on A-HMS showed at least two phases but did not plateau out.

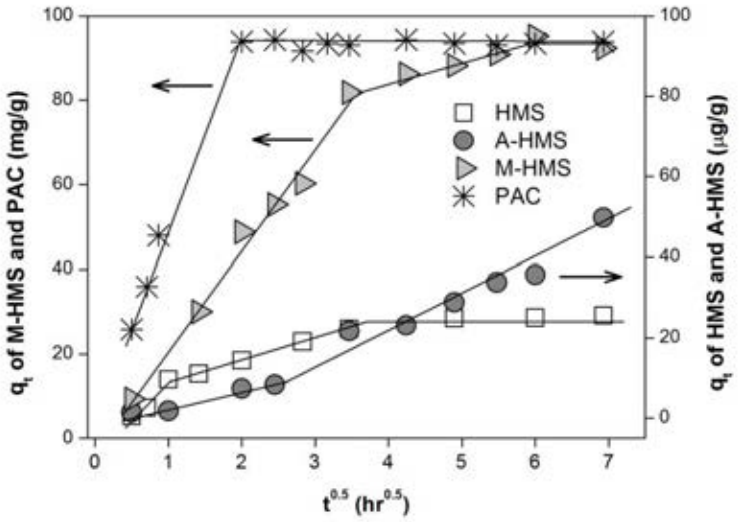

Figure 5.3 Plot of intraparticle diffusion model (Weber and Moris) for the adsorption of DCAN on HMS, A-HMS, M-HMS and PAC.

The external diffusion step occurring at initial period of adsorption process was measured by determining the rate constant (k_s) obtained from the slope of the first linear region where the larger value means the faster external diffusion. The rate constant of these adsorbents are listed in Table 5.3. Comparison between the parental HMS, A-HMS and OD-HMS, it can be seen that the order of the rate constant was OD-HMS > HMS > A-HMS. This is consistent with the level of hydrophobicity of the adsorbent surface, where the hydrophobic functional group might reduce the film resistance of water to mass transfer surrounding the adsorbent particle.

The intraparticle diffusion rate constant (k_{iP}) is determined from the slope of the second regime. The calculated values follow the sequence A-HMS > HMS > OD-HMS, and it implies that the pore size of the adsorbent might influence the adsorption rate. Due to the larger pore size of A-HMS, DCAN could diffuse into the pores more easily than the smaller pore size. Surprisingly, the intraparticle diffusion rate constant (k_{iP}) value of A-HMS, which would be expected to be a lower rate, was higher than film diffusion rate constant (k_s). The first stage was relatively slow which was shown that the existence of film diffusion was limited by a high hydrophilic surface characteristic of A-HMS (water contact angle = 40.18^o). The second stage was relatively fast and it might associate with the interaction of DCAN into the higher density adsorption sites (amino functional group) present in the pore of adsorbent. High affinity of amino functional group towards DCAN molecule could enhance the adsorption capacity and so the intrapaticle diffusion proceeded rapidly. Meanwhile, the gradient of diffusion occurred from bulk solution through interface layer might be changed resulted in a higher diffusion rate. Similar adsorption behavior has been reported as described by Cestari et al., (2006). They found that the red-dye uptake on aminopropyl-silica (Sil-NH_2) at 25 ^{o}C was slow at the initial period of time which was related to the occupation of the surface adsorption site.

Furthermore, the existence of a boundary layer effect for HMS, A-HMS and M-HMS, as indicated by the fact that the linear plot does not pass through the origin, suggesting that intraparticle diffusion is not the only rate-limiting step for DCAN adsorption.

Table 5.3 Intraparticle diffusion model parameters of DCAN adsorption on HMS, three functionalized HMS derivatives, and PAC adsorbents

Adsorbents	External diffusion	Intraparticle diffusion		
	k_s ($\mu g\ g^{-1}\ h^{-0.5}$)	k_{iP1} ($\mu g\ g^{-1}\ h^{-0.5}$)	Intercept (C_1)	R^2
PAC[a]	-	79,631	21,117	0.991
M-HMS[a]	24,949	5,205	62,875	0.977
HMS[b]	11.51	5.22	7.99	0.999
A-HMS[b]	3.97	8.33	11.10	0.961
OD-HMS[b]	14.29	1.82	18.00	0.975

[a] Initial DCAN concentration was 50 mg L^{-1}
[b] Initial DCAN concentration was 100 μg L^{-1}

5.3.2 Effect of Porous and Crystalline Structures

The q_t versus $t^{0.5}$ relations, are shown in Figure 5.4, display a differentiated linearity for all four adsorbents, indicating that multiple adsorption steps are associated in the adsorption process. The rate constant or intraparticle diffusion model on HMS, Ti-HMS, SBA-15, and NaY are summarized in Table 5.4.

In the first region, it can be seen that the external mass transfer is predominant at the initial of contact time. Comparing of the k_s values between silica-based mesoporous HMS and SBA-15 revealed, surprisingly, that the external diffusion rate of SBA-15 was 2.56-fold lower than that for HMS even though its pore size is larger. However, the external diffusion rate may be related to the particle size of the adsorbent. Because the ratio of external/internal surface area ratio of SBA-15, with its smaller particle, is larger than HMS with its larger particle size, this might make it difficult for the DCAN molecules to diffuse through the boundary layer.

The second region in Figure 5.4 represents the step at which the intraparticle diffusion starts to control the rate of adsorption. Here, the pore size of the adsorbent might influence the adsorption rate. Thus, for instance, the intraparticle diffusion rate constants (k_{iP1}) of the silica-based mesoporous adsorbents (i.e. HMS, Ti-HMS and SBA-15) were higher than that of the microporous NaY (Table 5.4). Consequently, DCAN can diffuse more easily in the larger pore size of mesoporus material than in the smaller pore size of NaY. Moreover, it can be seen that SBA-15 had four apparent mass transfer steps in the adsorption process, where the second region of the plot seems to refer to as the diffusion into the wider mesopores and, for the third region with the lowest slope, the adsorption into narrow micropores.

As seen, the existence of a boundary layer effect was appeared in all adsorbents as indicated by the linear plot does not pass though the origin, suggesting that intraparticle diffusion was not the only rate-controlling step for DCAN adsorption.

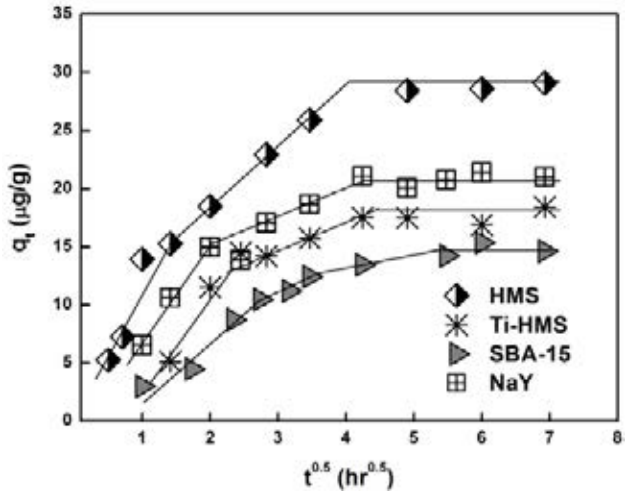

Figure 5.4 Plot of intraparticle diffusion model (Weber and Moris) for the adsorption of DCAN on HMS, Ti-HMS, SBA-15 and NaY

Table 5.4 Intraparticle diffusion model parameters of DCAN adsorption on HMS, Ti-HMS, SBA-15, and NaY adsorbents

Adsorbents	External diffusion	Intraparticle diffusion					
	k_s (µg $g^{-1}h^{-0.5}$)	k_{iP1} (µg $g^{-1}h^{-0.5}$)	C_1	R^2	k_{iP2} (µg $g^{-1}h^{-0.5}$)	C_2	R^2
HMS	11.506	5.219	7.985	0.999	-	-	-
Ti-HMS	9.183	2.326	7.646	0.918	-	-	-
SBA-15	4.490	2.653	3.083	0.944	0.867	9.552	0.961
NaY	7.433	2.295	9.493	0.997	-	-	-

5.4 CONCLUSIONS

In order to determine the most appropriate adsorption kinetic of the synthesized adsorbents, the experimental data were substituted to three kinetic models, i.e. pseudo-first-order, pseudo-second-order and intraparticle diffusion equations. The kinetic parameters and the best-fit model equation were identified based on the correlation coefficient (R^2) and the normalized standard deviation $\triangle q$ (%) values. The pseudo-second order model can be used to describe the adsorption kinetic of DCAN onto the synthesized adsorbents at a low solute concentration. The kinetic results were implied that the adsorption process was dependent on both the boundary layer effect and the intraparticle diffusion. Hydrophobic surface characteristic of adsorbent could reduce the film resistance of water to mass transfer surrounding the adsorbent particle. DCAN could diffuse more rapidly in a larger pore size of mesoporous materials that micropore zeolite.

CHAPTER VI

ADSORPTION ISOTHERMS, EFFECTS OF pH AND TEMPERATURE, AND MECHANISM OF ADSORPTION

6.1 INTRODUCTION

This study investigated the effects of the surface functional group, porosity and crystalline structures on the haloacetonitrile (HANs) adsorption efficiencies and mechanisms over inorganic porous materials, compared with powdered activated carbon (PAC). In order to determine the adsorption mechanism, two parameters of isotherm equations (Langmuir and Freundlich isotherm models) and three parameters (Sips isotherm model) were employed to determine the adsorption mechanism at high concentration of organic adsorbates whereas the Linear adsorption isotherm was also performed for HAN adsorption at low concentration (ppb level). In addition, the effects of pH and temperature on adsorption capacity were also investigated. Thermodynamic parameter as the change in free energy, enthalpy, and entropy of adsorption were also estimated. Towards a better understand of the adsorption mechanism, the adsorptive interactions between surface functional groups of adsorbents and HAN molecular structures were determined from Fourier-transform infrared (FT-IR) spectroscopy analysis.

6.2 ADSORPTION ISOTHERMS OF FIVE-HANs IN SINGLE SOLUTE SOLUTION

6.2.1 Effect of Surface Functional Group

Comparison on the effect of the different surface functional groups of the HMS derivatives on the five-HANs adsorption capacities, i.e. MCAN, DCAN, TCAN, MBAN and DBAN, at pH 7 is shown in Figure 6.1. Note that the data for HAN adsorption on PAC and M-HMS are plotted with a different Y-axis scale to the others due to the much higher adsorption capacity. To exclude the effect of differences in surface area between adsorbents, the adsorption capacities of the adsorbents were normalized for the surface area and are presented accordingly as μg m^{-2} for HMS, A-HMS and OD-HMS, and mg m^{-2} for M-HMS and PAC. Here,

M-HMS adsorbed the four HANs (i.e. MBAN, DCAN, DBAN, and TCAN) far more effectively than the parental HMS and the other two functionalized-HMS derivatives, excepted for MCAN.

Table 6.1 shows the molecular structure of five-HANs and charge distribution calculated by minimum energy optimization using MOPAC. Even though HAN adsorbates are neutral molecules, however, the positive and negative dipole in each atom can interact with surface functional groups via electrostatic interaction. As revealed in Figure 4.8 and Table 4.3 in Chapter 4, the surface of M-HMS exhibited a moderately negative charge at pH 7 (pH_{PZC} = 6.2), and so the mercapto-groups as well as the remaining silanol groups were ionized and so the HAN molecules were electrostatically adsorbed. Moreover, this result suggested that the hydrophobic surface (M-HMS, see below for OD-HMS) facilitated a higher adsorption capacity than the hydrophilic one (HMS and A-HMS) by probably reducing the competitive adsorption between water and HAN onto the adsorbents. Recently, Punyapalakul et al. (2009) pointed out that both electrostatic and hydrogen bonding interactions were interfered with by the presence of water especially at low concentrations of the adsorbate. In contrast, the hydrophobic OD-HMS adsorbent showed a lower adsorption performance even though its surface hydrophobicity was similar to M-HMS, as reflected by the contact angle (θ), OD-HMS (θ) = 89.83^{o} and M-HMS (θ) = 89.65^{o}, respectively. Hence, the much higher HAN adsorption capacity of M-HMS should be ascribed to the combination of its hydrophobic surface and ionizable mercapto-groups promoting the ion-dipole interaction, whereas the protonation / deprotonation of the octyl groups on OD-HMS surface cannot occur.

With respect to HMS, its negative surface charge could contribute to ion-dipole electrostatic interactions towards HAN adsorption at pH 7. However, that the observed adsorption capacity of HMS for HAN was lower than that for M-HMS might be caused by active surface competition between HANs and water molecules. Along these lines, Pan and Jaroniec (1996) reported that water molecules can be adsorbed onto the surface oxygen groups by hydrogen bonding. In our case study, the hydrophobic mercapto-groups can weaken the competition of water in aqueous solution and so result in the adsorption of HANs.

A-HMS presents a positive charge surface over the pH range used in this study due to protonation of the amino group. Since HANs contains N-atom with one pair of electrons and a high electronegativity (negative dipole), HANs can be electrostatically adsorbed onto the positively charge surface thus A-HMS had a much higher HAN adsorption capacity than that for the parental HMS and the octyl-functionalized HMS derivative (OD-HMS). These results strongly support the effects of the surface functional group of HMS derivatives on HAN adsorption.

Additionally, it was observed that the adsorption capacities of di-HANs and tri-HAN on the parental HMS and OD-HMS (excepted for A-HMS) were less than that of mono-HANs while the adsorption of five-HANs on M-HMS displayed a reversed behavior. It suggests that the adsorption capacities are likely to be related to the molecular structure of HANs, i.e. halogen atom type and degree of substitution (more discussion in Chapter 7: Adsorption selectivity).

The adsorption capacities of the five-HANs on M-HMS compared with PAC are shown in Figure 6.2. Interestingly, M-HMS was only the functionalized silica-based material that had a comparable adsorption capacity to PAC for HANs. As seen, the adsorption capacities of MCAN, MBAN and TCAN on M-HMS were higher than that for PAC whereas DCAN and DBAN adsorption capacities had slightly less than. The considerably higher adsorption capacity of PAC for di-HANs was probably caused by its heterogeneous surface that consists of various organic functional groups (Kumar et al., 2008; Tsai et al., 2008).

Table 6.1 Molecular structure of five-HANs and charge distribution

Molecular structure	Charges [a]									
	MCAN		MBAN		DCAN		DBAN		TCAN	
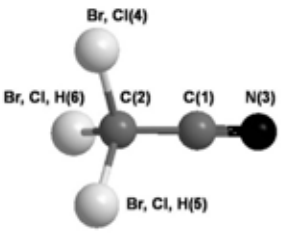	C(1)	-0.1304	C(1)	-0.1205	C(1)	-0.1254	C(1)	-0.1089	C(1)	+0.1136
	C(2)	-0.1323	C(2)	-0.2513	C(2)	-0.0239	C(2)	-0.2460	C(2)	-0.1298
	N(3)	-0.0537	N(3)	-0.0542	N(3)	-0.0177	N(3)	-0.0219	N(3)	-0.0027
	Cl(4)	-0.0838	Br(4)	+0.0094	Cl(4)	-0.0362	Br(4)	+0.0633	Cl(4)	+0.0044
	H(5)	+0.2002	H(5)	+0.2083	Cl(5)	-0.0364	Br(5)	+0.0632	Cl(5)	+0.0044
	H(6)	+0.2002	H(6)	+0.2083	H(6)	+0.2399	H(6)	+0.2504	Cl(6)	+0.0048

[a] Calculated by ChemOffice Ultra 2005.

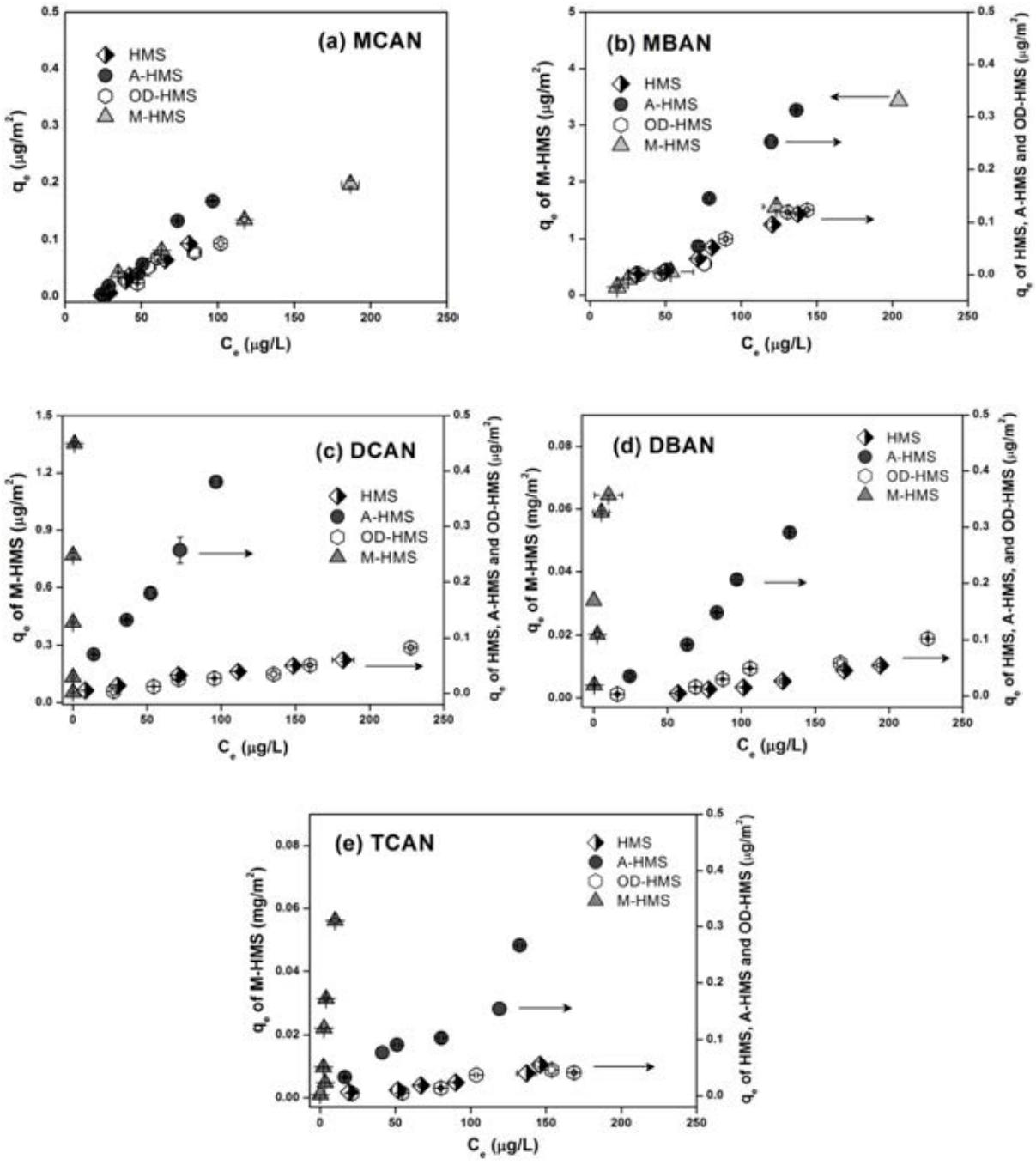

Figure 6.1 Effect of surface functional group on adsorption of HANs on HMS, A-HMS, OD-HMS and M-HMS at pH 7 with IS 10 mM (25 ^{o}C); (a) MCAN; (b) MBAN; (c) DCAN; (d) DBAN; and (e) TCAN

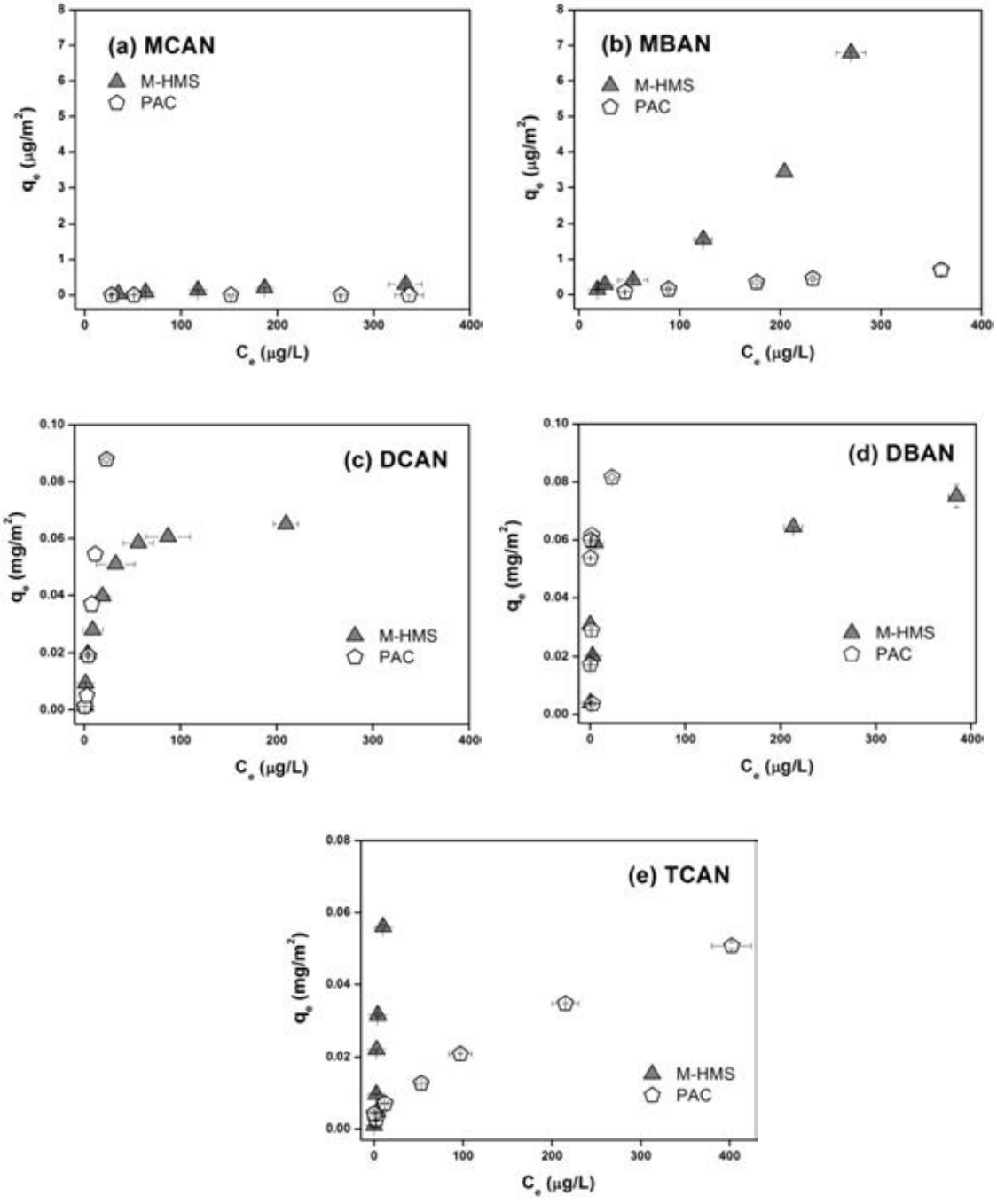

Figure 6.2 Comparison of adsorption capacities of five-HANs between M-HMS and PAC at pH 7 with IS 10 mM (25 ^{o}C); (a) MCAN; (b) MBAN; (c) DCAN; (d) DBAN; and (e) TCAN

6.2.2 Effect of Porous and Crystalline Structures

Comparison on the effect of porous and crystalline structures of adsorbents on the five-HANs adsorption capacities at pH 7 is shown in Figure 6.3. As seen in Figure 6.3(a) and (b) of MCAN and MBAN adsorption, respectively, Ti-HMS had the highest adsorption capacities of both mono-HANs (MCAN and MBAN). Of the three mesoporous adsorbents, although HMS had a somewhat similar mean pore size to Ti-HMS, the observed adsorption capacities of MCAN and MBAN were slightly and significantly lower, respectively, for HMS than that for Ti-HMS. This is probably due to the significantly higher pore volume of Ti-HMS, as determined by N_2 adsorption (Table 4.2 in Chapter 4). Thus, the accessibility of the mono-HANs molecules to the internal pores of Ti-HMS is better than that for HMS leading to a higher adsorption capacity. In addition, the Lewis acid site on the Ti-HMS surface, is a stronger acid than the weak acidic silanol group in the pure silica-based HMS and SBA-15, and so could enhance the adsorption capacity by the synergic adsorption of both surface functional groups. Previous reports have found that the active Lewis and Brönsted acid sites can promote adsorption by interacting with the nitrile (C≡N) and nitroso (N=NO) groups in the adsorbate molecules (Busca et al., 2008; Dai et al., 2009). Thus, the surface functional group of the adsorbent also plays an important role on adsorption.

However, the mesopore SBA-15 showed the lowest adsorption capacity of all four adsorbents for the two mono-HANs, compared with the other adsorbents (Fig. 5(a) and (b)). The negative surface charge derived from dissociation of silanol groups could contribute to the electrostatic interaction with the ion-dipole of the HANs and thus HAN adsorption. The significantly larger mean pore size (6.0 nm) of SBA-15 might reduce its ability to confine smaller sized adsorbates, such as these two mono-HANs. A similar result has been reported previously where the adsorption capacity of nitrosamine on SBA-15 was lower than on the smaller (2.22-fold) pore diameter of MCM-41 (2.7 nm) (Wei et al., 2009). Thus, the pore size is clearly likely to be a key factor controlling the mono-HANs adsorption.

In the case of NaY, the positively charged surface is due to the combination of the protonated silanol group, Lewis acid sites and the Na-cation at pH 7. Since the

N-atom (N3) of each HAN possesses a negative dipole, they can be electrostatically adsorbed onto the positively charged surface such as Na-cation of NaY. As seen, the adsorption of the mono-HANs exhibited a comparable adsorption capacity to that for HMS and Ti-HMS (excepting for the adsorption of MBAN that was less than Ti-HMS), although NaY has a relatively low surface area and pore volume (see Table 4.2 in Chapter 4). The adsorption capacities of mono-HANs on NaY may relate to the strength of the negative dipole of N-atom in the respective mono-HANs molecules. The two H-atoms of the mono-HANs provide the strongest negative dipole of N-atom (Table 6.1) which could be electrostatically attracted with Na-cation and Lewis acid site of NaY leading to a high adsorption capacity. Another one possible explanation for these results is that the small pore size (0.74 nm) and crystalline structure of NaY could be effective in retaining the mono-HANs. In this scenario, the crystalline structure and narrow diameter pore size (micropores) of zeolite NaY provides a delicate geometric confinement of small adsorbate molecules (Zhou and Zhu, 2005), and so suggests that the crystalline structure of the adsorbent can affect the adsorption capacity of mono-HANs.

The adsorption capacities of the di-HANs (DCAN and DBAN) on the four adsorbents (Figure 6.3(c) and (d)) were less than that of the mono-HANs, whereas, in contrast, SBA-15 showed a slightly higher capacity. However, the adsorption capacities are likely to be related to the molecular structure of the HANs in term of the amount of halogen atoms in the molecule and their molecular weight, as will be discussed in Chapter 7. Moreover, that the adsorption capacity of DBAN is higher than DCAN might be because of the stronger positive dipole of the H-atom in DBAN.

The TCAN adsorption isotherm (Figure 6.3e) showed the adsorption capacity followed the sequence Ti-HMS > NaY > SBA-15 > HMS and suggests that the Lewis acid sites of Ti-HMS and the Na-cation of NaY significantly influenced the adsorption capacities. According to the charge distribution of TCAN molecule (see Table 6.1), the positive and negative dipoles in TCAN molecule displayed the weak dipoles; however its structure has one pair of electrons with high electronegativity. Thus, the Lewis acid sites and Na-cation could interact with the lone pair of TCAN molecule leading to higher adsorption capacity. This supports the notion that the surface functional group plays a crucial role in HAN adsorption.

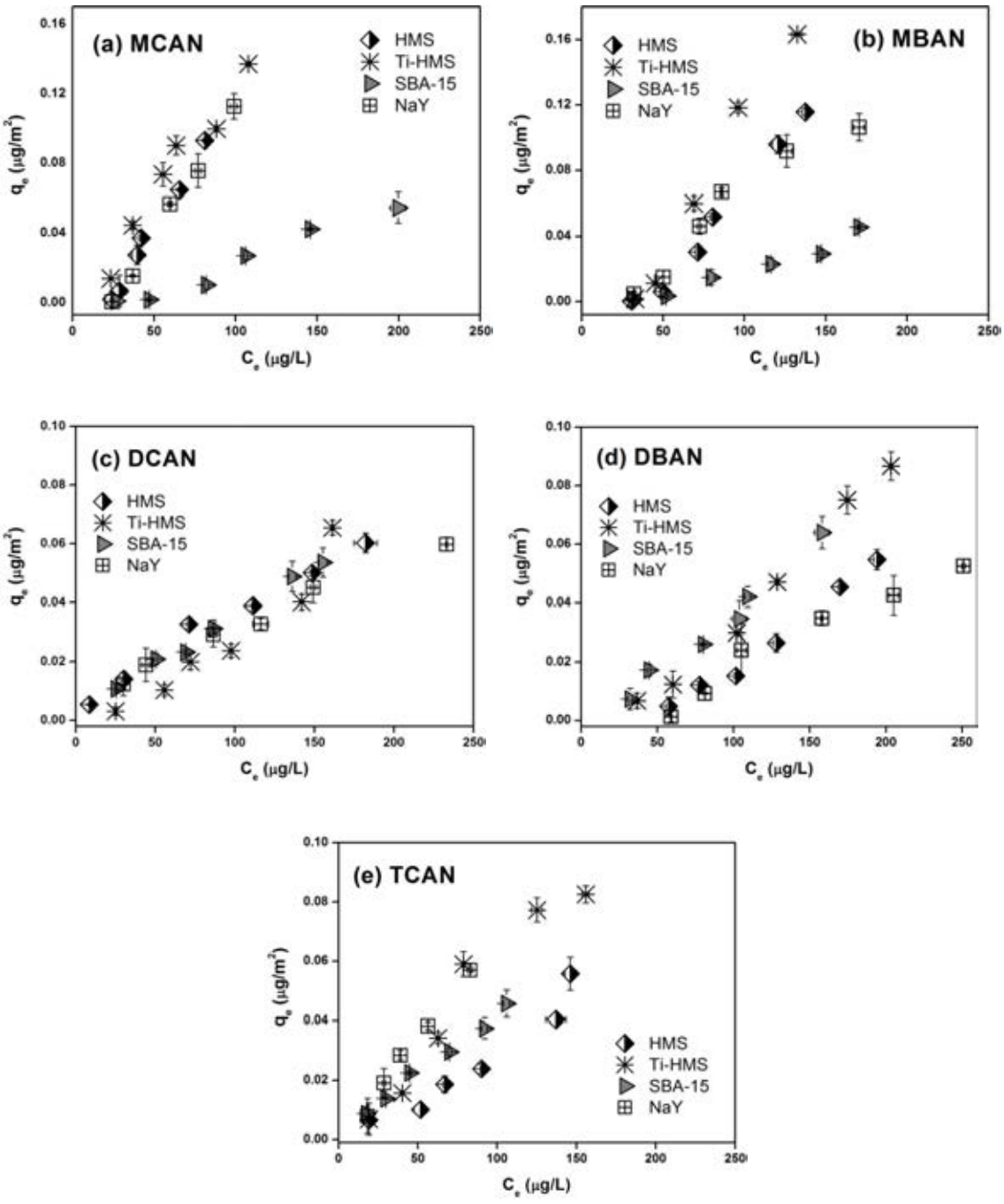

Figure 6.3 Effect of porous and crystalline structures on adsorption of five-HANs on HMS, Ti-HMS, SBA-15 and NaY at pH 7 with IS 10 mM (25 ^{o}C); (a) MCAN; (b) MBAN; (c) DCAN; (d) DBAN; and (e) TCAN

6.3 ISOTHERM MODELS

6.3.1 Isotherm Model of HAN Adsorption on M-HMS and PAC at High Concentration (ppm level)

In order to model the adsorption mechanism, Langmuir, Freundlich and Sips isotherm models were used to test the experimentally derived adsorption process data for correlation. The Langmuir model is based on the assumption of a homogeneous adsorbent surface with specific adsorption sites. The non-linear and linear equations can be defined as shown in Equations (6.1) and (6.2), respectively:

$$q_e = \frac{q_m K_L C_e}{1+K_L C_e} \qquad (6.1)$$

$$\frac{C_e}{q_e} = \frac{C_e}{q_m} + \frac{1}{q_m K_L} \qquad (6.2)$$

where q_m is the maximum adsorption capacity (mg g^{-1}) and K_L is Langmuir adsorption constant.

The Freundlich model is an empirical isotherm employed to describe non-ideal adsorption that involves heterogeneous surface. The non-linear and linear equations can be given as shown in Equations (6.3) and (6.4), respectively:

$$q_e = K_F {C_e}^{1/n} \qquad (6.3)$$

$$\ln(q_e) = \ln(K_F) + \frac{1}{n}\ln(C_e) \qquad (6.4)$$

where K_F is Freundlich constant related to the adsorption capacity (mg g^{-1}) and n is the adsorption intensity.

The Sips model is used as a compromise between the Langmuir and Freundlich models and as expected to describe heterogeneous surfaces much better. At low adsorbate concentrations, it reduces to a Freundlich model while it predicts a monolayer adsorption capacity characteristic of the Langmuir model at high adsorbate concentrations, and can be written as in Equation (6.5):

$$q_e = \frac{q_m K_S C_e^{1/n}}{1+K_S C_e^{1/n}} \qquad (6.5)$$

where K_S is the Sips adsorption constant (L mg^{-1}).

Figure 6.4 shows the adsorption isotherm of five-HANs on PAC and M-HMS at high concentration. Adsorption isotherm on PAC showed L-shaped in all five-HANs while H-shaped responded to di-HANs and tri-HANs adsorption on M-HMS, except L-shaped for mono-HANs (MCAN and MBAN). The adsorption capacity results were fitted with the three models by non-linear regression using the ORIGIN version 8.0 software. The results showed that the Sips model showed the best fitting for both PAC and M-HMS, supported by the R^2 high R^2 (> 0.91) values for the three isotherms, except DBAN adsorption (R^2 > 0.71). The low correlation coefficient (R^2) of DBAN on PAC and M-HMS might be because the trend of equilibrium isotherm seemed not to reach the plateau, and so the predicted data may not be well fitting.

Considering the Sips parameters, the Sips model is the best fit is reasonable due to its incorporation of the advantages of both the Langmuir and Freundlich equations, which can be applied either to homogeneous or heterogeneous surfaces. In this study, the exponent 1/*n* value of five-HANs for PAC was fairly close to unity (one), which means that the form of the DCAN adsorption equilibrium on PAC was more Langmuir like than Freundlich. Thus, the adsorption is limited with monolayer coverage on PAC surface. A similar model has been observed previously for adsorption of another nitrile adsorbate (namely acrylonitrile) by PAC and GAC (Kumar et al., 2008).

By contrary, the adsorption of di-HANs (DCAN and DBAN) on M-HMS tends towards a Freundlich isotherm with the value of exponent 1/*n* being less than half and near zero in the Sips and Freundlich models, respectively, and suggests that the adsorption process M-HMS is heterogeneous (mercapto-functional groups and silanol group). On the other hand, the adsorption of mono-HANs (MCAN and MBAN) and tri-HANs (TCAN) tend to Langmuir based on 1/*n* values closed to unity and high R^2 of Langmuir, suggesting that the adsorption mechanism may be a monolayer adsorption on heterogeneous surface of M-HMS.

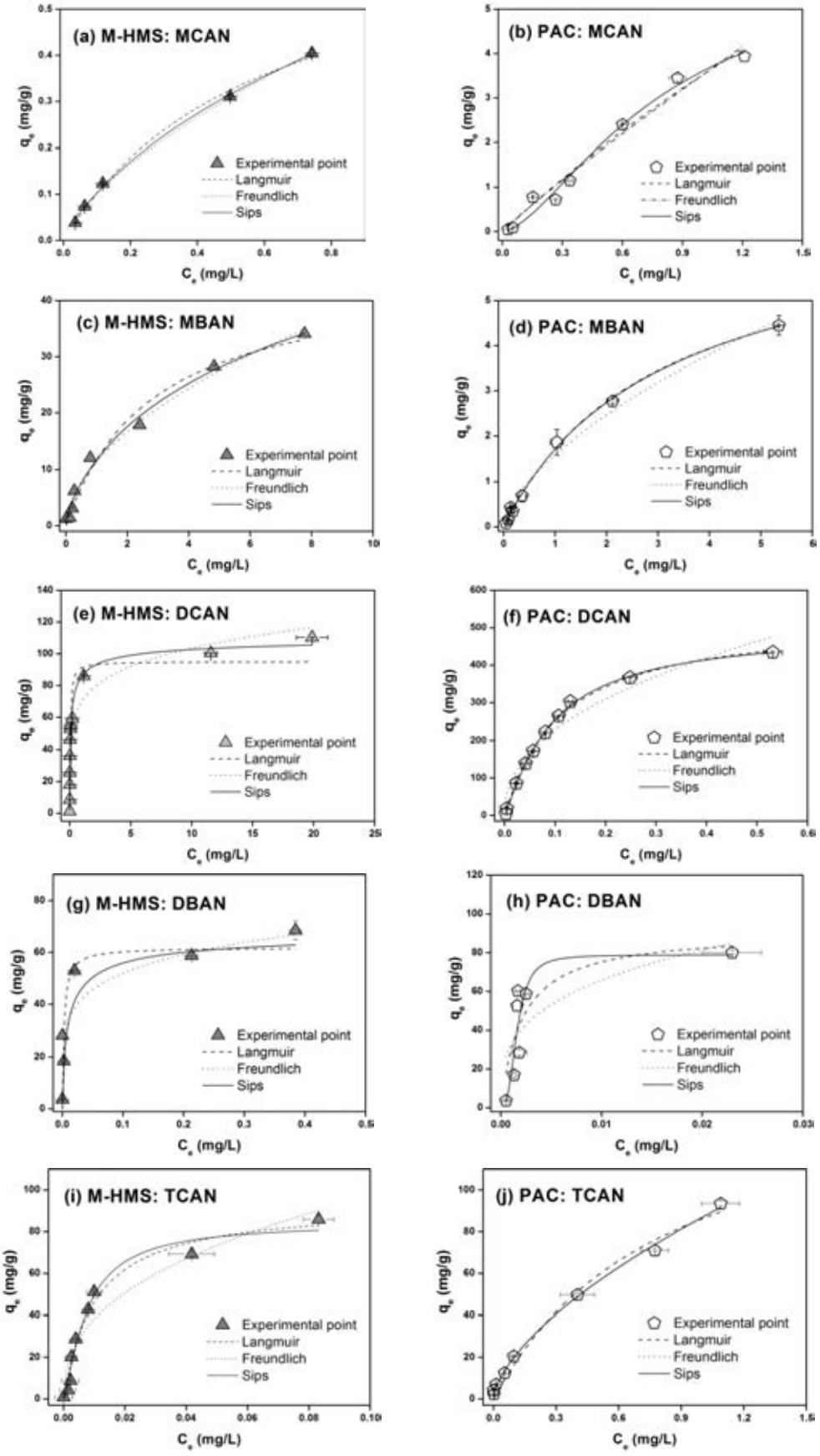

Figure 6.4 Comparison of the predicted and experimental data for the equilibrium adsorption of five-HANs on PAC and M-HMS adsorbents at pH 7 (25 ^{o}C)

Table 6.2 Isotherm parameters of Langmuir, Freundlich and Sips models for adsorption of HANs in single solute on M-HMS and PAC at pH 7 (25 ^{o}C)

Isotherms	HANs				
	MCAN	DCAN	TCAN	MBAN	DBAN
M-HMS					
Langmuir					
q_m (mg g^{-1})	0.72	92.61	93.22	45.17	61.88
K_L (L mg^{-1})	1.67	38.61	98.73	0.353	366.93
R^2	0.996	0.852	0.970	0.978	0.678
Freundlich					
1/n	0.69	0.16	0.40	0.54	0.19
K_F (mg g^{-1})	0.50	71.02	246.90	11.45	79.90
R^2	0.997	0.909	0.910	0.984	0.633
Sips					
q_m (mg g^{-1})	1.53	119.76	84.20	84.97	68.45
K_S (L mg^{-1})	0.45	2.34	536.69	0.16	21.44
1/n	0.80	0.42	0.67	0.70	0.48
R^2	0.997	0.967	0.972	0.984	0.712
PAC					
Langmuir					
q_m (mg g^{-1})	22.03	531.78	159.01	6.92	90.84
K_L (L mg^{-1})	0.19	9.00	1.18	0.33	483.52
R^2	0.971	0.9972	0.984	0.995	0.779
Freundlich					
1/n	0.92	0.44	0.63	0.63	0.31
K_F	3.52	629.26	86.92	1.60	269.73
R^2	0.971	0.939	0.985	0.984	0.774
Sips					
q_m (mg g^{-1})	6.10	495.33	186.26	7.25	78.84
K_S (L mg^{-1})	1.45	14.57	0.0005	0.31	7.1E+07
1/n	0.64	0.84	0.63	0.97	0.36
R^2	0.981	0.998	0.994	0.997	0.732

6.3.2 Isotherm Model of HAN Adsorption on HMS, Functionalized HMS Derivatives, SBA-15 and NaY at Low Concentration (ppb level)

The three isotherm models i.e. the Linear, Langmuir and Freundlich isotherm models are employed to describe the adsorption behavior on HMS, functionalized HMS derivatives, SBA-15 and NaY. Due to linear-shaped demonstration at low initial concentration of five-HANs adsorption, the adsorption isotherms of these adsorbents are also fitted with Linear isotherm, and the linear form of Langmuir and Freundlich equations as shown in Equations (6.2) and (6.4).

The Linear isotherm can be written as shown in Equation (6.6):

$$q_e = K_p C_e \qquad (6.6)$$

where K_p is linear partition coefficient that obtained from the slope of plotted q_e *versus* C_e.

The isotherm parameters of Linear, Langmuir and Freundlich were calculated using the ORIGIN version 8.0 software and the results are all listed in Table 6.3. Since the equilibrium concentration was low, the Linear isotherm was the best fitting to the experimental results with a high R^2 (> 0.91), except for the case of MCAN adsorption on NaY (R^2 = 0.855). A high K_p value indicates a high affinity of functional group on adsorbent surface for HAN adsorption. Comparison of the Langmuir and Freundlich parameters onto A-HMS, Ti-HMS, OD-HMS and NaY adsorbents, it was found that the data seemed to best fit with the Freundlich isotherm as evidenced from the R^2 values, which supports the heterogeneous distribution of surface functional groups on the their surface (i.e. silanol group and amine groups of A-HMS, silanol group and Lewis acid site of titanium substitution of Ti-HMS, octyl- and silanol groups of OD-HMS, Na-cation and silanol group of NaY). Meanwhile, the adsorption data of HMS and SBA-15 (only mono-HANs) fitted well with the Freundlich model rather than the Langmuir one, despite the fact that the surface of HMS and SBA-15 has a relative uniform silanol group distribution. One possible reason is that the Freundlich isotherm is more suitable at low adsorbate concentration than the Langmuir isotherm. On the other hand, the adsorption equilibrium of di-HANs (DBAN and DCAN) and tri-HAN on SBA-15 was likely to be described by both models. Here, it implies that a multilayer coverage may occur on homogeneous surface of silanol group uniformity on SBA-15 surface. Note, however, that the evaluation of the adsorption at high concentration of HANs is required further study for confirmation.

From these results, although the adsorption data seemed to be described by the Freundlich model compared with the Langmuir model, however, the values of 1/*n* are more than 1 (unity) in almost cases, indicative of unfavorable adsorption.

Therefore, the Linear isotherm model is recommended in this study due to at low concentration (ppb level) of adsorption experiments.

Table 6.3 Isotherm parameters of Linear, Langmuir, and Freundlich models for adsorption of five-HANs in single solute on HMS, functionalized HMS derivatives, SBA-15 and NaY

Materials	HANs	Linear		Langmuir			Freundlich		
		K_p	R^2	q_m (μg g^{-1})	K_L (L μg^{-1})	R^2	K_F (μg g^{-1})	*1/n*	R^2
HMS	MCAN	1.122	0.990	107.18	0.013	0.725	0.0002	3.007	0.876
	DCAN	0.237	0.958	140.85	0.015	0.993	1.563	1.261	0.996
	TCAN	0.189	0.926	12.41	0.004	0.983	0.028	1.245	0.987
	MBAN	0.731	0.924	96.15	0.024	0.902	0.286	3.502	0.935
	DBAN	0.263	0.984	102.56	0.005	0.920	0.004	1.749	0.981
Ti-HMS	MCAN	1.028	0.954	166.76	0.009	0.902	0.172	1.399	0.925
	DCAN	0.170	0.957	250.00	0.044	0.965	1.430	0.713	0.948
	TCAN	0.464	0.911	172.41	0.002	0.774	0.155	1.232	0.966
	MBAN	1.369	0.978	454.54	0.002	0.854	0.001	3.013	0.916
	DBAN	0.441	0.989	188.68	0.001	0.954	0.002	1.980	0.971
A-HMS	MCAN	0.577	0.897	49.03	0.009	0.849	0.055	1.479	0.863
	DCAN	0.953	0.982	625.0	0.001	0.899	0.208	1.186	0.991
	TCAN	0.414	0.908	53.48	0.002	0.745	0.084	0.852	0.896
	MBAN	0.831	0.952	23.41	0.006	0.768	0.0001	3.358	0.849
	DBAN	0.665	0.897	133.33	0.003	0.895	0.158	1.253	0.988
OD-HMS	MCAN	0.616	0.970	45.87	0.006	0.847	0.054	1.479	0.732
	DCAN	0.179	0.967	55.86	0.002	0.899	0.020	1.407	0.961
	TCAN	0.172	0.881	53.48	0.002	0.745	0.032	1.276	0.840
	MBAN	0.594	0.953	23.42	0.006	0.768	0.0005	3.009	0.863
	DBAN	0.246	0.958	32.89	0.003	0.874	0.002	1.969	0.879
SBA-15	MCAN	0.224	0.966	41.67	0.002	0.887	0.0003	2.266	0.995
	DCAN	0.215	0.962	118.48	0.003	0.991	2.679	1.152	0.991
	TCAN	0.229	0.994	60.98	0.007	0.999	0.823	0.756	0.988
	MBAN	0.197	0.960	61.39	0.006	0.852	0.001	2.041	0.975
	DBAN	0.280	0.979	133.33	0.002	0.966	0.075	1.248	0.960
NaY	MCAN	1.629	0.855	117.65	0.0016	0.9280	0.0001	3.071	0.940
	DCAN	0.150	0.985	95.24	0.0016	0.9216	0.007	1.966	0.873
	TCAN	0.581	0.948	90.09	0.0098	0.8003	0.128	1.315	0.987
	MBAN	0.504	0.933	222.22	0.0028	0.9646	0.006	1.915	0.916
	DBAN	0.168	0.955	72.99	0.0026	0.9805	0.0002	2.287	0.821

6.4 EFFECT OF pH ON DCAN ADSORPTION

The adsorption capacity of DCAN on the different adsorbents within the pH range of 5 - 9 with IS 10 mM at 25 ^{o}C was evaluated, with the results presented in Figure 6.5. The results indicated that increasing the pH resulted in a higher DCAN adsorption on all adsorbents. The surface of the HMS, OD-HMS, Ti-HMS, SBA-15 and NaY adsorbents is more negatively charged at pH 9, which is at a pH higher than their pH_{PZC}. The charge of the H-atom in the DCAN molecule, as calculated by ChemOffice Ultra 2005, is more positive (Table 6.1) comparing with other atom in DCAN molecular structure, and so the negative surface charges of these adsorbents could be electrostatically attracted by the positive dipole of the H-atom in DCAN molecules via ion-dipole electrostatic interaction. In addition, the density of the negative surface charge (per square meter) at pH 9 of the adsorbents was higher than that at pH 5 and 7 (Figure 4.8 in Chapter 4), leading to a higher adsorption capacity. For A-HMS, surface of A-HMS is positively charged at pH 5-9 based on pH_{PZC} value (pH_{PZC} = 9.5), however, at pH 9 the ratio of negative/positive charged moieties of A-HMS surface becomes higher than pH 5 and 7. This can increase the opportunity of negative groups on surface to interact with the positive dipole of H-atom in DCAN molecule.

However, that the adsorption capacity of M-HMS was not significantly affected by increasing the pH from 7 to 9, accords with the fact that the surface charge density of M-HMS did not change significantly within the pH range 7 - 10 (see Figure 4.8 in Chapter 4). For PAC, the observed adsorption capacity at pH 7 was slightly higher than at pH 9, both the effect of pH on the complex surface functional groups of PAC and its interaction with DCAN to alter the adsorption capacity is still unclear.

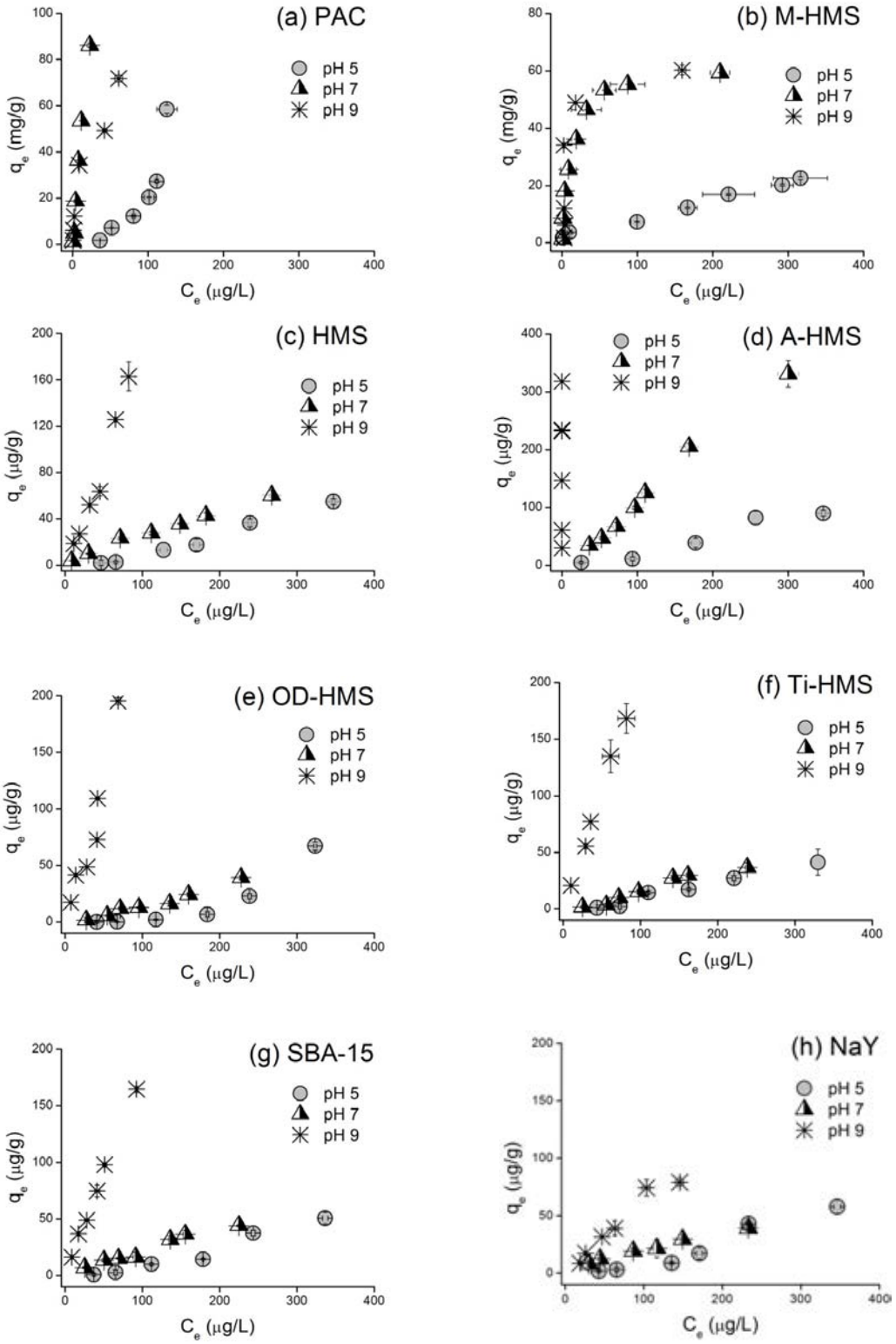

Figure 6.5 Effect of pH on the adsorption on DCAN at pH 5, 7 and 9 with IS 10 mM at 25 ^{o}C

6.5 EFFECT OF TEMPERATURE ON DCAN ADSORPTION OF M-HMS AND PAC

6.5.1 Adsorption Isotherm of DCAN on M-HMS and PAC at Various Temperatures

Temperature is an important parameter for the adsorption process. The effect of temperature on the adsorption of DCAN on M-HMS and PAC was investigated at three different of temperature (15, 25 and 40 ^{o}C). A plot of the DCAN adsorption capacity as a function of temperature of is shown in Figure 6.6. The result revealed that the temperature increased leading to an increased adsorption capacity of DCAN on PAC (Figure 6.6a) while the temperature did not affect the DCAN adsorption capacity on M-HMS at 25 ^{o}C to 40^{o}C significantly (Figure 6.6b).

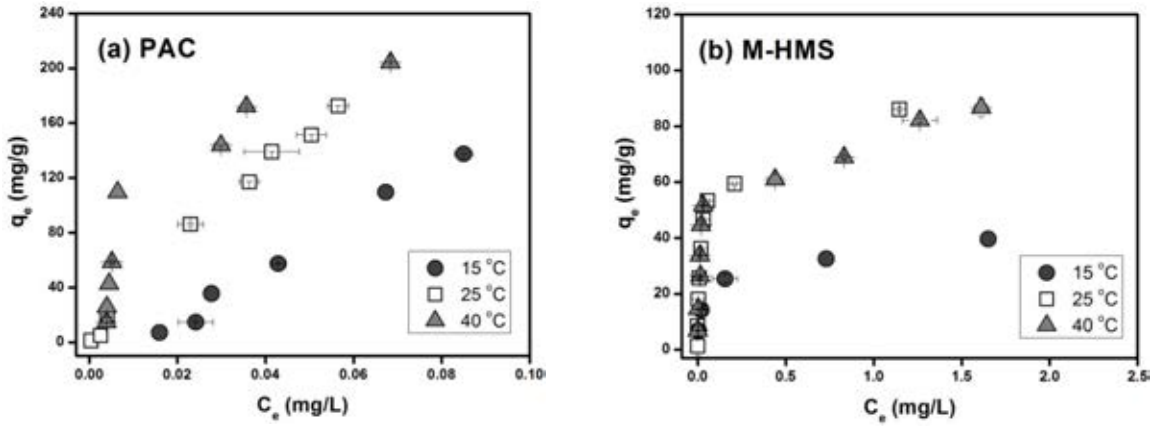

Figure 6.6 Effect of temperature on DCAN adsorption capacity on (a) PAC; and (b) M-HMS

6.5.2 Thermodynamic Parameters

By using the equilibrium constant (K_L) obtained from Langmuir model of each temperature, the Gibbs free energy (ΔG) can be calculated according to the following equation:

$$\Delta G = -RT\ lnK \qquad (6.7)$$

where ΔG is the free energy change (kJ mol^{-1}) and K corresponds to K_L in the Langmuir equation.

The Gibbs free energy (Δ*G*) is also related to the change in entropy (Δ*S*) and heat of adsorption (enthalpy, Δ*H*) at constant temperature, and can be calculated according to the Equation 6.8:

$$\ln K = -\frac{\Delta H}{RT} + \frac{\Delta S}{R} \qquad (6.8)$$

where Δ*H* is the change in enthalpy (kJ mol^{-1}); Δ*S* is the entropy change (kJ mol^{-1} K^{-1}), *R* is universal gas constant (8.314 J mol^{-1} K^{-1}), and *T* is the absolute temperature (^{o}K). The value of Δ*H* and Δ*S* can be calculated, respectively, from the slope and the intercept of the van't Hoff plot of ln*K* versus 1/*T*.

A plot of ln*K* versus 1/*T* of PAC and M-HMS are shown in Figure 6.7 and the calculated values of Δ*G*, Δ*H* and Δ*S* for adsorption of DCAN and Langmuir model parameters are summarized in Table 6.4.

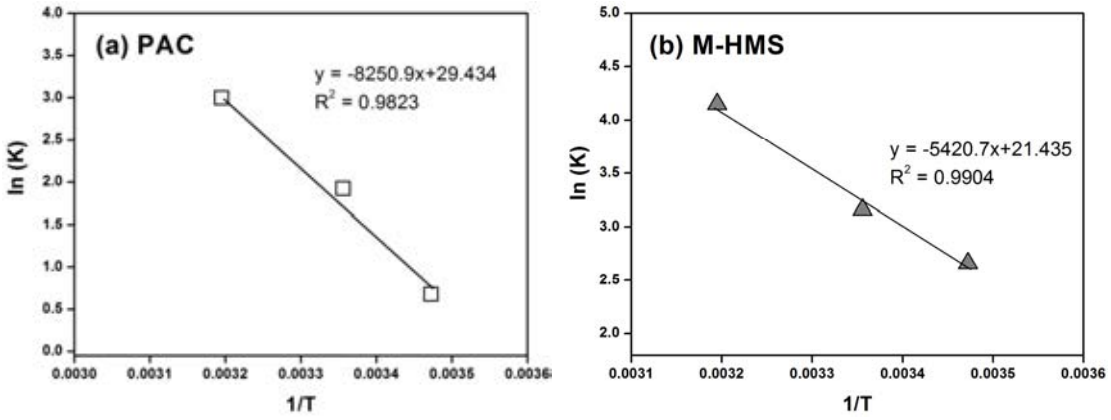

Figure 6.7 Plot of ln*K* vs. 1/*T* estimation of thermodynamic parameters for the adsorption of DCAN on PAC and M-HMS

As seen in Table 6.4, the negative Δ*G* values are obtained in all cases of DCAN adsorption on PAC and M-HMS, which was due to that the adsorption processes were spontaneous with high preference of DCAN on both adsorbents. In addition, the Δ*G* values decreased with an increased in temperature indicating that the spontaneous nature of adsorption of DCAN inversely proportional to the temperature and higher temperature favored the adsorption.

Table 6.4 Equilibrium constants and thermodynamic parameters for the adsorption of DCAN on PAC and M-HMS

Adsorbents	Temp	Langmuir model parameters			Thermodynamic parameters		
	(^{o}C)	q_m (mg g^{-1})	K_L (L mg^{-1})	R^2	ΔG (kJ mol^{-1})	ΔH (kJ mol^{-1})	ΔS (kJ mol^{-1} K^{-1})
PAC	15	383.12	1.98	0.9685	-1.63	68.18	0.24
	25	531.78	9.00	0.9972	-4.77		
	40	836.17	20.06	0.9730	-7.80		
M-HMS	15	41.76	14.34	0.8630	-6.37	45.27	0.18
	25	95.10	23.56	0.9124	-7.83		
	40	92.68	63.60	0.8800	-10.81		

The positive ΔH value obtained indicating that the adsorption process was endothermic in nature. The adsorption of endothermic processes could be due to the increase in temperature increased the rate of diffusion of the adsorbate molecules across the external boundary layer and in the internal pores of adsorbent particle, owing to decrease on viscosity of the solution (Wang and Zhu, 2007). Furthermore, Senthikumaar et al. (2006) suggested that the increased adsorption capacity with increase in temperature was due to the possibility of an increase in the mobility of adsorbate molecule in the adsorbent pores.

The ΔS value shows the affinity of the adsorbents for DCAN adsorption. From results, the positive ΔS values confirm a high affinity of DCAN molecules for the PAC and M-HMS surface. Usually adsorption of gases on solids is accompanied by a decrease in entropy as the molecules from the disordered gaseous state find an ordered arrangement on the solid surface (Asouhidou et al., 2009). In the case of adsorption in aqueous solution in this study, it was suggested that the possibility of some structure changes or readjustments in both adsorbates and adsorbents during the adsorption process may occur (Abe et al., 2009; Alkaram et al., 2009; Tan et al., 2009).

6.6 ADSORPTION MECHANISM

The adsorption of HANs in aqueous solution by inorganic porous materials from aqueous solution depends on the nature of adsorbate and surface functional group of the adsorbent. The expected adsorption mechanism between HANs and inorganic porous materials in this study are proposed in Table 6.5.

Table 6.5 Expected adsorption mechanism between the surface functional groups and HAN adsorbates

Adsorbents	Surface functional groups	Expected mechanism
1. Mesoporous material		
1. 1 Parental mesoporous material		
• HMS	Silanol	Ion-dipole electrostatic force and Hydrogen bonding
• SBA-15	Silanol	Ion-dipole electrostatic force and Hydrogen bonding
• Large pore SBA-CHX	Silanol	Ion-dipole electrostatic force and Hydrogen bonding
1.2 Transition element substituted HMS		
• Ti-HMS	Lewis acid site, Silanol	Covalent bonding , Ion-dipole electrostatic force and Hydrogen bonding
1.3 Organic functionalized HMS derivatives		
• A-HMS	Amino (-NH_2), Silanol	Ion-dipole electrostatic force and Hydrogen bonding
• OD-HMS	Octyl (-C_8H_{17}), Silanol	Ion-dipole electrostatic force and Hydrogen bonding
• M-HMS	Mercapto (-SH), Silanol	Covalent bonding , Ion-dipole electrostatic force and Hydrogen bonding
2. Microporous material		
• NaY zeolite	Na^+, Lewis acid site, Silanol	Ion-dipole electrostatic force and Hydrogen bonding
• PAC	Carboxyl, phenyl and oxygen-containing groups	Complexity interactions such as van der Waals force, and covalent bonding
3. Surfactant-modified adsorbent		
• PG-SBA-CHX	Cationic surfactant	Adsolubilization process, Ion-dipole electrostatic force and Hydrogen bonding

6.6.1 Adsorption Mechanism Evaluation from FT-IR Analysis

To investigate the adsorption mechanism, DCAN is selected as a model HAN for explanation. According to the molecular structure and the calculated charge distribution of the of DCAN molecule after its structure was optimized for minimum energy using MOPAC as shown in Table 6.6, there are two possible reactive sites for the adsorption on the adsorbents. The nitrogen atom (N3) of the nitrile group possesses some basicity and is prone to interact with electron-deficient sites, such as protons and Lewis acids. On the other end, the C≡N group and the two chloride atoms withdraw electrons from the methyl carbon (C2), leaving a positive charge on the hydrogen atom (H6). Besides the hydrophobic/hydrophilic characteristics of the adsorbent surface, two other important mechanisms, that is hydrogen bonding and electrostatic interaction (ion-dipole interaction), are proposed here to interpret the DCAN adsorption. Hydrogen bonding may occur via an interaction between the surface functional groups with –OH, –SH or $–NH_2$ moieties and the nitrogen atom of DCAN molecules. Furthermore, the surface functional groups ionizable under different pH conditions, for example ≡Si-O^-, ≡Si-R-S^-, ≡Si-R-NH_3^+, Na+, and Lewis acid site amongst others, can interact with the opposite charged positions of the DCAN molecules via electrostatic forces. Moreover, DCAN molecule can be both reversibly and irreversibly adsorbed on the M-HMS surface, which can be the result by interaction between the carbon (C1) of nitrile group and mercapto functional group (Patai, 1974).

Table 6.6 Charge characteristics of DCAN molecule

Molecular structure of DCAN	**Charges** [a]	
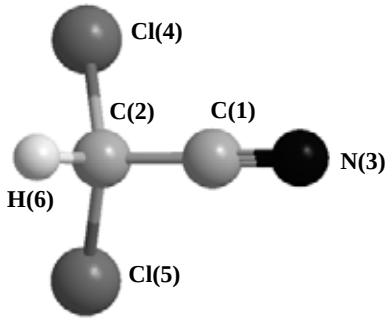	C (1)	-0.12548
	C (2)	-0.02396
	N (3)	-0.01778
	Cl (4)	-0.03625
	Cl (5)	-0.03648
	H (6)	+0.23995

[a] Calculated by ChemOffice Ultra 2005.

The adsorption mechanism can be proposed as follows:

(1) Hydrogen bonding

$\equiv Si\text{-}OH + N\equiv CCl_2CH \longrightarrow \equiv Si\text{-}OH \cdots N\equiv CCl_2CH$

$\equiv Si\text{-}R\text{-}NH_2 + N\equiv CCl_2CH \longrightarrow \equiv Si\text{-}R\text{-}NH_2 \cdots N\equiv CCl_2CH$

$\equiv Si\text{-}R\text{-}SH + N\equiv CCl_2CH \longrightarrow \equiv Si\text{-}R\text{-}SH \cdots N\equiv CCl_2CH$

(2) Ion-dipole electrostatic interaction

2.1 pH > pH_{PZC}

$\equiv Si\text{-}O^- + HCCl_2C\equiv N \longrightarrow \equiv Si\text{–}O^- \cdots HCCl_2C\equiv N$

$\equiv Si\text{-}R\text{-}NH^- + HCCl_2C\equiv N \longrightarrow \equiv Si\text{-}R\text{-}NH^- \cdots HCCl_2C\equiv N$

$\equiv Si\text{-}R\text{-}S^- + HCCl_2C\equiv N \longrightarrow \equiv Si\text{-}R\text{-}S^- \cdots HCCl_2C\equiv N$

2.2 pH < pH_{PZC}

$\equiv Si\text{-}OH_2^+ + N\equiv CCl_2CH \longrightarrow \equiv Si\text{–}OH_2^+ \cdots N\equiv CCl_2CH$

$\equiv Si\text{-}R\text{-}NH_3^+ + N\equiv CCl_2CH \longrightarrow \equiv Si\text{-}R\text{-}NH_3^+ \cdots N\equiv CCl_2CH$

$\equiv Si\text{-}R\text{-}SH_2^+ + N\equiv CCl_2CH \longrightarrow \equiv Si\text{-}R\text{-}SH_2^+ \cdots N\equiv CCl_2CH$

$Na^+ + N\equiv CCl_2CH \longrightarrow Na^+ \cdots N\equiv CCl_2CH$

(3) Covalent bonding

$\equiv Ti + N\equiv CCl_2CH \longrightarrow \equiv Ti - HN=CCl_2CH$

$\equiv Si\text{-}R\text{-}SH + N\equiv CCl_2CH \longrightarrow \equiv Si\text{-}R\text{-}S - HN=CCl_2CH$

To identify the adsorptive interaction during the surface adsorption, HMS and M-HMS were saturated with DCAN solution at 500 μg L^{-1} and 25 mg L^{-1}, respectively, (pH 7 with IS 10 mM) and FT-IR analysis was conducted on the surface of both adsorbents and the FT-IR spectra were analyzed by IGOR Pro 6.0 software. The C≡N stretching of the nitrile group has been reported to be located at around 2250 cm^{-1} (Kozyra et al., 2006; Busca et al., 2008). As shown in upper section of Figure 6.9, the spectrum of HMS (Figure 6.9a) and M-HMS (Figure 6.7b) showed two peaks. For the parental HMS, the downward shift of the minor peak at wavenumber of 2239 cm^{-1} can be assigned to the interaction of the silanol group ($\equiv Si\text{-}O^-$) and the positive dipole of the H-atom in DCAN molecule. The DCAN nitrile

group may be weak after interacting with the deprotonated silanol group (≡Si-O$^-$) via ion-dipole electrostatic interaction, causing a downward shift of the C≡N stretching. Due to the low concentration of DCAN solute in this study, the single intensive upward shift at wavenumber of 2331 cm^{-1} might be evidence of hydrogen bonding between the physisorbed water molecule on the HMS surface and the DCAN nitrile group. In the region of the O-H bending of the adsorbed water as shown in Figure 6.9c, the band at wavenumber of 1630 cm^{-1} represented the physisorbed water molecules. Interestingly, there was a new peak formed at 1701 cm^{-1} that corresponds to the C=N stretching, which might be caused by a weaker nitrile group due to ion-dipole electrostatic interactions. This result is consistent with the appearance of downward shift of the C≡N stretching at 2239 cm^{-1}.

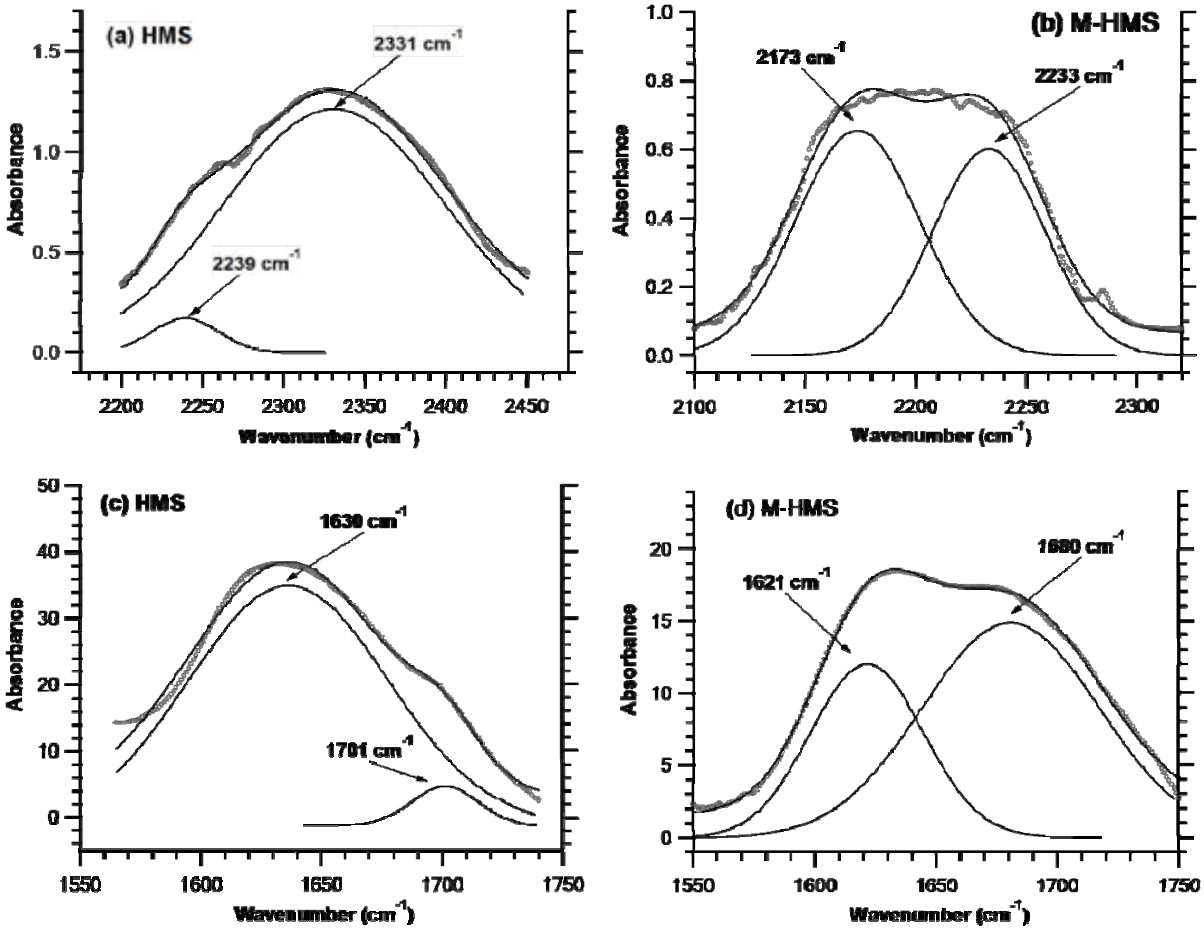

Figure 6.8 FT-IR spectra of HMS and M-HMS after DCAN adsorption at pH 7 in phosphate buffer: (a, b) region of C≡N stretching; and (c, d) region of O-H bending

In case of M-HMS, both peaks exhibited the downward shift to the lower wavenumber (Figure 6.7b). A minor peak at wavenumber of 2233 cm^{-1} can also be assigned to the ion-dipole electrostatic interaction between the mercapto group (≡Si-R-S^{-}) and positive dipole of H-atom as evidence on HMS. The lower downward shift at 2173 cm^{-1} as well as a new band at 1680 cm^{-1} corresponding to the C=N stretching might be due to the bond of the nitrile group to mercapto group of M-HMS (Figure 6.7d). This result indicates that DCAN molecule can be irreversibly adsorbed on M-HMS surface by interaction between ≡Si-R-S^{-} of mercapto group, which acts as a neucleophile, and carbon atom (C1) of nitrile group (electrophile) to form chemical bond. In comparison with HMS, the upward shift at around 2330 cm^{-1} was not observed for DCAN adsorption on M-HMS. It might be because the hydrophobic surface of M-HMS can reduce the physisorbed water molecule on its surface, which is consistent with a decreased in the absorbance and area of the peak at 1621 cm^{-1}.

In order to identify the presence of the hydrogen bonding interaction during the surface adsorption, HMS saturated with DCAN was prepared by equilibrating vacuum-dried mesoporous adsorbents in an organic solution of DCAN. Instead of water, n-hexane was used as the solvent to exclude any interference from the O-H stretching of physisorbed water molecules. As shown in Figure 6.10, free silanol groups (≡Si-OH) on the virgin HMS surface gave a sharp band at 3746 cm^{-1}. Upon adsorption of DCAN, a broad band from the C≡N stretching located at 2150 - 2300 cm^{-1} appeared whereas the O-H stretching band remained intact. A downward shift concomitant with the broadening of the O-H stretching is evidence of hydrogen bonding between nitrile and the hydroxyl groups (Kozyra et al., 2006; Busca et al., 2008). Therefore, it can be concluded that hydrogen bonding was not likely to be the major mechanism for the DCAN adsorption under the conditions investigated.

Form FT-IR results therefore indicated that ion-dipole electrostatic interaction was likely to be the main adsorption mechanism of HMS whereas both ion-dipole electrostatic interaction and chemisorption were identified as the mechanism that likely play an important role in HANs adsorption on M-HMS in this study.

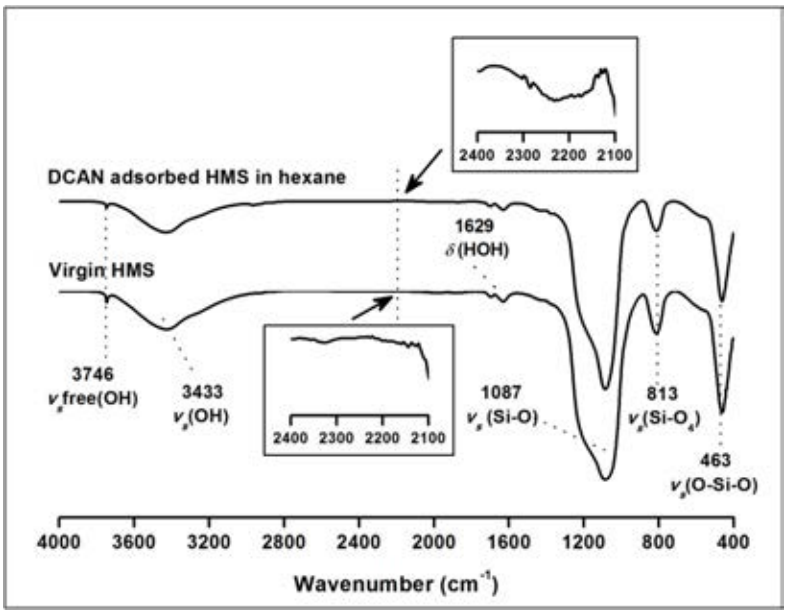

Figure 6.9 Representative FT-IR spectra of virgin HMS and DCAN adsorbed HMS in hexane

6.7 CONCLUSIONS

The surface functional groups, porosity and crystalline structure significantly affected the adsorption capacity of five-HANs. Interference by water molecules at low concentrations of adsorbate strongly affected the adsorption mechanism. The Sips isotherm model was successfully applied to describe the adsorption on PAC and M-HMS at high concentration whereas the experimentally derived isotherm data of the parental HMS, functionalized HMS derivatives, SBA-15 and NaY fitted well with the Linear isotherm due to at low concentration (ppb level) of adsorption experiments. The adsorption was favored at high pH due to a high negative surface charge density of adsorbent. In addition, the adsorption temperature increased leading to the increased adsorption capacity of DCAN adsorbed on adsorbent surface, indicating that the adsorption is controlled by endothermic process. The positive entropy suggests the possibility of some structure changes in both adsorbates and adsorbents during the adsorption process. The FT-IR analysis indicated that the adsorption mechanism involves a more complex interplay between an ion-dipole electrostatic interaction and chemisorption.

CHAPTER VII

ADSORPTION SELECTIVITY

7.1 INTRODUCTION

Activated carbon (AC) is well known as an adsorbent and has been widely used in the treatment of drinking/tap water. Although AC shows high adsorption capability for a number of disinfection by-product (DBPs), it does not seem to adsorb selectively; which would otherwise adsorb predominant pollutants of higher concentration. Selective adsorbents need to be developed, particularly in treating the pollutants with small molecular size, high molecular polarity and high solubility found at low concentration in water. Mesoporous silicates offer a number of potential advantages as adsorbents and their surface modification via the reaction of silanol groups with various organosilanes is very helpful in the improvement of the adsorption capacity and selectivity as a result of specific interactions between the surface functional groups and adsorbate molecules. In addition, DBPs usually occur in the water supply system as a mixture. The behavior of DBPs in a mixture may different and complicated, not as individual cases. Therefore, investigation of adsorption of a mixture of DBPs is required as a succeeding step for further application.

The objective of the study in this chapter is to investigate the mechanism of selective adsorption of adsorbents for adsorption of five different HANs in mixed solute solution comparing with the adsorption capacity of individual solute adsorption. The effect of molecular structure of HANs in terms of halogen type and degree of substitution of halogen atom on the selective adsorption of adsorbents was discussed. The effects of co-existing electrolytes in tap water and the presence of co-existing DBPs, i.e. trihalomethanes (THMs) and haloacetic acids (HAAs), on selective adsorptive adsorption of HANs were investigated. Also, adsorption selectivity of powder activated carbon (PAC) was also studied for comparison.

7.2 SELECTIVE ADSORPTION OF FIVE-HANs IN MIXED SOLUTE SOLUTION COMPARED WITH IN SINGLE SOLUTE SOLUTION

7.2.1 Selective Adsorption of M-HMS for five-HANs Adsorption Compared with PAC

Among the organic functionalized HMS derivatives, M-HMS could efficiently adsorb HANs superior to the other adsorbents. Thus, M-HMS was investigated the effect of molecular structure of HANs (halogen type and degree of substitution of halogen atom) on the selective adsorption compared with PAC. To exclude the effect of surface area, the adsorption capacities of the adsorbents were corrected for differences in surface area by presentation as mg m^{-2}. As seen in Figure 7.1a, the individual adsorption isotherms for the five different HAN adsorbates by M-HMS were ranked in the adsorption preference order of TCAN ≅ DBAN > DCAN > MBAN > MCAN on M-HMS. Tri-HAN and di-HANs, which had a high molecular weight, exhibited higher adsorption capacities on M-HMS compared with the mono-HANs. That the bromo-HANs had higher adsorption capacities than the chloro-HANs is due to the stronger positive dipole of the H-atom in bromo-HANs (Table 7.1). These results indicate that the adsorption capacities of the five different HANs on M-HMS are likely to be related to the molecular structure of each HAN, though this requires further research for confirmation. In contrast, PAC had the highest adsorption capacities for di-HANs followed by tri-HANs and mono-HANs, respectively (Figure 7.1b). The individual adsorption capacities of the five-HANs a on PAC then, in contrast, did not appear to directly relate to the types and amount of halogen atom in the molecule (Figure 7.1b).

The adsorption isotherms of the mixed solutes of all five-HANs together are shown in Figure 7.1(c) and (d) for M-HMS and PAC, respectively. It was clear that the active surfaces of PAC and M-HMS were competitively segregated for all five- HAN species in the mixed solute, causing a decreased adsorption capacity for each HAN. The order of adsorption capacities in the mixed solute on M-HMS was slightly different from the single solute results, being TCAN ≅ DCAN > DBAN > MBAN > MCAN. Thus, the DBAN adsorption capacity on M-HMS might be easily outcompeted and interrupted by the presence of the other HANs. However, on PAC

the order of adsorption capacities of all HANs was in the same as that seen with the single adsorbate (Figure 7.1d).

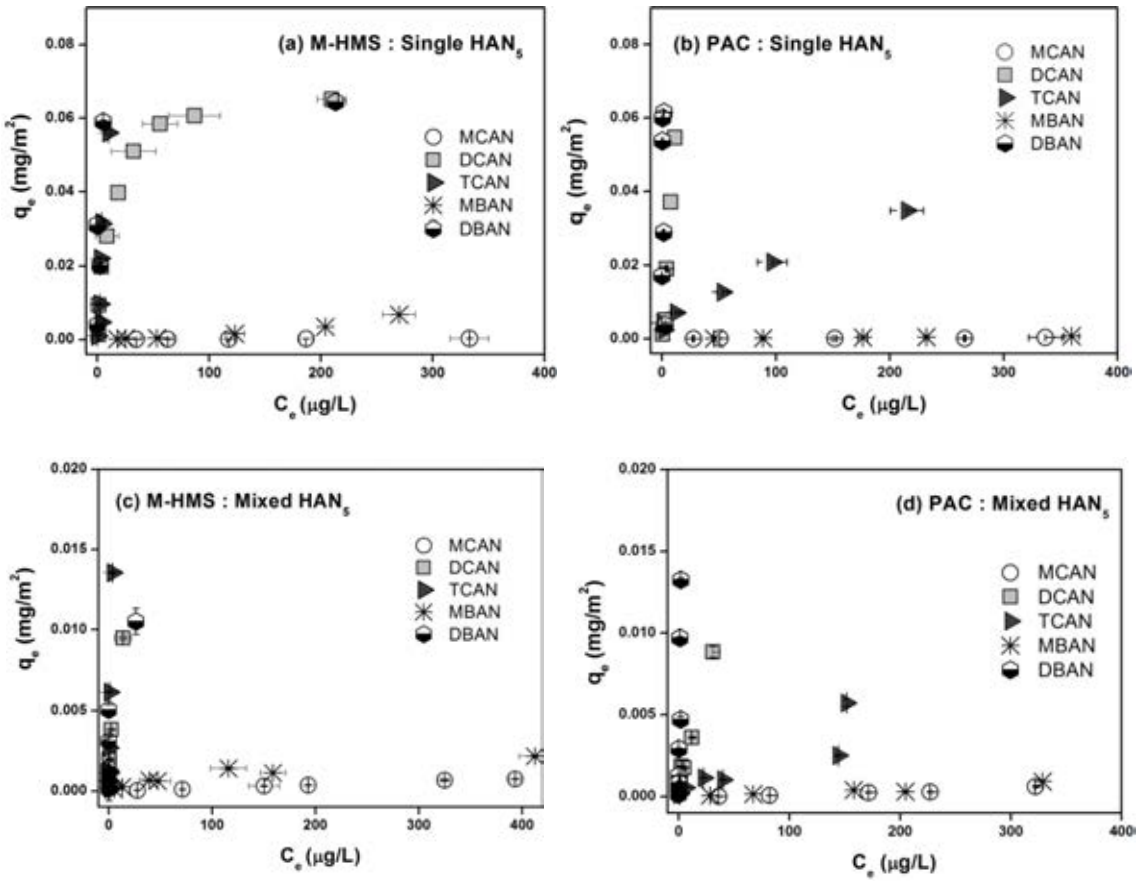

Figure 7.1 Adsorption isotherm of five-HANs as a (a, b) single solute; and (c,d) mixed solute on M-HMS and PAC at pH 7 with IS 10 mM

7.2.2 Effects of Porous and Crystalline Structures on Adsorption Selectivity

According to the results of adsorption isotherm of each HAN adsorbate in Chapter 6, the porous and crystalline structures of adsorbents seemed to affect the selectivity of those adsorbents. Therefore, the effects of porous and crystalline structures on selective adsorption in mixed solute solution were also investigated. Adsorption isotherms for the five-HAN_s alone (single solutes) on HMS, Ti-HMS, SBA-15 and NaY are shown in Figure 7.2 (a), (c), (e) and (g), respectively. The order of adsorption preference (highest to lowest) was MCAN > MBAN > DCAN > DBAN > TCAN on HMS, Ti-HMS and NaY, which implies that the adsorption capacities

may relate to the strength of the positive/negative dipole in mono-HANs molecule. Two H-atoms in mono-HANs can increase the opportunity of negatively charged surface of silanol group on HMS surface to interact with the positive dipole of H-atom in DCAN molecule whereas the strongest negative dipole of N-atom in mono-HANs molecule (Table 7.1) could interact with Lewis acid site of Ti-HMS and Na^+ of NaY leading to a higher adsorption capacity. Moreover, these selective adsorption behaviors might be linked to the surface characteristic of each adsorbent. The hydrophilic surface characteristics of all four adsorbents would be expected to selectively adsorb a hydrophilic adsorbate in order of mono-HANs > di-HANs > tri-HAN. However, except for SBA-15, the adsorption of the five-HAN_5 displayed a reverse order of adsorption preference (Figure 7.2e). For SBA-15, a larger molecular weight of tri-HANs was adsorbed more than the di-HANs and mono-HANs. Larger pore size might enhance the internal surface accessibility and let the larger molecular structure HANs be better adsorbed than on with smaller sized pores (Table 7.1). Regardless, these results indicate that the adsorption capacity of HAN_5 on the four adsorbents related to the molecular structure of HAN. Moreover, hydrophilic/hydrophobic nature of both adsorbent and adsorbate can influence on selective adsorption.

Table 7.1 Physicochemical properties and charge distribution of five-HANs

Parameters	**HANs**				
	MCAN	**MBAN**	**DCAN**	**DBAN**	**TCAN**
MW (g mol^{-1})	75.50	119.95	109.94	198.85	144.39
Width (A^o)	2.43	2.52	2.89	2.52	2.90
Length (A^o)	3.10	3.15	3.61	3.75	3.60
Solubility (mg mL^{-1})	100	50-100	10-50	50	< 1
Charges [a]					
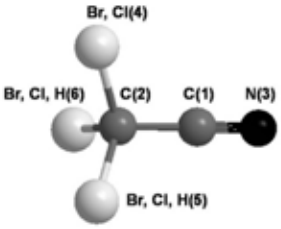	C(1) -0.1304	C(1) -0.1205	C(1) -0.1254	C(1) -0.1089	C(1) +0.1136
	C(2) -0.1323	C(2) -0.2513	C(2) -0.0239	C(2) -0.2460	C(2) -0.1298
	N(3) -0.0537	N(3) -0.0542	N(3) -0.0177	N(3) -0.0219	N(3) -0.0027
	Cl(4) -0.0838	Br(4) +0.0094	Cl(4) -0.0362	Br(4) +0.0633	Cl(4) +0.0044
	H(5) +0.2002	H(5) +0.2083	Cl(5) -0.0364	Br(5) +0.0632	Cl(5) +0.0044
	H(6) +0.2002	H(6) +0.2083	H(6) +0.2399	H(6) +0.2504	Cl(6) +0.0048

[a] Calculated by ChemOffice Ultra 2005

The adsorption isotherms for the five-HANs when presented in mixed solute on the four adsorbents are consistent with the notion that the active surfaces of each adsorbent had been divided between all five-HANs causing a decrease in the observed adsorption capacity of each HAN (Figure 7.2 (b), (d), (f) and (h)). The order of adsorption capacities in mixed solute of each HAN on HMS, Ti-HMS and NaY were significantly different from the single solute results (TCAN > DBAN ≅ DCAN > MBAN ≅ MCAN). The large molecular weight of the tri-HAN and the two di-HANs are more easily adsorbed than the smaller molecular weight of mono-HANs at low concentration. Unlike SBA-15, the order of adsorption capacities of all five-HANs was not different compared to that observed for the single HAN solute (Figure 7.2f), which might be caused by the higher accessibility to the active sites due to larger pore size.

7.3 EFFECT OF CO-EXISTING ELECTROLYTES IN TAP WATER ON ADSORPTION SELECTIVITY OF M-HMS AND PAC

Tap water contains many kinds of electrolytes (anions and cations) such as chloride, sulfate, sodium, magnesium ions and etc. which may affect the adsorption process by electrostatic interaction. In this study, the adsorption experiment was carried out in tap water and the five-HANs were mixed all at the same concentration. The concentration of electrolytes and the background concentration of HANs in tap water were determined by Ion chromatograph (IC) and GC/ECD, respectively, and are summarized in Table 7.2. The adsorption capacity of five-HANs was compared with that under DI water with IS 10 mM fixed by phosphate buffer.

Table 7.2 The tap water quality and concentration of electrolytes in tap water used in adsorption experiment

Parameters	**Tap water** [a]								
pH	7.15								
Conductivity[b] **(μmol cm^{-1})**	323								
TDS[b] **(mg L^{-1})**	202								
Ionic strength (mM)	4.6								
Electrolytes (mg L^{-1})	Na^+	Ca^{2+}	Mg^{2+}	Fe^{2+}	Br^-	Cl^-	F^-	NO_3^-	SO_4^{2-}
	23.57	1.34	32.06	1.73	ND[c]	23.31	0.21	1.98	33.38
Background HANs (μg L^{-1})	MCAN	DCAN	TCAN	MBAN	DBAN				
	0.3	13	ND[c]	ND[c]	ND[c]				

[a] Sampling on 11 February, 2011
[b] Average concentration from October 2009 to August 2010 obtained from http://www.mwa.co.th
[c] ND means not detected

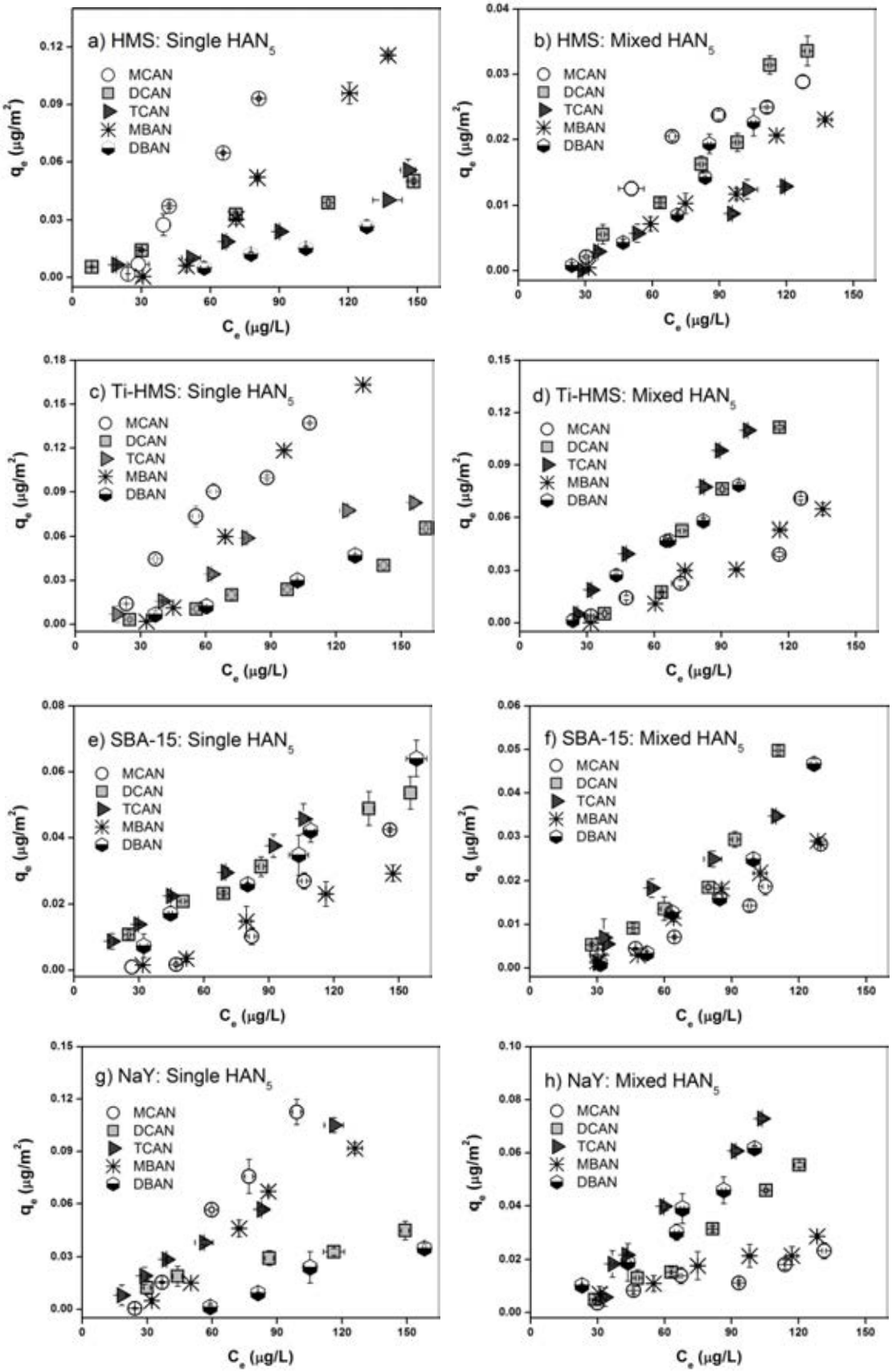

Figure 7.2 Adsorption isotherm of five-HANs (a, c, e, g) single solute; and (b, d, f, h) mixed solute on HMS, Ti-HMS, SBA-15 and NaY at pH 7 with IS 10 mM

As shown in Figure 7.3, the M-HMS adsorbent still displayed high adsorption capacity of each HAN in the presence of co-existing electrolytes in tap water (Figure 7.3c) and the order of adsorption capacities of all HANs was in the same as that seen with the mixed solute solution under DI water condition (Figure 7.3a). Considering the ionic strength (IS), it was found that the IS value of the tap water (IS = 4.6 mM), as calculated from the concentration of ions in tap water, was less ca. 2 times than that for DI water (IS 10 mM fixed by phosphate buffer) since a lower IS value usually weakens the electrostatic interaction and consequently decreases the adsorption capacity (Bjelopavlic et al., 1999). However, some literature have been reported that the adsorption of adsorbate did not change significantly at low IS value. For instance, Yu et al. (2008) found that the adsorption of perfluorooctane sulfonate (PFOS) on chitosan-based polymer adsorbent did not change with increasing of NaCl concentrations from 0 to 50 mM. The adsorption capacity of As(III) on surfactant-modified bentonite was not significantly affected when the IS increased from 0 to 500 mM (Su et al., 2011). Evidence from literature is consistent with the result obtained in this study. Moreover, the surface charge density of M-HMS at IS 4.6 mM (pH 7) is not significantly different from that for IS at 10 mM (Figure 7.4a). From these results, it can be concluded that common electrolytes in tap water did not affect the adsorption capacities and selectivity of M-HMS for five-HANs in the mixed solute solution.

For PAC, the order of adsorption capacities of five-HANs in the tap water on PAC was also similar to that in DI water; however, the adsorption capacity of TCAN was slightly higher. It might be caused that the ratio of positive/negative charge density of PAC at IS 4.6 mM (pH 7) is slightly higher than at IS 10 mM (Figure 7.4b) which can more interact with lone pair of TCAN molecule leading to a higher adsorption capacity. However, the adsorption phenomenon cannot be explained only by the surface charge characteristic. The heterogeneous surface of PAC that consists of various organic functional groups may affect the adsorption capacity also.

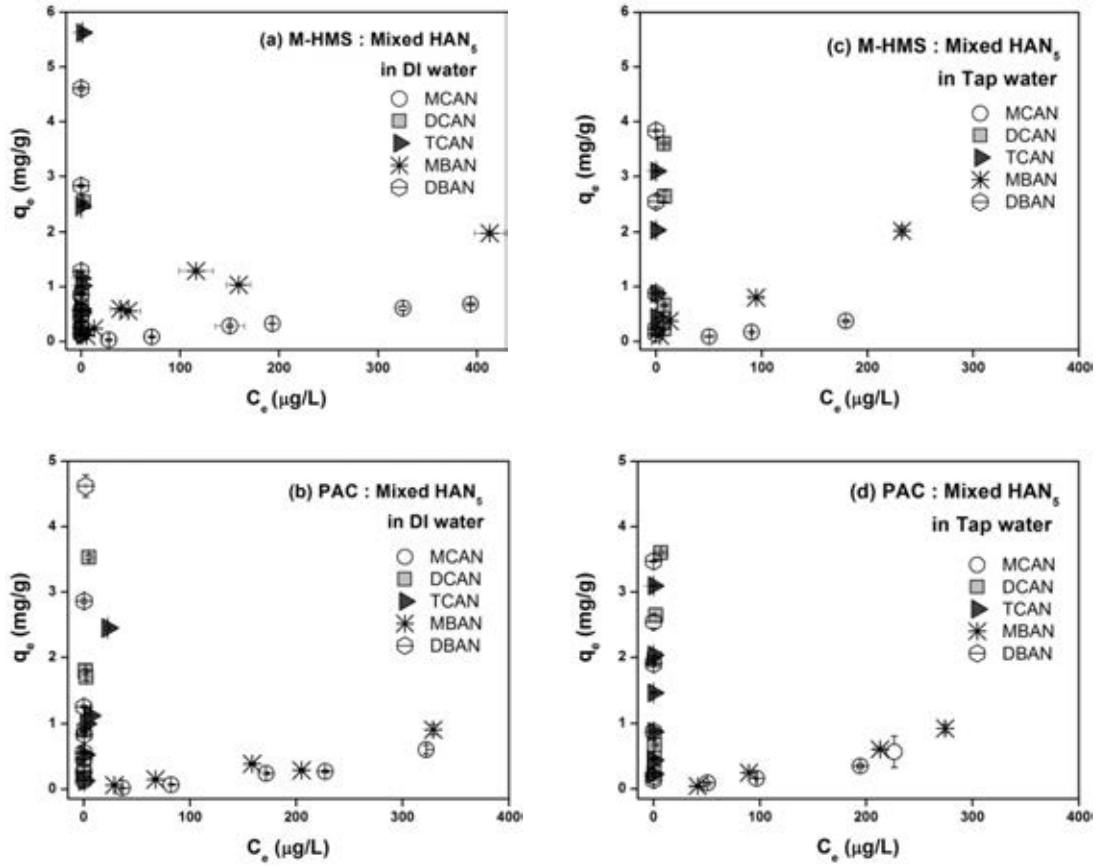

Figure 7.3 Adsorption isotherms of five-HANs in mixed solute solution (DI water) at pH 7 with IS 10 mM, comparing with adsorption isotherm of mixed solute in tap water on M-HMS and PAC

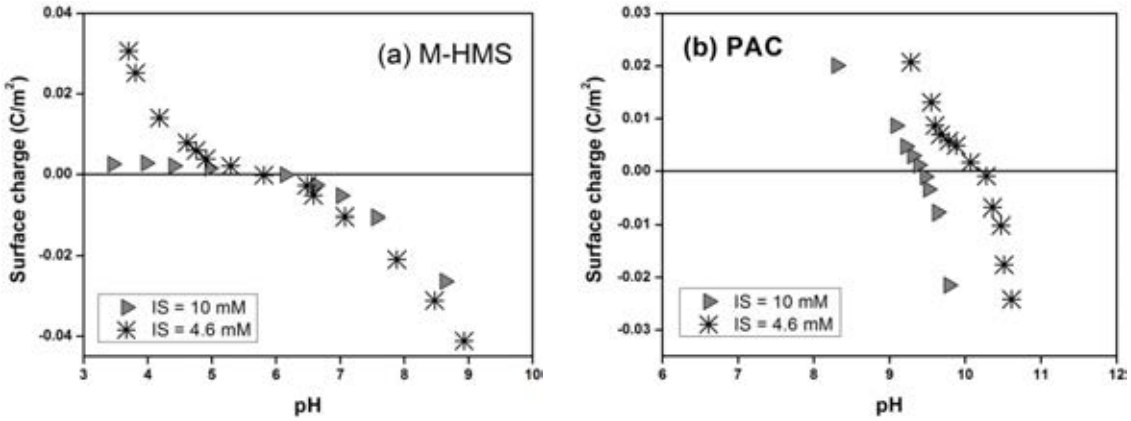

Figure 7.4 Surface charge density of M-HMS and PAC at pH 7 with IS 10 mM comparing with IS 4.6 mM of tap water

7.4 EFFECT OF CO-EXISTING DBPs ON ADSORPTION SELECTIVITY OF M-HMS AND PAC

As mentioned earlier, DBPs usually occur in the water supply as a mixture. Trihalomethanes (THMs) and haloacetic acids (HAAs) are the most dominant species of DBPs while the HANs represents the third major classes of DBPs. Therefore, this study was to investigate the selective adsorption of M-HMS on DCAN adsorption in the presence of other competitive DBPs, comparing with PAC. Trichloromethane (TCM) and dichloroacetic acid (DCAA) were used as a model of THMs and HAAs, respectively, due to the most abundance after water chlorination. The adsorption experiment was carried out in DI water at pH 7 (IS 10 mM) and the three species DBPs (i.e. DCAA, DCAN, and TCM) were mixed all at the same concentration.

Figure 7.5 (a) shows the adsorption isotherm of the three DBPs in mixed solute solution. Obviously, M-HMS could efficiently adsorb DCAN in the presence of co-existing DBPs, and the adsorption of three DBPs were ranked in the adsorption preference order of DCAN > TCM >> DCAA. For M-HMS, the combination of ion-dipole electrostatic interaction and van der Waals force caused by hydrophobicity are likely to be the main adsorption mechanism for TCM adsorption on M-HMS, considering the molecular structure and charge distribution of TCM (Table 7.3). At the pH range of study and pH_{PZC} of M-HMS of 6.2, the mercapto-groups as well as the remaining silanol groups were deprotonated to the dissociated forms as $\equiv$Si-R-S^- and $\equiv$Si-O^-, respectively, which can interact with the positive dipole of H-atom in TCM molecule. Beside, TCM is high hydrophobicity (Table 7.3) and the surface characteristic of M-HMS is also hydrophobicity based on the water contact angle (θ) = 89.65. Thus, the hydrophobicity of both adsorbate and adsorbent facilitated the van der Waals force. Surprisingly, the adsorption capacity of TCM was quite less than DCAN although the strength of positive dipole H-atom of DCAN (δ = 0.23995) and TCM (δ = 0.24071) is not different significantly (see Table 7.1 for DCAN and Table 7.3 for TCM). It might be caused that DCAN is a basic adsorbate comparing with TCM, and so DCAN may be favorable adsorbed on the acidic group of mercapto- and silanol group causing a higher adsorption capacity.

For DCAA adsorption on M-HMS, it can be seen that DCAA was slightly adsorbed on M-HMS. At pH 7, DCAA exists as anions in solution due to low pK_a value (about 1.30), while M-HMS surface is charged negatively, leading to increased electrostatic repulsion force between them. Thus, M-HMS may adsorb DCAA via ion dipole electrostatic interaction between positive dipole of H-atom (H7) of DCAA molecule (see Table 7.3) and negative charge surface of M-HMS. However, Patiparn et al. (2009) pointed out that the electrostatic interaction could not enhance the DCAA adsorption capacity at low concentration whereas the hydrogen bonding seemed to play an important role on DCAA adsorption (Punyapalakul et al., 2009). Thus, it is possible that the remaining neutral groups (mercapto- and silanol groups) can also adsorb DCAA by forming the hydrogen bonding with high electronegativity O-atom of C=O group.

In case of PAC, DCAN had highest adsorption capacity followed by TCM and DCAA, respectively (Figure 7.5b). Moreover, it was observed that the adsorption capacities of TCM and DCAA by PAC were higher than that by M-HMS. This might be caused by the surface complexity of functional group in PAC, it may induce many interactions towards TCM and DCAA adsorption such as electrostatic force, van der Waals force and covalent bonding resulted in higher adsorption capacities. However, the effect of complexity of surface functional groups of PAC and their interaction with the three DBPs is still unclear, and this requires further research for investigation.

Form these results, it can be concluded that the presence of co-existing DBPs (TCM and DCAA) did not affect the adsorption capacities and selectivity of M-HMS and PAC for DCAN adsorption in the mixed solute solution.

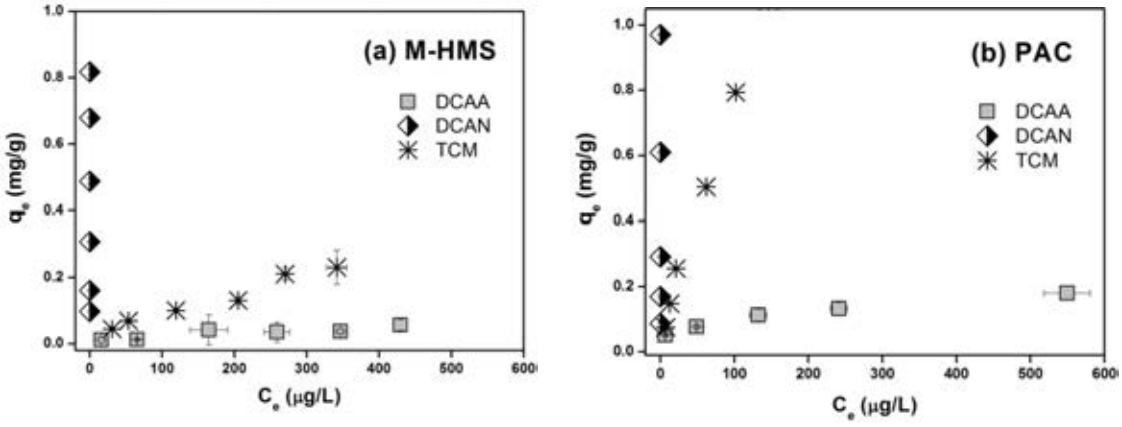

Figure 7.5 Adsorption isotherms of DCAA, DCAN and TCM on M-HMS and PAC adsorbents in mixed solute solution at pH 7 with IS 10 mM (Effect of co-existing DPBs on adsorption selectivity)

Table 7.3 Physicochemical properties and charge distribution of TCM and DCAA molecules

Parameters	**Trichloromethane (TCM)**		**Dichloroacetic acid (DCAA)**	
Molecular structure	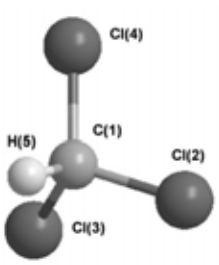		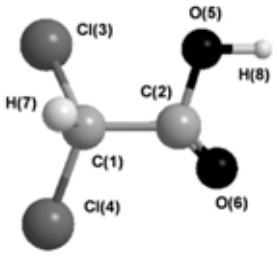	
MW (g mol^{-1})	119.38		128.90	
Solubility(mg mL^{-1})	8.0		miscible	
pK_a	-		1.30	
Charges [a]	C(1)	-0.1139	C(1)	-0.1274
	Cl(2)	-0.0422	C(2)	+0.3629
	Cl(3)	-0.0422	Cl(3)	-0.0393
	Cl(4)	-0.0423	Cl(4)	-0.0334
	H(5)	+0.2407	O(5)	-0.3519
			O(6)	-0.3391
			H(7)	+0.2334
			H(8)	+0.2948

[a] Calculated by ChemOffice Ultra 2005

7.5 CONCLUSIONS

This study investigated the effect of molecular structure of HANs, the effects of co-existing electrolytes in tap water and the competitive DBPs on the adsorption selectivity of adsorbents, comparing with PAC. The results revealed that the molecular structure of HANs obviously affected the adsorption capacity and selectivity over M-HMS whereas selective adsorption over PAC was not observed. Moreover, the different porous and crystalline structures of adsorbents (i.e. mesopore HMS, Ti-HMS, SBA-15 and micropore NaY) affected the selective adsorption of five-HANs as well as hydrophilic/hydrophobic nature of both adsorbent and adsorbate also influenced on their selective adsorption on hydrophilic adsorbents.

Furthermore, the effect of electrolyte in tap water and the presence of co-existing DBPs did not affect the adsorption capacities and selectivity of M-HMS and PAC in the mixed solute solution. The large adsorption affinity and selectivity for DCAN and TCM of M-HMS could be ascribed by the ion-dipole electrostatic interaction. As a selective adsorbent, M-HMS can be an alternative to PAC for removal DBPs such as THMs and HANs in aqueous solution. However, the further studies will be investigated to improve the adsorption capacity and selectivity of mercapto-functionalized HMS derivative (M-HMS) for HAA removal (such as bi-functional groups of mercapto- and amine group modification).

CHAPTER VIII

EFFECT OF SURFACTANT MODIFICATION ON ADSORPTION OF HALOACETONITRILES

8.1 INTRODUCTION

Surfactant-modified adsorbents have drawn much attention in separation process and have proved in the removal efficiency for various organic/inorganic compounds. The adsorbents can be modified by surfactant to form bilayer micelle structures, called “admicelle”, on their surface having the potential to solubilize organic molecules. In several research studies, various adsorbents such as metal oxides, zeolites, bentonites, montmorillonites and etc., have been used to modify surface by anionic/cationic surfactant adsorption. However, the adsorption of surfactant molecules on these adsorbents is limited due to small pore size and low specific surface area resulted in the amount of surfactant coverage on surface was low and limited to sites of external surface only. Even though the surfactant-modified adsorbent has been found to be a promising adsorbent for environmental approach, however; its use is sometimes problematic due to the loss of surfactant from the solid surface. In order to reduce the surfactant loss, polymerizable surfactants are of interest because the crosslink of adsorbed surfactant after polymerization is expected to increase a stability of the surfactant coverage on adsorbent surface.

This study investigated the effect of surfactant modification on adsorption of HANs. Large pore mesoporous silicate (SBA-CHX) was synthesized, which would expect to increase the amount of surfactant coverage on surface, and modified surface with polymerizable gemini surfactant (PG). The polymerization process was performed to increase the stability of admicelle structure on its adsorbent surface. The HAN adsorption study in aqueous solution by PG-modified mesoporous silicate was compared with the unmodified mesoporous silicate to investigate the effect of surfactant modification on HAN adsorption efficiency and mechanism. The adsorption kinetics, adsorption isotherms, the effect of pH of solution, selective adsorption of five-HAN_5 by comparing between single and mixed solutes, and surfactant leaching were also investigated under batch adsorption experiments.

8.2 SUMMARY OF THE PHYSICOCHEMICAL CHARACTERISTIC OF ADSORBENTS

The detailed physicochemical characteristic of the adsorbents, the parental SBA-CHX and PG surfactant-modified SBA-CHX (PG-SBA-CHX), was previously described in Chapter 4: Material characterization and just a brief description are shown here. The multipoint BET surface area, mean pore diameter and pore volume of the parental SBA-CHX were 765.8 m^2 g^{-1}, 23.41 nm and 448 mm^3 g^{-1}, respectively. The maximum adsorption capacity (q_{max}) of surfactant on SBA-CHX was 1.35 mmol g^{-1} derived from the initial PG concentration at 14 mmol L^{-1}. The surface characteristic of PG-SBA-CHX is hydrophobic surface ($\theta = 80.45^o$) while the parental SBA-CHX ($\theta = 32.56^o$) is hydrophilicity, based on the water contact angle values. The pH_{PZC} of parental SBA-CHX and PG-SBA-CHX were 3.5 and 9.6, respectively. The effective area per head molecule (94.04 A^{o2} $molecule^{-1}$) was 3 times higher than surface area of PG headgroup (32.26 A^{o2} $molecule^{-1}$) suggesting that the possibility of the remaining silanol groups on its surface which is available to interact with HAN molecules.

8.3 KINETIC STUDY AND INTRAPARTICLE DIFFUSION MECHANISM

8.3.1 Adsorption Kinetics of DCAN

The adsorption kinetic of DCAN on the parental SBA-CHX and surfactant-modified SBA-CHX plotted as a relative adsorption capacity (q_t) versus time are shown in Figure 8.1. DCAN was adsorbed on the parental SBA-CHX and attained equilibrium stage around 30 h whilst the adsorption of DCAN on PG-SBA-CHX showed at least two phases but did not plateau out at this time range of study. The equilibrium time of PG-SBA-CHX was ca. 60 h (data not shown). These results suggest that disorder of mesopore structure resulting from pore size expansion and surface modification with surfactant affected the time required to attain the equilibrium.

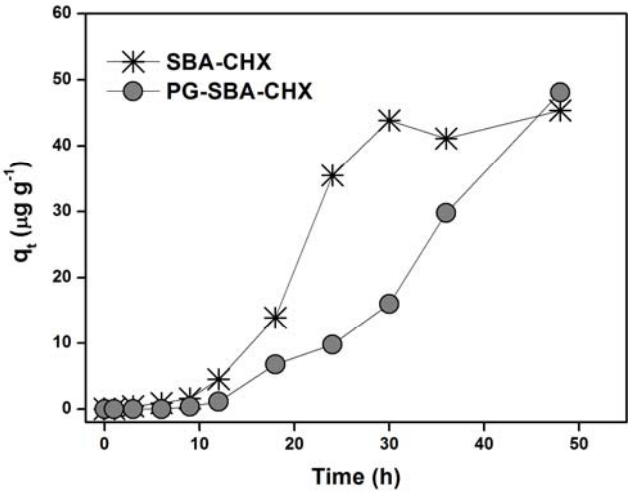

Figure 8.1 DCAN adsorption kinetics of SBA-CHX and PG-SBA-CHX at 100 μg L^{-1} in phosphate buffer at pH 7 with IS 10 mM

In order to investigate the adsorption mechanism, the pseudo-first-order and the pseudo-second-order models were used to fit with the experiment data. The linear form equations of the pseudo-first-order (Lagergren), the pseudo-second-order kinetic models and the initial adsorption rate, h (μg g^{-1} h^{-1}) at t = 0, based on the pseudo-second-order model are expressed as given in Equation (8.1) to (8.3):

$$\ln(q_e - q_t) = lnq_e - k_1 t \qquad (8.1)$$

$$\frac{t}{q_t} = \frac{1}{k_2 q_e^2} + \frac{t}{q_e} \qquad (8.2)$$

$$h = k_2 q_e^2 \qquad (8.3)$$

where q_t and q_e are the amount of DCAN adsorbed at any given time (t) and at equilibrium (μg g^{-1}), respectively, and k_1 and k_2 are the pseudo-first-order rate constant (h^{-1}) and the pseudo-second-order rate constant (g μg^{-1} h^{-1}).

Kinetic parameters along with the correlation coefficients (R^2) from the linear regression were calculated using the ORIGIN version 8.0 software and are shown in Table 8.1. The fitting results show that higher R^2 of the pseudo-second-order model. In addition, the effect of water on adsorption mechanism essentially can be

excluded due to at low concentration of DCAN in this study, therefore, the adsorbate concentration in the solution and the amount of active sites on the adsorbent surface are the key factors on the adsorption process in this study. Hence, the pseudo-second-order model is more suitable to describe the adsorption kinetic process on the parental SBA-CHX and PG-SBA-CHX at low solute concentration. Similar conclusions were found by Ho and McKay (1999) as a result of an analysis of data from the literature. They reported that the most of the adsorption systems follow a pseudo-second-order kinetic model.

Table 8.1 Kinetic parameters of DCAN adsorption on SBA-CHX and PG-SBA-CHX using the pseudo-first-order and pseudo-second-order models

Adsorbents	$q_{e,exp}$ (μg g^{-1})	Pseudo-first-order			Pseudo-second-order			
		$q_{e,cal}$ (μg g^{-1})	k_1 (h^{-1})	R^2	$q_{e,cal}$ (μg g^{-1})	k_2 (g μ$g^{-1}h^{-1}$)	R^2	h (μg $g^{-1}h^{-1}$)
SBA-CHX	45.37	58.74	0.059	0.745	46.08	0.0007	0.775	0.142
PG-SBA-CHX	50.13[a]	50.86	0.013	0.773	48.78	0.0005	0.829	0.108

[a] $q_{e,\ exp}$ of PG-SBA-CHX was obtained by prolonging the contact time to 72 h, and equilibrium time was ca. 60 h.

8.3.2 Intraparticle Diffusion Mechanism

Three consecutive mass transfer steps are associated with the adsorption of solute from solution by porous adsorbent (i) film or external diffusion, (ii) pore diffusion and (iii) adsorption at the site on the adsorbent surface. Thus, the intrapaticle diffusion model was also tested in this study, and the equation can be given in Equation (5.6) as shown in Chapter 5. However, the adsorption on surfactant-modified adsorbent (PG-SBA-CHX) may occur via different mechanisms or additional mechanisms due to the solubilization into the hydrophobic part of polymerized surfactant.

The plot of q_t versus $t^{0.5}$ of two adsorbents are shown in Figure 8.2, it was found that the data exhibited multi-linear plots in both adsorbents. For the parental SBA-CHX, the multi-linear of plot was due to the wide pore size distribution of synthesized adsorbents which was consequence of disordered mesopore structure. The external mass transfer (k_s) rate constant of SBA-CHX was relatively low which might be caused that the film diffusion was limited by a high hydrophilic surface

characteristic (water contact angle = 32.56^{o}). Furthermore, the second stage was relatively fast and it might associate with the interaction of DCAN into the adsorption sites present in the pore of adsorbent resulted in a higher internal pore diffusion rate. This adsorption phenomenon was similar to the adsorption behavior of a hydrophilic amino-functionalized HMS derivative (A-HMS) as described in Chapter 5. Moreover, the adsorption rate in the second region (intraparticle diffusion rate constant) of DCAN onto adsorbents had the following tendency: SBA-CHX > PG-SBA-CHX. But the adsorption of DCAN by SBA-CHX had a lower adsorption capacity towards the PG-SBA-CHX. This implies that a faster interaction or diffusion phenomena may occur in the large pore of SBA-CHX; however, the study in detail is still necessary to identify the phenomena.

In case of PG-SBA-CHX, it was found that the value k_s of PG-SBA-CHX was relatively slow and less than that for the parental SBA-CHX (Table 8.2) although its surface is high hydrophobic character which would expected to be a higher film diffusion rate due to reducing the water film resistance surrounding the adsorbent particle. As mention before, the adsorption on surfactant-modified adsorbent may occur via different mechanisms. Thus, it is possible that the slow rate at the initial period of adsorption might be caused that the DCAN is moderate hydrophilic adsorbate compared with the other HAN species resulting that it takes relatively long contact time to diffuse through the solution-surfactant admicelle structure interface and / or partition into the hydrophobic part of surfactant aggregated on external surface of adsorbent. Furthermore, the second region seemed to be both the external surface adsorption and particle diffusion which were concurrently occurred in adsorption process. It was observed that the rate constants of the second region of PG-SBA-CHX were lower than the parental adsorbent (Table 8.2). The different in adsorption mechanism on PG-SBA-CHX is by the partition process. This process (adsolubilization) might require long contact time for DCAN molecule partitioning into the admicelle structure of surfactant. This has previously been found that the diffusion rate of 2,4-dichlorophenol (2,4-DCP) form the particles surface into internal sites by pore diffusion of CTAB-bentonite was slower than that for the nature bentonite (Khenifi et al., 2009).

Moreover, the line plot of both adsorbents did not pass through the origin and so this confirmed the intraparticle diffusion was not the only rate-limiting step for DCAN adsorption.

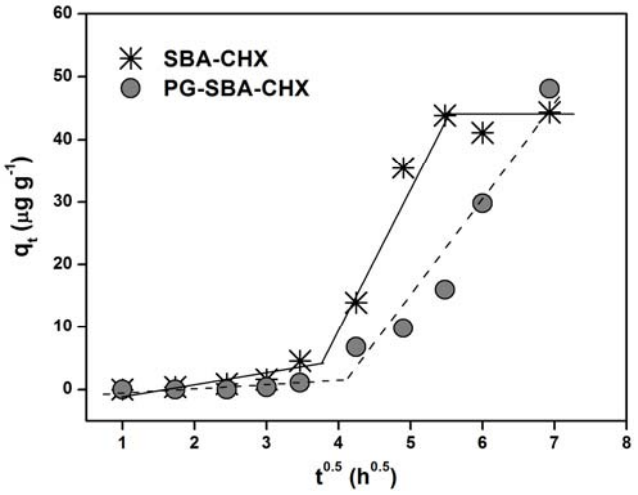

Figure 8.2 Plot of intraparticle diffusion model for the adsorption of DCAN on SBA-CHX and PG-SBA-CHX.

Table 8.2 Intraparticle diffusion parameters of DCAN adsorption on SBA-CHX and PG-SBA-CHX

Adsorbents	Intraparticle diffusion			
	k_s (μg g^{-1}h$^{-0.5}$)	k_{IP} (μg g^{-1}h$^{-0.5}$)	Intercept (*C*)	R^2
SBA-CHX	0.77	18.16	56.72	0.951
PG-SBA-CHX	0.38	13.43	50.80	0.911

8.4 EFFECT OF SURFACTANT MODIFICATION ON ADSORPTION OF HALOACETONITRILES

8.4.1 Proposed Adsorption Mechanism of HAN Adsorption on Surfactant-Modified Mesoporous Silicate

According to the characteristic of surfactant-modified adsorbent (PG-SBA-CHX) as described in Section 8.2, there are two important phenomena involving to the adsorption process, i.e. partition (or adsolubilization) and surface adsorption. The

partition process represents the distribution of a solute between two phases in which the solute is soluble, so called “adsolubilization”. This mechanism results from the change of surface characteristics from hydrophilicity to hydrophobicity due to the long alkyl chain of PG molecules. It is also associated with the hydrophobicity of organic adsorbates. Apart from the adsolubilization, PG surfactant is also capable of producing positive charges, i.e. cation derived from ammonium headgroup, on the surface of PG-SBA-CHX adsorbents and in turn creating more available active sites for adsorption.

Due to the remaining of silanol group on PG-SBA-CHX surface which is able to interact with HAN molecules. Surface adsorption includes hydrogen bonding and electrostatic interaction (ion-dipole interaction) based on the molecular structure of HANs and charge distribution consideration (Table 8.3). As discussion in Chapter 6, the ion-dipole electrostatic interaction was likely to be the main mechanism for adsorption in this study, thus the deprotonated (≡Si-O^-) / protonated (Si-OH_2^+) forms of remaining silanol groups are electrostatically adsorbed the opposite charge positions of the HANs molecules. The mechanism can be schematically illustrated as shown in Figure 5.3. Here, DCAN is selected as a model HANs for explanation.

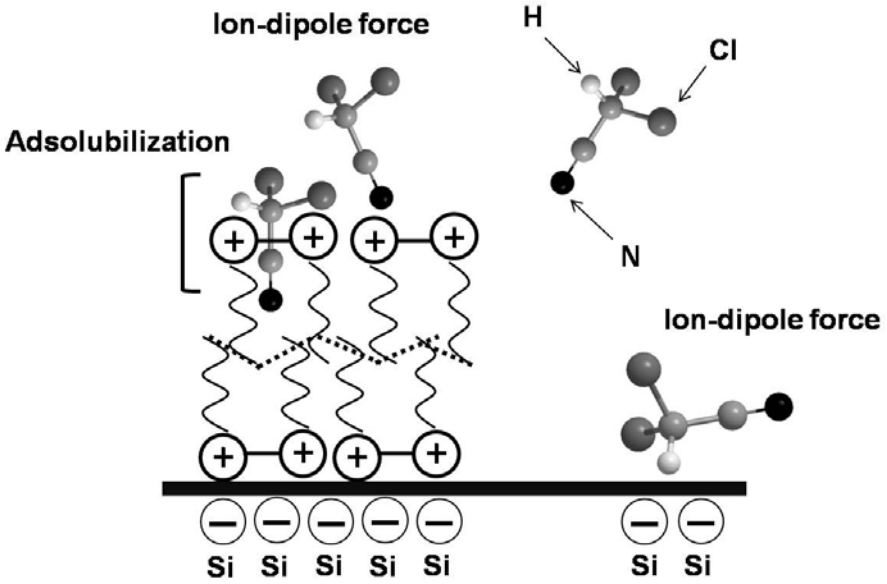

Figure 8.3 Model of DCAN adsorption mechanism on polymerizable gemini surfactant-modified mesoporous silicate

Table 8.3 Charge distribution and water solubility property of five-HANs

Molecular structure	Charges [a]									
	MCAN		MBAN		DCAN		DBAN		TCAN	
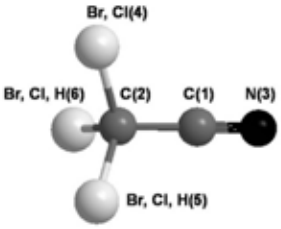	C(1)	-0.1304	C(1)	-0.1205	C(1)	-0.1254	C(1)	-0.1089	C(1)	+0.1136
	C(2)	-0.1323	C(2)	-0.2513	C(2)	-0.0239	C(2)	-0.2460	C(2)	-0.1298
	N(3)	-0.0537	N(3)	-0.0542	N(3)	-0.0177	N(3)	-0.0219	N(3)	-0.0027
	Cl(4)	-0.0838	Br(4)	+0.0094	Cl(4)	-0.0362	Br(4)	+0.0633	Cl(4)	+0.0044
	H(5)	+0.2002	H(5)	+0.2083	Cl(5)	-0.0364	Br(5)	+0.0632	Cl(5)	+0.0044
	H(6)	+0.2002	H(6)	+0.2083	H(6)	+0.2399	H(6)	+0.2504	Cl(6)	+0.0048
Water solubility (mg mL^{-1})	100		50-100		10-50		50		< 1	

[a] Calculated by ChemOffice Ultra 2005

8.4.2 Adsorption Isotherm of five-HANs in Single Solute Solution

Considering the partition process (adsolubilization) and hydrophobicity / hydrohilicity of HANs, an increased degree substitution of halogen atom in HANs molecules can increase the hydrophobicity of HANs (see Table 8.3), and so the hydrophobicity characteristic of admicelle structure (hydrophobic part of PG aggregation on adsorbent surface) would be expected to selectively adsorb a hydrophobic adsorbate in order of tri-HAN > di-HANs > mono-HANs.

The effect of surfactant modification on the adsorption capacities of the five-HANs adsorbates (MCAN, DCAN, TCAN, MBAN and DBAN) on the two adsorbents at pH 7 in single solute solution are shown in Figure 8.4. The parental SBA-CHX had higher adsorption capacities than PG-SBA-CHX in both mono-HANs (MCAN and MBAN). Negative surface charge derived from dissociation of silanol groups of parental SBA-CHX could contribute to ion-dipole electrostatic interaction towards positive dipole of H-atom in HAN molecules. For PG-SBA-CHX, mono-HANs can be electrostatically adsorbed on PG-SBA-CHX via interaction between positive charges of PG headgroup and negative dipole of N-atom of HAN molecules as well as between the remaining silanol groups (deprotonated form) and positive dipole of H-atom. Due to the low hydrophobicity of mono-HANs, they might not favor to partition into the admicelle structute suggesting that the surface adsorption might be likely plays an important role in the adsorption of mono-HANs by PG-SBA-CHX.

The adsorption capacities of the two di-HANs (DCAN and DBAN) on the two adsorbents are shown in Figure 8.4(c) and (d), respectively. As seen, the adsorption capacities of the both di-HANs on PG-SBA-CHX had significantly higher than the parental SBA-CHX. Moreover, di-HANs adsorption capacities were higher than that for mono-HANs. The di-HANs are more the hydrophobicity than the mono-HANs, thus allow a more significant hydrophobic interaction with such surface of PG-SBA-CHX. It can be concluded that the adsorption capacity of di-HANs might be enhanced due to the combination mechanism of the partition and the surface adsorption. For SBA-CHX, the adsorption capacity is also related to the molecular structure of HANs, i.e. a higher molecular weight and a stronger positive dipole of H-atom of di-HANs could be more adsorbed than mono-HANs.

The adsorption isotherms of TCAN on the two adsorbent are shown in Figure 8.4(e), the tri-HAN (TCAN) could be efficient adsorbed on the PG-SBA-CHX. These result also confirmed the supposed mechanism of the partition process (adsolubilization) that relates to the hydrophobicity of organic adsorbates. Consistent with this notion is that Mortland et al. (1986) pointed out that the relative energy of both adsorbate-solvent (i.e water) and adsorbate-adsorbent interactions affect the partitioning of adsorbate molecules between adsorbent and solvent (Mortland et al., 1986). In this study, the hydrophobic adsorbate (TCAN) can reduce its energy of interaction with water, consequently it could partition into the hydrophobic part of PG aggregation more easily than the hydrophilic adsorbate. For SBA-CHX, the adsorption of tri-HAN exhibited a comparable adsorption capacity to mono-HANs, although the positive dipole of TCAN molecule exhibits weaker values (Table 8.3). It might be caused that a larger pore size might enhance the internal surface accessibility and let the large molecular structure of TCAN can be adsorbed.

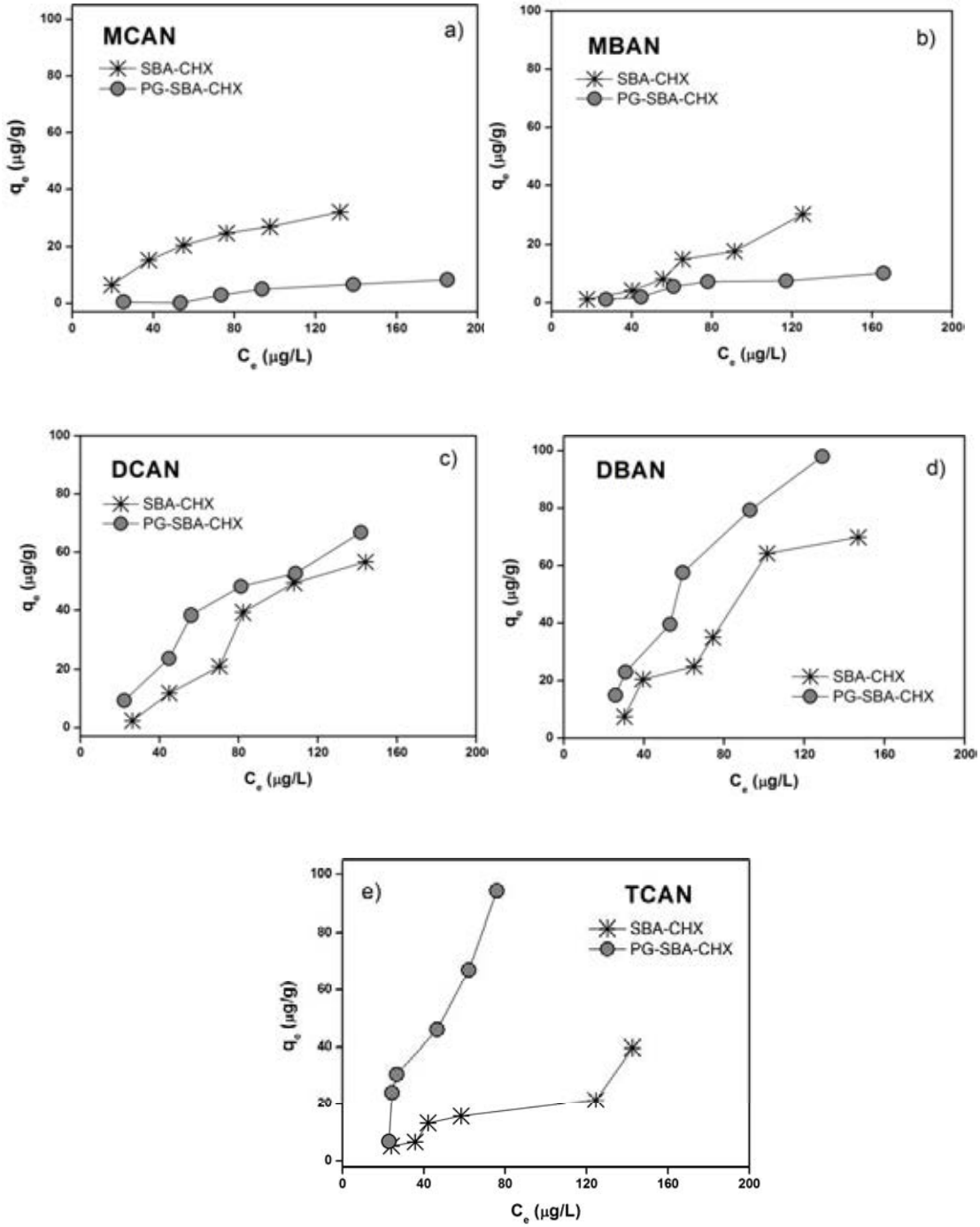

Figure 8.4 Adsorption isotherms of five-HANs on SBA-CHX and PG-SBA-CHX at pH 7 in phosphate buffer with IS 10 mM; (a) MCAN; (b) MBAN; (c) DCAN; (d) DBAN; and (e) TCAN

8.4.3 Isotherm Models

To investigate the adsorption mechanism of HANs on adsorbents in this study, three isotherm models including the Linear, Langmuir and Freundlich isotherm models, are used to analyze the experiment data. The Langmuir, and Freundlich Linear, equations are shown in Equations (6.2), (6.4) and (6.6), respectively (see Chapter 6).

The derived isotherm parameters and correlation coefficients (R^2) of the Linear, the Langmuir and the Freundlich models from the linear equations were calculated using the ORIGIN version 8.0 software and the results are all listed in Table 8.4. Since the equilibrium concentration was low, the Linear isotherm also fits well to the experimental results on both adsorbents with a high R^2 (> 0.89), except for the case of TCAN adsorption on SBA-CHX (R^2 = 0.851), which might be caused by at low concentration of HANs in this study.

Based on the correlation coefficients (R^2) of the Langmuir and the Freundlich parameters, the data seemed to best fit with the Freundlich isotherm model which is that the Freundlich isotherm is more suitable at low adsorbate concentration. Considering the K_F constants, the order of (highest to lowest) was TCAN > DBAN > DCAN >> MBAN > MCAN. The K_F value of TCAN was the highest value which was the greater partitioning of this adsorbate by PG-SBA-CHX. Moreover, some previous literature has been reported that the equilibrium adsorption conformed to both Langmuir and Freundlich models such as phenol and chlororinated phenol adsorption onto surfactant-modified bentonite and koalionite (Rawajfih and Nsour, 2006; Alkaram et al., 2009). The applicability of both models implies that the interaction between adsorbate molecules and adsorptive sites may be the pattern of monolayer adsorption while a heterogeneous surface of surfactant modified adsorbent. However, the adsorption experiments in this study were performed at low concentration, hence, the Linear isotherm model is also recommended in this study. Note, however, that the evaluation of the adsorption at high concentration of HANs is required further study for confirmation.

Table 8.4 Isotherm parameters of Linear, Langmuir and Freundlich models for adsorption of HANs in single solute on SBA-CHX and PG-SBA-CHX

Adsorbents	HANs	Linear		Langmuir			Freundlich		
		K_p	R^2	q_m (μg g^{-1})	K_L (L μg^{-1})	R^2	K_F (μg g^{-1})	*1/n*	R^2
SBA-CHX	MCAN	0.214	0.922	76.92	0.0044	0.982	0.580	0.817	0.945
	DCAN	0.517	0.953	84.75	0.0091	0.901	0.007	1.877	0.949
	TCAN	0.234	0.851	62.89	0.0034	0.907	0.023	1.003	0.895
	MBAN	0.275	0.966	52.55	0.0011	0.945	0.009	1.693	0.981
	DBAN	0.546	0.918	61.35	0.0041	0.775	0.094	1.342	0.798
PG-SBA-CHX	MCAN	0.052	0.961	26.38	0.0063	0.988	0.004	1.508	0.958
	DCAN	0.432	0.940	120.48	0.0022	0.901	0.443	1.041	0.942
	TCAN	1.386	0.951	263.16	0.0042	0.784	0.825	1.089	0.833
	MBAN	0.063	0.861	38.10	0.0086	0.905	0.021	1.252	0.887
	DBAN	0.753	0.942	178.54	0.0037	0.792	0.756	1.021	0.898

8.4.4 Effect of pH on DCAN Adsorption

The adsorption capacities of DCAN on the adsorbents at pH 5, 7, and 9 are presented in Figure 8.5. Increasing the pH of the solution from 5-7 and especially from 7 to 9 resulted in a higher DCAN adsorption on the two adsorbents. For SBA-CHX (Figure 8.5a), is charged more negatively at pH of 9 due to the increasing in the dissociation of silanol group which is considered as the major functional group on the surface of adsorbents. The charge of the H-atom of DCAN molecule is supposed to be more positive, as calculated by the ChemOffice Ultra 2005(Table 8.3). Therefore, the negative surface silanol charges could attract by the positive dipole of the DCAN H-atom (H6) via ion-dipole electrostatic interaction.

In case of PG-SBA-CHX (Fig. 9b), its surface was positively charged at pH between 5 and 9 (pH_{PZC} = 9.6). However the ratio of negative/positive charged moieties becomes higher with increasing pH, resulting in an enhancement of the ion-dipole electrostatic interaction with the DCAN molecule. Consistent with the result of amino-functionalized HMS (A-HMS) which has pH_{PZC} = 9.5, previously the result in this study indicated that the surface charge density significantly influenced the adsorption capacity of DCAN as described in Chapter 6. Comparison between PG-SBA-CHX and the parental SBA-CHX, the adsorption capacity of DCAN on SBA-CHX was 1.59-fold higher than that for the PG-SBA-CHX at pH 9 (SBA-CHX was

105.4 μg g^{-1} and PG-SBA-CHX was 66.31 μg g^{-1} at equilibrium concentration of 100 μg L^{-1} derived from the Linear adsorption isotherm). It might be caused that the small amount of remaining silanol groups and the positive charge of PG headgroup (ammonium group) may be balanced to neutral by hydroxide ion which is predominant species at high pH of solution, so resulted in the negative dipole of the N-atom in DCAN molecules could not interact with the positive charge of PG-SBA-CHX surface. Thus, the adsorption capacity was low.

At pH 5, the adsorption capacities of both adsorbent were lower than pH 7 and 9. Not only the density of negative charges was low, but also it might be due to the hydronium ion strongly completing with the positive H6 dipole of DCAN for the same negatively charged adsorptive sites on the surface or the two adsorbents. From these results, the interference of water molecule significantly affected the adsorption capacity of adsorbate at low concentration (Punyapalakul et al., 2009).

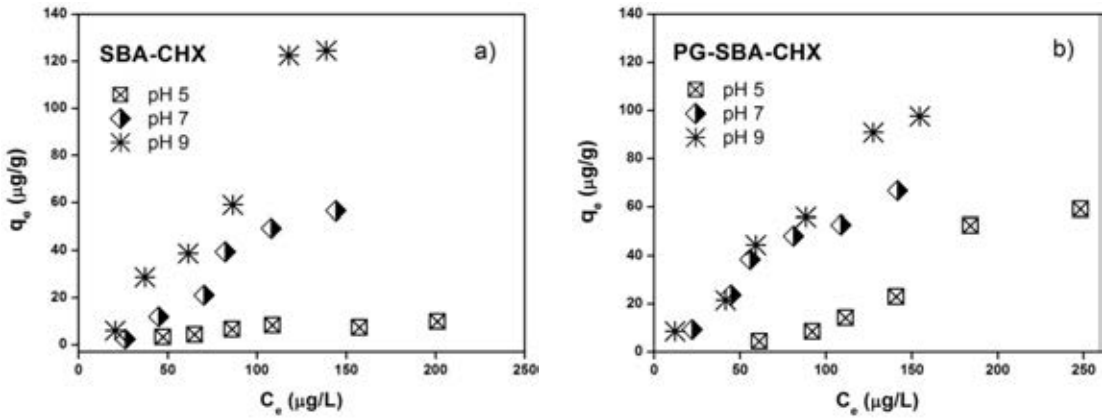

Figure 8.5 Effect of pH on the adsorption on DCAN at pH 5, 7 and 9 in phosphate buffer with IS 10 mM on (a) SBA-CHX and (b) PG-SBA-CHX.

8.4.5 Selective Adsorption of five-HANs in Mixed Solute Solution Compared with in Single Solute Solution

Adsorption isotherms for five-HAN_5 in single solute on the parental SBA-CHX and PG-SBA-CHX are shown in Figure 8.6(a) to (d). As seen in Figure 8.6a, the order of adsorption preference on the parental SBA-CHX was DBAN > DCAN >

TCAN ≅ MBAN ≅ MCAN on the parental SBA-CHX. This behavior might be related to its porous structure the strength of the positive dipole of di-HANs which could enhance the adsorption capacity. In addition, a large pore size may enhance the internal surface accessibility and let the larger molecular structure HANs can be adsorbed better than smaller one as discussion above. Consequently, the larger molecular weight of di-HANs and tri-HAN were more adsorbed than the mono-HANs. For PG-SBA-CHX, the adsorption preference was ranked in order of TCAN > DBAN > DCAN > MBAN ≅ MCAN. This could be linked to the hydrophobicity of HANs, because TCAN is the highest hydrophobicity (Table 8.3) at which it could more partition into the hydrophobic part of PG admicellle structure than di-HANs and mono-HANs.

The mixed five-HANs adsorption isotherms are shown in Figure 8.6(c) and (d). Interestingly, the adsorption capacity of each HAN on PG-SBA-CHX was less slightly than that in single solute results whereas a decreased adsorption capacity of each HANs revealed in the parental SBA-CHX. The amount of adsorptive sites by surface adsorption significantly influence to the adsorption capacity. Thus, the active sites of SBA-CHX were segregated for all five-HANs adsorbates resulting in a decreased adsorption capacity. On the contrary, at low concentration of HANs in this study might not affect the partition process of PG-SBA-CHX. In other words, the mixed five-HANs increased the overall concentration of adsorbate in aqueous solution which could contribute the predominant of partitioning process. Consistent with the notion of Rawajfih and Nsour (2006) that the sorption of organic solute was dominated by the surface adsorption at low concentrations and the partition (adsolubilization) was dominated at high concentration of adsorbate.

Furthermore, the order of adsorption capacity in mixed solute on the parental SBA-CHX was slightly different from the single solute results, being DBAN≅DCAN >TCAN > MBAN ≅ MCAN (Figure 8.6c), suggesting that the large molecular weight of the two di-HANs and tri-HAN are more easily adsorbed than the smaller molecular weight of mono-HANs at low concentration. The adsorption preference on PG-SBA-CHX was in the same as that seen in the single solute results (Figure 8.6d)

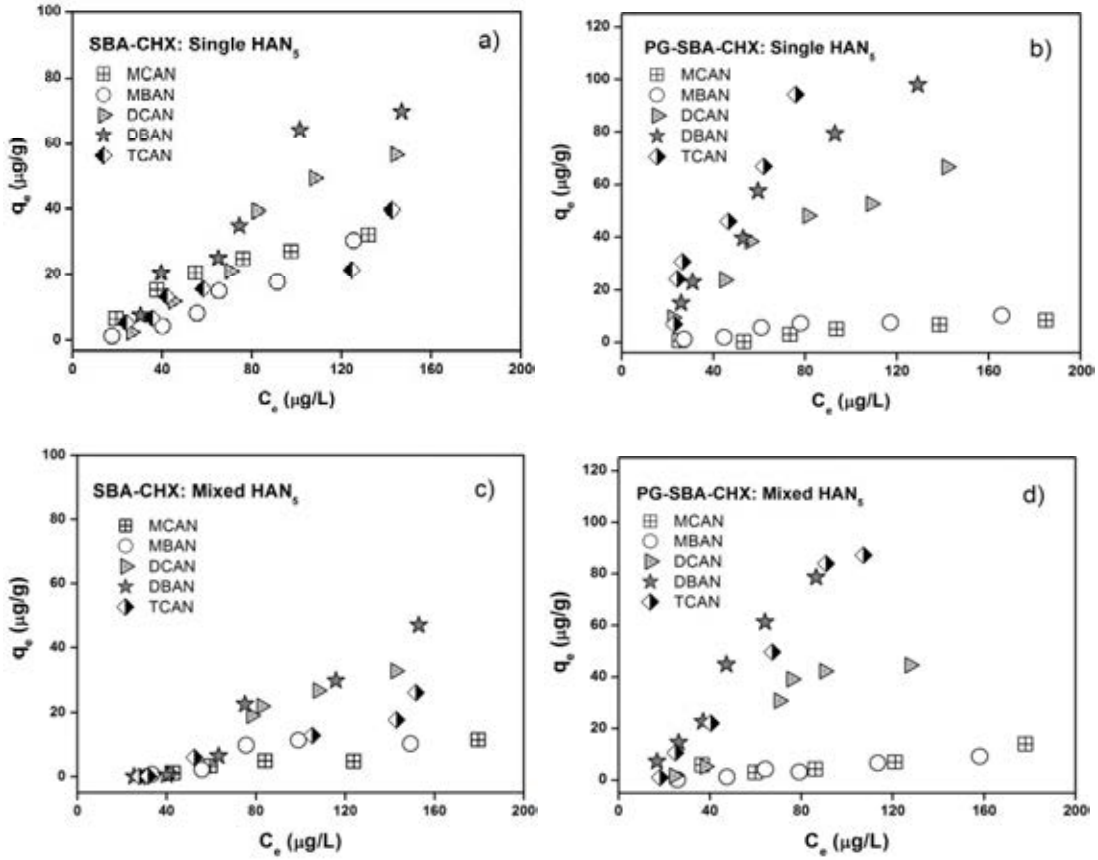

Figure 8.6 Adsorption isotherms of five-HAN$_s$ in single and mixed solutes on SBA-CHX and PG-SBA-CHX in phosphate buffer at pH 7 with IS 10 mM as a (a, b) in single solute; and (c,d) in mixed solute

8.5 SURFACTANT LEACHING STUDY

In order to determine the performance of polymerization process for fixing the bilayer of admicelle structure on the parental SBA-CHX, surfactant leaching test was employed with phosphate buffer at pH 7 by comparing the amount of surfactant leaching from solid surface between nonpolymerization PG-SBA-CHX and polymerization PG-SBA-CHX. As seen in Table 8.5 and Figure 8.7, the percentage of surfactant leaching of nonpolymerization PG-SBA-CHX and polymerization PG-SBA-CHX were 8.52% (retained 91.48%) and 1.89% (retained 98.11%), respectively. PG surfactant before polymerization was ca. 4.5 times higher desorbed from adsorbent surface than after polymerization. This result indicates that polymerization significantly reduces polymerizable surfactant leaching from adsorbent surface

consistent with previous reports described by Asnachinda et al. (2009) and Attaphong et al. (2010).

Table 8.5 Comparison of the surfactant leaching amount of PG-SBA-CHX before and after polymerization

	q_e of PG [a] (mmol g^{-1})	Leaching amount (mmol g^{-1})	Retained PG (%)	Leaching PG (%)
Non-polymerization	1.29	0.109	91.48	8.52
Polymerization	1.33	0.025	98.11	1.89

[a] Maximum adsorption capacity of PG on adsorbent surface.

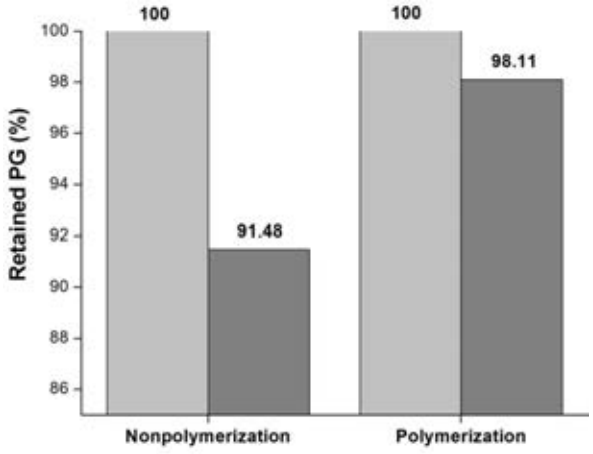

Figure 8.7 The percentage of retained PG surfactant of nonpolymerization PG-SBA-CHX and polymerization PG-SBA-CHX after washing with phosphate buffer (pH 7 with IS 10 mM) at 200 rpm for 24 h

8.6 COMPARISON OF PG-SBA-CHX WITH THE OTHER FUNCTIONALIZED HMS DERIVATIVES

The adsorption capacities of PG-SBA-CHX and other functionalized HMS derivatives (A-HMS, OD-HMS and Ti-HMS) for the five-HAN adsorption in single solute at equilibrium concentration 100 mg L^{-1} (pH 7) derived from the Linear adsorption isotherm are given in Table 8.5. Note that the data for five-HAN adsorption on M-HMS had the much higher adsorption capacities superior to the other functionalized HMS derivatives and PG-SBA-CHX. Comparing the results, PG-SBA-CHX could efficiently adsorb tri-HAN (TCAN) followed by di-HANs (DCAN and

DBAN) and their capacities reached 138.60, 43.2 and 75.30 mg g^{-1} for TCAN, DCAN, and DBAN, respectively; superior to other functionalized HMS derivatives. With the exception of the mono-HANs adsorption (MCAN and MBAN) PG-SBA-CHX exhibited quite lower adsorption capacity than the other which is because the low hydrophobicity of organic adsorbates may not be flavorable to partition process of PG-SBA-CHX. Thus, it can be concluded that the surfactant-modified adsorbent is revealed a high potential for use as an adsorbent for the removal of HANs which is high hydrophobic nature from aqueous solution.

Table 8.5 Comparison of the adsorption capacities of five-HANs onto PG-SBA-CHX and the other functionalized HMS derivatives

HANs	Adsorbents	q_e (μg g^{-1})[a]
MCAN	PG-SBA-CHX	5.20
	A-HMS	57.72
	OD-HMS	61.64
	Ti-HMS	102.82
DCAN	PG-SBA-CHX	43.20
	A-HMS	95.33
	OD-HMS	17.87
	Ti-HMS	16.98
TCAN	PG-SBA-CHX	138.60
	A-HMS	41.38
	OD-HMS	17.19
	Ti-HMS	46.39
MBAN	PG-SBA-CHX	6.30
	A-HMS	83.08
	OD-HMS	59.36
	Ti-HMS	136.92
DBAN	PG-SBA-CHX	75.30
	A-HMS	66.54
	OD-HMS	24.56
	Ti-HMS	44.08

[a] q_e at equilibrium concentration of 100 μg L^{-1} derived from Linear adsorption isotherm

8.7 CONCLUSIONS

Surfactant-modified adsorbent was synthesized by adsorption polymerizable gemini surfactant (PG) on mesoporous silicate (SBA-CHX). In kinetic studies, DCAN adsorption on surfactant-modified adsorbent and unmodified adsorbent followed the pseudo-second order model. The adsorption rate of surfactant-modified adsorbent seemed to be controlled by surface adsorption and intraparticle diffusion and surface adsorption. The adsorption capacities of HANs can be improved after surface modification by surfactant especially the adsorption of the hydrophobic HANs. The adsorption mechanism involved partition and surface adsorption (i.e. ion-dipole electrostatic interaction). The partition process related to the hydrophobicity of organic adsorbates. The experimental isotherm data fitted well with the Linear isotherm model due to at low concentration of adsorbates. Interference by water molecules at low concentrations of DCAN strongly affected the adsorption mechanism. In addition, the high degree of substitution of halogen atom in HAN molecule can increase the hydrophobicity property which significantly affected the adsorption selectivity by the partition process. The partition was predominant at high concentration of adsorbate. The polymerization of polymerizable surfactant could reduce the surfactant leaching from adsorbent surface.

CHAPTER IX

REGENERATION STUDY

9.1 INTRODUCTION

Activated carbon and synthetic adsorbents are widely use in adsorption process. The regeneration of adsorbent is one of the important factors which affect the overall cost of the adsorbent process. It is well known that regeneration of activated carbons by thermal process is sometimes problematic due to carbon lost and attrition during heating of each cycle. Even though the adsorption capacity of synthetic adsorbents is almost less than that of activated carbon, however, their regeneration is suggested to be easier because of the uniformity of surface functional groups and crystalline structure. Mesoporous silicate, is one of the synthetic adsorbents, is possible to be an alternative adsorbent to activated carbon. Various regeneration methods for those mesoporous silicates have been studied in previous literature such as solvent extraction, desorption by acidic/akaline solution and etc. However, the effective regeneration depends on adsorbate/adsorbent interaction.

In order to evaluate the possibility of regeneration for HAN saturated adsorbents, regeneration experiments have been performed by (i) solvent extraction process and (ii) extraction by aqueous solution in the pH range 5 to 9. Also, regeneration study of powder activated carbon (PAC) was also studied for comparison.

9.2 REGENERATION EFFICIENCY OF DCAN ADSORBED HMS, M-HMS AND PAC

To study the regeneration efficiency of DCAN adsorbed adsorbents, in this study, M-HMS was chosen due to excellence DCAN adsorption efficiency and for representative of functionalized HMS derivative. The parental HMS and PAC were also studied for comparison. The DCAN adsorbed HMS, M-HMS and PAC were extracted by various kinds of eluant solvent (such as methanol, ethanol, acetone, and

MtBE), as well as various pH values of phosphate buffer solution (pH 5, 7, and 9) at 25 ^{o}C for 24 h. The eluant strength (ε^{o}) of methanol, ethanol, acetone, and MtBE are 0.95, 0.88, 0.56 and 0.2, respectively. Ratio extract solution/adsorbent was fixed at 500 v/w (mL g^{-1}) for M-HMS and PAC, and 250 v/w (mL g^{-1}) for HMS due to low DCAN adsorbed on HMS surface.

Table 9.1 shows the DCAN regeneration efficiencies of the parental HMS, M-HMS and PAC. It was found that regeneration efficiency percentage in all cases were quite low, although, these conditions were expected to weaken the adsorptive interaction between the adsorbate and adsorbent surface.

For M-HMS, an irreversible adsorbed DCAN result was consistent with the FT-IR evidences, as described in Chapter 6, The FT-IR spectra (Figure 6.9d) exhibited a new band at wavenumber of 1680 cm^{-1} corresponding to the C=N stretching caused by the interaction between ≡Si-R-S^{-} of mercapto group which acts as a strong neucleophile, and carbon atom of nitrile group (electrophile) to form a chemical bond. It seems likely that adsorption mechanism can be assumed as follows: the ion-dipole electrostatic interaction facilitated the interaction of nitrile and mercapto groups and then the formation of chemical bond was occurred. Moreover, this also consisted with the notion in literature described by Patai (1974) that the nitrile group can undergo an addition reaction with thiol group resulting in the formation of a carbon-sulfur bond. Thus, it can be concluded that the adsorption of DCAN was chemisorbed on M-HMS surface. The interaction between mercapto groups of M-HMS and DCAN can be supposed as follows:

$$\equiv \text{Si-R-SH} + \text{N}\equiv\text{CCl}_2\text{CH} \longrightarrow \equiv \text{Si-R-S}\text{——}\text{HN}=\text{CCl}_2\text{CH} \qquad (9.1)$$

In case of HMS, it is possible that the dissociate silanol group (≡Si-O^{-}) can interact with nitrile group and form a chemical bond which might be because the –OH moiety of silanol group is a neucleophile character as same as –SH moiety (or thiol group). However, the –OH moiety is a weaker neucleophile compared with the strong neucleophile of thiol group, and the FT-IR evidence is still unclear to confirm this mechanism. In addition, the strength of interaction between adsorbate and silica

surface is always variable and dependent on adsorption active sites (Bui and Choi, 2009). In this case, the heterogeneity of silica surface with several types of silanol group, for example ≡Si-O¯, ≡Si-OH, ≡Si-O····H····O-Si≡ and etc., might be strong interaction resulted in the irreversible adsorption.

For PAC, low regeneration efficiency was revealed as M-HMS and HMS. It might be caused that the complexity of surface functional group of PAC may contribute the irreversible adsorption. PAC surface consists of various organic functional groups such as carbonyl, carboxyl, phenyl and oxygen-containing groups which can introduce various interactions between DCAN and its surface functional groups such as covalent bonding, hydrogen bonding, electrostatic force and etc. Moreover, Tamon et al. (1996) reported that irreversibility of electron-donating compounds adsorption such as phenol and aniline was observed on activated carbon, whereas reversible adsorption was observed for the electron-attracting compound (such as nitrobenzene). Evidence of this literature supports the result obtained in this study that the nitrile group of DCAN is an electron-donating group, thus the irreversible adsorption of DCAN might occur. However, the further research to investigate the effect of surface complexity of PAC on adsorption mechanism is required.

Tables 9.1 Regeneration efficiencies of DCAN from HMS, M-HMS and PAC by extraction method

Adsorbents	q_e [a]	**Regeneration efficiency (%)** [b]						
	(mg g^{-1})	**Phosphate buffer extraction**			**Solvent extraction**			
		pH 5	**pH 7**	**pH 9**	**Acetone**	**Methanol**	**Ethanol**	**MtBE**
HMS	0.057	0.1483	0.0001	-	0.2436	-	0.0000	1.0686
M-HMS	44.54	0.0071	0.0028	0.0014	0.1084	0.0158	0.0445	0.1025
PAC	85.51	0.0025	0.0022	0.0005	0.1487	0.0286	0.0234	0.1705

a Pre-adsorption of DCAN at pH 7 in phosphate buffer with IS 10 mM (25 °C) at equilibrium concentration in range 5 to 80 μg L^{-1}

b All regeneration experiments were performed under duplicate condition.

9.3 CONCLUSIONS

The possible of adsorbent regeneration by extraction with solvent and various pH aqueous solutions was evaluated. The mechanism of adsorbent regeneration by extraction is expected to weaken the adsorptive interaction between the adsorbate and adsorbent surface. The results showed that regeneration efficiencies percentage of the three adsorbents (HMS, M-HMS and PAC) were quite low due to DCAN irreversible adsorption on their surface. The evidences of irreversible adsorption in this study and the appearance of the C=N stretching based on FT-IR spectra also confirmed the chemisorbed DCAN on M-HMS surface (see Figure 6.9d in Chapter 6). The ion-dipole electrostatic interaction facilitated the interaction of nitrile and mercapto groups and then the formation of chemical bond was occurred. The parental HMS was also displayed the irreversible adsorption of DCAN, however, the mechanism is still unclear and cannot be concluded now. In addition, the complexity of surface functional group contributed the irreversible adsorption of DCAN on PAC which might be related to the electron donating group of nitrile in DCAN molecule. However, further research to investigate the effect of surface functional group complexity of PAC on adsorption mechanism is required.

CHAPTER X

CONCLUSIONS AND RECOMMENDATIONS

10.1 CONCLUSIONS

The main objective of this study is to investigate the removal of haloacetonitriles (HANs) in aqueous solution by adsorption on various surface-modified inorganic porous materials. Hexagonal mesoporous silicate (HMS) was synthesized and modified surface with various organic functional groups (amino-, mercapto- and octyl groups) to investigate the effect of surface functional group on adsorption efficiency and mechanism compared with powder activated carbon (PAC). In addition, HMS then modified by substitution of titanium in silicate structure to investigate the relationship between the porous structure and the resultant adsorption capacities, compared to the similar mesopore SBA-15. Zeolite NaY was used so as to investigate the effect of a crystalline structure. Furthermore, mesoporous silicate SBA-CHX was modified surface by polymerizable gemini surfactant (PG-SBA-CHX) adsorption to investigate the effect of surface modification by surfactant on HAN adsorption efficiency. These adsorbents were characterized their physicochemical properties. The adsorption kinetics, adsorption isotherms and mechanism, the effects of pH of solution and temperature, selective adsorption of HAN_5 by comparing single and mixed solutes, and surfactant desorption were also investigated under batch adsorption experiments.

According to the physicochemical property characterization results, the different levels of disorder of the mesopore structures upon incorporation of the functional groups were exhibited based on XRD and N_2 adsorption isotherms, which are dependent upon the type of organosilanes present in the synthesis mixtures and functionalization method. Elemental analysis data and FT-IR spectra demonstrated the presence of the organic functional groups and PG surfactant coverage on the adsorbent surface, including polymerization degree. Surface characteristic of adsorbents, i.e. surface charge and hydrophilic/hydrophobic characteristic, were change after surface modification with organosilanes and surfactant.

For kinetic adsorption study, the pseudo-second order model can be used to describe the adsorption kinetic of DCAN onto the synthesized adsorbents at a low solute concentration. The kinetic results were implied that the adsorption process was dependent on both the boundary layer effect and the intraparticle diffusion. Hydrophobic surface characteristic of the adsorbent could reduce the film resistance of water to mass transfer surrounding the adsorbent particle. The pore size of the adsorbent affected the boundary layer thickness.

For adsorption isotherm studies, the results indicated that the surface functional groups, porosity and crystalline structure significantly affected the adsorption capacity of five-HANs. The mercapto-functionalized HMS derivative (M-HMS) could efficiently adsorb HANs superior to the other HMS derivatives and had a higher adsorption capacity of HANs comparable to PAC. Interference by water molecules at low concentrations of adsorbate strongly affected the adsorption mechanism. The Sips isotherm model was successfully applied to describe the adsorption on PAC and M-HMS at high concentration whereas the experimentally derived isotherm data of the parental HMS, functionalized HMS derivatives, SBA-15 and NaY fitted well with the Linear isotherm due to at low concentration (ppb level) of adsorption experiments. The adsorption was favored at high pH due to a high negative surface charge density of adsorbent. In addition, the adsorption temperature increased leading to the increased adsorption capacity of DCAN adsorbed on adsorbent surface, indicating that the adsorption is controlled by endothermic process. The positive entropy suggests the possibility of some structure changes in both adsorbates and adsorbents during the adsorption process. The FT-IR analysis indicated that the adsorption mechanism was involved a more complex interplay between an ion-dipole electrostatic interaction and chemisorption.

For adsorption selectivity studies, the results revealed that the molecular structure of HANs obviously affected the adsorption capacity and selectivity over M-HMS whereas selective adsorption over PAC was not observed. Moreover, the different porous and crystalline structures of adsorbents (mesopore HMS, Ti-HMS, SBA-15 and micropore NaY) affected the selective adsorption of five-HANs as well as hydrophilic/hydrophobic nature of both adsorbent and adsorbate also influenced

their selective adsorption. Furthermore, the effect of electrolyte in tap water and the presence of co-existing DBPs did not affect the adsorption capacities and selectivity of M-HMS and PAC in the mixed solute solution.

The influence of surfactant-modified surface of mesoporous silicate SBA-CHX on the adsorption of HANs indicated that the adsorption capacities of HANs can be improved after surface modification with surfactant especially the adsorption of the hydrophobic HANs. The adsorption mechanism involved partition and surface adsorption (i.e. ion-dipole electrostatic interaction). The partition process related to the hydrophobicity of organic adsorbates. The experimental isotherm data fitted well with the Linear isotherm model due to at low concentration of adsorbates. Interference by water molecules at low concentrations of DCAN strongly affected the adsorption mechanism. In addition, the high degree of substitution of halogen atom in HAN molecule can increase the hydrophobicity property which significantly affected the adsorption selectivity by the partition process. The partition was predominant at high concentration of adsorbate. The polymerization of polymerizable surfactant could reduce the surfactant leaching from adsorbent surface.

For adsorbent regeneration studies, the results indicated that regeneration efficiency percentage of the three adsorbents (HMS, M-HMS and PAC) were quite low due to DCAN irreversible adsorption on their surface. The evidences of irreversible adsorption in this study and the appearance of the C=N stretching based on FT-IR spectra also confirmed the chemisorbed DCAN on M-HMS surface. The ion-dipole electrostatic interaction facilitated the interaction of nitrile and mercapto groups and then the formation of chemical bond was occurred. The parental HMS was also displayed the irreversible adsorption of DCAN, however, the mechanism is still unclear and cannot be concluded now. In addition, the complexity of surface functional group contributed the irreversible adsorption of DCAN on PAC which might be related to the electron donating group of nitrile in DCAN molecule.

10.2 ENGINEERING SIGNIFICANCE

Adsorption mechanism data of HAN adsorption on various types of organic functional groups were investigated towards a better understanding the most

important role of adsorptive interaction force. Those obtained information can be applied for the development of adsorbents and to design the sequence of multiple steps adsorption process or combining with the conventional activated carbon to ensure safety of drinking/tap water for halogenic micropolutants especially DBPs. Moreover, the obtained information of adsorption capacity, selectivity and regeneration ability of each functional group and porous structure will be applied to design sequence of filter unit to obtain final highest adsorption capacity of overall contaminants with long time cycle period and recyclable by reasonable and safety method.

10.3 RECOMMENDATIONS AND FUTURE WORK

As results, mercapto-functionalized HMS derivative (M-HMS) can be an alternative to PAC for removal DBPs such as THMs and HANs in aqueous solution. However, further studies will be investigated to improve the adsorption capacity and selectivity of M-HMS for HAA removal. Bi-functional group mesoporous silicate of mercapto- and amine group modification with various ratios is of interest for this approach. Even though the regeneration efficiency of M-HMS and PAC were quite low due to HAN irreversible adsorption on their surface, however, the study of regeneration ability and reuse efficiency of used adsorbent after THMs and HAAs adsorption requires further investigation. In addition, cost-benefit analysis will be investigated comparing with commercial adsorbents such as PAC and the other treatment methods.

REFERENCES

Abe, M., et al. Polymerized assemblies of cationic gemini surfactants in aqueous solution. Journal of Colloid and Interface Science 330 (2009): 250-253.

Abe, M., Tsubone, K., Koike, T., Tsuchiya, K., Ohkubo, T., and Sakai, H. Polymerizable cationic gemini surfactant. Langmuir 22 (2006): 8293-8297.

Adak, A.,Bandyopadhyay, M., and Pal, A. Removal of crystal violet dye from wastewater by surfactant-modified alumina. Separation and Purification Technology 44 (2005): 139-144.

Aguado, J., Arsuaga, J.M., Arencibia, A., Lindo, M., and Gascón, V. Aqueous heavy metals removal by adsorption on amine-functionalized mesoporous silica. Journal of Hazardous Materials 163 (2009): 213-221.

Ahmaruzzaman, M., and Laxmi Gayatri, S. Batch adsorption of 4-nitrophenol by acid activated jute stick char: Equilibrium, kinetic and thermodynamic studies. Chemical Engineering Journal 158 (2010): 173-180.

Al-Ghouti, M.A.,Khraisheh, M.A.M.,Allen, S.J., and Ahmad, M.N. The removal of dyes from textile wastewater: a study of the physical characteristics and adsorption mechanisms of diatomaceous earth. Journal of Environmental Management 69 (2003): 229-238.

Alkaram, U.F.,Mukhlis, A.A., and Al-Dujaili, A.H. The removal of phenol from aqueous solutions by adsorption using surfactant-modified bentonite and kaolinite. Journal of Hazardous Materials 169 (2009): 324-332.

Alkilany, A.M., and Murphy, C.J. Gold Nanoparticles with a Polymerizable Surfactant Bilayer: Synthesis, Polymerization, and stability evaluation Langmuir 25 (2009): 13874-13879.

Amy, G., and Cho, J. Interactions between natural organic matter (NOM) and membranes: Rejection and fouling. Water Science and Technology 40 (1999): 131-139.

Amy, G.L.,Tan, L., and Davis, M.K. The effects of ozonation and activated carbon adsorption on trihalomethane speciation. Water Research 25 (1991): 191-202.

Anbia, M., and Lashgari, M. Synthesis of amino-modified ordered mesoporous silica as a new nano sorbent for the removal of chlorophenols from aqueous media. Chemical Engineering Journal 150 (2009): 555-560.

Asnachinda, E.,Khaodhiar, S., and Sabatini, D.A. Effect of ionic head group on admicelle formation by polymerizable surfactants. Journal of Surfactant Detergent 12 (2009): 379–386.

Asouhidou, D.D.,Triantafyllidis, K.S.,Lazaridis, N.K., and Matis, K.A. Adsorption of Remazol Red 3BS from aqueous solutions using APTES- and cyclodextrin-modified HMS-type mesoporous silicas. Colloids and Surfaces A: Physicochemical and Engineering Aspects 346 (2009a): 83-90.

Asouhidou, D.D., Triantafyllidis, K.S., Lazaridis, N.K., Matis, K.A., Kim, S.-S., Pinnavaia, T.J. Sorption of reactive dyes from aqueous solutions by ordered hexagonal and disordered mesoporous carbons. Microporous and Mesoporous Materials 117 (2009b): 257-267.

Ates, N.,Yilmaz, L.,Kitis, M., and Yetis, U. Removal of disinfection by-product precursors by UF and NF membranes in low-SUVA waters. Journal of Membrane Science 328 (2009): 104-112.

Athens, G.L.,Shayib, R.M., and Chmelka, B.F. Functionalization of mesostructured inorganic-organic and porous inorganic materials. Current Opinion in Colloid & Interface Science 14 (2009): 281-292.

Attaphong, C.,Asnachinda, E.,Charoensaeng, A.,Sabatini, D.A., and Khaodhiar, S. Adsorption and adsolubilization of polymerizable surfactants on aluminum oxide. Journal of Colloid and Interface Science 344 (2010): 126-131.

Babi, K.G., Koumenides, K.M., Nikolaou, A.D., Makri, C.A., Tzoumerkas, F.K., and Lekkas, T.D. Pilot study of the removal of THMs, HAAs and DOC from drinking water by GAC adsorption. Desalination 210 (2007): 215-224.

Bichsel, Y., and von Gunten, U. Formation of Iodo-trihalomethanes during disinfection and oxidation of Iodide-containing waters. Environmental Science & Technology 34 (2000): 2784-2791.

Bjelopavlic, M.,Newcombe, G., and Hayes, R. Adsorption of NOM onto Activated Carbon: Effect of surface Charge, ionic strength, and pore volume distribution. Journal of Colloid and Interface Science 210 (1999): 271-280.

Bui, T.X., and Choi, H. Adsorptive removal of selected pharmaceuticals by mesoporous silica SBA-15. Journal of Hazardous Materials 168 (2009): 602-608.

Bull, R.J., et al. Evaluation of mutagenic and carcinogenic properties of brominated and chlorinated acetonitriles: By-products of chlorination. Fundamental and Applied Toxicology 5 (1985): 1065-1074.

Busca, G.,Montanari, T.,Bevilacqua, M., and Finocchio, E. Removal and recovery of nitriles from gaseous streams: An IR study of acetonitrile adsorption on and desorption from inorganic solids. Colloids and Surfaces A: Physicochemical and Engineering Aspects 320 (2008): 205-212.

Cao, L.,Man, T., and Kruk, M. Synthesis of Ultra-Large-Pore SBA-15 Silica with Two-Dimensional Hexagonal Structure Using Triisopropylbenzene As Micelle Expander. Chemistry of Materials 21 (2009): 1144-1153.

Cancho, B., Ventura, F., and Galceran, M.T. Behavior of halogenated disinfection By-products in the water treatment plant of barcelona, spain. Bulletin of Environmental Contamination and Toxicology 63 (1999): 610-617.

Cestari, A.R.,Vieira, E.F.S.,Vieira, G.S., and Almeida, L.E. The removal of anionic dyes from aqueous solutions in the presence of anionic surfactant using aminopropylsilica--A kinetic study. Journal of Hazardous Materials 138 (2006): 133-141.

Charoensaeng, A.,Sabatini, D., and Khaodhiar, S. Styrene solubilization and adsolubilization on an aluminum oxide surface using linker molecules and extended surfactants. Journal of Surfactants and Detergents 11 (2008): 61-71.

Cho, J.,Amy, G.,Pellegrino, J., and Yoon, Y. Characterization of clean and natural organic matter (NOM) fouled NF and UF membranes, and foulants characterization. Desalination 118 (1998): 101-108.

Choi, H.-D., Jung, W.-S., Cho, J.-M., Ryu, B.-G., Yang, J.-S., and Baek, K. Adsorption of Cr(VI) onto cationic surfactant-modified activated carbon. Journal of Hazardous Materials 166 (2009): 642-646.

Chong, A.S.M.,Zhao, X.S.,Kustedjo, A.T., and Qiao, S.Z. Functionalization of large-pore mesoporous silicas with organosilanes by direct synthesis. Microporous and Mesoporous Materials 72 (2004): 33-42.

Chutia, P.,Kato, S.,Kojima, T., and Satokawa, S. Adsorption of As(V) on surfactant-modified natural zeolites. Journal of Hazardous Materials 162 (2009): 204-211.

Ciesla, U., and Schuth, F. Review: Ordered mesoporous materials. Microporous and mesoporous Material 27 (1999): 131-149.

Dai, X.,Zou, L.,Yan, Z., and Millikan, M. Adsorption characteristics of N-nitrosodimethylamine from aqueous solution on surface-modified activated carbons. Journal of Hazardous Materials 168 (2009): 51-56.

Damjanovic, L.,Rakic, V.,Rac, V.,Stosic, D., and Auroux, A. The investigation of phenol removal from aqueous solutions by zeolites as solid adsorbents. Journal of Hazardous Materials 184 (2010): 477-484.

Daniel, F.B.,Schenck, K.M., and Mattox, J.K. Genotoxic properties of haloacetonitriles: drinking water by-products of chlorine disinfection. Fundamental and Applied Toxicology 6 (1986): 447-453.

Dickson, J., and O'Haver, J. Adsolubilization of naphthalene and naphthol in CnTAB admicelles. Langmuir 18 (2002): 9171-9176.

EPA Method 551.1, 1990. Determination of Chlorination Disinfection Byproducts, chlorinated solvents, and Halogenated Pesticides/Herbicides in Drinking Water by Liquid-Liquid Extraction and Gas Chromatography with Electron-capture Detection. National Exposure Research Laboratory, Office of Research and Development, U.S. Environmental Protection Agency, Cincinnati, OHIO.

EPA Method 552.2, 1990. Determination of Haloacetic Acids and Dalapon in Drinking Water by Liquid-Liquid Extraction, Derivatization and Gas Chromatography with Electron-capture Detection. National Exposure Research Laboratory, Office of Research and Development, U.S. Environmental Protection Agency, Cincinnati, OHIO.

Esumi, K. Adsorption and adsolubilization of surfactants on titanium dioxides with functional groups. Colloids and Surfaces A: Physicochemical and Engineering Aspects 176 (2001): 25-34.

Esumi, K.,Nakao, T., and Ito, S. Fixation of Polymerizable surfactant on alumina by UV irradiation. Journal of Colloid and Interface Science 156 (1993): 256-257.

Esumi, K.,Watanabe, N., and Meguro, K. Polymerization of styrene adsolubilized in polymerizable surfactant bilayer on alumina. Langmuir 7 (1991): 1775-1778.

Foo, K.Y., and Hameed, B.H. Insights into the modeling of adsorption isotherm systems. Chemical Engineering Journal 156 (2010): 2-10.

Ghiaci, M.,Kia, R.,Abbaspur, A., and Seyedeyn-Azad, F. Adsorption of chromate by surfactant-modified zeolites and MCM-41 molecular sieve. Separation and Purification Technology 40 (2004): 285-295.

Gimbert, F.,Morin-Crini, N.,Renault, F.,Badot, P.-M., and Crini, G. Adsorption isotherm models for dye removal by cationized starch-based material in a single component system: Error analysis. Journal of Hazardous Materials 157 (2008): 34-46.

Glezer, V.,Harris, B.,Tal, N.,Iosefzon, B., and Lev, O. Hydrolysis of haloacetonitriles: LINEAR FREE ENERGY RELATIONSHIP, kinetics and products. Water Research 33 (1999): 1938-1948.

Gopal, K.,Tripathy, S.S.,Bersillon, J.L., and Dubey, S.P. Chlorination byproducts, their toxicodynamics and removal from drinking water. Journal of Hazardous Materials 140 (2007): 1-6.

Grunwald, A.,Stastny, B.,Slavickova, K., and Slavicek, M. Formation of haloforms during chlorination of Natural Waters. Acta Polytechnica 42 (2002): 56-59.

Gu, F.N.,Zhou, Y.,Wei, F.,Wang, Y., and Zhu, J.H. Creating the adsorptive sites with high performance toward nitrosamines in mesoporous silica MCM-41 by alumina modifier. Microporous and Mesoporous Materials 126 (2009): 143-151.

Gűnay, A.,Arslankaya, E., and Tosun, I. Lead removal from aqueous solution by natural and pretreated clinoptilolite: Adsorption equilibrium and kinetics. Journal of Hazardous Materials 146 (2007): 362-371.

Han, R., Zhang, J., Han, P., Wang, Y., Zhao, Z., Tang, M. Study of equilibrium, kinetic and thermodynamic parameters about methylene blue adsorption onto natural zeolite. Chemical Engineering Journal 145 (2009): 496-504.

Ho, Y.S., and McKay, G. Pseudo-second order model for sorption processes. Process Biochemistry 34 (1999): 451-465.

Hoffmann, F.,Cornelius, M.,Morell, J.R., and Freba, M. Silica-Based Mesoporous organic-inorganic hybrid materials. Angewandte Chemie International Edition 45 (2006): 3216-3251.

Huang, C.-H.,Chang, K.-P.,Ou, H.-D.,Chiang, Y.-C., and Wang, C.-F. Adsorption of cationic dyes onto mesoporous silica. Microporous and Mesoporous Materials 141 (2011): 102-109.

Imperor-Clerc, M., Davidson, P., Davidson, A. Existence of a microporous corona around the mesopores of silica-based SBA-15 materials templated by triblock copolymers. Journal of the American Chemical Society 122 (2000): 11925-11933.

Inumaru, K., Nakano, T., and Yamanaka, S. Molecular selective adsorption of alkylphenols and alkylanilines from water by alkyl-grafted mesoporous alumina: A comparative study to alkyl-grafted mesoporous silica. Microporous and Mesoporous Materials 95 (2006): 279-285.

Jacangelo, J.G.,DeMarco, J.,Owen, D.M., and Randtke, S.J. Selected processes for removing NOM: an overview. Journal of American Water Works Association 87 (1995): 64-77.

Jang, S.H.,Kim, M.J.,Ko, J.R., and Ahn, W.S. Catalytic properties of Ti-HMS with high titanium loadings. Bulletin of the Korean Chemical Society 26 (2005): 1214-1218.

Jin, X.,Jiang, M.-q.,Shan, X.-q.,Pei, Z.-g., and Chen, Z. Adsorption of methylene blue and orange II onto unmodified and surfactant-modified zeolite. Journal of Colloid and Interface Science 328 (2008): 243-247.

Khenifi, A.,Zohra, B.,Kahina, B.,Houari, H., and Zoubir, D. Removal of 2,4-DCP from wastewater by CTAB/bentonite using one-step and two-step methods: A comparative study. Chemical Engineering Journal 146 (2009): 345-354.

Kim, J., and Kang, B. DBPs removal in GAC filter-adsorber. Water Research 42 (2008): 145-152.

Kimura, K., et al. Rejection of organic micropollutants (disinfection by-products, endocrine disrupting compounds, and pharmaceutically active compounds) by NF/RO membranes. Journal of Membrane Science 227 (2003): 113-121.

Kozyra, P., Salla, I., Montanari, T., Datka, J., Salagre, P., and Busca, G. FT-IR study of the adsorption of carbon monoxide and of some nitriles on Na-faujasites: Additional insight on the formation of complex interactions. Catalysis Today 114 (2006): 188-196.

Krasner, S.W.,Weinberg, H.S., and Richardson, S.D. Occurrence of a New Generation of Disinfection Byproducts. Environmental Science&Technology 40 (2006): 7155-7178.

Kumar, A., Prasad, B., and Mishra, I.M. Adsorptive removal of acrylonitrile by commercial grade activated carbon: Kinetics, equilibrium and thermodynamics. Journal of Hazardous Materials 152 (2008): 589-600.

Kumar, K.V., and Kumaran, A. Removal of methylene blue by mango seed kernel powder. Biochemical Engineering Journal 27 (2005): 83-93.

Langmuir, I. The constitution and fundamental properties of solid and liquids. Part I. Solid. Journal of the American Chemical Society 38 (1916): 2221-2295.

Lee, B., Kim, Y., Lee, H., and Yi, J. Synthesis of functionalized porous silicas via templating method as heavy metal ion adsorbents: the introduction of surface hydrophilicity onto the surface of adsorbents. Microporous and Mesoporous Materials 50 (2001): 77-90.

Lee, W.,Westerhoff, P., and Croul, J.-P. Dissolved organic nitrogen as a precursor for chloroform, dichloroacetonitrile, *n*-Nitrosodimethylamine, and trichloronitromethane. Environmental Science & Technology 41 (2007): 5485-5490.

Li, J., Wang, L., Qi, T., Zhou, Y., Liu, C., Chu, J., and Zhang, Y. Different N-containing functional groups modified mesoporous adsorbents for Cr(VI) sequestration: Synthesis, characterization and comparison. Microporous and Mesoporous Materials 110 (2008): 442-450.

Liang, X., et al. Preparation, characterization of thiol-functionalized silica and application for sorption of Pb2+ and Cd2+. Colloids and Surfaces A: Physicochemical and Engineering Aspects 349 (2009): 61-68.

Linssen, T.,Cassiers, K.,Cool, P., and Vansant, E.F. Mesoporous templated silicates: an overview of their synthesis, catalytic activation and evaluation of the stability. Advances in Colloid and Interface Science 103 (2003): 121-147.

Liu, Q.-S.,Zheng, T.,Wang, P.,Jiang, J.-P., and Li, N. Adsorption isotherm, kinetic and mechanism studies of some substituted phenols on activated carbon fibers. Chemical Engineering Journal 157 (2010): 348-356.

Lu, G.Q., and Zhao, X.S., 2004. Nanoporous material-An overview. Nanoporous materials-science and engineering. Imperial College, pp. 1-12.

Luna-Xavier, J.-L.,Guyot, A., and Bourgeat-Lami, E. Synthesis and characterization of silica/poly (methyl methacrylate) nanocomposite latex particles through emulsion polymerization using a cationic azo initiator. Journal of Colloid and Interface Science 250 (2002): 82-92.

Maria Chong, A.S., Zhao, X.S., Kustedjo, A.T., and Qiao, S.Z. Functionalization of large-pore mesoporous silicas with organosilanes by direct synthesis. Microporous and Mesoporous Materials 72 (2004): 33-42.

Mortland, M.M., Sun, S., and Boyd, S.A. Clay-organic complexes as adsorbents for phenol and chlorophenols. Clays and Clay Minerals 34 (1986): 581-585.

Nadeem, M.,Shabbir, M.,Abdullah, M.A.,Shah, S.S., and McKay, G. Sorption of cadmium from aqueous solution by surfactant-modified carbon adsorbents. Chemical Engineering Journal 148 (2009): 365-370.

Najm, I.N.,Snoeyink, V.L.,Lykins, B.W., and Adams, J.Q. Using powdered activated carbon: a critical review. Journal of American Water Works Association 83 (1991): 65-76.

Nayyar, S.P.,Sabatini, D.A., and Harwell, J.H. Surfactant adsolubilization and modified admicellar sorption of nonpolar, polar, and ionizable organic contaminants. Environmental Science & Technology 28 (1994): 1874-1881.

Nguyen, T.P.B., Lee, J.-W., Shim, W.G., and Moon, H. Synthesis of functionalized SBA-15 with ordered large pore size and its adsorption properties of BSA. Microporous and Mesoporous Materials 110 (2008): 560-569.

Nikolaou, A., Golfinopoulos, S., Rizzo, L., Lofrano, G., Lekkas, T., and Belgiorno, V. Optimization of analytical methods for the determination of DBPs: Application to drinking waters from Greece and Italy. Desalination 176 (2005): 25-36.

Nowinska, K.,F₀rmaniak, R.,Kaleta, W., and Waclaw, A. Heteropoly compounds incorporated into mesoporous material structure. Applied Catalysis A: General 256 (2003): 115-123.

Oei, B.C.,Ibrahim, S.,Wang, S., and Ang, H.M. Surfactant modified barley straw for removal of acid and reactive dyes from aqueous solution. Bioresource Technology 100 (2009): 4292-4295.

Oliver, B.G. Dihaloacetonitriles in drinking water: algae and fulvic acid as precursors. Environmental Science & Technology 17 (1983): 80-83.

Özcan, A., and Özcan, A.S. Adsorption of Acid Red 57 from aqueous solutions onto surfactant-modified sepiolite. Journal of Hazardous Materials 125 (2005): 252-259.

Pan, D., Jaroniec, M. Adsorption and thermogravimetric studies of unmodified and oxidized active carbons. Langmuir 12 (1996): 3657-3665.

Paria, S., and Khilar, K.C. A review on experimental studies of surfactant adsorption at the hydrophilic solid-water interface. Advances in Colloid and Interface Science 110 (2004): 75-95.

Patai, S. The Chemistry of the Thiol Group: Part 2. London: John Wiley and Sons, 1974.

Plewa, M.J., Wargner, E.D., Muellner, M.G., and Hsu, K.M., Richardson, S.D., 2008. Comparative mammalian cell toxicity of N-DBPs and C-DBPs. Symposoum Series 995, Washington, District of Columbia, US.

Pongprayoon, T.,Yanumet, N., and O'Rear, E.A. Admicellar Polymerization of styrene on Cotton. Journal of Colloid and Interface Science 249 (2002): 227-234.

Punyapalakul, P., and Takizawa, S. Effect of organic grafting modification of hexagonal mesoporous silicate on haloacetic acid removal. Environmental Engineering Research 41 (2004): 247-256.

Punyapalakul, P., and Takizawa, S. Effect of surface functional group on adsorption of organic pollutants on hexagonal mesoporous silicate. Water Science & Technology: Water Supply 6 (2006): 17-25.

Punyapalakul, P., and Takizawa, S. Selective adsorption of nonionic surfactant on hexagonal mesoporous silicates (HMSs) in the presence of ionic dyes. Water Research 40 (2006): 3177-3184.

Punyapalakul, P.,Soonglerdsongpha, S.,Kanlayaprasit, C.,Ngamcharussrivichai, C., and Khaodhiar, S. Effects of crystalline structures and surface functional groups on the adsorption of haloacetic acids by inorganic materials. Journal of Hazardous Materials 171 (2009): 491-499.

Qin, Q.,Ma, J., and Liu, K. Adsorption of anionic dyes on ammonium-functionalized MCM-41. Journal of Hazardous Materials 162 (2009): 133-139.

Ratasuk, C.,Kositanont., C., and Ratanatamskul., C. Removal of haloacetic acids by ozone and biologically active carbon. ScienceAsia 34 (2008): 293-298.

Rawajfih, Z., and Nsour, N. Characteristics of phenol and chlorinated phenols sorption onto surfactant-modified bentonite. Journal of Colloid and Interface Science 298 (2006): 39-49.

Richardson, S.D. Disinfection by-products and other emerging contaminants in drinking water. TrAC Trends in Analytical Chemistry 22 (2003): 666-684.

Rockmann, R., and Kalies, G. Characterization and adsorptive application of ordered mesoporous silicas. Applied Surface Science 253 (2007): 5666-5670.

Rosen, M.J. Surfactant and Interfacial Phenomena. 3. New Jersey: John Wiley & Sons, Inc., 2004.

Rouquerol, F.,Rouquerol, J., and Kenneth, S., 1999. Introduction of adsorption by Powders and Porous Solids: Principle, Methodology and Applications. Academic Press, pp. 1-26.

Ruiz, B., Cabrita, I., Mestre, A.S., Parra, J.B., Pires, J., Carvalho, A.P., and Ania, C.O. Surface heterogeneity effects of activated carbons on the kinetics of paracetamol removal from aqueous solution. Applied Surface Science 256 (2010): 5171-5175.

Samuel, D.F., and Osman, M.A. Adsorption process for water treatment. Boston: Butterworth Publishers, 1987.

Saphanuchart, W.,Saiwan, C., and O'Haver, J.H. Effect of adsolubilized solutes on 2-D structure of cationic admicelles. Colloids and Surfaces A: Physicochemical Engineering Aspects 307 (2007): 71-76.

Senthilkumaar, S., Kalaamani, P., Porkodi, K., Varadarajan, P.R., and Subburaam, C.V. Adsorption of dissolved Reactive red dye from aqueous phase onto activated carbon prepared from agricultural waste. Bioresource Technology 97 (2006): 1618-1625.

Shaarani, F.W., and Hameed, B.H. Ammonia-modified activated carbon for the adsorption of 2,4-dichlorophenol. Chemical Engineering Journal 169 (2011): 180-185.

Shi, L.Y.,Wang, Y.M.,Ji, A.,Gao, L., and Wang, Y. In situ direct bifunctionalization of mesoporous silica SBA-15. Journal of Materials Chemistry 15 (2005): 1392-1396.

Siddiqui, M.S., and Amy, G.L. Factors affecting DBP formation during ozone–bromide reactions. Journal of the American Water Works Association 85 (1993): 63-72.

Siriviriyanun, A.,ORear, E.A., and Yanumet, N. Modification of polyester fabric properties by surfactant-aided surface polymerization. Journal of Applied Polymer Science 103 (2007): 4059-4064.

Smart, M.M., Rada, R.G., and Donnermeyer, G.N. Determination of total nitrogen in sediments and plants using persulfate digestion. An evaluation and comparison with the Kjeldahl procedure. Water Research 17 (1983): 1207-1211.

Su, J.,Huang, H.-G.,Jin, X.-Y.,Lu, X.-Q., and Chen, Z.-L. Synthesis, characterization and kinetic of a surfactant-modified bentonite used to remove As(III) and As(V) from aqueous solution. Journal of Hazardous Materials 185 (2011): 63-70.

Sue-aok, N., Srithanratana, T., Rangsriwatananon, K., and Hengrasmee, S. Study of ethylene adsorption on zeolite NaY modified with group I metal ions. Applied Surface Science 256 (2010): 3997-4002.

Taguchi, A., and SchÜth, F. Ordered mesoporous materials in catalysis. Microporous and Mesoporous Materials 77 (2005): 1-45.

Tamon, H., Atsushi, M., and Okazaki, M. On Irreversible Adsorption of Electron-Donating Compounds in Aqueous Solution. Journal of Colloid and Interface Science 177 (1996): 384-390.

Tan, I.A.W.,Ahmad, A.L., and Hameed, B.H. Adsorption isotherms, kinetics, thermodynamics and desorption studies of 2,4,6-trichlorophenol on oil palm empty fruit bunch-based activated carbon. Journal of Hazardous Materials 164 (2009): 473-482.

Tanev, P.T., and Pinnavaia, T.J. Mesoporous Silica Molecular Sieves Prepared by Ionic and Neutral Surfactant Templating: A Comparison of Physical Properties Chemistry of Materials 8 (1996): 2068-2079.

Tanev, P.T.,Chibwe, M., and Pinnavaia, T.J. Titanium-containing mesoporous molecular sieves for catalytic oxidation of aromatic compounds. Nature 368 (1994): 321-323.

Tao, Q., Xu, Z., Wang, J., Liu, F., Wan, H., and Zheng, S. Adsorption of humic acid to aminopropyl functionalized SBA-15. Microporous and Mesoporous Materials 131 (2010): 177-185.

Thorsen, T. Membrane filtration of humic substances - State of the art. Water Science and Technology 40 (1999): 105-112.

Trehy, M.L.,Yost, R.A., and Miles, C.J. Chlorination byproducts of amino acids in natural waters. Environmental Science & Technology 20 (1986): 1117-1122.

Tsai, J.-H., Chiang, H.-M., Huang, G.-Y., and Chiang, H.-L. Adsorption characteristics of acetone, chloroform and acetonitrile on sludge-derived adsorbent, commercial granular activated carbon and activated carbon fibers. Journal of Hazardous Materials 154 (2008): 1183-1191.

Tung, H.-H.,Unz, R.F., and Xie, Y.F. HAA removal by GAC adsorption. Journal of American Water Works Association. 98 (2006): 107-112.

Uyak, V.,Koyuncu, I.,Oktem, I.,Cakmakci, M., and Toroz, I. Removal of trihalomethanes from drinking water by nanofiltration membranes. Journal of Hazardous Materials 152 (2008): 789-794.

Uyak, V.,Yavuz, S.,Toroz, I.,Ozaydin, S., and Genceli, E.A. Disinfection by-products precursors removal by enhanced coagulation and PAC adsorption. Desalination 216 (2007): 334-344.

Valsaraj, K.T.,Jain, P.M.,Kommalapati, R.R., and Smith, J.S. Reusable adsorbents for dilute solution separation. 1. Adsorption of phenanthrene on surfactant-modified alumina. Separation and Purification Technology 13 (1998): 137-145.

Visvanathan, C.,Marsono, B.D., and Basu, B. Removal of THMP by nanofiltration: Effects of interference parameters. Water Research 32 (1998): 3527-3538.

Wang, S., and Zhu, Z.H. Effects of acidic treatment of activated carbons on dye adsorption. Dyes and Pigments 75 (2007): 306-314.

Weber, W.J., and Morris, J.C. Kinetics of adsorption on carbon from solution. Journal of the Sanitary Engineering Division of American Society of Civil Engineers 89 (1963): 31-60.

Wei, F., Gu, F.N., Zhou, Y., Gao, L., Yang, J., and Zhu, J.H. Modifying MCM-41 as an efficient nitrosamine trap in aqueous solution. Solid State Sciences 11 (2009): 402-410.

Wei, Q., Nie, Z., Hao, Y., Chen, Z., Zou, J., and Wang, W. Direct synthesis of thiol-ligands-functionalized SBA-15: Effect of 3-mercaptopropyltrimethoxysilane concentration on pore structure. Materials Letters 59 (2005): 3611-3615.

West, C.C., and Harwell, J.H. Surfactants and subsurface remediation. Environmental Science & Technology 26 (1992): 2324-2330.

WHO. Guildelines for drinking water quality: incorporating 1st and 2nd addenda. Volume 1, Recommendations (2008): – 3rd ed.

Wu, F.-C., Tseng, R.-L., Huang, S.-C., and Juang, R.-S. Characteristics of pseudo-second-order kinetic model for liquid-phase adsorption: A mini-review. Chemical Engineering Journal 151 (2009): 1-9.

Xie, Y.F., and Zhou, H. Use of BAC for HAA removal - Part 2, column study. Journal of American Water Works Association 94 (2002): 126-134.

Yu, Q.,Deng, S., and Yu, G. Selective removal of perfluorooctane sulfonate from aqueous solution using chitosan-based molecularly imprinted polymer adsorbents. Water Research 42 (2008): 3089-3097.

Zepeda, T.A., et al. Synthesis and Characterization of Ti-HMS and CoMo/Ti-HMS Oxide Materials with Varying Ti Content. Chemistry of Materials 17 (2005): 4062-4073.

Zhan, Y.,Lin, J., and Zhu, Z. Removal of nitrate from aqueous solution using cetylpyridinium bromide (CPB) modified zeolite as adsorbent. Journal of Hazardous Materials 186 (2011): 1972-1978.

Zhang, X.,Li, A.,Jiang, Z., and Zhang, Q. Adsorption of dyes and phenol from water on resin adsorbents: Effect of adsorbate size and pore size distribution. Journal of Hazardous Materials 137 (2006): 1115-1122.

Zhao, D., et al. Triblock Copolymer Syntheses of Mesoporous Silica with Periodic 50 to 300 Angstrom Pores. Science 279 (1998): 548-552.

Zhao, Y.X.,Ding, M.Y., and Chen, D.P. Adsorption properties of mesoporous silicas for organic pollutants in water. Analytica Chimica Acta 542 (2005): 193-198.

Zhou, C.F., and Zhu, J.H. Adsorption of nitrosamines in acidic solution by zeolites. Chemosphere 58 (2005): 109-114.

APPENDICES

APPENDIX A
GC Chromatogram of HANs, TCM and DCAA

Table A-1 Five-HANs and Trichloromethane Determination by Gas Chromatograph followed the EPA Method 551.1 (Column HP-1, GC/ECD)

Retention time (min)	5.083	5.524	6.170	7.709	15.409
HANs	MCAN	TCAN	DCAN	MBAN	DBAN
Detection Limit	0.15-0.18 μg L^{-1} or ppb				

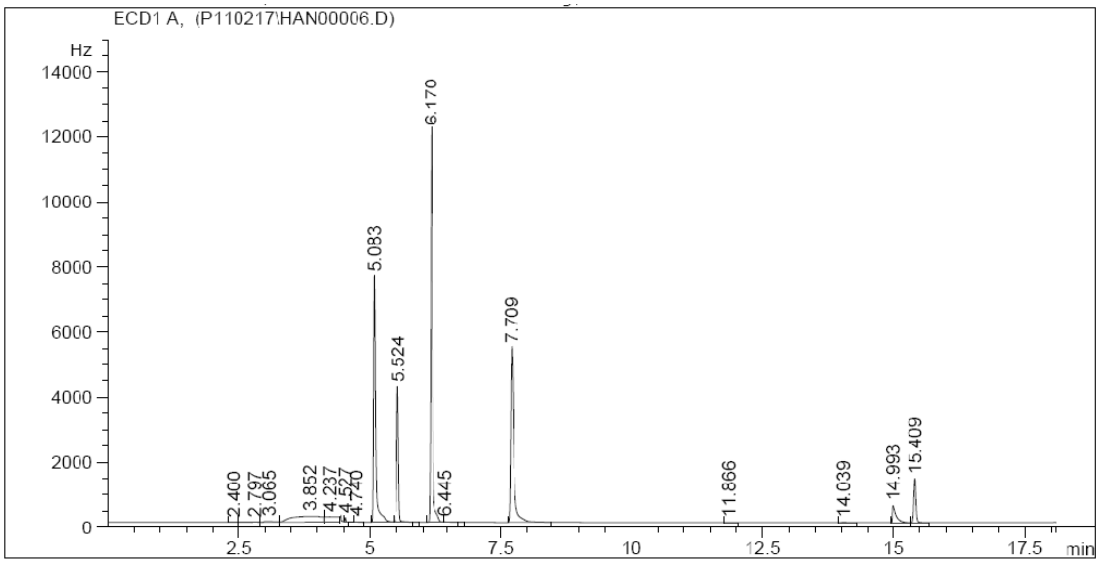

Figure A-1 Chromatogram of Five-HANs

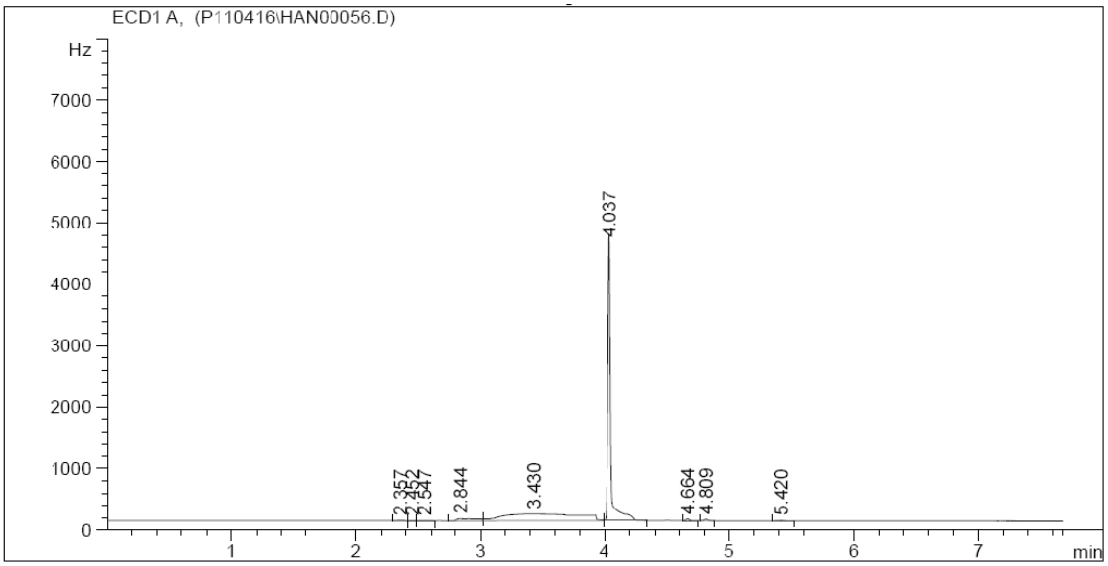

Figure A-2 Chromatogram of Trichloromethane (TCM); Rentention time 4.037 min.

Table A-2 Dichloroacetic acid (DCAA) Determination by Gas Chromatograph followed the EPA Method 552.2 (Column VF-X, GC/ECD)

Retention time (min)	7.482	8.876
Substances	DCAA	2,3-dibromopropionic acid (Surrogate standard)

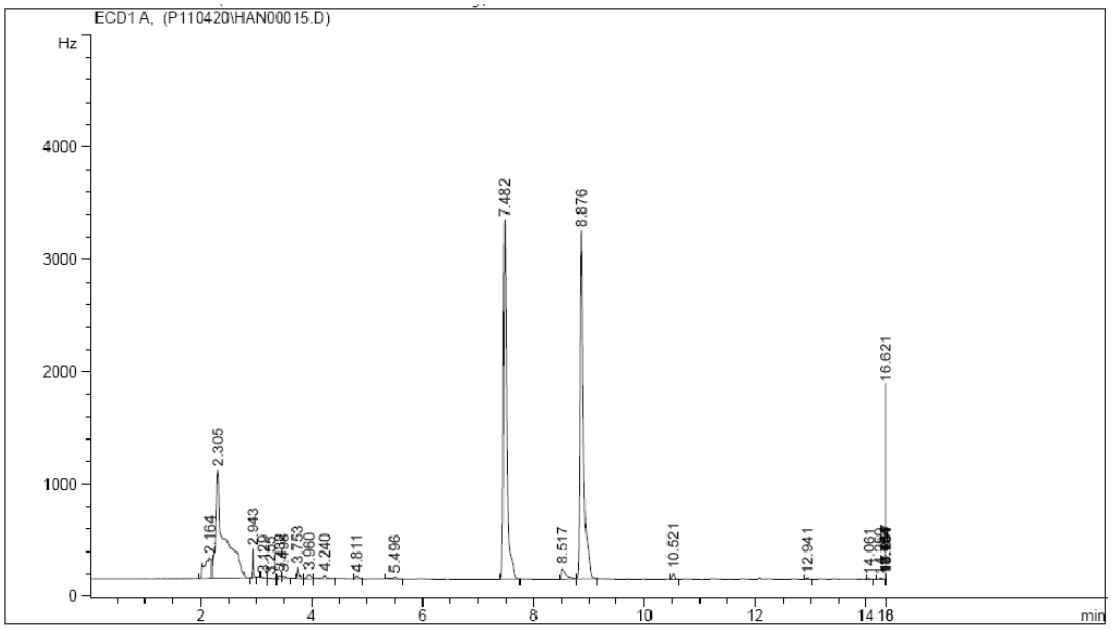

Figure A-3 Chromatogram of Dichloroacetic acid (DCAA)

APPENDIX B
Data of Physicochemical Characterization of Adsorbents

1. Surface Charge density determination by Acid-Base Titration Method

Table B-1 Data from calculation of surface charge density of HMS

Sample	pH	Surface charge (C/m^2)
1	3.39	0.0388
2	3.60	0.0166
3	3.78	0.0138
4	4.06	0.0041
5	4.37	0.0029
6	4.99	-9.2838E-5
7	5.42	-0.0016
8	5.97	-0.0038
9	6.70	-0.01575
10	7.24	-0.0386
11	8.23	-0.0627
12	8.56	-0.1023
13	8.94	-0.2157

Table B-2 Data from calculation of surface charge density of A-HMS

Sample	pH	Surface charge (C/m^2)
1	9.67	-0.0826
2	9.60	-0.0290
3	9.58	-0.0113
4	9.57	-0.0024
5	9.53	0.0062
6	9.51	0.0135
7	9.50	0.0204
8	9.38	0.0346
9	9.38	0.0760

Table B-3 Data from calculation of surface charge density of M-HMS

Sample	pH	Surface charge (C/m^2)
1	8.63	-0.0263
2	7.56	-0.0105
3	7.01	-0.0053
4	6.62	-0.0026
5	6.14	-3.7050E-5
6	4.96	0.0016
7	4.40	0.0022
8	3.97	0.0028
9	3.45	0.0026

Table B-4 Data from calculation of surface charge density of OD-HMS

Sample	pH	Surface charge (C/m^2)
1	3.36	0.0224
2	3.58	0.0145
3	3.75	0.0086
4	4.01	9.8053E-4
5	4.20	-0.0046
6	4.48	-0.0097
7	4.57	-0.0010
8	4.67	-0.0123
9	5.35	-0.0230
10	6.42	-0.0405
11	7.86	-0.0867
12	8.69	-0.1296
13	9.09	-0.2251

Table B-5 Data from calculation of surface charge density of Ti-HMS

Sample	pH	Surface charge (C/m^2)
1	3.99	0.0267
2	4.27	0.0123
3	4.55	0.0058
4	5.24	0.0011
5	8.74	-0.0579
6	8.15	-0.0293
7	7.30	-0.0119
8	6.57	-0.0030
9	5.82	-4.2730E-4
10	3.63	0.0760
11	3.84	0.0386
12	9.17	-0.1249
13	8.90	-0.0869

Table B-6 Data from calculation of surface charge density of SBA-15

Sample	pH	Surface charge (C/m^2)
1	5.88	-0.0039
2	6.40	-0.0073
3	6.80	-0.0147
4	7.61	-0.0295
5	8.08	-0.0445
6	8.30	-0.0592
7	8.78	-0.0717
8	5.24	-8.3218E-4
9	4.87	0.0017
10	4.57	0.0033
11	4.37	0.0084
12	4.15	0.0193
13	3.95	0.0273
14	3.67	0.0421

Table B-7 Data from calculation of surface charge density of NaY

Sample	pH	Surface charge (C/m^2)
1	9.94	-0.0993
2	9.46	-0.0416
3	9.05	-0.0217
4	8.33	-0.0116
5	7.88	1.7855E-4
6	7.58	0.0098
7	7.31	0.0191
8	7.00	0.0383
9	6.69	0.0969

Table B-8 Data from calculation of surface charge density of PAC

Sample	pH	Surface charge (C/m^2)
1	9.78	-0.0215
2	9.63	-0.0078
3	9.51	-0.0034
4	9.47	-0.0010
5	9.38	0.0012
6	9.30	0.0030
7	9.21	0.0047
8	9.08	0.0087
9	8.30	0.0201

2. Surface Charge Determination by Zeta Potential Analyzer

Table B-9 Surface charge of PG-SBA-CHX

Sample	pH	Surface charge (mV)
1	3.39	39.32
2	3.60	35.25
3	3.78	26.24
4	4.06	23.11
5	4.37	14.59
6	4.99	13.11
7	5.42	9.56
8	5.97	-6.328

Table B-10 Surface charge of SBA-CHX

Sample	pH	Surface charge (mV)
1	3.02	8.753
2	3.95	-10.70
3	5.07	-18.53
4	6.11	-24.02
5	7.05	-25.77
6	8.00	-27.96
7	8.97	-30.53
8	9.99	-39.57
9	3.02	8.75

APPENDIX C
Data of Adsorption Kinetics

Table C-1 Data from Adsorption kinetic of HMS, A-HMS, M-HMS, OD-HMS, Ti-HMS, NaY , SBA-15 and PG-SBA-CHX at initial concentration of DCAN at 100 μg L^{-1} and M-HMS and PAC at 50 mg L^{-1} (pH 7 with IS 10 mM)

HMS		**Ti-HMS**		**A-HMS**		**OD-HMS**		**SBA-15**	
***t* (h)**	q_t	***t* (h)**	q_t	***t* (h)**	q_t	***t* (h)**	q_t	***t* (h)**	q_t
0	0.00	0	0	0	0.00	0	0.00	0	0.00
0.25	5.26	2	5.09	0.25	1.40	1	3.62	1	3.01
0.50	7.25	4	11.50	1	1.80	2	5.82	3	4.46
1	13.94	6	14.50	4	7.40	4	6.03	5.50	8.70
2	15.26	8	14.21	6	8.30	6	11.76	7.50	10.46
4	18.47	12	15.71	12	21.70	10	13.90	10	11.20
8	22.94	18	17.51	18	23.11	12	14.92	12	12.43
12	25.91	24	17.47	24	28.80	18	15.95	18	13.43
24	28.43	36	17.88	30	33.76	24	16.62	30	14.22
36	28.59	48	18.41	36	35.62	30	16.31	36	15.35
48	29.10			48	49.78	36	17.76	48	14.63
				60	73.45	48	18.94		
				72	74.01				

NaY		**SBA-CHX**		**PG-SBA-CHX**		**M-HMS**		**PAC**	
***t* (h)**	q_t	***t* (h)**	q_t	***t* (h)**	q_t	***t* (h)**	q_t	***t* (h)**	q_t
0	0.00	0	0	0	0	0	0.00	0	0.00
1	6.52	1	0.00	1	0.00	0.25	4.70	0.25	22.11
2	10.60	3	0.40	3	0.00	0.50	21.18	0.50	32.71
4	14.97	6	0.87	6	0.00	0.75	26.52	0.75	45.34
6	13.83	9	1.60	9	0.35	2	26.47	1	91.35
8	17.06	12	4.52	12	1.10	4	46.22	2	93.06
12	18.67	18	13.91	18	6.75	6	53.00	4	93.59
18	21.04	24	35.47	24	9.78	8	58.26	8	91.34
24	20.05	30	43.85	30	16.00	12	80.97	10	93.11
30	20.75	36	41.12	36	29.77	18	85.57	12	92.69
36	21.39	48	45.37	48	46.78	24	87.67	18	94.06
48	20.69			60	49.64	30	90.48	24	93.15
				72	50.13	36	92.02	36	93.14
						48	92.97	48	93.60

Note: Unit of adsorption capacity at time (q_t) of M-HMS and PAC is mg g^{-1}.
Unit of adsorption capacity at time (q_t) of HMS, functionalized-HMS derivatives, SBA-15, NaY, SBA-CHX and PG-SBA-CHX is μg g^{-1}.

APPENDIX D
Data of Adsorption Isotherms

1. Adsorption isotherm of Five-HANs in Single Solute Solution

Table D-1 Data of adsorption isotherms of five-HANs in single solute solution on HMS in phosphate buffer at pH 7 with IS 10 mM (25 ^{o}C)

MCAN			DCAN			TCAN		
C_0 (μg/L)	q_e (μg/m^2)	C_e (μg/L)	C_0 (μg/L)	q_e (μg/m^2)	C_e (μg/L)	C_0 (μg/L)	q_e (μg/m^2)	C_e (μg/L)
25.08	0.002	24.14	10	0.005	8.42	22.68	0.007	19.16
32.25	0.007	28.69	20	0.014	14.61	56.28	0.010	51.70
55.73	0.028	39.57	40	0.014	30.16	85.06	0.019	66.90
61.54	0.037	42.07	75	0.033	71.10	116.83	0.024	90.16
99.22	0.065	65.55	100	0.039	111.37	170.13	0.030	137.13
128.56	0.093	81.07	150	0.050	148.51	183.09	0.056	146.06
			200	0.060	182.17			
			300	0.085	267.32			
MBAN			**DBAN**					
C_0 (μg/L)	q_e (μg/m^2)	C_e (μg/L)	C_0 (μg/L)	q_e (μg/m^2)	C_e (μg/L)			
30.71	0.0005	30.70	59.85	0.0049	57.35			
52.84	0.0061	49.61	83.96	0.0121	77.67			
81.78	0.0204	71.30	109.11	0.0152	101.54			
106.25	0.0519	80.50	139.54	0.0265	128.03			
169.10	0.0758	126.59	192.41	0.0454	169.72			
195.61	0.1157	137.37	222.84	0.0547	194.16			

Table D-2 Data of adsorption isotherms of five-HANs in single solute solution on Ti-HMS in phosphate buffer at pH 7 with IS 10 mM (25 ^{o}C)

MCAN			DCAN			TCAN		
C_0 (μg/L)	q_e (μg/m^2)	C_e (μg/L)	C_0 (μg/L)	q_e (μg/m^2)	C_e (μg/L)	C_0 (μg/L)	q_e (μg/m^2)	C_e (μg/L)
26.70	0.014	23.43	26.27	0.003	25.01	22.68	0.007	19.13
47.15	0.045	36.84	58.08	0.006	55.72	56.38	0.016	51.16
71.92	0.073	55.44	78.35	0.020	71.96	74.43	0.034	62.78
84.21	0.090	63.57	108.56	0.024	97.55	100.49	0.059	78.70
111.19	0.100	88.24	163.57	0.040	141.94	148.85	0.077	125.11
133.95	0.137	107.84	182.91	0.065	161.34	183.09	0.083	155.83
MBAN			**DBAN**					
C_0 (μg/L)	q_e (μg/m^2)	C_e (μg/L)	C_0 (μg/L)	q_e (μg/m^2)	C_e (μg/L)			
33.07	0.002	32.75	59.85	0.008	56.80			
47.65	0.011	45.05	83.96	0.012	80.29			
82.95	0.060	69.01	109.11	0.030	102.16			
113.96	0.118	86.09	139.54	0.047	128.77			
172.87	0.173	132.46	192.41	0.075	174.63			
186.10	0.192	142.07	222.84	0.087	203.39			

Table D-3 Data of adsorption isotherms of five-HANs in single solute solution on A-HMS in phosphate buffer at pH 7 with IS 10 mM (25 ^{o}C)

MCAN			DCAN			TCAN		
C_0 (μg/L)	q_e (μg/m^2)	C_e (μg/L)	C_0 (μg/L)	q_e (μg/m^2)	C_e (μg/L)	C_0 (μg/L)	q_e (μg/m^2)	C_e (μg/L)
25.08	0.0047	24.17	50.00	0.133	36.24	22.68	0.033	16.39
32.25	0.0190	28.63	75.00	0.180	52.46	56.19	0.077	41.35
55.73	0.0408	48.03	100.00	0.257	72.12	74.43	0.121	50.98
61.54	0.0574	50.76	150.00	0.380	96.47	100.49	0.103	80.42
99.22	0.1335	73.64	200.00	0.479	110.48	148.85	0.155	119.04
128.56	0.1682	96.58	300.00	0.784	168.69	183.09	0.266	132.54
MBAN			**DBAN**					
C_0 (μg/L)	q_e (μg/m^2)	C_e (μg/L)	C_0 (μg/L)	q_e (μg/m^2)	C_e (μg/L)			
30.71	0.0030	31.40	30.37	0.035	24.44			
52.84	0.0100	50.89	74.33	0.092	63.32			
81.78	0.0545	71.48	97.78	0.149	83.40			
106.25	0.1455	78.85	123.00	0.206	97.00			
169.10	0.2526	119.76	187.77	0.290	132.69			
195.61	0.3129	136.47	262.86	0.413	185.85			

Table D-4 Data of adsorption isotherms of five-HANs in single solute solution on OD-HMS in phosphate buffer at pH 7 with IS 10 mM (25 ^{o}C)

MCAN			DCAN			TCAN		
C_0 (μg/L)	q_e (μg/m^2)	C_e (μg/L)	C_0 (μg/L)	q_e (μg/m^2)	C_e (μg/L)	C_0 (μg/L)	q_e (μg/m^2)	C_e (μg/L)
26.70	0.0020	26.01	28.76	0.0036	27.51	22.68	0.0044	21.18
55.30	0.0230	47.34	58.59	0.0121	54.43	56.28	0.0051	54.52
71.92	0.0515	54.20	79.96	0.0250	71.23	85.06	0.0139	80.14
84.21	0.0683	60.72	104.68	0.0268	95.36	116.83	0.0372	103.70
111.19	0.0774	84.58	147.07	0.0343	135.25	170.13	0.0464	153.70
133.95	0.0935	101.77	177.53	0.0508	159.82	183.09	0.0414	168.57
MBAN			**DBAN**					
C_0 (μg/L)	q_e (μg/m^2)	C_e (μg/L)	C_0 (μg/L)	q_e (μg/m^2)	C_e (μg/L)			
33.07	0.0009	32.74	47.36	0.0034	46.65			
47.65	0.0018	47.00	74.33	0.0162	68.91			
82.95	0.0214	75.48	97.78	0.0299	87.33			
113.96	0.0686	89.81	123.00	0.0492	106.02			
172.87	0.1193	130.60	187.77	0.0589	167.09			
186.10	0.1236	143.56	262.86	0.1025	226.27			

Table D-5 Data of adsorption isotherms of five-HANs in single solute solution on SBA-15 in phosphate buffer at pH 7 with IS 10 mM (25 ^{o}C)

MCAN			DCAN			TCAN		
C_0 (μg/L)	q_e (μg/m^2)	C_e (μg/L)	C_0 (μg/L)	q_e (μg/m^2)	C_e (μg/L)	C_0 (μg/L)	q_e (μg/m^2)	C_e (μg/L)
27.18	0.0009	26.74	30.44	0.0108	25.35	23.54	0.0107	17.60
47.36	0.0017	47.15	60.33	0.0209	50.39	37.99	0.0169	29.84
86.79	0.0102	82.07	80.09	0.0232	69.06	59.83	0.0225	44.90
118.90	0.0270	106.30	101.33	0.0313	86.49	85.20	0.0316	70.00
165.85	0.0424	145.90	159.63	0.0488	136.15	111.07	0.0375	92.08
225.14	0.0545	199.66	182.04	0.0536	155.34	124.72	0.0427	105.93
MBAN			**DBAN**					
C_0 (μg/L)	q_e (μg/m^2)	C_e (μg/L)	C_0 (μg/L)	q_e (μg/m^2)	C_e (μg/L)			
32.40	0.0015	31.76	35.66	0.0073	32.22			
53.23	0.0035	51.97	52.83	0.0172	44.58			
86.68	0.0148	79.66	92.49	0.0260	80.16			
127.37	0.0231	116.30	120.16	0.0347	103.83			
160.50	0.0293	147.32	129.39	0.0421	109.32			
192.08	0.0456	170.39	191.96	0.0640	158.14			

Table D-6 Data of adsorption isotherms of five-HANs in single solute solution on NaY in phosphate buffer at pH 7 with IS 10 mM (25 ^{o}C)

MCAN			DCAN			TCAN		
C_0 (μg/L)	q_e (μg/m^2)	C_e (μg/L)	C_0 (μg/L)	q_e (μg/m^2)	C_e (μg/L)	C_0 (μg/L)	q_e (μg/m^2)	C_e (μg/L)
24.43	0.0004	24.31	34.60	0.0124	29.94	19.39	0.008	18.27
37.47	0.0054	36.84	51.30	0.0189	44.03	34.32	0.019	28.64
75.90	0.0568	59.78	97.61	0.0292	86.43	38.48	0.033	28.96
102.55	0.0756	77.02	129.04	0.0329	116.27	67.98	0.038	56.31
143.09	0.1126	99.08	166.17	0.0451	149.20	100.74	0.060	82.90
			256.24	0.0598	233.11	148.76	0.105	116.27
MBAN			**DBAN**					
C_0 (μg/L)	q_e (μg/m^2)	C_e (μg/L)	C_0 (μg/L)	q_e (μg/m^2)	C_e (μg/L)			
33.07	0.0047	32.11	59.50	0.0012	59.12			
47.65	0.0151	50.18	83.86	0.0092	81.21			
82.95	0.0462	72.48	114.12	0.0240	105.25			
113.96	0.0671	86.00	168.88	0.0349	158.09			
172.87	0.0918	126.03	217.63	0.0426	205.23			
186.10	0.1064	170.47	270.20	0.0525	250.96			

Table D-7 Data of adsorption isotherms of five-HANs in single solute solution on SBA-CHX in phosphate buffer at pH 7 with IS 10 mM (25 ^{o}C)

MCAN			DCAN			TCAN		
C_0 (µg/L)	q_e (µg/g)	C_e (µg/L)	C_0 (µg/L)	q_e (µg/g)	C_e (µg/L)	C_0 (µg/L)	q_e (µg/g)	C_e (µg/L)
23.75	6.46	19.53	27.67	2.39	26.26	27.06	5.23	24.02
46.93	15.26	37.73	51.75	11.86	44.91	41.95	6.59	35.73
67.41	20.49	54.88	72.98	21.07	70.30	51.11	15.29	42.07
90.39	24.79	76.16	103.56	45.45	82.19	67.52	21.80	55.15
112.23	27.05	97.50	138.67	49.40	107.96	117.23	51.60	86.48
151.11	32.23	132.10	178.15	56.66	144.15	132.97	64.19	95.00
MBAN			**DBAN**					
C_0 (µg/L)	q_e (µg/g)	C_e (µg/L)	C_0 (µg/L)	q_e (µg/g)	C_e (µg/L)			
18.30	1.18	17.62	34.80	7.46	30.32			
42.58	4.16	40.16	51.40	20.45	39.49			
60.40	8.16	55.64	76.40	14.31	67.88			
74.05	14.92	65.38	93.28	35.03	74.41			
100.83	17.70	91.31	138.97	64.23	101.44			
143.15	30.43	125.46	189.54	69.86	146.88			

Table D-8 Data of adsorption isotherms of five-HANs in single solute solution on PG-SBA-CHX in phosphate buffer at pH 7 with IS 10 mM (25 ^{o}C)

MCAN			DCAN			TCAN		
C_0 (µg/L)	q_e (µg/g)	C_e (µg/L)	C_0 (µg/L)	q_e (µg/g)	C_e (µg/L)	C_0 (µg/L)	q_e (µg/g)	C_e (µg/L)
25.60	0.51	25.32	27.67	9.38	22.18	27.06	6.85	22.86
53.41	0.17	53.31	58.53	23.75	44.82	38.64	24.12	24.30
75.16	2.96	73.47	78.46	38.46	55.94	44.76	30.59	26.58
96.81	5.07	93.68	109.34	48.19	81.12	67.52	46.00	46.58
142.41	6.64	138.62	139.91	52.72	108.73	117.23	67.00	62.00
190.00	8.37	185.07	180.63	66.76	141.71	132.97	94.24	75.89
MBAN			**DBAN**					
C_0 (µg/L)	q_e (µg/g)	C_e (µg/L)	C_0 (µg/L)	q_e (µg/g)	C_e (µg/L)			
27.90	1.14	27.22	34.80	14.94	25.83			
45.78	1.92	44.67	51.40	23.00	30.90			
64.22	5.57	60.85	76.40	39.62	52.97			
82.21	7.18	77.97	93.28	57.57	59.39			
121.42	7.52	117.10	138.97	79.34	92.95			
171.71	10.18	165.69	189.54	98.00	129.06			

Table D-9 Data of adsorption isotherms of five-HANs in single solute solution on M-HMS in phosphate buffer at pH 7 with IS 10 mM (25 ^{o}C)

MCAN			DCAN			TCAN		
C_0 (mg/L)	q_e (mg/m^2)	C_e (μg/L)	C_0 (mg/L)	q_e (mg/m^2)	C_e (mg/L)	C_0 (mg/L)	q_e (mg/m^2)	C_e (μg/L)
0.06	0.00004	34.74	1	0.001	0.001	0.5	0.0010	0.00
0.11	0.00008	63.14	5	0.009	0.001	2.5	0.0047	3.37
0.19	0.00014	117.42	10	0.020	0.004	5.2	0.0097	2.21
0.30	0.00020	186.70	15	0.028	0.009	11.9	0.0221	2.47
0.50	0.00031	333.01	20	0.040	0.019	16.8	0.0315	3.93
0.67	0.00034	497.19	25	0.051	0.033	29.8	0.0561	9.91
			30	0.058	0.056			
			35	0.065	0.210			
			47.9	0.094	1.147			
			70	0.110	11.577			
			85	0.121	19.872			

MBAN			DBAN		
C_0 (mg/L)	q_e (mg/m^2)	C_e (μg/L)	C_0 (mg/L)	q_e (mg/m^2)	C_e (μg/L)
0.09	0.00014	18.0	1.07	0.0040	0.29
0.18	0.00029	25.4	5.47	0.0202	2.42
0.28	0.00041	53.3	8.41	0.0310	0.00
0.96	0.00157	123.2	16.07	0.0590	5.21
2.13	0.00343	204.0	17.32	0.0644	213.13
3.77	0.00679	270.0	21.10	0.0751	384.45

Table D-10 Data of adsorption isotherms of five-HANs in single solute solution on PAC in phosphate buffer at pH 7 with IS 10 mM (25 ^{o}C)

MCAN			DCAN			TCAN		
C_0 (mg/L)	q_e (mg/m^2)	C_e (μg/L)	C_0 (mg/L)	q_e (mg/m^2)	C_e (μg/L)	C_0 (mg/L)	q_e (mg/m^2)	C_e (μg/L)
0.06	0.00005	27.60	1	0.001	0.0004	1.39	0.0024	1.8
0.11	0.00009	50.99	5	0.005	0.0026	2.49	0.0043	0.0
0.19	0.00007	151.62	10	0.019	0.004	4.05	0.0071	12.0
0.34	0.00012	265.83	60	0.088	0.023	7.31	0.0127	53.0
0.53	0.00034	336.70	70	0.119	0.036	11.89	0.0209	96.8
			80	0.142	0.041	20.00	0.0347	215.0
			90	0.154	0.050	29.80	0.0507	402.1
			100	0.176	0.056			
			110	0.199	0.071			
			130	0.226	0.081			
			140	0.238	0.088			
			150	0.270	0.107			
			170	0.290	0.109			
			180	0.309	0.130			
			210	0.374	0.248			

MBAN			DBAN		
C_0 (mg/L)	q_e (mg/m^2)	C_e (μg/L)	C_0 (mg/L)	q_e (mg/m^2)	C_e (μg/L)
0.09	0.00008	45.4	1.1	0.004	2.50
0.18	0.00016	88.8	5.5	0.017	0.00
0.38	0.00035	176.4	8.4	0.029	1.28
0.50	0.00046	232.1	16.1	0.054	0.28
0.76	0.00070	359.7	17.32	0.062	1.69
1.00	0.00094	415.4	16.88	0.060	0.51

2. Effect of pH solution on Adsorption of DCAN

Table D-11 Data of adsorption isotherms of DCAN on HMS in phosphate buffer at pH 5,7 and 9 with IS 10 mM (25 ^{o}C)

pH 5			pH 7			pH 9		
C_0 (µg/L)	q_e (µg/g)	C_e (µg/L)	C_0 (µg/L)	q_e (µg/g)	C_e (µg/L)	C_0 (µg/L)	q_e (µg/g)	C_e (µg/L)
46.86	1.99	46.49	10	3.843	8.42	25.09	18.52	11.42
67.53	2.68	65.59	40	10.03	30.16	38.68	26.80	18.46
136.90	13.21	127.32	75	23.33	71.10	69.26	51.90	31.82
183.24	17.55	170.02	100	27.71	111.37	91.03	63.63	45.04
265.92	36.50	239.13	150	35.63	148.51	158.28	125.58	65.18
387.73	54.88	347.21	200	42.88	182.17	203.05	162.89	82.32

Table D-12 Data of adsorption isotherms of DCAN on Ti-HMS in phosphate buffer at pH 5,7 and 9 with IS 10 mM (25 ^{o}C)

pH 5			pH 7			pH 9		
C_0 (µg/L)	q_e (µg/g)	C_e (µg/L)	C_0 (µg/L)	q_e (µg/g)	C_e (µg/L)	C_0 (µg/L)	q_e (µg/g)	C_e (µg/L)
44.55	1.07	43.72	26.27	1.75	25.01	25.09	20.75	10.10
74.91	2.28	73.27	58.08	3.28	55.72	69.26	58.98	26.54
120.62	14.46	110.19	78.35	9.97	71.96	91.03	77.02	35.58
174.96	17.26	162.46	108.56	15.18	97.55	158.28	134.85	61.37
240.84	27.09	221.05	163.57	27.46	141.94	203.05	168.30	81.82
360.00	41.26	329.61	182.91	29.68	161.34			

Table D-13 Data of adsorption isotherms of DCAN on A-HMS in phosphate buffer at pH 5,7 and 9 with IS 10 mM (25 ^{o}C)

pH 5			pH 7			pH 9		
C_0 (µg/L)	q_e (µg/g)	C_e (µg/L)	C_0 (µg/L)	q_e (µg/g)	C_e (µg/L)	C_0 (µg/L)	q_e (µg/g)	C_e (µg/L)
28.90	4.73	25.50	50	34.73	36.24	21.76	29.89	0.108
101.59	10.97	93.58	75	47.17	52.46	44.39	60.80	0.091
201.87	38.93	177.32	100	67.28	72.12	107.27	146.55	0.073
323.00	82.25	256.92	150	99.65	96.47	171.94	232.25	0.078
412.06	90.08	346.59	200	125.52	110.48	170.66	234.14	0.077
			300	205.46	168.69	232.79	318.17	0.076

Table D-14 Data of adsorption isotherms of DCAN on OD-HMS in phosphate buffer at pH 5,7 and 9 with IS 10 mM (25 ^{o}C)

pH 5			pH 7			pH 9		
C_0 (µg/L)	q_e (µg/g)	C_e (µg/L)	C_0 (µg/L)	q_e (µg/g)	C_e (µg/L)	C_0 (µg/L)	q_e (µg/g)	C_e (µg/L)
37.85	0.00	40.95	28.76	1.70	27.51	20.36	17.32	7.42
67.20	0.15	67.28	58.59	5.77	54.43	44.17	41.43	13.81
119.05	2.14	117.48	79.96	11.94	71.23	63.20	48.58	28.16
189.09	6.83	184.08	104.68	12.79	95.36	95.04	72.71	41.32
255.48	22.95	238.61	147.07	16.35	135.25	122.60	109.26	42.02
372.76	67.26	323.59	177.53	24.21	159.82	210.96	195.40	68.58
			260.33	39.25	227.69			

Table D-15 Data of adsorption isotherms of DCAN on SBA-15 in phosphate buffer at pH 5,7 and 9 with IS 10 mM (25 ^{o}C)

pH 5			pH 7			pH 9		
C_0 (µg/L)	q_e (µg/g)	C_e (µg/L)	C_0 (µg/L)	q_e (µg/g)	C_e (µg/L)	C_0 (µg/L)	q_e (µg/g)	C_e (µg/L)
37.85	0.88	37.20	30.44	7.03	25.35	20.36	16.24	8.74
67.20	2.79	65.19	60.33	13.64	50.39	44.17	36.93	17.31
119.05	10.16	111.70	80.09	15.20	69.06	63.20	48.82	28.12
189.09	14.44	178.50	101.33	16.53	91.30	95.04	74.75	41.35
270.65	37.52	243.40	159.63	31.91	136.15	122.60	97.84	51.17
372.76	50.68	336.42	182.04	36.73	155.34	210.96	164.56	92.49
			256.48	44.13	224.76			

Table D-16 Data of adsorption isotherms of DCAN on NaY in phosphate buffer at pH 5,7 and 9 with IS 10 mM (25 ^{o}C)

pH 5			pH 7			pH 9		
C_0 (µg/L)	q_e (µg/g)	C_e (µg/L)	C_0 (µg/L)	q_e (µg/g)	C_e (µg/L)	C_0 (µg/L)	q_e (µg/g)	C_e (µg/L)
44.50	1.85	42.61	34.60	8.08	29.94	25.09	8.56	18.77
67.53	3.05	65.25	51.30	12.33	44.03	38.68	17.30	25.63
141.76	8.77	135.37	97.61	19.09	86.43	69.26	31.55	46.50
183.24	17.22	170.68	129.04	21.47	116.27	91.03	39.00	62.83
265.92	42.85	233.36	166.17	29.43	149.20	158.28	74.23	103.27
387.73	57.76	346.30	256.24	39.03	233.11	203.05	79.00	145.57

Table D-17 Data of adsorption isotherms of DCAN on SBA-CHX in phosphate buffer at pH 5,7 and 9 with IS 10 mM (25 ^{o}C)

pH 5			pH 7			pH 9		
C_0 (μg/L)	q_e (μg/g)	C_e (μg/L)	C_0 (μg/L)	q_e (μg/g)	C_e (μg/L)	C_0 (μg/L)	q_e (μg/g)	C_e (μg/L)
46.70	3.28	47.26	27.67	2.39	26.26	23.98	5.94	20.52
67.48	4.27	65.03	51.75	11.86	44.91	54.37	28.66	37.26
90.26	6.56	86.04	72.98	21.07	70.30	84.49	38.79	61.44
113.35	8.27	108.61	103.56	45.45	82.19	121.88	59.02	86.47
160.73	7.32	157.37	138.67	49.40	107.96	190.32	122.52	117.86
206.72	9.87	201.11	178.15	56.66	144.15	211.76	124.55	138.80

Table D-18 Data of adsorption isotherms of DCAN on PG-SBA-CHX in phosphate buffer at pH 5,7 and 9 with IS 10 mM (25 ^{o}C)

pH 5			pH 7			pH 9		
C_0 (μg/L)	q_e (μg/g)	C_e (μg/L)	C_0 (μg/L)	q_e (μg/g)	C_e (μg/L)	C_0 (μg/L)	q_e (μg/g)	C_e (μg/L)
63.77	4.45	61.22	27.67	9.38	22.18	17.17	8.59	12.16
97.17	8.51	92.11	58.53	23.75	44.82	54.37	21.52	41.52
119.80	14.22	111.43	78.46	38.46	55.94	85.62	44.44	59.21
154.81	22.97	140.90	109.34	48.19	81.12	121.88	55.88	88.35
214.11	52.45	184.14	139.91	52.72	108.73	181.24	90.88	127.49
282.33	59.11	248.21	180.63	66.76	141.71	211.76	97.58	154.60

Table D-19 Data of adsorption isotherms of DCAN on M-HMS in phosphate buffer at pH 5,7 and 9 with IS 10 mM (25 ^{o}C)

pH 5			pH 7			pH 9		
C_0 (mg/L)	q_e (mg/g)	C_e (μg/L)	C_0 (mg/L)	q_e (mg/g)	C_e (μg/L)	C_0 (mg/L)	q_e (mg/g)	C_e (mg/L)
1.01	1.74	1.13	1	1.233	1.00	1.00	1.70	0.003
1.09	1.85	1.98	5	8.55	1.33	3.65	6.14	0.004
2.11	3.58	9.75	10	18.05	3.63	7.03	11.99	0.003
4.29	7.26	99.74	15	25.64	8.68	20.20	34.00	0.003
7.27	12.22	166.52	20	36.19	18.87	29.27	48.87	0.018
10.15	16.83	221.01	25	46.48	32.51	35.26	60.24	0.159
12.08	20.12	292.19	30.8	53.27	56.22			
13.59	22.56	316.22	35	55.30	87.00			
			47.9	59.37	209.68			

Table D-20 Data of adsorption isotherms of DCAN on PAC in phosphate buffer at pH 5,7 and 9 with IS 10 mM (25 ^{o}C)

pH 5			pH 7			pH 9		
C_0 (mg/L)	q_e (mg/g)	C_e (µg/L)	C_0 (mg/L)	q_e (mg/g)	C_e (µg/L)	C_0 (mg/L)	q_e (mg/g)	C_e (µg/L)
1.01	1.70	36.39	1	1.25	0.400	1.00	1.72	0.783
4.31	7.20	51.88	5	5.00	2.600	3.63	6.16	1.093
7.27	12.22	80.84	10	18.71	4.060	7.03	12.08	2.288
10.15	17.03	91.07	20	36.30	7.654	20.20	34.31	8.960
12.08	20.35	101.48	30	53.45	11.250	29.27	49.20	42.428
13.59	22.49	108.06	60	86.08	22.979	41.69	71.79	61.108
16.40	27.27	111.61						
34.94	58.49	124.98						

3. Effect of Temperature on Adsorption Capacity of DCAN on M-HMS and PAC

Table D-21 Data of adsorption isotherms of DCAN on M-HMS in phosphate buffer at temperature 15, 25 and 40 ^{o}C (pH 7with IS 10 mM)

15 ^{o}C			25 ^{o}C			40 ^{o}C		
C_0 (mg/L)	q_e (mg/g)	C_e (mg/L)	C_0 (mg/L)	q_e (mg/g)	C_e (mg/L)	C_0 (mg/L)	q_e (mg/g)	C_e (mg/L)
4.07	6.82	0.00	1	1.233	0.001	4.07	6.84	0.001
8.60	14.26	0.02	5	8.55	0.001	8.60	14.56	0.002
15.37	25.38	0.16	10	18.05	0.004	15.37	26.41	0.016
20.14	32.50	0.73	15	25.64	0.009	20.14	33.70	0.013
26.23	39.65	1.65	20	36.19	0.019	26.23	44.54	0.019
30.98	47.62	3.23	25	46.48	0.033	30.98	51.59	0.031
			30	53.27	0.056	34.52	52.95	0.440
			35	59.37	0.210	41.69	68.91	0.832
			47.9	86.08	1.147	46.81	78.15	1.263
			70	100.45	11.577	49.89	83.63	1.611
			85	110.39	19.872			

Table D-22 Data of adsorption isotherms of DCAN on PAC in phosphate buffer at at temperature 15, 25 and 40 ^{o}C (pH 7with IS 10 mM)

15 ^{o}C			25 ^{o}C			40 ^{o}C		
C_0 (mg/L)	q_e (mg/g)	C_e (mg/L)	C_0 (mg/L)	q_e (mg/g)	C_e (mg/L)	C_0 (mg/L)	q_e (mg/g)	C_e (mg/L)
4.07	7.02	0.02	1	1.25	0.0004	8.60	14.56	0.00
8.60	14.66	0.02	5	5	0.0026	33.69	58.51	0.01
20.44	35.54	0.03	10	18.71	0.004	63.27	109.58	0.01
33.69	57.44	0.04	60	86.08	0.023	85.51	143.84	0.03
63.27	109.50	0.07	70	117.08	0.036	100.33	172.07	0.04
82.97	137.49	0.09	80	139.14	0.041	118.47	204.19	0.07
100.33	173.55	0.17	90	151.32	0.050	164.16	278.74	0.12
118.47	203.43	0.19	100	172.49	0.056			
164.16	280.51	0.26						

4. Adsorption Selectivity

4.1 Adsorption isotherm of Five-HANs in Mixed Solute Solution

Table D-23 Data of adsorption isotherms of five-HANs in mixed solute solution on HMS in phosphate buffer at pH 7 with IS 10 mM (25 ^{o}C)

MCAN			DCAN			TCAN		
C_0 (μg/L)	q_e (μg/m^2)	C_e (μg/L)	C_0 (μg/L)	q_e (μg/m^2)	C_e (μg/L)	C_0 (μg/L)	q_e (μg/m^2)	C_e (μg/L)
31.55	0.0021	30.44	40.80	0.0056	37.86	28.68	0.0001	28.73
57.13	0.0126	50.62	68.93	0.0104	63.50	36.17	0.0029	35.69
79.63	0.0205	68.90	90.41	0.0162	81.92	56.27	0.0057	53.28
102.20	0.0237	89.69	107.85	0.0195	98.05	100.26	0.0088	95.65
124.11	0.0249	111.27	128.78	0.0314	112.61	112.15	0.0125	102.45
142.79	0.0288	127.34	147.34	0.0336	129.39	126.20	0.0129	119.29
MBAN			**DBAN**					
C_0 (μg/L)	q_e (μg/m^2)	C_e (μg/L)	C_0 (μg/L)	q_e (μg/m^2)	C_e (μg/L)			
31.71	0.0005	31.47	24.41	0.0008	23.98			
62.92	0.0072	59.19	49.18	0.0043	46.92			
80.21	0.0103	74.81	75.67	0.0085	71.19			
103.86	0.0118	97.65	91.24	0.0143	83.68			
126.20	0.0206	115.58	95.44	0.0193	85.50			
149.66	0.0231	137.34	117.46	0.0226	105.35			

Table D-24 Data of adsorption isotherms of five-HANs in mixed solute solution on Ti-HMS in phosphate buffer at pH 7 with IS 10 mM (25 ^{o}C)

MCAN			DCAN			TCAN		
C_0 (μg/L)	q_e (μg/m^2)	C_e (μg/L)	C_0 (μg/L)	q_e (μg/m^2)	C_e (μg/L)	C_0 (μg/L)	q_e (μg/m^2)	C_e (μg/L)
31.55	0.0038	31.76	40.80	0.0052	37.85	28.68	0.0050	25.81
52.57	0.0143	47.56	67.18	0.0175	63.29	36.17	0.0188	31.99
76.68	0.0226	71.75	83.96	0.0527	72.42	56.27	0.0395	47.62
102.20	0.0603	88.12	107.85	0.0762	90.43	100.26	0.0775	82.26
124.11	0.0392	115.85	127.46	0.1150	100.79	112.15	0.0983	89.33
142.79	0.0709	125.48	140.77	0.1115	115.97	126.20	0.1099	101.77
MBAN			**DBAN**					
C_0 (μg/L)	q_e (μg/m^2)	C_e (μg/L)	C_0 (μg/L)	q_e (μg/m^2)	C_e (μg/L)			
31.71	0.0001	31.63	24.41	0.0013	23.68			
62.92	0.0110	60.48	49.18	0.0273	43.10			
80.21	0.0299	73.67	75.67	0.0470	65.38			
103.86	0.0305	96.76	77.84	0.0472	66.90			
126.20	0.0532	116.12	95.44	0.0582	81.95			
149.66	0.0648	135.26	115.25	0.0785	97.80			

Table D-25 Data of adsorption isotherms of five-HANs in mixed solute solution on SBA-15 in phosphate buffer at pH 7 with IS 10 mM (25 ^{o}C)

MCAN			DCAN			TCAN		
C_0 (μg/L)	q_e (μg/m^2)	C_e (μg/L)	C_0 (μg/L)	q_e (μg/m^2)	C_e (μg/L)	C_0 (μg/L)	q_e (μg/m^2)	C_e (μg/L)
31.69	0.0030	29.92	30.11	0.0053	27.59	30.84	0.0011	30.33
49.28	0.0045	47.18	50.46	0.0092	46.11	36.89	0.0055	34.30
67.82	0.0071	64.48	66.34	0.0136	59.93	36.31	0.0070	33.05
104.81	0.0143	98.04	87.53	0.0185	79.60	63.04	0.0183	54.37
113.96	0.0187	105.09	105.39	0.0293	91.46	93.41	0.0248	81.59
143.05	0.0282	129.74	134.34	0.0497	110.87	126.23	0.0347	109.85
MBAN			**DBAN**					
C_0 (μg/L)	q_e (μg/m^2)	C_e (μg/L)	C_0 (μg/L)	q_e (μg/m^2)	C_e (μg/L)			
30.90	0.0015	30.17	31.98	0.0010	31.52			
49.52	0.0030	48.12	53.81	0.0034	52.20			
69.47	0.0114	64.09	69.42	0.0128	63.41			
94.13	0.0182	85.51	92.27	0.0160	84.69			
112.99	0.0217	102.69	111.45	0.0248	99.69			
142.09	0.0290	128.42	148.73	0.0467	126.70			

Table D-26 Data of adsorption isotherms of five-HANs in mixed solute solution on NaY in phosphate buffer at pH 7 with IS 10 mM (25 ^{o}C)

MCAN			DCAN			TCAN		
C_0 (μg/L)	q_e (μg/m^2)	C_e (μg/L)	C_0 (μg/L)	q_e (μg/m^2)	C_e (μg/L)	C_0 (μg/L)	q_e (μg/m^2)	C_e (μg/L)
30.64	0.0036	29.89	31.00	0.0049	28.83	34.55	0.0058	33.23
47.79	0.0083	46.10	52.58	0.0130	47.80	40.34	0.0183	36.66
70.84	0.0139	67.36	74.36	0.0153	63.03	47.71	0.0218	42.97
95.40	0.0112	93.27	100.88	0.0316	81.55	67.26	0.0398	59.72
117.48	0.0181	113.88	124.65	0.0458	105.45	103.89	0.0607	91.88
136.29	0.0233	131.49	144.16	0.0554	120.39	118.51	0.0729	103.60
MBAN			**DBAN**					
C_0 (μg/L)	q_e (μg/m^2)	C_e (μg/L)	C_0 (μg/L)	q_e (μg/m^2)	C_e (μg/L)			
32.46	0.0071	30.88	25.24	0.0103	22.99			
57.99	0.0109	55.09	47.41	0.0189	43.62			
79.53	0.0177	74.86	71.96	0.0303	65.35			
102.17	0.0214	98.10	74.62	0.0391	67.97			
122.83	0.0214	116.99	99.84	0.0458	86.49			
133.92	0.0288	128.38	121.91	0.0617	100.27			

Table D-27 Data of adsorption isotherms of five-HANs in mixed solute solution on SBA-CHX in phosphate buffer at pH 7 with IS 10 mM (25 ^{o}C)

MCAN			DCAN			TCAN		
C_0 (μg/L)	q_e (μg/g)	C_e (μg/L)	C_0 (μg/L)	q_e (μg/g)	C_e (μg/L)	C_0 (μg/L)	q_e (μg/g)	C_e (μg/L)
40.01	0.00	42.98	25.40	0.00	31.68	25.62	0.10	27.81
61.52	3.38	59.55	40.96	1.07	41.42	31.06	0.21	31.62
88.72	4.97	84.09	89.03	19.05	77.95	54.63	6.00	52.35
125.09	4.82	123.77	98.43	22.03	82.51	111.89	12.856	105.21
186.21	11.51	179.57	124.86	26.91	107.77	159.25	17.75	143.00
247.32	19.13	236.16	161.83	32.99	142.54	166.02	26.25	151.60
MBAN			**DBAN**					
C_0 (μg/L)	q_e (μg/g)	C_e (μg/L)	C_0 (μg/L)	q_e (μg/g)	C_e (μg/L)			
30.67	0.00	33.44	25.37	0.05	25.34			
57.07	2.24	55.77	41.92	0.52	40.04			
81.34	9.80	75.64	66.99	6.49	63.22			
105.55	11.35	98.99	88.18	22.63	75.08			
153.80	10.29	149.23	133.09	30.03	115.77			
229.82	25.07	212.36	180.44	47.03	152.90			

Table D-28 Data of adsorption isotherms of five-HANs in mixed solute solution on PG-SBA-CHX in phosphate buffer at pH 7 with IS 10 mM (25 ^{o}C)

MCAN			DCAN			TCAN		
C_0 (μg/L)	q_e (μg/g)	C_e (μg/L)	C_0 (μg/L)	q_e (μg/g)	C_e (μg/L)	C_0 (μg/L)	q_e (μg/g)	C_e (μg/L)
40.01	5.83	36.60	25.40	1.71	24.40	18.74	0.97	18.18
61.52	2.91	59.84	40.96	5.26	37.93	31.06	10.60	24.94
88.72	4.19	86.17	89.03	30.79	70.28	53.95	22.16	40.46
125.09	6.92	121.09	98.43	39.17	75.82	96.05	49.65	67.39
186.21	13.94	178.21	114.34	42.26	90.07	138.99	84.04	90.73
247.32	19.06	236.05	153.94	44.58	127.58	158.94	87.28	107.32
MBAN			**DBAN**					
C_0 (μg/L)	q_e (μg/g)	C_e (μg/L)	C_0 (μg/L)	q_e (μg/g)	C_e (μg/L)			
25.88	0.15	25.79	21.0	7.24	16.77			
48.16	1.17	47.48	34.7	14.61	26.28			
66.80	4.18	64.26	50.8	22.67	37.00			
80.97	3.19	79.13	73.0	44.81	47.17			
117.29	6.66	113.47	99.3	61.30	64.07			
163.54	9.21	158.09	133.0	78.65	86.46			

Table D-29 Data of adsorption isotherms of five-HANs in mixed solute solution on M-HMS in phosphate buffer at pH 7 with IS 10 mM (25 ^{o}C)

MCAN			DCAN			TCAN		
C_0 (mg/L)	q_e (mg/m^2)	C_e (μg/L)	C_0 (mg/L)	q_e (mg/m^2)	C_e (mg/L)	C_0 (mg/L)	q_e (mg/m^2)	C_e (μg/L)
0.05	0.0001	27.85	0.12	0.0002	0.15	0.08	0.0001	0.86
0.12	0.0001	71.42	0.22	0.0004	0.18	0.13	0.0002	0.07
0.31	0.0003	150.39	0.53	0.0010	0.37	0.34	0.0006	0.22
0.38	0.0004	193.12	0.51	0.0010	0.68	0.30	0.0006	0.53
0.68	0.0007	325.07	1.08	0.0020	0.89	0.67	0.0013	0.08
0.79	0.0007	393.38	1.02	0.0019	0.38	0.60	0.0011	0.75
1.39	0.0013	671.70	2.08	0.0038	2.53	1.46	0.0027	0.14
			5.15	0.0095	14.00	3.34	0.0062	1.09
			10.76	0.0200	240.34	7.12	0.0135	3.98
						7.54	0.0143	20.93
						13.75	0.0253	36.44

MBAN			DBAN		
C_0 (mg/L)	q_e (mg/m^2)	C_e (μg/L)	C_0 (mg/L)	q_e (mg/m^2)	C_e (μg/L)
0.06	0.0001	5.39	0.08	0.0001	0.00
0.15	0.0003	13.10	0.15	0.0003	0.00
0.39	0.0007	39.62	0.33	0.0006	0.00
0.37	0.0006	47.45	0.27	0.0005	0.00
0.87	0.0014	115.99	0.75	0.0014	0.00
0.76	0.0011	159.02	0.49	0.0009	0.00
1.59	0.0022	412.56	1.68	0.0031	0.00
			2.74	0.0051	0.000
			5.54	0.0105	26.28
			7.65	0.0132	705.67

Table D-30 Data of adsorption isotherms of five-HANs in mixed solute solution on PAC in phosphate buffer at pH 7 with IS 10 mM (25 ^{o}C)

MCAN			DCAN			TCAN		
C_0 (mg/L)	q_e (mg/m^2)	C_e (μg/L)	C_0 (mg/L)	q_e (mg/m^2)	C_e (μg/L)	C_0 (mg/L)	q_e (mg/m^2)	C_e (μg/L)
0.05	0.0001	36.30	0.12	0.0002	0.13	0.08	0.0001	0.42
0.12	0.0001	82.13	0.22	0.0004	0.24	0.13	0.0002	0.89
0.31	0.0002	171.57	0.53	0.0009	0.70	0.34	0.0006	2.17
0.38	0.0003	227.21	0.51	0.0009	0.83	0.30	0.0005	0.76
0.68	0.0006	322.21	1.08	0.0018	1.64	0.68	0.0011	6.05
0.79	0.0005	481.39	1.02	0.0017	2.37	0.60	0.0010	2.11
1.39	0.0012	677.48	2.08	0.0036	4.84	1.46	0.0025	22.47
			5.15	0.0088	11.90	3.34	0.0057	40.00
			10.76	0.0188	30.93	7.12	0.0122	144.26
			15.21	0.0263	45.87	7.54	0.0128	151.65
			22.01	0.0373	65.59	13.75	0.0231	141.56

MBAN			DBAN		
C_0 (mg/L)	q_e (mg/m^2)	C_e (μg/L)	C_0 (mg/L)	q_e (mg/m^2)	C_e (μg/L)
0.06	0.0001	28.58	0.08	0.0001	0.000
0.15	0.0002	67.42	0.15	0.0003	0.000
0.39	0.0004	158.35	0.33	0.0006	0.000
0.37	0.0003	204.96	0.27	0.0005	0.000
0.87	0.0009	328.74	0.75	0.0013	0.000
0.76	0.0005	493.63	0.49	0.0009	0.165
1.59	0.0014	789.74	1.68	0.0029	0.186
			2.74	0.0047	1.69
			5.54	0.0097	1.11
			7.65	0.0133	1.88
			11.15	0.0190	1.86

4.2 Effect of Electrolyte in Tap Water on Adsorption of Mixed Five-HANs

Table D-31 Data of adsorption isotherms of five-HANs in mixed solute solution on M-HMS in tap water at pH 7.15 with IS 4.6 mM (25 ^{o}C)

MCAN			DCAN			TCAN		
C_0 (mg/L)	q_e (mg/g)	C_e (μg/L)	C_0 (mg/L)	q_e (mg/g)	C_e (μg/L)	C_0 (mg/L)	q_e (mg/g)	C_e (μg/L)
0.11	0.09	50.16	0.15	0.23	7.55	0.14	0.23	0.055
0.20	0.17	90.50	0.29	0.46	7.61	0.27	0.44	0.059
0.40	0.38	179.47	0.40	0.66	7.79	0.52	0.88	0.063
1.00	0.82	517.42	0.00	0.00	0.00	0.88	1.47	0.000
1.44	0.87	934.56	1.56	2.63	8.24	1.20	2.03	0.097
			2.12	3.60	7.47	1.82	3.09	0.168
MBAN			**DBAN**					
C_0 (mg/L)	q_e (mg/g)	C_e (μg/L)	C_0 (mg/L)	q_e (mg/g)	C_e (μg/L)			
0.07	0.11	3.56	0.08	0.14	0.00			
0.24	0.38	12.76	0.14	0.23	0.00			
0.57	0.81	94.57	0.52	0.88	0.00			
1.43	2.02	232.59	0.00	0.00	0.00			
1.94	2.42	525.44	1.50	2.54	0.00			
			2.25	3.83	0.00			

Table D-32 Data of adsorption isotherms of five-HANs in mixed solute solution on PAC in tap water at pH 7.15 with IS 4.6 mM (25 ^{o}C)

MCAN			DCAN			TCAN		
C_0 (mg/L)	q_e (mg/m^2)	C_e (μg/L)	C_0 (mg/L)	q_e (mg/m^2)	C_e (mg/L)	C_0 (mg/L)	q_e (mg/m^2)	C_e (μg/L)
0.11	0.09	50.61	0.15	0.24	0.67	0.14	0.23	0.075
0.20	0.16	96.83	0.29	0.47	0.76	0.27	0.44	0.067
0.40	0.35	194.35	0.40	0.67	1.06	0.52	0.88	0.066
0.79	0.57	226.33	1.18	1.97	0.97	0.88	1.47	0.040
1.00	0.75	560.77	1.56	2.64	2.23	1.20	2.03	0.063
1.44	0.98	869.21	2.12	3.60	6.98	1.82	3.09	0.170
MBAN			**DBAN**					
C_0 (mg/L)	q_e (mg/m^2)	C_e (μg/L)	C_0 (mg/L)	q_e (mg/m^2)	C_e (μg/L)			
0.07	0.04	41.42	0.08	0.14	0.000			
0.24	0.25	89.75	0.11	0.19	0.000			
0.57	0.61	212.93	0.52	0.88	0.000			
1.11	0.92	274.28	1.15	1.91	0.000			
1.43	1.29	666.59	1.50	2.54	0.000			

4.3 Adsorption of DCAN in the presence of Co-existing DBPs (TCM and DCAA)

Table D-33 Data of adsorption isotherms of DCAA, DCAN and TCM in mixed solute solution on M-HMS in phosphate buffer at pH 7 with IS 10 mM (25 ^{o}C)

DCAA			DCAN			TCM		
C_0 (μg/L)	q_e (mg/g)	C_e (μg/L)	C_0 (μg/L)	q_e (mg/g)	C_e (μg/L)	C_0 (μg/L)	q_e (mg/g)	C_e (μg/L)
22.44	0.011	15.86	56.63	0.097	0.026	51.62	0.045	30.68
73.11	0.013	65.43	93.31	0.161	0.029	90.46	0.069	53.37
170.20	0.042	164.66	177.22	0.307	0.037	143.50	0.101	119.09
266.79	0.035	258.77	280.21	0.487	0.041	240.28	0.131	204.93
365.11	0.037	346.74	391.37	0.678	0.046	360.24	0.211	269.91
455.37	0.057	429.28	475.10	0.817	0.067	425.30	0.230	341.37

Table D-34 Data of adsorption isotherms of DCAA, DCAN and TCM in mixed solute solution on PAC in phosphate buffer at pH 7 with IS 10 mM (25 ^{o}C)

DCAA			DCAN			TCM		
C_0 (μg/L)	q_e (mg/g)	C_e (μg/L)	C_0 (μg/L)	q_e (mg/g)	C_e (μg/L)	C_0 (μg/L)	q_e (mg/g)	C_e (μg/L)
36.43	0.052	6.52	50.55	0.088	0.037	61.99	0.075	7.33
94.70	0.078	49.22	99.64	0.170	0.022	112.50	0.148	12.70
198.76	0.113	132.26	171.91	0.292	0.039	178.16	0.256	21.15
318.50	0.133	241.48	354.52	0.610	0.071	444.89	0.504	61.91
653.37	0.180	549.69	558.71	0.970	0.110	643.08	0.794	101.85
871.36	0.277	711.27	766.41	1.328	0.204	835.54	1.074	146.68

APPENDIX E
JOURNAL ARTICLE

1) Prarat, P., Ngamcharussrivichai, C., Khaodhiar, S., and Punyapalakul, P. **Adsorption characteristics of haloacetonitriles on functionalized silica-based porous materials in aqueous solution**. Journal of Hazardous Materials 192 (2011): 1210-1218.

2) Prarat, P., Ngamcharussrivichai, C., Khaodhiar, S., and Punyapalakul, P. **Effect of porous and crystalline structures of inorganic porous silicates on their adsorption of dilute aqueous haloacetonitriles**. Submitted to Journal of Hazardous Materials on August, 2011.

3) Prarat, P., Ngamcharussrivichai, C., Khaodhiar, S., and Punyapalakul, P. **Adsorption property of haloacetonitriles on polymerizable surfactant-modified mesoporous silicate in aqueous solution through adsolubilization**. Expected to ready for submission to Colloids and Surfaces A: Physicochemical and Engineering Aspects in October, 2011.

BIOGRAPHY

Miss Panida Prarat was born in Bangkok province. After she graduated high school in the Demonstration School of Ramkhumhaeng University, Bangkok, she studied in Faculty of Science and Technology at Thammasat University. She graduated Bachelor's degree of Science of Environmental Science in 2001. Three year later, she received her Master's degree of Science in Environmental Science, Chulalongkorn University. She pursued her philosophy of Doctoral Degree studies in the International Postgraduate Program in Environmental Management, Chulalongkorn University in October, 2008, and finished her philosophy of Doctoral Degree in September, 2011.